



# Construction et Analyse de Nouveaux Codes Spatio-Temporels pour les Systèmes Ultra Large Bande par Impulsions

Chadi Abou Rjeily

## ► To cite this version:

Chadi Abou Rjeily. Construction et Analyse de Nouveaux Codes Spatio-Temporels pour les Systèmes Ultra Large Bande par Impulsions. domain\_other. Télécom ParisTech, 2006. Français. NNT: . pastel-00001968

HAL Id: pastel-00001968

<https://pastel.hal.science/pastel-00001968>

Submitted on 19 Oct 2006

**HAL** is a multi-disciplinary open access archive for the deposit and dissemination of scientific research documents, whether they are published or not. The documents may come from teaching and research institutions in France or abroad, or from public or private research centers.

L'archive ouverte pluridisciplinaire **HAL**, est destinée au dépôt et à la diffusion de documents scientifiques de niveau recherche, publiés ou non, émanant des établissements d'enseignement et de recherche français ou étrangers, des laboratoires publics ou privés.



## THÈSE

présentée pour obtenir le grade de **Docteur**  
de l' **École Nationale Supérieure des Télécommunications**

Spécialité : Communications et Électronique

par

**Chadi Abou-Rjeily**

***Construction et Analyse de Nouveaux Codes Spatio-Temporels pour les  
Systèmes Ultra Large Bande par Impulsions***

Jury composé de :

Président	Helmut Böelcskei
Rapporteurs	Emanuele Viterbo Raymond Knopp
Examinateur	Ghaya Rekaya-Ben Othman
Directeurs de thèse	Jean-Claude Belfiore Norbert Daniele



---

# Remerciements

Je tiens à remercier toutes les personnes qui ont contribué au bon déroulement de cette thèse. À toutes les personnes qui m'ont soutenu au cours de ces trois années.

Je remercie tout particulièrement Jean-Claude Belfiore, qui a accepté d'être mon directeur de thèse et qui m'a donnée l'occasion de débuter dans le monde de la recherche. À remercier aussi son attention, sa disponibilité et ses divers conseils, remarques et encouragements. À remercier son suivi avec enthousiasme et persévérance le développement de ma thèse. Je remercie également Norbert Daniele qui a assuré mon encadrement à CEA Grenoble. Ce travail n'aurait pas pu être ce qu'il est sans son encadrement, patience et conseils.

Je tiens aussi à exprimer mes remerciements à tous les membres du jury. À Helmut Böelcskei qui m'a fait l'honneur de présider ce jury. À Ghaya Rekaya-Ben Othman qui a accepté d'en être le examinateur. Je remercie également Emanuele Viterbo et Raymond Knopp d'avoir acceptés de rapporter ma thèse et qui ont également contribués avec leurs suggestions à améliorer la qualité du manuscrit.

Je remercie Laurent Ouvry et Jean-Michel Leger de CEA Grenoble de m'avoir accueilli au sein de leurs laboratoires.

Merci à mes amis collègues de CEA qui ont rendu cette période aussi agréable qu'enrichissante. À Benoit, Samuel, Michael, Youssef, Julien, Sébastien, Jean-Benoit, Manuel, Christophe, Moussa, Raphi, Laurent, Mathieu, Sylvie, Nicolas. Coté ENST : Elias, Sheng, Emilio, Sylvain, Anne-Laure, Ihsan, Lydia, Ghalid, Ghassan.

Enfin, je voudrais remercier mes parents de m'avoir apporté leur affection pour arriver jusqu'ici et de m'avoir soutenu dans les moments difficiles. À mes frères Elie, Fadi et Jean sans lesquels la vie serait trop ennuyeuse. À mes proches et mes amis.

*"If I have seen further it is by standing on the shoulders of giants "*

Sir Isaac Newton



# Abstract

Providing high data rates with good quality of service for a large number of radio terminals communicating with each other over a wireless channel constitutes the major challenge for the fourth generation (4G) wireless networks. The basic technologies necessary to implement the vision of a target data rate in the order of 1 Gbits/s are the subject of extensive research and investigation. In this context, the ultra-wideband (UWB) technology is a strong candidate for 4G wireless personal area networks (WPANs). This technology provides the advantage of low cost terminals that can coexist with the existing wireless communication systems.

In this thesis, we present the construction of UWB transmitters and receivers over multi-antenna channels. The multi-antenna techniques can further enhance the data rate, quality and communication ranges of the existing UWB solutions.

Given the carrier-less nature of the UWB transmissions, most of the existing space-time (ST) coding schemes (the best known ones in any case) can not be associated with this nonconventional technique. While phase rotations can be exploited to achieve the transmit diversity in conventional narrow-band and wide-band systems, the very large bandwidth occupied by the transmitted UWB pulses renders the phase reconstitution at the receiver side practically infeasible.

In our work, we propose novel families of ST codes that can be associated with carrier-less UWB transmissions. At a first time, we adapt the mathematical tools based on cyclic division algebras to construct new totally-real coding schemes over the field of rational numbers. At a second time, we show that additional performance gains can be obtained when applying additional intra-symbol coding on the pulses used to convey a given information symbol. Finally, and unlike the classical approach of constructing ST codes over infinite fields, we propose a new approach for the construction of modulation-specific codes that can be associated with pulse position modulation (PPM) and with hybrid pulse position and amplitude modulation (PPAM). The new modulation-specific codes show the best known performance among the existing ST-UWB schemes. In some situations, these codes satisfy all the construction constraints of the perfect codes in addition to the constraint of being totally real.

We also consider the problem of constructing distributed ST-UWB codes that permit to profit from the spatial diversity in a distributed manner. Novel amplify-and-forward and decode-and-forward strategies are proposed and investigated over the indoor UWB channels. Throughout our work, we present analytical, semi-analytical and numerical analysis of the proposed solutions over realistic indoor highly frequency-selective channels. Issues related to the transceiver design and decoding strategies of practical multi-antenna UWB systems are also studied.



# Contents

<b>Remerciements</b>	<b>i</b>
<b>Abstract</b>	<b>iii</b>
<b>Contents</b>	<b>v</b>
<b>Résumé de la thèse en Français</b>	<b>ix</b>
<b>List of Figures</b>	<b>xxvii</b>
<b>List of Acronyms</b>	<b>xxxi</b>
<b>List of Notations</b>	<b>xxxiii</b>
<b>1 Introduction</b>	<b>1</b>
1.1 Ultra-Wideband communications . . . . .	1
1.1.1 Introduction . . . . .	1
1.1.2 Waveforms . . . . .	2
1.1.3 Modulation Schemes . . . . .	3
1.1.4 Time Hopping UWB . . . . .	4
1.1.5 UWB channel models . . . . .	7
1.1.6 Receivers . . . . .	8
1.2 Definitions from algebraic number theory . . . . .	9
1.3 Multiple-Input-Multiple-Output communications . . . . .	13
1.3.1 Introduction . . . . .	13
1.3.2 Diversity and Multiplexing Tradeoff . . . . .	14
1.3.3 Design criteria of Space-Time codes . . . . .	15
1.3.4 Space-Time Block Codes . . . . .	16
1.3.5 Cooperative Diversity . . . . .	24
1.4 MIMO-UWB communication systems . . . . .	26
1.4.1 Space-Hopping with IR-UWB . . . . .	26
1.4.2 Coherent Rate-1 Space-Time codes for IR-UWB . . . . .	27
1.4.3 Non-coherent Rate-1 Space-Time codes for IR-UWB . . . . .	28
1.4.4 Spatial Multiplexing with IR-UWB . . . . .	29
1.4.5 MIMO-UWB systems using orthogonal pulses . . . . .	30

1.5	Thesis outline and contributions . . . . .	30
<b>2</b>	<b>Receiver Design and Performance Analysis</b>	<b>33</b>
2.1	System Model . . . . .	34
2.1.1	Rake receivers . . . . .	36
2.1.2	Correlation receivers . . . . .	39
2.1.3	Despreadering . . . . .	40
2.2	Rate-1 coherent ST-coded systems . . . . .	40
2.2.1	Transceiver Structure . . . . .	40
2.2.2	Conditional Error probability with bi-orthogonal PPAM . . . . .	41
2.2.3	Error probability with PAM . . . . .	42
2.2.4	Achieved diversity order over the IEEE 802.15.3a channel models . . . . .	42
2.3	Diversity-Multiplexing Tradeoff over the 802.15.3a channel models . . . . .	44
2.3.1	Statistical characterization . . . . .	45
2.3.2	Achieved Tradeoffs . . . . .	47
2.4	Interference model . . . . .	50
2.4.1	Inter Symbol Interference . . . . .	50
2.4.2	Multi User Interference . . . . .	52
2.4.3	Performance with MMSE receivers . . . . .	54
2.4.4	Designing the amplitude-spreading sequences . . . . .	55
2.5	Numerical Results . . . . .	57
2.5.1	All-digital systems based on direct sampling . . . . .	57
2.5.2	Coded systems over realistic indoor channels . . . . .	57
2.5.3	Coverage extension offered by the MIMO techniques . . . . .	59
<b>3</b>	<b>Full-Rate ST codes</b>	<b>61</b>
3.1	Partial Transmit Diversity Using Modified Hermite Pulses . . . . .	61
3.2	Inter-Symbol Coding (ISC) . . . . .	63
3.2.1	$2 \times 2$ codes . . . . .	65
3.2.2	$3 \times 3$ code . . . . .	66
3.2.3	$4 \times 4$ code . . . . .	66
3.2.4	$5 \times 5$ code . . . . .	67
3.2.5	$6 \times 6$ code . . . . .	67
3.2.6	Balanced codes . . . . .	68
3.2.7	Relation with the TAST codes . . . . .	69
3.2.8	Coding Gain . . . . .	69
3.2.9	ISC with hybrid PPM-PAM constellations . . . . .	70
3.3	Inter-Pulse Coding (IPC) . . . . .	72
3.3.1	Code Construction . . . . .	72
3.3.2	IPC with hybrid PPM-PAM constellations . . . . .	74
3.4	Modulation-specific ST codes . . . . .	75
3.4.1	Construction 1: Achieving full transmit diversity via position permutation . . . . .	75
3.4.2	Construction 2: Achieving full transmit diversity via position combining . . . . .	79
3.4.3	Comparison with codes from cyclic division algebras . . . . .	81

3.5	Numerical Results . . . . .	82
3.5.1	Performance with PAM . . . . .	82
3.5.2	Performance with hybrid PPM-PAM . . . . .	86
3.5.3	Construction 1 versus Construction 2 . . . . .	90
3.5.4	Performance in the presence of MUI . . . . .	91
<b>4</b>	<b>Cooperative Diversity</b>	<b>93</b>
4.1	System design with the AF scheme . . . . .	93
4.1.1	Diversity combining at the relays . . . . .	94
4.1.2	Systems with feedback . . . . .	94
4.1.3	System model . . . . .	95
4.2	Code construction for the NAF scheme . . . . .	97
4.2.1	Inter Symbol Coding (ISC) . . . . .	97
4.2.2	Inter Pulse Coding (IPC) . . . . .	100
4.2.3	Modulation-specific codes . . . . .	101
4.3	Code construction for the DF scheme . . . . .	103
4.3.1	Coherent systems . . . . .	103
4.3.2	Differential systems . . . . .	105
4.3.3	Selective Relaying and Fixed Relaying . . . . .	108
4.4	Numerical Results . . . . .	109
4.4.1	The NAF strategy . . . . .	109
4.4.2	The DF strategy . . . . .	114
<b>5</b>	<b>Decoding the multi-dimensional constellations</b>	<b>119</b>
5.1	Problem formulation . . . . .	119
5.2	Layered space-time detection . . . . .	120
5.3	Sphere detection based on Pohst enumeration (SD) . . . . .	122
5.3.1	SD with PPM-PAM constellations (algorithm 0) . . . . .	122
5.3.2	SD with PPM-PAM constellations (algorithm 1) . . . . .	123
5.3.3	SD with PPM-PAM constellations (algorithm 2) . . . . .	124
5.4	Sphere detection based on Schnorr-Euchner enumeration (SE) . . . . .	127
5.4.1	SE with PAM constellations . . . . .	127
5.4.2	SE with PPM constellations . . . . .	128
5.4.3	SE with PPM-PAM constellations . . . . .	130
5.4.4	SE with a Fano-like metric bias . . . . .	134
5.5	Numerical Results . . . . .	135
<b>Conclusion and Perspectives</b>		<b>139</b>
<b>A</b>	<b>SIMO-UWB channel measurements and characterization</b>	<b>141</b>
<b>B</b>	<b>Performance of bi-orthogonal Signalling</b>	<b>145</b>
<b>C</b>	<b><math>-1</math> is not a norm in <math>\mathbb{Q}(\sqrt{3})</math></b>	<b>149</b>

<b>D Properties of construction 1</b>	<b>151</b>
D.1 Diversity Order . . . . .	151
D.2 Coding Gain . . . . .	155
D.3 Information Losses . . . . .	157
<b>E Properties of construction 2</b>	<b>161</b>
E.1 Choice of $\Omega$ . . . . .	161
E.2 Diversity Order with 2-PPM . . . . .	162
E.3 Coding Gain with 2-PPM . . . . .	163
<b>List of Publications</b>	<b>167</b>
<b>Bibliography</b>	<b>171</b>

# Resumé en Français

## Introduction

Le plus grand défi des réseaux personnels sans fil de quatrième génération (4G) est de fournire un très haut débit avec une bonne qualité de service à un grand nombre d'utilisateurs qui partagent les mêmes ressources d'un canal radio. Les solutions techniques qui peuvent répondre aux besoins très haut débit (de l'ordre de 1 Gbits/s) des réseaux personnels sans fil de quatrième génération sont l'objet d'une intense activité de recherche à travers le monde. Dans ce contexte, les systèmes de transmissions à bande extrêmement large sont une solution adaptée à ces besoins. La technique ultra large bande (ULB) consiste à émettre des impulsions de très courte durée. Etant donnée que la transmission s'effectue directement en bande de base, les terminaux basés sur les transmissions ULB sont potentiellement bas coût et capable de coexister avec les autres systèmes de communication sans fil.

Ce rapport de thèse présente des nouvelles méthodes d'émission et de réception basées sur les transmissions ULB pour les canaux à antennes multiples. Dans ce contexte, les techniques multi-antennes sont capables d'améliorer les performances et d'augmenter le débit des systèmes ULB par impulsion.

Les codes spatio-temporels optimaux permettant d'atteindre les meilleures performances sont désormais connus pour un émetteur à  $n \geq 2$  antennes et un récepteur ayant au moins  $n$  antennes. Ces codes, appelés les codes parfaits, initialement développés pour les signaux à bande étroite peuvent être aussi appliqués aux systèmes à large bande de type OFDM, MC-CDMA ou DSSS-CDMA. Par contre, ces codes ne peuvent pas être associés aux signaux ULB impulsifs. En effet, les codes parfaits sont à coefficients complexes et portent par conséquent une information de phase. Or, les systèmes ULB ont pour spécificité de travailler directement en bande de base. Pour ces formes d'ondes étant donné la bande passante (de l'ordre de quelques GHz), il devient alors excessivement difficile de récupérer l'information de phase.

Dans ce travail, nous proposons la construction de nouvelles familles de codes espace-temps pour les systèmes de communications ULB impulsifs. Dans un premier temps, les outils mathématiques basés sur les algèbres cycliques de division ont été adaptés pour la construction d'un schéma de codage espace temps totalement réel sur le corps des nombres rationnels. Dans les systèmes ULB impulsifs, plusieurs impulsions sont utilisées pour la transmission de chaque symbole d'information. En profitant de la présence de ces impulsions, nous avons proposé une autre famille de codes basée sur l'introduction du codage d'impulsion ainsi que du codage conjoint symbole-impulsion. Cette famille de code a permis d'améliorer les performances.

À cause de leur très bonne résolution temporelle, les systèmes ULB sont mieux adaptés aux modulations par position. Dans un deuxième temps, et contrairement à l'approche classique de construction des codes espace-temps sur des corps infinis, nous proposons des nouvelles constructions spécifiques aux

modulations de positions (PPM) ou aux modulations conjointes de position et d'amplitude (PPAM). Ces constructions profitent des caractéristiques de ces constellations multidimensionnelles et non linéaires, elles permettent d'obtenir une famille de code présentant les meilleures performances parmi tous les schémas de codage espace-temps ULB existant dans la littérature. Dans certains cas, cette famille de codes totalement réels satisfait toutes les contraintes de construction des codes parfaits complexes.

Enfin, nous nous sommes intéressés à des nouvelles constructions de codes distribués pour les systèmes ULB coopératifs. En particulier, nous proposons trois familles de codes algébriques pour la stratégie de coopération type "amplify-and-forward". La première famille introduit un codage entre les symboles adjacents en se basant sur les algèbres cycliques de division. La deuxième famille est basée sur le codage inter-impulsion et elle permet d'atteindre des bons niveaux de performance avec une complexité réduite. Ces deux familles de code permettent d'atteindre un ordre de diversité maximal avec un gain de codage qui ne s'évanouit pas avec la taille de la constellation et ce pour n'importe quel nombre de relais. Ces codes peuvent être associés avec les constellations PAM, PPM et PPAM. La troisième famille de code présente l'avantage d'une énergie moyenne uniforme par relais et par symbole. Elle est spécifique aux constellations PPM et PPAM avec lesquelles elle présente les meilleures performances connues. Dans certains cas, cette famille de code peut atteindre un gain de codage qui ne s'évanouit pas avec la taille de la constellation. Nous présentons aussi des nouvelles techniques de coopération pour la stratégie type "decode-and-forward" pour les systèmes ULB cohérents et non cohérents.

Tout le long de notre travail, nous présentons une analyse analytique, semi-analytique et numérique des solutions proposées sur des canaux ULB sélectifs en fréquence proposés en standardisation (IEEE 802.15.3a). Nous présentons aussi des schémas pratiques de transmission, réception et décodage des systèmes multi-antennes ULB et des systèmes coopératifs ULB. Les simulations sur des canaux ULB réalistes valident les propositions théoriques et montrent l'utilité de combiner les techniques multi-antennes et les techniques coopératives avec les transmissions ULB impulsionales.

## Généralités sur les systèmes multi-antennes ULB

Durant ces dernières années la communauté de la recherche a développée des nombreuses solutions pour les réseaux personnels sans fil de quatrième génération (4G). Parmi les solutions qui promettent des améliorations significatives dans les performances, on peut citer le codage et la modulation adaptative, les algorithmes de codage itératifs, le codage espace-temps, les techniques multi-antennes, les modulations multi-porteuses et les systèmes radio à bande extrêmement large. Plus particulièrement, la technique de transmission ultra large bande (ULB) par impulsion promet des solutions attrayantes et innovantes pour les systèmes de communications sans fil, les applications radar, l'imagerie médicale et les systèmes de positionnement.

Aujourd'hui les transmissions ULB qui consistent à émettre des impulsions de très courte durée (bande fréquentielle de plusieurs GHz) sont toujours considérées comme non conventionnelles. Cette technique, d'abord utilisée pour des applications radar, a trouvé peu à peu des applications dans le domaine des télécommunications. L'ère moderne de l'ULB a commencé en 1993 quand Robert Scholtz a présenté une stratégie d'accès multiple adaptée aux communications radio de type impulsionales. Associé à un schéma d'accès multiple variable, les techniques ULB impulsionales peuvent permettre d'une part des applications radar ou des liens point à point, mais aussi des communications plus complexes mettant en réseaux plusieurs terminaux radios. Étant donné que la bande occupée par ces

impulsions peut être commune avec des bandes allouées à d'autres services de radiocommunication, des contraintes très rigides ont été adoptées sur le niveau d'émission des terminaux radio ULB. Par exemple, aux USA la "Federal Communications Commission" (FCC) permet l'émission des signaux ULB dans la bande de fréquence [3.1 10.6] GHz avec une densité spectrale de puissance très faible de -41.25 dBm/MHz. Ce faible niveau peut être très contraignant sur le débit et sur la portée des systèmes ULB.

Dans ce rapport de thèse, nous nous intéressons aux systèmes ULB impulsionnels. Une autre solution technique qui permet de profiter de la bande ULB est la solution multi-band OFDM où la bande passante est divisée en plusieurs sous bandes de 528 MHz. Chaque sous bande est composée de 128 sous porteuses modulée en QPSK en générale. La solution OFDM est bien adaptée aux systèmes haut débit et les sous porteuses peuvent être choisies d'une façon dynamique pour limiter l'interférence avec les systèmes à bande étroite. En générale, cette technique nécessite des traitements FFT lourds et la variation du niveau de puissance sur une bande extrêmement large constitue un grand défi pour la conception des circuits RF. En effet, il y a un grand débat sur les avantages et les inconvénients des solutions multi-bande et impulsionale et les organismes de standardisation n'ont pas tranchés pour une solution ou une autre. Dans la littérature, beaucoup de travail a été consacré aux systèmes OFDM (mono-antenne et multi-antennes). Les systèmes multi-antennes impulsionnels, sujet peu exploré constituent à la fois un nouveau défi, et une solution potentielle pour les systèmes très haut débit.

Grâce à leur très bonne résolution temporelle, les systèmes ULB impulsionnels peuvent être associés avec les modulations par amplitude (PAM), les modulations par position (PPM) ou les modulations conjointes d'amplitude et de position (PPAM). Pour les systèmes ULB haut débit, l'augmentation de l'efficacité spectrale est obtenue en augmentant les niveaux d'amplitude de la modulation PAM ce qui introduit des pertes non négligeables au niveau des performances du système. D'autre part, pour les modulations PPM l'augmentation de l'efficacité spectrale est obtenue en augmentant le nombre de positions de modulation cependant cette solution augmente la complexité du récepteur.

Le canal de propagation ULB est un canal sélectif en fréquence. La réponse impulsionale du canal est composée d'un très grand nombre de multi-trajets et l'étalement du canal peut être cent fois plus important que la durée de l'impulsion transmise. Cette caractéristique du canal de propagation implique des conséquences directes sur la conception du récepteur. Pour profiter de cette diversité de multi-trajet, les récepteurs de type Rake sont souvent utilisés. Ces récepteurs combinent des versions différentes du signal émis qui ceux sont propagés par des chemins différents. Mais, étant donné l'étalement du canal, l'énergie du signal émis est étalée sur des centaines de multi-trajets et par conséquent l'énergie intégrée par chaque doigt du Rake est faible. D'autre part, la complexité du Rake augmente avec son nombre de doigts, et par conséquent, en pratique les récepteurs profitent d'une partie limitée de la diversité offerte par le canal ULB. Une autre catégorie de récepteur ULB est réalisée à l'aide de corrélateurs de type filtres adaptées au canal ou à une partie du canal. La différence entre un Rake et un récepteur à base de corrélations et que la seconde approche ne souffre pas de l'interférence intra-impulsion. En d'autres termes, le récepteur à base de corrélations arrive à résoudre les multi-trajets séparés d'une durée plus petite que la largeur de l'impulsion. Etant donnée la bonne résolution temporelle des récepteurs à base de corrélations, l'amplitude est souvent quantifiée sur un nombre très limité de niveaux.

D'autre part, les techniques multi-antennes sont capables d'améliorer la qualité des communications sur un canal radio. Les ressources limitées du système, comme par exemple le spectre et la puissance, peuvent être exploitées d'une façon plus efficace pour augmenter la capacité du canal par rapport à un canal avec une antenne de transmission et une antenne de réception. En d'autres termes, le degré spatial additionnels de liberté donne la possibilité de transmettre des flux de données indépendants à traverse

le canal et de les séparer coté réception. De ce point de vue, les techniques multi-antennes permettent d'augmenter le débit des systèmes sans fil. Les techniques multi-antennes peuvent être également employées pour combattre les phénomènes d'évanouissement.

Sur les canaux radio sans fil, il est possible d'obtenir un gain de multiplexage et un gain de diversité à la fois. Mais, désormais, il existe un compromis entre ces deux gains. Dans ce contexte, le compromis diversité-multiplexage d'un canal multi-antennes est nettement plus élevé que le compromis atteint par un canal mono-antenne. D'autre part, des solutions exclusives à l'ULB ont été proposées où deux impulsions orthogonales destinées à l'estimation du canal et à la transmission de données sont transmises simultanément pour améliorer le débit et les performances des systèmes multi-antennes ULB.

Une diversité de transmission maximale qui est égale au nombre des antennes de transmissions peut être obtenu dans le cas où le flux de donnée transmis est convenablement codé par un schéma de codage espace-temps approprié, ST pour space-time en Anglais. Les codes ST peuvent être classés en deux catégories : les codes ST par treillis et les codes ST en bloc. Dans la suite de ce rapport, nous nous intéressons aux techniques de codage par bloc parce que la complexité de leur décodage est moins élevée que celle des codes par treillis. Plusieurs familles de codes ont été proposées dans la littérature. Le premier code est le code d'Alamouti pour les systèmes avec deux antennes de transmissions. Ce code permet d'atteindre la diversité maximale de transmission sans réduction en débit par rapport aux systèmes mono-antenne. La dernière génération de codes ST linéaires correspond aux codes parfaits qui permettent d'atteindre la meilleure performance avec n'importe quel nombre d'antennes de transmission. Dans ce rapport, nous prenons les codes parfaits comme référence avec laquelle nous comparons nos codes qui sont adaptés aux communications ULB.

Dans le domaine des réseaux de capteur, les contraintes d'encombrement des terminaux radios constituent une limite pratique au nombre d'antennes qui peut être implémenté sur chacun de ces terminaux. Dans ce contexte, les différents nœuds peuvent coopérer entre eux pour profiter de la diversité spatiale d'une façon distribuée en formant un réseau virtuel d'antennes. Considérons le cas d'un réseau sans fil composé d'un certain nombre de nœuds équipé d'une seule antenne chacun. On considère le cas pratique des terminaux qui peuvent recevoir ou transmettre à un moment donnée (pas d'émission et de réception en même temps). Dans ce contexte, les nœuds voisins peuvent aider un certain nœud source à transmettre son message vers sa propre destination. Ces nœuds réagissent comme des relais pendant la communication entre la source et sa destination. Dans ce contexte là, plusieurs stratégies de coopération permettent d'obtenir des gains de performances très importants par rapport aux systèmes non coopératifs.

Les caractéristiques des canaux ULB et l'application des techniques non conventionnelles des transmissions avec des nouvelles modulations nécessitent la construction de codes ST et de schémas de coopération appropriés. L'état de l'art sur les systèmes multi-antennes ULB n'est pas très fourni. En général, les solutions proposées dans la littérature consistent à associer des transmissions ULB avec des codes ST orthogonaux (dont le débit peut être au mieux égal à 1 symbole par utilisation du canal). Une autre approche basée sur du multiplexage spatial permet d'augmenter le débit mais qui ne permet pas de tirer profit de la diversité de transmission. L'analyse des performances est basée sur des approximations des propriétés du canal et est souvent limité à des stratégies simples de transmission et de réception. Quelques codes orthogonaux de débits unitaires ont été aussi proposés pour les systèmes ULB non-cohérents utilisant des modulations PPM où la réception est basée sur l'intégration de l'énergie.

Dans ce mémoire de thèse, nous présentons une application des techniques multi-antennes pour les systèmes ULB impulsionnels. En particulier, nous présentons la construction de nouvelles familles de code ST par bloc adaptées aux transmissions ULB par impulsion. Nous présentons aussi la construction

de nouvelles familles de code ST distribués qui peuvent être associées aux systèmes ULB coopératifs. Nous nous intéressons aussi à l'architecture des récepteurs multi-antennes ULB et au problème de décodage avec les constellations multidimensionnelles et non-linéaires utilisées avec ces systèmes. Les systèmes proposés dans cette thèse sont exploitables dans les applications de réseaux personnels sans fil à très haut débit.

## Modèle et performances des systèmes ULB sur des canaux à antennes multiples

Dans le deuxième chapitre, nous présentons le modèle du système que nous appliquerons tout le long de la thèse. Nous considérons un système multi-antennes ULB où la connaissance du canal est disponible coté réception uniquement. Nous faisons l'hypothèse de synchronisation parfaite entre l'émetteur et le récepteur. Le schéma d'accès multiple par des sauts temporels est considéré et toutes les antennes du même utilisateur partagent la même séquence de saut temporel et, par conséquent, le niveau d'interférence moyen est le même que dans les réseaux mono antenne.

Le canal est typiquement un canal sélectif en fréquence. Etant donné la très courte durée des impulsions émises, les différences de temps de propagation doivent être prises en compte. D'autre part, les temps d'arrivée des différents trajets multiples sont complètement différents d'une antenne à l'autre. Nous adoptons trois approches pour générer les canaux multi-antennes ULB. Dans une première approche, nous faisons l'hypothèse que la distance qui sépare deux antennes du même réseau d'antennes est grande par rapport à la longueur d'onde correspondante à la fréquence minimale de la bande fréquentielle occupée. Dans ce cas, les différents sous-canaux sont non-correlés et, par conséquent, ils sont générés indépendamment utilisant les modèles du canal mon-antenne ULB proposés par le IEEE (les modèles IEEE 802.15.3.a). La deuxième approche consiste d'utiliser les modèles semi-déterministes du canal mono-antenne. Ces modèles qui prennent l'aspect spatial de l'environnement en considération peuvent être adaptés pour générer des canaux multi-antennes. La troisième approche consiste de simuler les performances du système sur une base de données générée par des mesures effectuées avec des réseaux d'antennes dans la bande fréquentielle [3 5] GHz.

Les récepteurs considérés sont de type Rake et à base de corrélations. Pour les Rake, on distingue entre les Rakes non-sélectifs qui combinent les premiers trajets et les Rakes sélectifs qui combinent uniquement les trajets les plus forts entre une antenne de transmission et une antenne de réception. Les Rakes sélectifs profitent d'une meilleure diversité de multi-trajets mais au coût d'une complexité beaucoup plus élevée que celle des Rake non-sélectifs. Les récepteurs à base de corrélations sont équivalents aux Rakes qui combinent la totalité des multi-trajets avec une résolution temporelle très élevée. Leur réalisation pratique est associée avec un échantillonnage sur un nombre très limité des niveaux d'amplitude (typiquement, échantillonnage sur 1 bit).

Dans les systèmes ULB impulsions, plusieurs impulsions sont utilisées pour la transmission de chaque symbole d'information. Ces répétitions sont introduites pour lutter contre l'interférence multi-utilisateur. En d'autres termes, et étant donné le faible niveau de puissance imposé sur les transmissions ULB, ces répétitions servent aussi à améliorer le niveau d'énergie capturée au récepteur en permettant des intégrations cohérentes. Pour les systèmes à antennes multiples, on peut profiter de ces répétitions pour introduire un nouveau type de codage inter-impulsion. Ce codage peut améliorer les performances et diminuer la complexité par rapport aux schémas de codage espace-temps plus classiques et qui sont

basés sur le codage inter-symbole. Nous proposons un schéma simple de codage ST qui profite à la fois de la diversité de multi-trajets et d'espace avec un débit qui est égale à 1 symbole par utilisation du canal pour n'importe quel nombre d'antennes de transmission et de réception. Quand le nombre de répétitions est plus grand que le nombre d'antennes de transmission, le même symbole d'information peut être transmis par les différentes antennes tandis que des séquences orthogonales attribuées aux impulsions de chaque symbole permettent d'introduire une orthogonalité entre les différents flux de données.

Des expressions explicites de la probabilité d'erreur conditionnelle sont données quand ce schéma de codage est utilisé avec les modulations PPM ou les modulations PPM plus polarité. Pour les modulations de polarité, une expression approximative de la probabilité d'erreur est donnée. Dans ce cas, la distribution statistique de la somme des variables aléatoires qui suivent une loi lognormale peut être approximée par une loi lognormale. Cette approximation permet d'intégrer la probabilité d'erreur conditionnelle et d'obtenir une expression explicite de la probabilité d'erreur.

Nous démontrons l'équivalence entre les critères de construction de codes ST sur un canal de Rayleigh et leur construction sur les canaux du standard IEEE 802.15.3a. D'une façon plus explicite, un gain en diversité plus élevé est équivalent à une variance plus faible pour la loi lognormale qui décrit la variation globale de l'énergie intégrée provenant des différents trajets de propagation entre émetteur et récepteur. De la même façon, le gain de codage est relié à la moyenne de cette distribution. Donc le canal multi-antenne codé par ce schéma de codage est équivalent à un canal mono-antenne ayant la même distribution mais avec une variance plus petite et une moyenne plus grande que chacun des sous canaux entre l'émetteur et le récepteur. La variance et la moyenne de cette distribution équivalente du canal à antennes multiples varient en fonction du produit entre le nombre d'antennes de transmission et le nombre d'antennes de réception, ce produit qui correspond au nombre total de canaux entre l'émetteur et le récepteur. Cette dépendance montre que les codes proposés profitent de la diversité maximale de transmission étant donné que la diversité maximale de réception est assurée par ces récepteurs cohérents.

Nous poursuivons ce chapitre par une caractérisation statistique des canaux IEEE 802.15.3a. En particulier pour les systèmes mono-antenne, l'énergie intégrée dans une fenêtre temporelle de n'importe quelle durée peut être approximée par une loi lognormale. De la même façon pour les canaux multi-antennes, la valeur maximale entre les valeurs propres de la matrice du canal peut aussi être approximée par une loi lognormale. Grâce à cette étude statistique, nous avons proposé des expressions approximatives du compromis diversité-multiplexage pour des canaux mono-antenne et des systèmes multi-antennes codés par le code ST de débit unitaire. De la même façon, nous proposons des bornes inférieures et supérieures des compromis diversité-multiplexage des canaux multi-antennes.

Cette étude montre que pour les canaux IEEE 802.15.3a, un gain de diversité infini peut être obtenu avec les systèmes mono-antennes et multi-antennes pour les valeurs asymptotiques du rapport signal-sur-bruit (RSB). Mais pour ces valeurs, les compromis varient comme le logarithme du RSB et pas linéairement avec le RSB comme dans le cas des canaux de Rayleigh. Par conséquent, le codage ST présente un avantage majeur pour les valeurs pratiques du RSB. En effet, étant donné cette variation logarithmique, le régime asymptotique correspondant à une diversité infinie est atteint pour des valeurs très élevées du RSB. Dans les systèmes pratiques, il est impossible d'atteindre ces RSB et il est toujours possible d'obtenir un gain de diversité pour les valeurs pratiques du RSB. Dans ce cas, les résultats montrent qu'il est beaucoup plus avantageux (en termes de performance et complexité) d'utiliser des systèmes multi-antennes avec des Rakes ayant un nombre limité de doigts que d'utiliser des systèmes mono-antennes avec des Rakes ayant un nombre très grand de doigts afin de combiner la totalité des multi-trajets. Ces améliorations de compromis diversité-multiplexage offertes par les techniques multi-

antennes sont importantes particulièrement pour les gains de multiplexage élevés.

Dans un deuxième temps, nous nous intéressons à l'Interférence Inter-Symboles (IIS) et à l'Interférence Multi-Utilisateurs (IMU). Nous proposons un modèle qui prend en compte ces interférences pour des systèmes synchrones et asynchrones. Ce modèle est ensuite utilisé pour analyser les performances des systèmes ULB multi-antennes en présence de ces interférences avec des récepteurs linéaires de type MMSE (Minimum Mean Square Error).

En se basant sur le modèle d'interférence, nous proposons une nouvelle technique qui peut être appliquée pour la réduction des niveaux d'IMU. Dans ce contexte, des études récentes montrent une réduction des niveaux d'IMU dans le cas où des séquences aléatoires d'étalement en amplitude sont associées aux séquences de sauts temporels. Nous étudions le problème d'IMU avec les systèmes mono-antenne et multi-antennes et nous proposons une méthode plus appropriée pour la génération de ces séquences.

L'analyse est basée sur une borne supérieure de la probabilité d'erreur qui correspond à la réduction de l'interférence entre deux utilisateurs en négligeant l'interférence des autres utilisateurs. Cette approche permet de proposer un critère simple pour la construction de ces matrices d'étalement. La propriété de l'inclusion est respectée par cette construction ce qui évite la mise à jour des matrices des différents utilisateurs chaque fois qu'un utilisateur accède ou sort du réseau. La construction d'une famille de matrices d'étalement qui respecte ce critère de construction est ensuite présentée. Cette technique de construction qui est inspirée des codes ST non-cohérents peut être appliquée avec n'importe quel nombre d'antennes de transmission. Les séquences d'étalement générées sont très courtes par rapport aux autres séquences appliquées dans les systèmes CDMA.

La dernière partie de ce chapitre est consacrée aux simulations sur les canaux IEEE 802.15.3a et sur des canaux multi-antennes issues d'une campagne de mesure que nous avons effectuée au CEA-LETI. Cette analyse numérique montre l'intérêt de l'association des techniques multi-antennes avec les systèmes ULB impulsifs. Pour un ordre de diversité donnée, la diversité spatiale peut apporter beaucoup plus que la diversité de multi-trajets en particulier pour les grandes valeurs de RSB. Limité par les réalisations pratiques des récepteurs, la diversité de multi-trajets peut être insuffisante même si la diversité du canal est très élevée.

Les campagnes de mesure montrent que la corrélation spatiale entre les réponses des sous-canaux est faible à cause de l'interaction limitée entre les différents multi-trajets ceci est du à la faible durée des impulsions. Dans ce contexte, les récepteurs à base de corrélations utilisant des filtres adaptés à la réponse entière du canal sont attractifs parce que l'interférence co-canal devient faible et des gains de multiplexage très élevés avec des bonnes performances peuvent être obtenus avec des récepteurs MMSE. D'autre part, les systèmes ayant des Rakes avec un nombre limité des doigts souffrent des niveaux non négligeables d'évanouissement. Même si cet évanouissement est moins sévère que dans les systèmes à bande étroite, il introduit des pertes non négligeables. Dans ce contexte, la diversité spatiale peut apporter des améliorations supplémentaires en termes de taux d'erreur binaire.

Finalement, une étude du bilan de liaison avec des impulsions respectant la masque du FCC montre les gains importantes en termes de l'extension de la portée des réseaux WPANs ULB en appliquant les techniques multi-antennes. Dans ce contexte, des débits de l'ordre de 100 Mbits/s à une distance de 10 m sont envisageables sur le modèle de canal IEEE CM2 avec six antennes à l'émission et à la réception. Dans les mêmes conditions le cas mono antenne permet seulement une portée de 1m. Les simulations prennent en compte les aspects pratiques des récepteurs ULB comme, par exemple, l'échantillonnage sur un bit et l'estimation non parfaite du canal.

## Construction des codes ST pour les systèmes multi-antennes ULB

Dans le troisième chapitre, nous considérons le problème de la construction des schémas de codage qui transmettent avec un débit maximal égal au nombre des antennes de transmission. Du fait de l'absence d'une fréquence porteuse, les flux de données codées transmis par les différentes antennes doivent être totalement réels. Limitant la communication dans la bande de base constitue une contrainte très forte du point de vue de construction des codes ST à débit maximale. Malgré cette contrainte, les transmissions impulsionales présentent un certain nombre de dégrées de libertés qui peuvent être exploités pour la construction des schémas de codage appropriés.

Le premier dégrée réside dans la possibilité de transmettre des formes impulsionales différentes. Le deuxième dégrée de liberté est lié à la transmission de chaque symbole d'information à l'aide de plusieurs impulsions. Enfin, les spécificités des modulations PPM et PPAM peuvent être exploitées pour la construction de schémas de codage adaptés.

Pour profiter du premier dégrée de liberté, nous proposons un nouveau schéma de diversité basé sur l'utilisation des impulsions de Hermite. Les formes des impulsions transmises par les différentes antennes sont constituées de fonctions d'Hermite d'ordres différents. D'une manière équivalente, les impulsions transmises par les différentes antennes sont orthogonales entre elles. Ce schéma s'applique sur un bloc contenant un nombre de symboles d'information égal au nombre des antennes de transmission. Dans un premier temps, une rotation réelle appropriée est appliquée entre les impulsions transmises dans chacune des positions PPM et correspondantes au bloc des symboles considérés. Cette rotation permet d'atteindre un ordre de diversité maximale. Dans un deuxième temps, les versions retournées des symboles sont transmis par les différents sous-espaces générés par les différentes formes d'ondes.

L'interférence intra-impulsion générée par la propagation dans des canaux très sélectifs en fréquence réduit le niveau d'orthogonalité entre les différents signaux reçus. Les simulations sur les canaux IEEE 802.15.3a montrent que l'association des impulsions d'Hermite avec de la diversité de modulation permet d'atteindre des niveaux de performance élevés avec une complexité de décodage qui est une fonction du nombre d'antennes de transmission. Un autre avantage est que les récepteurs linéaires simples peuvent atteindre des niveaux de performances plus élevés que dans le cas classique à cause de l'orthogonalité introduite par l'utilisation des impulsions de Hermite. Par exemple, un système avec trois antennes de transmission utilisant des impulsions de Hermite permet de transmettre trois fois plus rapidement qu'un système mono-antenne avec des meilleures performances en utilisant des décodeurs MMSE simples. Dans ce cas, les systèmes multi-antennes n'utilisant pas des impulsions de Hermite permettent d'atteindre des meilleures performances que les systèmes mono-antennes simplement avec des décodeurs non-linéaires basées sur le critère de maximum de vraisemblance.

Le désavantage est que le nombre des filtres adaptés nécessaires en réception augmente avec le nombre d'antennes à l'émission. Les simulations montrent que les performances de ce schéma de codage sont nettement meilleures que celles des systèmes multi-antennes non-codés associés à un récepteur utilisant un Rake avec  $P$  fois plus de doigts où  $P$  est le nombre d'antennes de transmission.

Les algèbres cycliques de division constituent le principal outil mathématique utilisé pour la construction des dernières familles de code ST qui transmettent à débit maximale et qui profitent d'un ordre de diversité maximale. Ces codes sont en général construits sur des corps infinis et ils sont associés aux modulations QAM, PAM ou PSK. La première approche adoptée dans ce chapitre pour la construction des codes ST à diversité maximale et débit maximal est basée sur les algèbres cycliques totalement réels considérés sur le corps des nombres entiers. Les codes proposés peuvent être associés avec n'importe

quelle modulation PAM, PPM ou PPAM. Avec ces constellations, cette première famille de codes permet d'atteindre un gain de codage qui ne diminue pas avec la taille de la constellation.

D'autre part, la contrainte d'avoir des mots de code totalement réels implique un désavantage sur les codes construits des algèbres cycliques de division totalement réels. Pour les systèmes équipés de plus de trois antennes de transmission, il est impossible de construire des mots de codes basés sur les algèbres cycliques de division et qui ont un niveau d'énergie moyen uniforme par antenne et par temps symbole. Dans ce cas, les codes proposés sont construits sur le sous-corps maximal du corps cyclotomique et le choix approprié d'une base permet de transmettre une constellation qui est une simple rotation de la constellation d'origine (avant codage). Pour les systèmes équipés avec deux antennes de transmission, nous montrons qu'il existe un compromis entre l'efficacité énergétique et l'efficacité de forme. Dans ce cas, nous proposons la construction des deux familles de codes. La première famille de codes est associée avec l'entier  $-1$  et permet de maximiser le gain de codage parmi tous les codes ayant un niveau d'énergie moyen. Par contre, ce code introduit des pertes de forme. La deuxième famille est associée avec l'entier  $2$  et le nombre d'or. La constellation transmise est une rotation de la constellation d'origine mais l'énergie n'est pas distribuée d'une façon uniforme entre les différents symboles d'information. Malgré le niveau de performance très élevé atteint par cette première famille de codes, elle reste moins performante que les codes parfaits et le gain de codage atteint par la nouvelle construction est une fraction du meilleur gain de codage connu et qui est atteint par les codes parfaits à mots de codes complexes.

Dans un deuxième temps, nous avons profité de la présence des répétitions des impulsions pour améliorer les performances de cette première famille de code en distribuant l'énergie disponible à la transmission d'une façon plus équilibré entre les différentes couches de chaque mot de code. Ce schéma de codage conjoint par symbole et par impulsion est obtenu en appliquant une permutation cyclique d'ordre  $P$  d'une façon périodique sur le bloc de  $P^2$  symboles avant d'appliquer les niveaux d'amplitude sur les différentes impulsions.

Nous proposons aussi une troisième famille de codes basée sur le codage inter-impulsion. Nous montrons que ce schéma de codage est l'extension optimale des codes construits à partir des algèbres cycliques de division. Cette extension est obtenue dans le cas où les différents flux de données peuvent être séparés coté réception à l'aide de plusieurs séquences orthogonales associées aux impulsions utilisées pour la transmission de chaque symbole d'information.

Par rapport au codage inter-symbole, le codage inter-impulsion présente l'avantage d'une complexité plus réduite avec des meilleures performances. En effet, la complexité de décodage optimal des deux premières familles de codes augmente avec  $P^2$ . Par contre, la complexité de décodage de la troisième famille de codes est une fonction de  $P$  (le nombre d'antennes à la transmission). En plus, le gain de codage est optimal est ne diminue pas avec la taille de la constellation. Le désavantage est que ce schéma de codage peut être appliqué simplement dans le cas où le nombre d'antenne de transmission est plus petit que le nombre d'impulsions transmises par symbole.

Dans la dernière partie de ce chapitre, nous introduisons la notion de codages spécifiques aux modulations. En particulier, nous présentons la construction de nouvelles familles de codes qui peuvent être associées avec les modulations PPM ou les modulations PPAM avec un nombre donné de positions de modulation. L'avantage par rapport aux codes construits à partir des algèbres cycliques de division est que l'efficacité énergétique peut être obtenue avec n'importe quel nombre d'antennes de transmission. En générale le gain de codage diminue avec le nombre de niveaux d'amplitude. Par contre, dans certains cas, le gain de codage est constant avec n'importe quel nombre de niveaux d'amplitude.

D'une façon plus explicite, nous présentons la construction des deux familles de codes. La première

famille est basée sur la permutation des impulsions où une simple permutation cyclique entre les impulsions permet d'atteindre un ordre de diversité maximal. Pour cette famille de codes, le nombre des positions de modulation pour lequel le code atteint la diversité maximale est une fonction croissante du nombre des antennes à l'émission. Plus précisément, pour les constellations  $M\text{-PPM-}M'\text{-PAM}$  avec  $P$  antennes de transmission, la première construction permet d'atteindre le niveau maximal de diversité de transmission pour toutes les valeurs de  $M'$  et pour  $M \geq 2P - 1$  ou pour les valeurs de  $M$  respectant  $\varphi(M) \geq P$  où  $\varphi(\cdot)$  est la fonction d'Euler.

La deuxième famille des codes spécifiques est basée sur la combinaison des impulsions. Dans ce cas, une extension additionnelle de la constellation non-codée permet d'atteindre la diversité maximale avec n'importe quel nombre d'antennes de transmission et pour toutes les constellations PPM ou PPAM ayant un nombre pair de positions de modulation. Comme la première famille de codes spécifiques, la deuxième construction permet de transmettre une énergie moyenne constante par antenne et par symbole. Cette famille de code est particulièrement intéressante avec les modulations PPM binaires. Dans ce cas, le gain de codage est le même que le gain de codage atteint avec les codes parfaits complexes pour n'importe quel nombre d'antennes de transmission.

Dans les cas où les deux familles permettent d'atteindre une diversité maximale, la première famille présente un niveau de performance légèrement plus élevé. Cette différence en performances est visible particulièrement avec les constellations ayant un grand nombre des niveaux de modulation d'amplitude.

D'une façon générale, les codes construits à partir des algèbres cycliques de divisions permettent d'atteindre un gain de codage ne s'évanouissant pas avec l'efficacité spectrale de la constellation transmise. Le désavantage est la perte de l'efficacité énergétique. D'autre part, les codes spécifiques permettent d'atteindre cette efficacité énergétique avec un gain de codage qui risque de diminuer avec le nombre des niveaux de modulation d'amplitude. Pour les canaux IEEE 802.15.3a, nous pouvons constater que l'efficacité énergétique est plus importante que le critère d'un gain de codage fixe pour les raisons suivantes :

- Sur le canal de Rayleigh, les codes ST ayant un gain de codage qui est indépendant de la taille de la constellation sont capables d'atteindre le compromis diversité-multiplexage du canal. Par contre, pour les canaux ULB, il n'y a pas une relation directe entre la contrainte d'un gain de codage constant et du compromis diversité-multiplexage atteint. En absence de cette relation, le critère d'avoir un gain de codage ne s'évanouissant pas avec la taille de la constellation devient moins important que l'efficacité énergétique.
- D'autre part, pour les constellations  $M\text{-PPM-}M'\text{-PAM}$ , l'efficacité spectrale peut être augmentée en augmentant la valeur de  $M$ . Contrairement à la réduction du gain de codage qui est associé à l'augmentation de la valeur de  $M'$ , l'augmentation du nombre des positions de modulation n'implique pas une réduction du gain de codage.

Les codes spécifiques sont intéressants parce que la structure des codes est indépendante du nombre des niveaux de modulation d'amplitude. Cette structure est simplement dépendante de la dimensionnalité de la constellation transmise (nombre d'antennes de transmission et le nombre des positions PPM). Dans plusieurs cas, les codes spécifiques totalement réels répondent aux mêmes critères de construction que les codes parfaits complexes et les niveaux des performances atteints sont très semblables. En plus, cette nouvelle famille de code est à mots de codes entièrement réels et, par conséquent, peut être associée aux transmissions ULB dans la bande de base.

Une analyse numérique effectuée sur des canaux réaliste montre que les performances des codes spécifiques sont meilleurs que celles des codes construits à partir des algèbres cycliques de division. D'une façon plus générale, les systèmes ULB pratiques sont associés avec des modulations PPM ou des modulations PPAM ayant un nombre limité de niveaux d'amplitude car les performances diminuent très rapidement lorsque l'ordre de modulation PAM augmente. Dans ce contexte, l'efficacité énergétique est plus importante que la propriété d'avoir un gain de codage ne s'évanouissant pas avec la taille de la constellation et les modulations spécifiques sont mieux adaptées à la nature impulsionale de la transmission.

## **Construction des codes ST distribués pour les systèmes coopératifs ULB**

Dans le quatrième chapitre, nous étudions les systèmes ULB coopératifs. Dans ce contexte, les terminaux radios coopèrent pour profiter de la diversité spatiale d'une façon distribuée. En particulier, considérons la communication entre une source et une destination. Dans le mode coopératif, des terminaux radio qui se trouvent dans le voisinage d'une source et de sa destination peuvent aider ces derniers à établir leur communication d'une façon plus fiable. Dans la suite nous considérons le cas des terminaux radios équipés d'une seule antenne et qui ne peuvent pas transmettre et recevoir en même temps.

Dans la suite, nous considérons les réseaux coopératifs où  $K$  relais peuvent aider la source à transmettre son message vers sa propre destination. Tous les schémas de coopération que nous considérons permettent d'atteindre un ordre de diversité spatiale égale à  $K + 1$ . En plus, cette diversité est atteinte en transmettant dans une fenêtre TDMA de la source uniquement. Pendant la phase de coopération, la source et ses  $K$  relais partagent la même séquence de sauts temporels.

Cette technique de coopération non-orthogonale est très intéressante. Étant donné que les relais transmettent dans la fenêtre TDMA de la source, ces relais peuvent se coopérer avec la source même dans le cas où ils ont leurs propres données à transmettre vers leurs destinations respectives. De la même façon, la source peut devenir un relai pendant la transmission d'un de ses voisins. En d'autres termes, l'application des stratégies de coopération non-orthogonales correspond à une meilleure utilisation des ressources du canal radio.

Dans un premier temps, nous considérons la stratégie de coopération basée sur la technique "Amplify-and-Forward" (AF) où chaque relai transmet une version amplifiée du signal qu'il a reçu antérieurement. Pour ces systèmes, la sélectivité en fréquence des canaux ULB implique des conséquences directes sur la structure du récepteur et des différents relais. Pour les relais, nous choisissons de combiner un certain nombre de multi-trajets avant la retransmission du signal. Cette solution permet de réduire d'une façon très significative l'interférence intra-symbole à la destination et évite l'implémentation des Rakes avec un nombre excessif de doigts.

D'autre part, les différences de temps de propagation associées aux canaux entre les différents relais et la destination peuvent être comparables avec la durée des impulsions ULB. Alors, étant donnée la grande résolution temporelle des impulsions ULB, il faut différencier les systèmes avec voie de retour des systèmes sans voie de retour entre la destination et chaque relai. Dans le premier cas, les différents temps de propagation sont compensés et les premiers trajets, correspondants aux canaux entre chaque relai et la destination, sont alignés à la destination. Dans le deuxième cas, le délai du premier doigt du Rake à la destination est égal au temps d'arrivée du premier trajet entre la source et la destination.

Des simulations sur des canaux ULB réalistes montrent que le retour entre la destination et les relais

permet d'améliorer les performances d'une façon très significative. Plus précisément, les canaux avec un trajet direct (les canaux CM1 de la recommandation IEEE 802.15.3a) sont plus sensibles à l'absence de synchronisation entre les différents relais et la destination. Dans ce cas, il n'est pas improbable de ne pas combiner le trajet direct et le plus court entre un relai et la destination. Pour ces canaux, la différence entre les niveaux des performances des systèmes avec ou sans voie de retour est plus manifeste. D'autre part, cette dégradation de performance devient moins visible pour les systèmes utilisant des Rakes avec un grand nombre de doigts.

Pour la stratégie AF, nous proposons la construction de quatre nouvelles familles de codes spatio-temporels distribués et adaptés aux systèmes ULB impulsionnels. Comme les codes ST proposés en chapitre 3, les codes ST distribués que nous proposons dans ce chapitre sont des codes à mots de codes totalement réels. Tous les codes que nous introduisons dans ce chapitre n'introduisent pas une réduction du débit binaire par rapport aux systèmes non coopératifs.

La première famille de codes est basée sur les algèbres cycliques de division. Cette famille de codes est basée sur le principe de codage inter-symbole. En d'autres termes, les amplitudes des différentes impulsions utilisées pour la transmission de chaque symbole d'information sont égales. D'une manière équivalente, cette famille de codes peut être associée même avec les systèmes ULB très haut débits n'appliquant aucune répétition d'impulsions. Cette famille de codes peut être appliquée avec n'importe quel nombre de relais et avec toutes les constellations PAM, PPM ou PPAM. Avec ces modulations, le gain de codage obtenu est indépendant de l'efficacité spectrale de la constellation transmise. Dans ce cas, la constellation transmise est une simple rotation de la constellation non codée.

Par contre, du fait de la contrainte des transmissions totalement réelles, l'énergie n'est pas distribuée d'une façon homogène entre les différents symboles d'information. Plus précisément, les mots de code sont composés des plusieurs couches où chaque couche contient un certain nombre des symboles d'information. Mais, ces couches ne sont pas protégées d'une façon égale contre le bruit et les erreurs de décision sur les symboles contenus dans les couches les moins protégées sont plus fréquentes. En d'autres termes, du fait de la contrainte des transmissions totalement réelles, ces codes sont moins performants que certains codes proposés pour les systèmes à bande étroite.

Cet inconvénient a orienté nos recherches vers une deuxième famille de codes qui profite de la présence de plusieurs impulsions pour introduire un codage conjoint des symboles et des impulsions. Dans ce contexte, le code basé sur les algèbres cycliques de divisions est appliqué périodiquement sur des versions permutees du flux de donnée source. Cette technique d'entrelacement permet de distribuer l'énergie disponible d'une façon plus équilibrée entre les symboles transmis par la source et les différents relais. Ce code à énergie moyenne uniforme par symbole d'information et par relai peut être appliqué si  $N_f > 1$  où  $N_f$  est le nombre d'impulsions utilisées pour la transmission d'un symbole d'information. Comme la première famille de codes, le gain de codage ne s'évanouit pas avec la taille de la constellation transmise. Pour ces deux familles de codes, le décodage doit être effectué dans un espace réel de dimension  $4K$ .

D'autre part, l'entrelacement introduit des gains importants en performances par rapport aux codes construits des algèbres cycliques de division. Par exemple, pour les faibles valeurs du rapport signal sur bruit, la première famille de codes introduit une perte en performances par rapport aux systèmes non-coopératifs. Etant donné que toutes les constructions proposées sont des constructions asymptotiques, le gain de diversité n'est pas visible pour ces RSB. D'autre part, le bruit additionnel introduit par les relais rend les décisions prises à la destination plus erronées. Par contre, pour ces mêmes intervalles de RSB, les performances de la deuxième famille de code sont nettement meilleures que celles des systèmes

non-coopératifs. Cette comparaison montre l'importance de l'équilibre énergétique dans la construction des codes ST distribués.

La troisième famille de code est basée sur le codage inter-impulsions où les impulsions utilisées pour la transmission de chaque symbole d'information sont encodées de façon indépendante des valeurs des impulsions utilisées pour la transmission d'un autre symbole. Cette famille de code présente l'avantage d'une complexité de décodage plus réduite car dans ce cas chaque mot de code contient  $2K$  symboles. Comme les deux premières familles de codes, le gain de codage ne s'évanouit pas avec la taille de la constellation transmise. En plus, le codage inter-impulsions peut être appliqué avec toutes les constellations PAM, PPM et PPAM. Par contre, cette famille de codes ne peut être appliquée que si le nombre d'impulsions par symbole est strictement plus grand que quatre fois le nombre de relais.

La deuxième et la troisième famille de codes profitent de la répétition des impulsions pour augmenter l'efficacité énergétique et améliorer les performances. La quatrième famille de codes que nous proposons permet d'atteindre cette efficacité énergétique même dans les systèmes ULB très haut débit où les répétitions des impulsions peuvent être absentes. Cette famille de codes est spécifique aux constellations multidimensionnelles PPM et PPAM. En d'autres termes, les trois premières familles de codes peuvent être associées avec n'importe quel sous ensemble de  $\mathbb{Z}^{4K}$  tandis que le gain en diversité de la quatrième code est atteint à cause de la structure particulière des constellations PPM et PPAM.

En particulier, considérons une constellation  $M\text{-PPM-}M'\text{-PAM}$ . La quatrième famille de code permet d'atteindre une diversité spatiale de l'ordre de  $K + 1$  pour  $M \geq 2$  et pour toutes les valeurs de  $M'$ . Pour les constellations ayant une dimensionnalité suffisamment grande (en particulier,  $M \geq 4K + 1$ ), le gain de codage est indépendant de la valeur de  $M'$ . Par rapport aux trois premières familles de codes, la quatrième famille présente l'avantage d'une bonne efficacité énergétique même en absence des répétitions des impulsions. Par contre, la quatrième famille ne peut pas être associée avec les modulations PAM.

Pour  $M > 2$ , la quatrième famille de codes est basée sur une permutation cyclique entre les positions nominales de modulation et par conséquent elle n'introduit aucune extension additionnelle de la constellation avec les modulations PPM et PPAM. Pour  $M = 2$ , cette construction introduit une permutation cyclique et un changement de polarité. Par conséquent, pour les constellations bidimensionnelles, cette famille de codes n'introduit aucune extension additionnelle de la constellation qu'avec les constellations PPAM.

Des résultats numériques sont donnés sur des canaux ULB 802.15.3a et sur les canaux obtenus à partir des techniques de “ray tracing”. Les résultats montrent l'importance de l'efficacité énergétique. La deuxième famille de codes permet d'atteindre les meilleurs niveaux de performance. La troisième famille de codes permet d'atteindre des niveaux de performance comparables avec une complexité réduite. Pour les constellations multidimensionnelles, le schéma de codage spécifique est meilleur que pour la première famille de codes et il permet de se rapprocher des performances de la deuxième famille de codes sans répétitions des impulsions.

Les simulations sur les canaux obtenus à partir des techniques de “ray tracing” montrent le gain énergétique additionnel obtenu par la coopération dans des réseaux sans fil de type “indoor”. Les résultats montrent aussi l'impact de la position de chaque relais sur les performances globales du système. Dans ce contexte, il est préférable de se coopérer avec les nœuds qui sont dans le voisinage de la source qu'avec les nœuds qui se trouvent dans le voisinage de la destination. D'autre part, le gain énergétique permet à la première famille de codes, basée sur le codage inter-symboles, d'avoir de meilleures performances que les systèmes non-coopératifs pour toutes les valeurs pratiques du RSB.

Dans un deuxième temps, nous considérons la stratégie de coopération basée sur la technique “Decode-

and-Forward” (DF). Dans ce cas, chaque relai peut décoder le flux de données qu’il reçoit et l’encoder avec un schéma de codage qui peut être potentiellement différent. Nous considérons les techniques DF avec les systèmes ULB cohérents, non cohérents et différentiels.

Le schéma cohérent est basé sur le codage conjoint des symboles et des impulsions et il peut être associé avec n’importe quel nombre de relais quand au moins deux impulsions sont utilisées pour la transmission de chaque symbole de l’information. Ce schéma est basé sur la diversité de modulation. Le décodage dans chaque relai est effectué symbole par symbole. Ce schéma de codage peut être appliqué avec toutes les constellations PAM, PPM et PPAM.

Le schéma de codage est périodique de période  $(K + 1)N_f$  impulsions où  $K$  est le nombre de relais et  $N_f$  est le nombre d’impulsions par symbole. Pendant la première moitié de la période de coopération, la source transmet  $K + 1$  symboles d’informations. Dans ce cas,  $N_f/2$  impulsions sont utilisées pour la transmission de chaque symbole (au lieu de  $N_f$  dans le cas non-coopératif). Pendant la deuxième moitié de la période de coopération, la source transmet des versions codées de ces  $K + 1$  symboles d’information. Le codage est basé sur l’association d’une séquence d’étalement d’amplitude avec la première ligne d’une matrice de rotation totalement réelle de dimensions  $(K + 1) \times (K + 1)$  et qui permet d’atteindre la diversité maximale de modulation.

Chaque relai reçoit les impulsions transmises pendant la première moitié de la période de coopération. Pendant la deuxième moitié de la période de coopération, tous les relais transmettent simultanément. Dans ce cas, chaque relai transmet une version codée de ses décisions concernant les  $K + 1$  symboles d’information. Le codage au  $k$ -ième relai est basé sur l’association d’une séquence d’étalement d’amplitude avec la  $(k + 1)$ -ième ligne de la matrice de rotation atteignant la diversité maximale de modulation. Les séquences d’étalements associés aux relais et à la source pendant la deuxième moitié de la période de coopération sont orthogonales.

Les études montrent que les performances sont très dépendantes de la façon avec laquelle l’énergie totale disponible est distribuée entre la source et ses relais. Les performances du système basculent entre deux cas extrêmes. Dans le premier cas, les niveaux de transmission des relais sont très élevés mais les décisions prises par les relais sont peu fiables. Dans le deuxième cas, des versions codées des décisions fiables des symboles d’information sont transmises par les relais avec un faible niveau d’énergie. Les performances optimales correspondent à un compromis entre ces deux cas et à une meilleure distribution énergétique entre la source et les relais d’une part et entre les deux moitiés de chaque période de coopération d’autre part. Ce compromis dépend des caractéristiques des différents canaux de propagation et du nombre de doigts de Rake utilisé à chaque relai.

Pour les systèmes différentiels et non cohérents, la diversité spatiale est atteinte par un codage inter impulsions. Ces deux systèmes ne nécessitent pas l’estimation du canal côté récepteur et sont mieux adaptés aux réseaux de capteurs simples à bas cout. Le nombre de relais toléré par ces schémas de codage est dépendant du nombre d’impulsions par symbole. En générale, le nombre de relais doit être plus petit que le nombre de répétitions des impulsions.

Les systèmes différentiels peuvent être associés avec toutes les modulations à module constant comme la modulation de polarité, les modulations PPM et les modulations bi-orthogonales PPM avec polarité. Dans ce cas, l’information est déterminée par la différence de phase et/ou le décalage temporel relatif entre deux impulsions consécutives. Coté réception, la comparaison des vecteurs de décision associées à des impulsions consécutives permet de déterminer l’amplitude et la position des symboles d’information. En d’autres termes, chaque impulsion constitue une référence pour la détection de l’impulsion suivante. Pour ces systèmes, les performances peuvent être améliorées en améliorant la

qualité du signal de référence. Dans ce cas, les systèmes avec retour de décision permettent d'améliorer les performances et de se rapprocher des performances des systèmes cohérents pour des valeurs suffisamment larges du rapport signal sur bruit.

Les systèmes non cohérents sont basés sur l'entrelacement des impulsions, utilisées pour la transmission de chaque symbole, entre la source et ses relais. Ces systèmes peuvent être associés avec des modulations PPM et le récepteur est basé sur l'intégration d'énergie. D'autre part, ce schéma non-cohérent ne nécessite pas une synchronisation très précise entre la source, la destination et les relais.

Les techniques DF sont associées avec du reliage sélectif. Dans ce cas, un relai participe à la communication entre une source et sa destination uniquement s'il est capable de décoder correctement un certain nombre de symboles d'apprentissage. Pour le reliage non sélectif, les performances sont détériorées par les décisions très erronées dans un certain nombre de relais. Dans ce cas, les gains de diversité des schémas DF ne sont visibles que aux valeurs très élevées et non réalisables du RSB. D'autres algorithmes de sélection de relais se basant sur les positions des différents nœuds sont aussi envisageables. Dans ce cas, le système proposé profite des potentiels de positionnement très élevés offerts par les systèmes ULB à cause de leur très haute résolution temporelle.

Des simulations sur des canaux réalistes montrent des gains importants en diversité. En plus du gain en diversité, des gains énergétiques importants sont obtenus. Ce dernier point présente un grand intérêt étant donné les très faibles niveaux de puissance tolérée en ULB. Les simulations montrent que l'association de la stratégie DF avec des modulations différentielles PPM non orthogonales et récepteurs avec retour de décision permet d'atteindre des débits très élevés avec des niveaux de performances importants et une complexité réduite. Dans ce cas, nous réalisons un débit important en utilisant des constellations PPM de grande efficacité spectrale. La durée de chaque symbole est maintenue constante en utilisant des modulations non-orthogonales. Les pertes en performances introduites par l'interférence entre les différentes positions PPM peuvent être remédiées avec l'implémentation d'un récepteur avec retour de décision.

## Décodage des constellations multidimensionnelles et non linéaires

Le dernier chapitre de cette thèse est consacré au problème du décodage des constellations multidimensionnelles PPM ou PPAM. Considérons une constellation  $M$ -PPM ou  $M$ -PPM- $M'$ -PAM. Ces constellations sont de dimension  $M$  et chaque symbole d'information est représenté par un vecteur de taille  $M$  dont uniquement une composante prend une valeur non nulle. D'autre part, les techniques de décodage par sphère permettent d'atteindre les performances des décodeurs optimaux à base de maximum de vraisemblance. Par contre, ces décodeurs peuvent être associés exclusivement avec des lattices des points ou avec des hyper cubes appartenant à ces lattices (par exemple, les constellations PAM ou QAM finies multidimensionnelles). Par conséquent, même si le code spatio-temporel appliqué est linéaire, la constellation multidimensionnelle transmise est non linéaire et les techniques de décodage par sphère ne peuvent pas être appliquées parce que les différentes composantes des vecteurs transmis ne sont pas indépendantes.

Considérons un système multi-antennes non codé avec  $P$  antennes de transmission associé avec une constellation  $M$ -PPM- $M'$ -PAM. Les vecteurs d'information sont de taille  $PM$  et sont composées de  $P$  sous vecteurs de taille  $M$  chacune et sont multiples entiers des colonnes de la matrice d'identité de taille  $M \times M$ . Par conséquent, le réseau d'antennes est composé de  $P$  sous réseaux ayant chacun  $M$  antennes

virtuelles parmi les quelles une seule antenne peut être active à un moment donné. Par contre, à cause de l’interférence co-canal et de la sélectivité en fréquence des canaux ULB, chaque antenne peut interférer avec les autres  $PM - 1$  antennes. D’autre part, l’hyper cube généré de dimension  $PM$  contient  $(M' + 1)^{MP}$  points parce que l’amplitude de l’impulsion dans chaque position peut prendre  $M'$  valeurs non nulles et une valeur nulle qui signifie l’absence du signal. Par contre, parmi ces points seulement  $(MM')^P$  points sont valables. Dans ce cas, la sortie d’un décodeur par sphère peut être égale à un point non valable qui n’appartient pas à la constellation transmise.

Les constellations 2-PPM-2-PAM constituent une exception. Dans ce cas, et même si les différentes composantes de chaque vecteur d’information ne sont pas indépendantes, une rotation adaptée rend ces composantes indépendantes. Dans ce cas, l’algorithme de décodage par sphère peut être appliqué sans modifications sur cette version tournée de la constellation. Dans un deuxième temps, une rotation inverse permet de déterminer la valeur du vecteur de l’information transmis.

Dans ce chapitre, nous proposons des modifications non triviales qui permettent l’association des techniques de décodage par sphère avec les sous ensembles finis et non linéaires correspondants aux modulations PPM ou PPAM. D’autre part, nous considérons l’adaptation des techniques de décodage sous optimales, tel que V-BLAST et l’algorithme de Fano, pour ces constellations. Pour les codes spatio-temporels linéaires avec  $P$  antennes et  $T$  symboles d’informations par mot de code,  $P$  doit être remplacé par la valeur  $PT$ .

Les décodeurs sous optimaux de type V-BLAST peuvent être directement appliqués avec les constellations  $M$ -PPM- $M'$ -PAM. Dans ce cas, les procédures d’annulation de l’interférence et de décision doivent être appliquées aux groupes composés des  $M$  colonnes consécutives de la matrice du canal et pas à chaque colonne comme avec les modulations PAM ou QAM. La même procédure est appliquée pour la détermination de l’ordre avec lequel les différents flux de données doivent être décodés.

Pour les techniques de décodage par sphère, nous adaptons les stratégies d’énumération de Pohst et de Schnorr-Euchner pour les constellations multidimensionnelles. Nous proposons trois algorithmes basés sur la stratégie de Pohst. Le premier algorithme est une solution triviale qui constitue la référence de temps pour comparer les différentes approches de décodage. Cet algorithme est aussi présenté pour démontrer que cette solution intuitive est largement sous-optimale motivant la proposition des nouvelles solutions ayant des temps de convergence nettement plus courts.

Dans ce cas, la validité de chacun de  $P$  sous vecteurs est testé d’une façon continue sur chacun de  $M$  niveaux de ce sous vecteur. Ce test assure qu’une partie composée de  $m$  composantes d’un sous vecteur ne contient plus qu’une valeur non-nulle et que cette partie contient exactement une seule valeur non nulle pour  $m = M$ . Dans le cas où la valeur testée à un certain niveau d’un sous vecteur n’est pas valable, un noeud adjacent sur le niveau considéré est testé.

Le deuxième algorithme est basé sur le principe suivant. Pour un certain niveau, l’intervalle de validité (correspondant aux points appartenant à la sphère considérée) est adapté d’une façon continue en fonction des points testés aux autres niveaux. En d’autres termes, si la valeur testée correspondante à un certain niveau est différente de zéro, les autres composantes (avec des indices plus petits) correspondantes aux premières positions nominales de modulations du même sous vecteur sont forcées de prendre la valeur zéro indépendamment des intervalles de validité à ces niveaux. Cette solution consiste à forcer l’algorithme à tester uniquement les points valables. Il évite de calculer et de parcourir plusieurs intervalles de validité correspondants aux plusieurs niveaux.

Le troisième algorithme consiste à déterminer d’une façon conjointe l’intervalle de validité à chaque niveau en prenant en compte que dans ce cas, les autres niveaux appartenant au même sous vecteur

doivent prendre des valeurs nulles. En d'autres termes, les équations de test d'appartenance à la sphère sont groupées et résolues conjointement après chaque  $M$  niveaux. Dans ce cas, si  $PM$  correspond à la taille du vecteur de l'information, algorithme 3 consiste à résoudre  $P$  groupes de  $M$  équations au lieu de résoudre les  $PM$  équations consécutivement l'une après l'autre. Cette solution conjointe est rendue possible grâce à la structure des symboles PPM ou PPAM transmises.

Une analyse numérique montre que le troisième algorithme présente le meilleur temps de convergence. Par exemple, pour les systèmes MIMO  $2 \times 2$  non-codés avec un rapport du signal sur bruit de 20 dB, algorithme 3 converge 10 fois plus rapidement que algorithme 0 avec les constellations ayant 16 dimensions avec 8 niveaux d'amplitude dans chaque dimension. Par rapport au premier et deuxième algorithme, le gain en termes de temps de convergence augmente avec les valeurs de  $M$  et  $M'$ . Dans ce dernier cas, le pourcentage des points valables dans la lattice considérée devient très faible et les deux premiers algorithmes vont tester beaucoup des points non valables avant la convergence vers le point valable le plus proche.

La seconde approche consiste à adapter l'énumération de Schnorr-Euchner aux modulations PPM et PPAM. Dans ce cas, le temps de convergence de l'algorithme de décodage peut être amélioré si l'ordre avec lequel les points appartenant à l'intervalle de validité, déterminé à chaque niveau du vecteur testé, est déterminé d'une façon efficace. La technique d'énumération de Schnorr-Euchner consiste de tester ces points dans l'ordre croissant de la distance Euclidienne (par rapport au point reçu). Cette technique peut être appliquée d'une façon efficace avec les modulations PAM ou QAM. Dans ce chapitre, nous appliquons le même principe avec une façon plus adaptée aux modulations PPM et PPAM.

Pour les modulations  $M$ -PPM, chacun de  $P$  sous vecteurs peut prendre  $M$  valeurs possibles. Nous proposons une méthode simple pour arranger ces valeurs par ordre croissant de distance Euclidienne. Dans ce cas, l'énumération de Schnorr-Euchner est remplacée par une autre technique d'énumération qui prend en compte la structure des constellations PPM. Pour les modulations  $M$ -PPM- $M'$ -PAM, nous proposons un algorithme simple qui permet de parcourir les  $MM'$  points valables sur chacun de  $P$  niveaux d'une façon itérative par ordre croissant de distance Euclidienne. L'algorithme détermine d'une façon efficace si le prochain test doit être appliqué sur le même niveau ou si l'algorithme doit tester un point appartenant à un niveau différent et qui appartient au même sous vecteur. La complexité de cette solution n'augmente pas avec  $M'$ . Par contre, elle augmente avec  $M$  simplement parce que les opérations matricielles sont appliquées à des matrices d'ordres plus élevés. Ces algorithmes associés aux modulations PPM et PPAM possèdent les meilleurs temps de convergence parmi toutes les autres versions modifiées des décodeurs par sphère.

Finalement, l'algorithme de Fano est adaptées aux constellations PPM et PPAM permettant d'atteindre plusieurs niveaux de compromis entre performance et complexité. Ce variant des algorithmes de décodage par sphère introduit une fonction de cout additionnelle qui dépend de la variance du bruit et des normes des valeurs propres de la matrice de Gramm associée à la matrice du canal. Cette technique permet de réduire la complexité de décodage en réduisant le nombre des points testés. Cette solution introduit des pertes en performances tout en gardant le même niveau de diversité.

Pour toutes les algorithmes proposés, et comme les techniques de décodage par sphère classiques, la complexité est indépendante de  $M'$ . Elle dépend uniquement de  $P$  et  $M$  qui déterminent la dimensionnalité de la constellation. En d'autres termes, ils sont adaptés aux systèmes très hauts débits ayant une grande efficacité spectrale.



# List of Figures

1.1	Structure of a TH-UWB signal. . . . .	5
1.2	TH-UWB signal with polarity randomization. $N_f = 4$ , $N_c = 3$ , $T_g = 0$ , $\delta = T_w$ and the TH sequence is $\{1, 0, 2, 1\}$ . The polarity randomization is given by $\{1, -1, 1, -1\}$ . A 4-PPM-4-PAM constellation is used. The 16 information symbols are mapped onto the amplitude ( $a$ ) and the position ( $p$ ) of the pulses. The pulses represented by solid and dashed lines correspond to $(a, p) = (1, 0)$ and $(a, p) = (-3, 2)$ respectively. . . . .	6
1.3	The NAF protocol with $K$ relays. . . . .	25
2.1	Schematic representation of a MIMO-UWB SRake receiver. . . . .	38
2.2	Bounds on the performance of single antenna systems and of the $(4 \times 1)$ orthogonal code over the IEEE 802.15.3a CM2 channel model. . . . .	43
2.3	Exact and approximated CDF of the energy integrated in a duration of $T_i$ over CM2. $\Gamma$ corresponds to the maximum channel delay spread. . . . .	46
2.4	PDF of $\alpha_{max}$ over CM2. Solid and dashed lines correspond to the simulated distributions and their lognormal approximations respectively. . . . .	46
2.5	D-MG tradeoffs over CM1 at a SNR of 15 dB and 30 dB with $T_i = 5$ ns. . . . .	51
2.6	D-MG tradeoffs over CM4 at a SNR of 20 dB. . . . .	51
2.7	Performance of spatial multiplexing over CM2 with 4-PPM-2-PAM, correlation receivers and MMSE detectors. . . . .	58
2.8	Performance of the rate-1 coded system over the measured channels with 2-PAM for different numbers of Rake fingers. . . . .	58
2.9	The achieved data rate vs. the communications distance at a SER of $10^{-3}$ with 4-PPM-2-PAM, MMSE detectors and a 3-finger PRake. . . . .	60
3.1	The orthogonality induced by the use of modified Hermite pulses over CM1. . . . .	62
3.2	A schematic representation of error-balancing with 3 transmit antennas. . . . .	68
3.3	The coding gain $d_M(\gamma)$ of $C_{2,rot}(\gamma)$ in eq. (3.19) for $M = 2, 4, 8, 16$ . . . . .	71
3.4	The coding gain of ISC with 3 transmit antennas and 2-PAM. . . . .	71
3.5	Performance on CM2 with PAM constellations at a rate of 4 bits PCU. . . . .	83
3.6	Performance on CM2 with 2 transmit antennas, 2 receive antennas and a PRake with 6 fingers. . . . .	83
3.7	Performance of $3 \times 3$ systems over CM3 and CM4 with 2-PAM and a 1-finger PRake. . . .	85
3.8	Performance of $5 \times 5$ systems over CM1 and CM2 with 2-PAM and a 1-finger PRake. . . .	85

3.9	Performance on CM2 with 6 transmit antennas, 6 receive antennas and a 1-finger PRake at 6 bits PCU. . . . .	86
3.10	Performance on CM2 with 8-PPM-8-PAM, $P = 3$ , $Q = 1$ and $L = 8$ using ML and MMSE receivers. . . . .	87
3.11	Performance on CM1 with 2-PPM-2-PAM and a 1-finger Rake. . . . .	87
3.12	ISC versus construction 1 (STC1) on CM2. . . . .	88
3.13	ISC versus construction 2 on CM2 with 2-PPM and $L = 1$ . . . . .	88
3.14	ISC versus construction 2 on the Kunisch-Pamp channel model (profile 3) using 4-PPM, $P = 3$ , $Q = 1$ and $L = 5$ . $d$ corresponds to the inter-antenna separation. . . . .	89
3.15	The new modulation-specific codes (NC) versus the perfect codes (PC) on CM2. . . . .	89
3.16	Construction 1 versus construction 2 with 3 transmit antennas, 3 receive antenna and 6-PPM- $M'$ -PAM constellations over CM2. A 1-finger PRake is used. . . . .	90
3.17	Performance with $P = Q = 2$ , 2-PAM and 5 fingers PRake with $K$ interfering users in a synchronous environment. The dotted lines associated with each curve correspond to the Gaussian approximation. . . . .	92
3.18	Performance of IPC in the presence of MUI with $P = Q = 2$ and 7 fingers PRake in an asynchronous environment at 25 dB. . . . .	92
4.1	Performance on CM2 with one relay, 2-PAM and a 5-finger PRake. . . . .	109
4.2	Performance on CM2 with 2-PAM and a 5-finger PRake using 2 and 4 relays. . . . .	110
4.3	Performance on CM2 with 2-PAM and a 1-finger PRake using 3 and 5 relays. . . . .	110
4.4	The modulation-specific PPM-PAM code versus ISC and balanced-ISC over CM2. . . . .	112
4.5	The modulation-specific code (MSC) versus ISC with one relay and 2-PPM- $M'$ -PAM constellations over CM1. A 5-finger PRake is used. . . . .	112
4.6	Impact of the synchronization errors over CM2. 4-PAM constellations are used and the receiver is equipped with a 8-finger PRake. . . . .	113
4.7	Performance with 2-PAM and a 5-finger PRake. $\epsilon = 0$ corresponds to perfect feedback while $\epsilon \neq 0$ corresponds to no feedback. . . . .	113
4.8	Map of the studied environment. . . . .	115
4.9	Performance in the studied environment with 4-PAM, 4-fingers PRake and 2 relays. The relays can occupy any position in rooms (A), (B) and (C) and they participate in the communication between REF <sub>2</sub> and REF <sub>4</sub> . . . . .	115
4.10	Fixed-Relaying versus Selective-Relaying on CM2 with coherent systems, 2-PAM and a 5-finger PRake using 1, 2 and 3 relays. . . . .	117
4.11	The impact of the energy distribution among the two halves of the cooperation period. Coherent systems are used with 1 relay, 2-PAM and a 4-finger PRake. . . . .	117
4.12	Performance of non-coherent systems on CM2 with 4-PPM and a 5-finger PRake using 1 and 2 relays. . . . .	118
4.13	Performance of decision-feedback differential systems on CM2 with 4-PPM-2-PAM and a 10-finger PRake using 1 relay. . . . .	118
5.1	The 3-PPM-4-PAM constellation (in filled circles). The stars corresponds to a {4-PAM} <sup>3</sup> constellation. . . . .	121

5.2	Solid and dashed lines correspond to algorithm 1 and algorithm 2 respectively. 2 transmit antennas, 2 receive antennas and a 1-finger PRake are used. . . . .	126
5.3	The Schnorr-Euchner enumeration with a 1-dimensional 4-PAM constellation. The black points correspond to the 4-PAM amplitude levels ( $\{\pm 1, \pm 3\}$ ) while the gray points correspond to the infinite extension of the 4-PAM (the set of odd integers). Dashed lines are used each time the enumeration results in a point that falls outside the boundaries of the 4-PAM constellation. The plotted parabola corresponds to the squared Euclidean distance between the received point and the visited lattice point. . . . .	128
5.4	The enumeration with a 2-dimensional 2-PPM-4-PAM constellation. This enumeration must be performed jointly between the points of the x-axis and the y-axis that correspond to the two modulation positions. . . . .	131
5.5	Convergence of SE with respect to algorithm 2 with a 1-finger PRake on CM2. . . . .	134
5.6	Performance of spatial multiplexing with 5 transmit antennas, 5 receive antennas and a 1-finger PRake on CM2. A 4-PPM-4-PAM constellation is used. . . . .	136
5.7	Complexity of the decoding algorithms with 4-PPM-4-PAM, 5 transmit antennas, 5 receive antennas and a 1-finger PRake on CM2. Spatial multiplexing is used. . . . .	136
5.8	Performance of the diversity scheme using modified Hermite pulses on CM2. A 4-PPM-4-PAM constellation is used with 5 transmit antennas, 5 receive antennas and a 1-finger PRake. . . . .	137
5.9	Complexity of the decoding algorithms with 4-PPM-4-PAM, 5 transmit antennas, 5 receive antennas and a 1-finger PRake on CM2. The diversity scheme using modified Hermite pulses is applied. . . . .	137
A.1	Map of the explored environment. . . . .	141
A.2	Fading margin over a 4-element linear antenna array of length 25.5 cm. . . . .	143
A.3	Spatial correlation among the channels received by two antennas separated by 8.5 cm and 25.5 cm respectively. . . . .	143
A.4	Spatial correlation among the signals at the output of a Rake receiver. . . . .	144
B.1	The different integration areas. . . . .	147



# List of Acronyms

- AWGN : Additive White Gaussian Noise
- MIMO : Multiple Input Multiple Output
- SISO : Single Input Single Output
- ST : Space-Time
- STBC : Space-Time Block Code
- IR : Impulse Radio
- UWB : Ultra Wide-Band
- TH : Time Hopping
- DSSS : Direct Sequence Spread Spectrum
- CDMA : Code Division Multiple Access
- TDMA : Time Division Multiple Access
- OFDM : Orthogonal Frequency Division Multiplexing
- WPAN : Wireless Personal Area Networks
- FCC : Federal Communications Commission
- RF : Radio Frequency
- FFT : Fast Fourier Transform
- QAM : Quadrature Amplitude Modulation
- PPM : Pulse Position Modulation
- PAM : Pulse Amplitude Modulation
- PPAM : Pulse Position Amplitude Modulation
- BPSK : Binary Phase Shift Keying
- BER : Bit Error Rate

- SER : Symbol Error Rate
- PEP : Pairwise Error Probability
- SNR : Signal to Noise Ratio
- LOS : Line Of Sight
- NLOS : Non-Line Of Sight
- AOA : Angle Of Arrival
- CSI : Channel State Information
- TAST : Threaded Algebraic Space Time
- ISC : Inter Symbol Coding
- IPC : Inter Pulse Coding
- ISI : Inter Symbol Interference
- MUI : Multi-User Interference
- PRake : Partial-Rake
- SRake : Selective-Rake
- ARake : All-Rake
- D-MG : Diversity-Multiplexing Gain
- PCU : Per Channel Use
- MRC : Maximum Ratio Combining
- EGC : Equal Gain Combining
- MMSE : Minimum Mean Square Error
- ML : Maximum Likelihood
- CDA : Cyclic Division Algebra
- SD : Sphere Decoder

# List of Notations

- $i = \sqrt{-1}$
- $\mathbb{N}$  : the set of natural integers
- $\mathbb{Z}$  : the ring of integers
- $\mathbb{Q}$  : the field of rational numbers
- $*$  : convolution
- $\otimes$  : Kronecker product
- $\delta(\cdot)$  : Dirac function
- $\varphi(\cdot)$  : Euler's totient function
- $X^T$  : the transpose of matrix  $X$
- $\text{rank}(X)$  : the rank of matrix  $X$
- $\det(X)$  : the determinant of matrix  $X$
- $\text{trace}(X)$  : the trace of matrix  $X$
- $\text{maxdiag}(X)$  : the maximum diagonal element of matrix  $X$
- $I_n$  : the  $n \times n$  identity matrix
- $e_m$  : the  $m$ -th column of the  $I_n$
- $1_{m \times n}$  : the  $m \times n$  matrix whose entries are all equal to 1
- $\mathbf{0}_{m \times n}$  : the  $m \times n$  matrix whose entries are all equal to 0
- $\mathbf{0}_m$  : the  $m$ -dimensional vector whose entries are all equal to 0
- $\|x\|$  : the Euclidean norm of vector  $x$
- $\mathcal{N}(\mu, \sigma^2)$  a Gaussian random variable with mean  $\mu$  and variance  $\sigma^2$
- $N_{\mathbb{K}/\mathbb{Q}}(x)$  : the algebraic norm of an element  $x$  in the field extension  $\mathbb{K}/\mathbb{Q}$
- $\text{Tr}_{\mathbb{K}/\mathbb{Q}}(x)$  : the algebraic trace of an element  $x$  in the field extension  $\mathbb{K}/\mathbb{Q}$

- $d_{\mathbb{K}}$  : the discriminant of the field  $\mathbb{K}$
- $\text{diag}(X_1, \dots, X_n)$  : places the matrices  $X_1, \dots, X_n$  on the principal diagonal
- $\text{vec}(X)$  : stacks the columns of the matrix  $X$  in a single vector
- $\Im(x)$  : the imaginary part of the complex number  $x$
- $\Re(x)$  : the real part of the complex number  $x$
- $x^*$  : the complex conjugate of  $x$

# Chapter 1

## Introduction

### 1.1 Ultra-Wideband communications

#### 1.1.1 Introduction

During the last years, the research community has developed a number of promising solutions for the fourth-generation (4G) wireless networks. Among the solutions that promise significant improvements in system performance we can mention adaptative coding and modulation, iterative (turbo) decoding algorithms, space-time coding, multi-antenna techniques, multi-carrier modulation, multi-user detection and ultra-wideband (UWB) radio. In particular, UWB is a fast emerging technology with uniquely attractive features inviting major advances in wireless communications, networking, radar, imaging, and positioning systems.

The history of UWB is as old as that of radio itself. In fact, the very first wireless transmission, via the Marconi Spark Gap Emitter, was essentially an UWB signal. Despite this, UWB is always referred to as unconventional radio. Early works on UWB systems showed their interest in radar and military applications. The modern era in UWB started in 1993 when Robert Scholtz wrote a landmark paper that presented a multiple access technique for UWB communication systems [1]. With a variable multiple access scheme, UWB became capable of supporting not only radar and point-to-point communications but wireless networks as well. Another important landmark has been the publication in 2002 of the Federal Communications Commission (FCC) Order and Report regulating the use of UWB systems in the USA [2]. Very low transmission levels in the order of -41.25 dBm/MHz were allowed in the bandwidth [3.1 10.6] GHz. This resulted in growing research activities in the industry, academic institutions and government agencies.

The adoption of the FCC regulations provoked different technological solutions all capable of meeting the FCC emission mask. In particular, we can differentiate between multi-carrier (MC) and impulse radio (IR) solutions.

The MC-UWB solution is based on the Orthogonal Frequency Division Multiplexing (OFDM) technique using multiple simultaneous carriers. In this approach, the UWB spectrum is divided into a number of sub-bands of 528 MHz each. Each sub-band comprises 128 carriers modulated using QPSK on OFDM tones. OFDM is suitable for high data rate. It is used in Asymmetrical Digital Subscriber Line (ADSL) services, power line networking (HomePlug), IEEE 802.11n (high speed 802.11) and IEEE 802.20 (MAN). OFDM is a mature technology and it is well suited for avoiding interference. At the expense of an additional layer of control in the physical layer, the carriers can be chosen to avoid inter-

ference to (and from) narrow-band systems. However, high speed FFT processing is required and the continuous variation in the power over a very wide bandwidth is challenging for the circuits (especially for the power amplifiers).

Unlike classical communications, IR-UWB does not use a modulated sinusoidal carrier to convey information. Instead, the transmitted signal is a series of short-duration baseband pulses. This results in simple and cheap digital circuits. On the other hand, highly precise synchronization is required.

The relative advantages and disadvantages of IR-UWB and MC-UWB are controversial issues and have been debated extensively in the standardization bodies. In January 2006, this debate resulted in disbanding the IEEE 802.15.3 task-group created three years earlier to define a standard for short-range and high data rate (up to 480 Mbits/s) wireless communications. On the other hand, the IEEE 802.15.4 task-group adopted IR-UWB for low data rate sensor networks.

This work focuses on IR-UWB. While the multi-antenna IR-UWB is a new topic, much information on OFDM (single-antenna and multi-antenna cases) is available in the recent technical research. IR-UWB has a number of appealing advantages:

- The very large bandwidth could potentially offer rates in the order of Gbits/s.
- Low-complexity and low-cost radio terminals. This arises essentially from the baseband nature of the transmitted signal. In conventional radio systems, a radio frequency (RF) mixing stage is necessary to translate the baseband signal to a frequency that has desirable propagation properties. In IR-UWB, the generated short pulses occupy a bandwidth that spans frequencies commonly used as carrier frequencies. In other words, these pulses can propagate without the need of additional up-conversion. At the receiver side, local oscillators can be omitted and the reverse down conversion process is not required.
- The fine temporal resolution results in very precise localization capabilities.
- Immunity against multi-path fading. Due to the narrow temporal pulses, the interaction between multi-path components is severely limited as compared to narrow-band signals.
- The noise-like signals allow coexistence, low probability of interception and resistance to jamming.

### 1.1.2 Waveforms

Perhaps the most famous pulse shapes used in UWB communications are the Gaussian waveform and its derivatives. The very short pulses occupy a very large bandwidth. In general, the frequency responses of the RF circuitry and antennas are not flat over these frequency ranges. In all that follows,  $w(t)$  is used to designate the pulse observed at the destination. In other words, all distortions (if any) introduced by the RF components, transmit antennas and receive antennas are included in  $w(t)$ .

Designate by  $B$  the -10 dB bandwidth occupied by  $w(t)$  and denote by  $f_0$  the center frequency of this band. A Gaussian pulse occupying a bandwidth  $B$  can be expressed as [3]:

$$w(t) = \sqrt{\pi\alpha} \frac{\beta}{2} \cos(2\pi f_0 t) e^{(-\pi\alpha\frac{\beta}{2}t^2)} \quad (1.1)$$

where  $\alpha = 0.93$  is a normalization factor that is introduced since the bandwidth is defined at the -10 dB points.

Another popular waveforms in the literature of UWB are the modified Hermite pulses. These pulses are known for their orthogonality properties and were used to achieve high data rates in single-antenna systems by transmitting several pulses during the same modulation position [4, 5].

The modified Hermite polynomial of order  $p$  can be expressed as [4]:

$$w_p(t) = (-1)^p \exp\left(\frac{t^2}{4\Gamma_p}\right) \frac{d^p}{dt^p} \left( \exp\left(-\frac{t^2}{2\Gamma_p}\right) \right) \quad (1.2)$$

where  $\Gamma_p$  regulates the width of the  $p$ -th order pulse. Multiplying eq. (1.2) by a sinusoidal waveform along with an appropriate choice of  $\Gamma_p$  [5] results in pulses respecting the FCC mask [2]. For a given center frequency and bandwidth, the best value of  $\Gamma_p$  that fits the FCC mask can be only obtained by computer simulations.

### 1.1.3 Modulation Schemes

In this section, we provide a brief review of the modulation schemes that are associated with IR-UWB. Since IR-UWB is a carrier-less technology, it can be associated uniquely with totally-real modulations.

#### Pulse Amplitude Modulation

In  $M'$ -ary Pulse Amplitude Modulations (PAM), the amplitude of each transmitted pulse can take one of  $M'$  possible values. In this case,  $\log_2(M')$  information bits are mapped onto these  $M'$  amplitudes. The transmitted signal set can be expressed as:

$$\mathcal{S}_{M'-\text{PAM}} = \{(2m' - 1 - M')w(t) ; m' = 1, \dots, M'\} \quad (1.3)$$

where  $w(t)$  is the pulse waveform.

Each signal in  $\mathcal{S}_{M'-\text{PAM}}$  can be represented by a unique point in a 1-dimensional signal space. In this signal space, the  $M'$ -ary PAM signal constellation is the set of points whose coordinates belong to the set:

$$\mathcal{C}_{M'-\text{PAM}} = \{(2m' - 1 - M') ; m' = 1, \dots, M'\} \quad (1.4)$$

PAM is a good candidate for IR-UWB [6]. In most cases, IR-UWB systems were associated with 2-PAM. However, high data rate systems must use modulations of higher orders (larger values of  $M'$ ) even though this choice results in performance losses [7].

#### Pulse Position Modulation

While Pulse Position Modulation (PPM) is a classical modulation for optical communications, it remains untraditional for wireless communications. The interest in PPM increased with IR-UWB that has a very fine time resolution [8]. In  $M$ -ary PPM, information is conveyed by the temporal shift of a pulse. The transmitted signal set is given by:

$$\mathcal{S}_{M-\text{PPM}} = \{w(t - \tau_m) ; m = 0, \dots, M - 1\} \quad (1.5)$$

In this case, the  $m$ -th information symbol corresponds to shifting the position of  $w(t)$  by  $\tau_m$  for  $m = 0, \dots, M - 1$ . A linear and non-overlapping PPM constellation corresponds to the choice  $\tau_m = m\delta$  where  $\delta$  is the nominal modulation delay.

The signals of  $S_{M\text{-PPM}}$  are orthogonal to each other. They can be represented in a  $M$ -dimensional signal space. In this space, the  $M$ -PPM constellation is defined by the set:

$$\mathcal{C}_{M\text{-PPM}} = \{e_{m+1} ; m = 0, \dots, M-1\} \quad (1.6)$$

where  $e_m$  is the  $m$ -th column of the  $M \times M$  identity matrix  $I_M$ . In other words, each point of the constellation is defined by a  $M$ -dimensional vector having  $M - 1$  zero components and exactly one component that equals to 1 and that corresponds to the position of the transmitted pulse. Unlike PAM, the performance of PPM is enhanced by increasing the cardinality of the constellation [7].

### Pulse Position Amplitude Modulation

In hybrid  $M$ -ary PPM and  $M'$ -ary PAM constellations, the information is mapped onto both the amplitudes and the positions of the transmitted pulses. The signal set is composed of  $MM'$  signals and is given by:

$$\mathcal{S}_{M\text{-PPM}-M'\text{-PAM}} = \{(2m' - 1 - M')w(t - \tau_m) ; m' = 1, \dots, M' ; m = 0, \dots, M-1\} \quad (1.7)$$

The special case of  $M' = 2$  corresponds to the bi-orthogonal constellations that have been considered with UWB systems [9, 10]. Recently, hybrid PPAM constellations with higher values of  $M'$  were considered in [11]. It was shown that these constellations offer a good compromise between performance and complexity. In fact, for  $M'$ -PAM increasing the value of  $M'$  does not increase the complexity of the receiver (the constellation always has one dimension). However, this increase in the data rate is associated with performance losses [7]. On the other hand, the performance of  $M$ -PPM is enhanced by increasing  $M$  at the expense of an increased receiver complexity.

The  $MM'$  information symbols can be represented by  $M$ -dimensional vectors that belong to the signal set:

$$\mathcal{C}_{M\text{-PPM}-M'\text{-PAM}} = \{(2m' - 1 - M')e_{m+1} ; m' = 1 \dots M' ; m = 0 \dots M-1\} \quad (1.8)$$

Among the  $M$  components of each element of eq. (1.8), only one value can be different from zero. Note that PPM and PAM follow as special cases of PPAM.

#### 1.1.4 Time Hopping UWB

Different users sharing the same physical channel interfere with each other. In order to limit the effect of this harmful interference, different multiple access techniques were considered in IR-UWB. Among these techniques, we can cite the time hopping (TH) and the direct sequence (DS) spread spectrum. UWB systems are inherently spread spectrum systems. The use of spreading codes is solely for accommodating multiple users.

In DS-UWB, pulses are transmitted continuously. For a given information symbol, the amplitudes of these pulses are determined from a spreading sequence. In TH-UWB, a pseudo-random sequence determines the positions of the transmitted pulses. TH is an interference avoidance strategy while direct sequence (DS) is an interference suppression technique. In general, DS-UWB is associated with PAM [12]. However, recently DS-UWB was used for multiple access with PPM [13].

In TH-UWB systems, an additional pseudo-random temporal shift avoids the catastrophic collision between the pulses transmitted by the different users. In this case, each information symbol is conveyed by  $N_f$  consecutive pulses. These pulse repetitions are introduced for the following reasons:

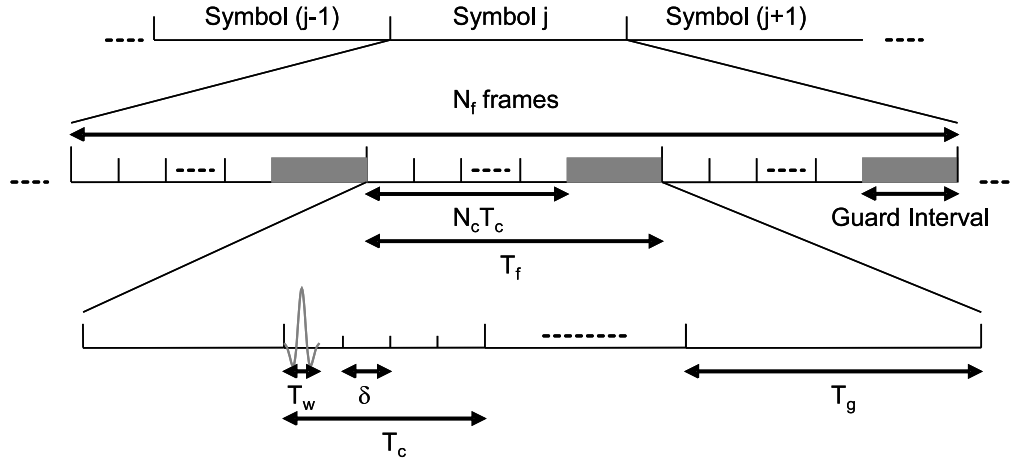


Figure 1.1: Structure of a TH-UWB signal.

- In order to avoid interference in cases where the channel is not shared in a TDMA manner.
- Given the very low transmission levels imposed by the regulatory organizations [2], these repetitions enhance the energy capture at the receiver side.

For TH systems, the signal transmitted from the  $k$ -th user can be expressed as [1, 14]:

$$s^{(k)}(t) = \sqrt{\frac{E_s \mathcal{E}_k}{N_f}} \sum_{j=-\infty}^{\infty} a_j^{(k)} \sum_{n=0}^{N_f-1} b_{j,n}^{(k)} w(t - jT_s - nT_f - c_{j,n}^{(k)} T_c - d_j^{(k)} \delta) \quad (1.9)$$

where:

- $w(t)$  is the pulse waveform of duration  $T_w$ . It normalized to have a unit energy:  $\int_0^{T_w} |w(t)|^2 dt = 1$ .
- $\mathcal{E}_k$  is the transmission level of the  $k$ -th user. It is determined with respect to the energy of the first user ( $\mathcal{E}_0 = 1$ ).
- $E_s$  is the average energy transmitted per information symbol.
- $N_f$  is the number of pulses used to transmit one information symbol.
- $T_f$  is the average separation between two consecutive pulses.
- $T_s = N_f T_f$  is the symbol duration.
- $T_c$  is the chip duration.
- $N_c$  is the number of chips per time frame (of duration  $T_f$ ).
- $T_g = T_f - N_c T_c$  is a guard interval introduced at the end of each time frame. Inter-frame interference can be eliminated by choosing  $T_g$  to be larger than the channel delay spread.

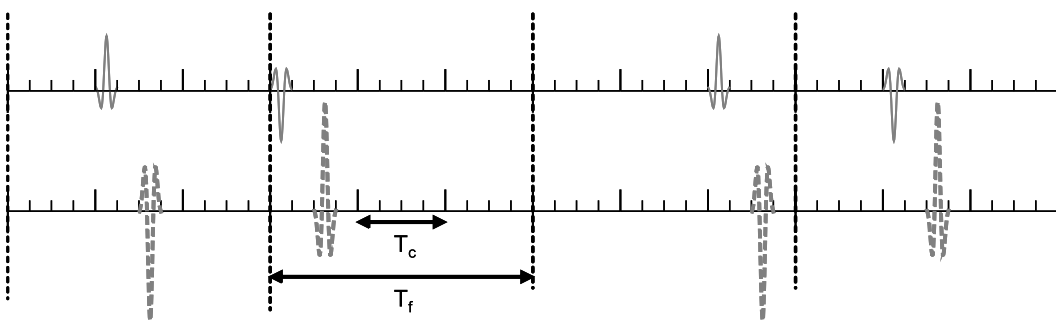


Figure 1.2: TH-UWB signal with polarity randomization.  $N_f = 4$ ,  $N_c = 3$ ,  $T_g = 0$ ,  $\delta = T_w$  and the TH sequence is  $\{1, 0, 2, 1\}$ . The polarity randomization is given by  $\{1, -1, 1, -1\}$ . A 4-PPM-4-PAM constellation is used. The 16 information symbols are mapped onto the amplitude ( $a$ ) and the position ( $p$ ) of the pulses. The pulses represented by solid and dashed lines correspond to  $(a, p) = (1, 0)$  and  $(a, p) = (-3, 2)$  respectively.

- $c_{j,n}^{(k)} \in \{0, \dots, N_c - 1\}$  is the additional time shift (normalized by  $T_c$ ) applied on the  $n$ -th pulse of the  $j$ -th information symbol of the  $k$ -th user.
- $\delta$  is the separation between two consecutive modulation positions.
- $a_j^{(k)}$  is the amplitude of the  $j$ -th information symbol of the  $k$ -th user. For PPM,  $a_j^{(k)} = 1$  for all values of  $j$  and  $k$ .
- $d_j^{(k)}$  is the position of the  $j$ -th information symbol of the  $k$ -th user. For PAM,  $d_j^{(k)} = 0$  for all values of  $j$  and  $k$ .
- $\{b_{j,n}^{(k)}\}$  is an additional amplitude spreading sequence. This sequence can be exploited for encoding the different pulses of a given user. In the same way, it can be used in order to introduce different signatures between the data flows transmitted by the different users.

The structure of a TH-UWB signal is presented in Fig. 1.1. Time hopping also corresponds to pseudo-random dithering. In fact, without the additional time shifts (determined by  $c_{j,n}^{(k)}$ ), all consecutive pulses are separated by  $T_f$ . This results in spectral lines in the frequency response of the transmitted signal. This can result in important interference to narrow-band systems.

For PAM and for independent and identically distributed information symbols, the mean of  $S_{M'}\text{-PAM}$  in eq. (1.3) is equal to zero. This results in an additional smoothing of the power spectrum density. On the other hand, for PPM, dithering by the TH sequence can be insufficient. In this case, an additional polarity randomization of the pulses must be applied [15]. In eq. (1.9), this dithering is included in the sequence  $\{b_{j,n}^{(k)}\}$ . Fig. 1.2 illustrates an example of a polarity-randomized pulse train.

For DS-UWB systems, the transmitted signal is obtained from eq. (1.9) by setting  $T_f = T_c$ ,  $N_f = N_c$  and by eliminating the TH sequence  $\{c_{j,n}^{(k)}\}$ .

In this work, we focus on TH with PAM, PPM and PPAM constellations. As discussed later, the extension to DS systems is straightforward since the space-time coding schemes that we propose are independent from the multiple access scheme.

### 1.1.5 UWB channel models

The UWB propagation channel is typically a frequency-selective multi-path channel. However, there are some differences between these channels and wideband channels. The main difference is the very large number of resolvable multi-path components. The energy contained in a very short pulse is dispersed over a duration that can be hundreds of times larger than the pulse-width. Wideband channels are modeled by tapped-delay lines where the arrivals of the multi-path components take place at integer multiples of the pulse-width [16]. Given the high frequency selectivity of UWB channels, modeling these channels by tapped-delay lines is inappropriate since several multi-path components can arrive during the duration of one pulse [17, 18]. This introduces intra-pulse interference and the impulse response of an UWB channel is the sum of a very large number of delayed, attenuated and distorted replicas of the transmitted pulse.

Modeling the single-antenna UWB channel has been the subject of extensive research (refer to [17, 18] and the many references therein). However, only limited references studied the multi-antenna channels.

#### Single-Input-Single-Output UWB channels

Two approaches were adopted for modeling the UWB channel. The first approach corresponds to “site-specific” or “deterministic” modeling [19, 20]. This corresponds to modeling the interaction of the electromagnetic signal with a known physical environment. This results in a good comprehension of the impact of some propagation phenomena on the system performance. The second approach is the “statistical” modeling. In this domain, the IEEE society adopted two channel models for high data rate [17] and low data rate [18] WPANs. These recommendations are based on the statistical model proposed in [21] where a clustering phenomenon is observed in indoor channels. In other words, the channel is modeled as the superposition of different clusters each composed of a certain number of rays. From [17, 18], an UWB channel can be modeled based on four parameters that characterize a given environment. Namely, the cluster arrival rate, the ray arrival rate within a cluster, the cluster decay factor and the ray decay factor. Unlike [21] where the amplitudes of the rays followed a Rayleigh distribution, it was found that these amplitudes can be well approximated by a lognormal distribution [17, 18].

#### Multiple-Input-Multiple-Output UWB channels

For the moment, the IEEE has not adopted an UWB channel model in the MIMO context. In [22, 23], a MIMO-UWB channel model was proposed based on the extension of a space-variant SISO-UWB channel model. In this model, the clusters are supposed to be generated by some reflectors whose positions are known. Based on the positions of the reflectors, receive antennas and transmit antennas, the different arrival times of the first ray of each cluster can be determined deterministically assuming free-space propagation. At a second time, the remaining rays of each cluster are generated randomly. [23] remains a simplified model. On one hand, it is a quasi-deterministic model that is highly dependant on the positions of the reflectors in a certain indoor environment. On the other hand, in [23], Rayleigh fading is observed on the different multi-path components. This observation contradicts the results of more extended channel sounding campaigns that prescribed a lognormal amplitude distribution [17, 18].

Perhaps the most extensive work on characterizing the MIMO-UWB channels is the one proposed in [24,25]. The authors of [24,25] observed that the variation of the total received energy over a local area

is very low. Given the very short duration of the pulses, the interaction between the different multi-path components is limited resulting in limited fading. However, the energy collected over a limited part of the channel delay spread can change significantly over local areas implying high fading margins. Given the very large number of multi-path components, practical systems (for example Rake receivers) combine a limited number of multi-path components. For these systems, the spatial fading is more pronounced. In this case, exploiting the spatial diversity can be beneficial.

Another observation made in [24, 25] is that UWB signals generally exhibit low spatial correlation despite the low variation in the signal level. Even though the interaction between the multi-path components is limited, the relative positions of these components can change substantially from one receive antenna to another co-located one given the short duration of the pulses. Following from the fact that there are several directions of arrival, the signals seen by different antennas can be very different. However, even though the spatial correlation of the entire impulse responses is low, the correlation among some portions of these responses can be more pronounced. In particular, the portions of the channel taken around the strongest arriving rays are more correlated than other portions.

Similar results on the spatial correlation were observed in [26] and [27]. In [27] it was observed that only the first bin presents high correlation levels in line-of-sight (LOS) situations while the correlations at all of the remaining bins are lower than 0.3. The SIMO-UWB channel measurements and characterization that we performed are summarized in Appendix A.

In [28], a spatial model for UWB systems is proposed based on the extension of the 2-cluster SISO model proposed in [29]. The authors observed a lack of significant clustering in their channel measurements and proposed a new model in which each channel is composed of only two clusters. The first arriving cluster has strong multi-path components while the second one is slowly decaying with diffuse multi-path components. While the rays of the first cluster arrive from approximately the same angle-of-arrival (AOA), the AOAs of the diffuse rays are uniformly distributed over all directions. Generating the AOAs of the first cluster from a Laplacian distribution with a small variance and the AOAs of the second cluster from a uniform distribution over  $[0 \ 2\pi]$ , the SISO model in [29] can be extended to the SIMO case.

### 1.1.6 Receivers

#### Rake Receivers

A very popular receiver structure that is widely used with multi-path channels is the Rake receiver [7]. Rake receivers capture the energy contained in the signal components that have propagated through the channel by different paths. In particular, an  $L$ -th order Rake captures the energy of  $L$  multi-path components. The integrated energy and the diversity order increase with  $L$  at the expense of an increased receiver complexity. In UWB systems, given the very large number of multi-path components, an All-Rake (A-Rake) receiver that combines all of the multi-path components is practically infeasible [30]. In practical systems, Rake receivers with limited number of fingers must be used. Therefore, despite the very large multi-path diversity offered by the frequency selective UWB channels, practical UWB systems only profit from a limited part of this diversity.

We can differentiate between Partial-Rake (PRake) and Selective-Rake (SRake) receivers [31]. A  $L$ -th order PRake combines the first  $L$  arriving multi-path components while a SRake combines the strongest  $L$  multi-path components. In general, Rake receivers are followed by a multi-path combining

stage. For example in coherent systems, maximum-ratio-combining (MRC) or equal-gain-combining (EGC) is performed. In  $L$ -th order PRakes, MRC and EGC necessitate the estimation of  $L$  amplitude and polarity values respectively. In addition to these quantities, SRakes necessitate the estimation of the arrival times of the strongest multi-path components. However, the energy captured by a SRake can be much more important than the energy captured by a PRake especially in non-line-of-sight (NLOS) situations where the magnitudes of the first arriving rays can be very small.

### Correlation receivers

In this case, the first stage of the receiver consists of a filter matched to the channel response rather than the received pulse waveform as with Rake receivers. This is equivalent to evaluating the cross-correlations between the received signal and a reference signal that is constructed during a training phase. Given the very large channel delay spreads of the UWB channels, constructing the reference signal can be practically infeasible. The practical implementation of these systems consists of all-digital receivers based on direct sampling [9, 32]. In this case, the received signal and the reference signals are sampled at a very high sampling rate (20 Gsample/s) and quantized over a small number of quantization levels (typically 3 levels for the reference signal and 2 levels for the received signal) [9].

Another suboptimal solution corresponds to the transmitted-reference (TR) systems [33]. In TR systems, each information-carrying pulse is preceded by a reference pulse. At the receiver side, the received data signal is correlated with the preceding noisy reference signal. The disadvantages include the additional energy transmitted for non data bearing pulses and performance losses induced by the use of a noisy reference signal.

## 1.2 Definitions from algebraic number theory

In this section, we will introduce some notations and definitions that are useful for the remaining parts of this work. Interested readers are referred to [34, 35] for more details.

### Definition 1.1 field extension

Let  $\mathbb{K}$  and  $\mathbb{L}$  be two fields.  $\mathbb{K}$  is called a **field extension** of  $\mathbb{L}$ , denoted by  $\mathbb{K}/\mathbb{L}$ , if  $\mathbb{L}$  is a subfield of  $\mathbb{K}$ .

### Definition 1.2 algebraic numbers

If  $\theta \in \mathbb{K}$  is the root of a monic polynomial:  $f(x) = \sum_{j=0}^n a_j x^j \in \mathbb{L}[x]$  and  $\theta$  is not the root of such a polynomial of degree less than  $n$ , then  $\theta$  is called **algebraic** over  $\mathbb{L}$  with degree  $n$ . If  $\theta$  is not algebraic, then it is called **transcendental**. If  $\mathbb{L} = \mathbb{Q}$ ,  $\theta$  is called an **algebraic number**. If  $f(x) \in \mathbb{Z}[x]$ , then  $\theta$  is called an **algebraic integer**.

For example, the  $n$ -th root of unity  $\omega_n = \exp\left(\frac{2\pi i}{n}\right)$  is an algebraic integer whose degree over  $\mathbb{Q}$  is equal to  $\varphi(n)$ , the Euler's function, that corresponds to the number of integers in the set  $\{1, \dots, n-1\}$  that are relatively prime with  $n$ . For example,  $\omega_3$  is of degree 2 and it is a solution of the quadratic monic polynomial  $x^2 + x + 1 = 0$ .

### Definition 1.3 simple field extension

Let  $\theta$  be algebraic over  $\mathbb{L}$  with degree  $n$ . The field extension  $\mathbb{L}(\theta)$  is formed from the adjunction of  $\theta$  to the field  $\mathbb{L}$  and is called a **simple field extension**. It is the smallest field containing both  $\mathbb{L}$  and  $\theta$ . A

synonymous definition of the **degree** occurs when the field  $\mathbb{K} = \mathbb{L}(\theta)$  is considered as a vector space over  $\mathbb{L}$ . In this case, we can say that  $\mathbb{L}(\theta)$  has degree  $n$  over  $\mathbb{L}$ .  $\mathbb{Q}(\theta)$  is called an **algebraic number field** of degree  $n$  over  $\mathbb{Q}$  generated by  $\theta$ .

For example, let  $\theta = 2\cos\left(\frac{2\pi}{N}\right)$  and  $n = \varphi(N)/2$ .  $\mathbb{Q}(\theta) = \left\{\sum_{j=0}^{n-1} a_j \theta^j ; a_0, \dots, a_{n-1} \in \mathbb{Q}\right\}$  is an algebraic number field with degree  $n$  over  $\mathbb{Q}$ .

#### Definition 1.4 field-basis

If  $\alpha \in \mathbb{L}(\theta)$ , then it can be written in the form  $\alpha = \sum_{j=0}^{n-1} \alpha_j \theta^j$  where  $\alpha_0, \dots, \alpha_{n-1} \in \mathbb{L}$  are unique. In other words, the set  $\{1, \theta, \dots, \theta^{n-1}\}$  forms a **field-basis** over  $\mathbb{L}(\theta)$ .

#### Definition 1.5 minimal polynomial

If  $\theta$  is algebraic over  $\mathbb{L}$ , then it has a unique monic irreducible function over  $\mathbb{L}$  called the **minimal polynomial** of  $\theta$  over  $\mathbb{L}$  and denoted by  $\mu_{\theta, \mathbb{L}}(x)$ . In other words, every polynomial in  $\mathbb{L}[x]$  for which  $\theta$  is a root must be divisible by  $\mu_{\theta, \mathbb{L}}(x)$  whose degree is equal to the degree of  $\theta$  over  $\mathbb{L}$ . If the  $n$  roots of  $\mu_{\theta, \mathbb{L}}(x)$  are distinct, then  $\mathbb{K} = \mathbb{L}(\theta)$  is called a Galois extension.

For example, the field  $\mathbb{Q}(\sqrt{5}) = \{a + b\sqrt{5} ; a, b \in \mathbb{Q}\}$  is generated by the basis  $\{1, \sqrt{5}\}$ . The minimal polynomial of the primitive element  $\sqrt{5}$  is equal to  $x^2 - 5$  and it is irreducible over  $\mathbb{Q}$ . The roots of this polynomial are equal to  $\pm\sqrt{5}$  and consequently  $\mathbb{Q}(\sqrt{5})$  is a Galois extension of  $\mathbb{Q}$ .

#### Definition 1.6 Galois group

Let  $\mathbb{K}/\mathbb{L}$  be a field extension. If  $\sigma$  is an embedding of  $\mathbb{K}$  in  $\mathbb{C}$  that fixes  $\mathbb{L}$  pointwise, namely  $\sigma(l) = l \forall l \in \mathbb{L}$ , then  $\sigma$  is called an  **$\mathbb{L}$ -isomorphism** of  $\mathbb{K}$ . The set of such  $\mathbb{L}$ -isomorphisms forms a group that is called the **Galois group** denoted by  $\text{Gal}(\mathbb{K}/\mathbb{L})$ . If  $\mathbb{K} = \mathbb{L}(\theta)$  has a minimal polynomial  $\mu_{\theta, \mathbb{L}}(x)$ , then each element of the Galois group permutes the roots of  $\mu_{\theta, \mathbb{L}}(x)$  in a fixed way.

#### Definition 1.7 conjugates of an algebraic number

If  $\mathbb{K} = \mathbb{Q}(\theta)$  is an algebraic number field of degree  $n$  over  $\mathbb{Q}$ , there exists exactly  $n$  embeddings  $\{\sigma^j ; j = 0, \dots, n-1\}$  of  $\mathbb{K}$  in  $\mathbb{C}$ . If  $\alpha \in \mathbb{K}$ , then  $\sigma^j(\alpha)$  is called the  $j$ -th **conjugate** of  $\alpha$  with  $\sigma^0(\alpha) = \alpha$ . Furthermore, the  $n$  conjugates of  $\theta$  are precisely the  $n$  roots of the minimal polynomial  $\mu_{\theta, \mathbb{Q}}(x)$ . When we apply the embedding  $\sigma^i$  to an arbitrary  $\alpha \in \mathbb{K}$ , the properties of the  $\mathbb{L}$ -isomorphisms imply that:

$$\sigma^i(\alpha) = \sigma^i\left(\sum_{j=0}^{n-1} \alpha_j \theta^j\right) = \sum_{j=0}^{n-1} \sigma^i(\alpha_j) \sigma^i(\theta^j) = \sum_{j=0}^{n-1} \alpha_j \theta_i^j \quad (1.10)$$

where  $\theta_0, \dots, \theta_{n-1}$  are the roots of  $\mu_{\theta, \mathbb{Q}}(x)$  with  $\theta_0 = \theta$ . If  $\sigma^i(\alpha) \geq 0$  for  $i = 0, \dots, n-1$ , then  $\alpha$  is called **totally-positive**.

Consider the maximal real subfield of the cyclotomic field  $\mathbb{Q}(\theta)$  with  $\theta = 2\cos\left(\frac{2\pi}{N}\right)$  and  $n = \varphi(N)/2$ . The  $j$ -th conjugate of  $\theta$  is given by  $\theta_j = \sigma^j(\theta) = 2\cos\left(\frac{2(j+1)\pi}{N}\right)$  for  $j = 0, \dots, n-1$  (with  $\theta_0 = \theta$ ). The  $j$ -th element of the Galois group  $\{\sigma^j\}_{j=0}^{n-1}$  is equivalent to applying a cyclic permutation of degree  $j$  over the elements of the set  $\{\theta_j\}_{j=0}^{n-1}$ .

#### Definition 1.8 ring of integers and integral basis

Let  $\mathbb{K} = \mathbb{Q}(\theta)$ . The set of algebraic integers of  $\mathbb{K}$  is called the **ring of integers** of  $\mathbb{K}$  and it is denoted by  $\mathcal{O}_{\mathbb{K}}$ . A basis of  $\mathcal{O}_{\mathbb{K}}$  over  $\mathbb{Z}$ , or simply a  $\mathbb{Z}$ -basis, is called an **integral basis** of  $\mathbb{K}$ . Any element of  $\mathcal{O}_{\mathbb{K}}$  can be expressed as  $\sum_{j=0}^{n-1} \alpha_j \omega^j$  where  $\alpha_0, \dots, \alpha_{n-1} \in \mathbb{Z}$  and  $\{1, \omega, \dots, \omega^{n-1}\}$  is the integral basis.

For example,  $\mathcal{O}_{\mathbb{Q}(\sqrt{2})}$  is generated by the integral basis  $\{1, \sqrt{2}\}$  while  $\mathcal{O}_{\mathbb{Q}(\sqrt{5})} = \mathbb{Z}(\theta) = \{a + b\theta ; a, b \in \mathbb{Z}\}$  where  $\theta = \frac{1+\sqrt{5}}{2}$  is the Golden number.

### Definition 1.9 norms, traces and discriminants

Let  $\mathbb{K}$  be an algebraic number field of degree  $n$  over  $\mathbb{L}$ . For each element  $\alpha \in \mathbb{K}$ ,  $\text{Tr}_{\mathbb{K}/\mathbb{L}}(\alpha) = \sum_{j=0}^{n-1} \sigma^j(\alpha) \in \mathbb{L}$  is called the **relative trace** of  $\alpha$  in  $\mathbb{K}/\mathbb{L}$ . In the same way,  $N_{\mathbb{K}/\mathbb{L}}(\alpha) = \prod_{j=0}^{n-1} \sigma^j(\alpha) \in \mathbb{L}$  is called the **relative norm** of  $\alpha$  in  $\mathbb{K}/\mathbb{L}$ . If  $\alpha \in \mathcal{O}_{\mathbb{K}}$ , then  $\text{Tr}_{\mathbb{K}/\mathbb{L}}(\alpha) \in \mathcal{O}_{\mathbb{L}}$  and  $N_{\mathbb{K}/\mathbb{L}}(\alpha) \in \mathcal{O}_{\mathbb{L}}$ .  $\text{Tr}_{\mathbb{K}/\mathbb{Q}}(\alpha)$  and  $N_{\mathbb{K}/\mathbb{Q}}(\alpha)$  are called the **absolute trace** and **absolute norm** respectively. Designate by  $\mathcal{D}$  the  $n \times n$  matrix whose  $(i, j)$ -th component is equal to  $\sigma^{i-1}(\omega_j)$  where  $\{\omega_1, \dots, \omega_n\}$  is an integral basis of  $\mathcal{O}_{\mathbb{K}}$ . The **relative discriminant** of  $\mathbb{K}$  as a field extension of  $\mathbb{L}$  is defined by  $d_{\mathbb{K}/\mathbb{L}} = \det(\mathcal{D})^2$ .  $d_{\mathbb{K}/\mathbb{Q}}$  is called the **absolute discriminant** of  $\mathbb{K}$ .

For example, let  $x = a + b\sqrt{5}$  be an element of  $\mathbb{K} = \mathbb{Q}(\sqrt{5})$ , then  $N_{\mathbb{K}/\mathbb{Q}}(x) = (a + b\sqrt{5})(a - b\sqrt{5}) = a^2 - 5b^2$  and  $\text{Tr}_{\mathbb{K}/\mathbb{Q}}(x) = (a + b\sqrt{5}) + (a - b\sqrt{5}) = 2a$ . In the same way,  $x$  can be written as  $x = a' + b'\theta$  where  $\theta$  is the Golden number and  $(a', b') = (a - b, 2b)$ . In this case:

$$\begin{aligned} N_{\mathbb{K}/\mathbb{Q}}(x) &= (a' + b'\theta)(a' + b'\bar{\theta}) = a'^2 - b'^2 + a'b' = a^2 - 5b^2 \in \mathbb{Q} \\ \text{Tr}_{\mathbb{K}/\mathbb{Q}}(x) &= (a' + b'\theta) + (a' + b'\bar{\theta}) = 2a' + b' = 2a \in \mathbb{Q} \end{aligned}$$

where  $\bar{\theta} = \sigma(\theta) = \frac{1-\sqrt{5}}{2}$ . Let:

$$\mathcal{D} = \begin{bmatrix} 1 & \theta \\ 1 & \bar{\theta} \end{bmatrix}$$

then:  $\det(\mathcal{D} \mathcal{D}^T) = d_{\mathbb{K}/\mathbb{Q}} = 5$ .

### Definition 1.10 signature

Let  $\sigma^0, \dots, \sigma^{n-1}$  be the embeddings of  $\mathbb{K}$  in  $\mathbb{C}$ . Designate by  $r_1$  (resp.  $2r_2$ ) the number of values of  $j$  for which  $\sigma^j(\mathbb{K}) \subseteq \mathbb{R}$  (resp.  $\sigma^j(\mathbb{K}) \not\subseteq \mathbb{R}$ ).  $(r_1, r_2)$  is called the **signature** of  $\mathbb{K}$ . An algebraic field is called **totally real** when all its embeddings are real ( $r_2 = 0$ ). In the same way, a field is **totally complex** when  $r_1 = 0$ .

$\mathbb{Q}(\sqrt{5})$  is totally real with signature  $(2, 0)$  while  $\mathbb{Q}(i)$  is totally complex with signature  $(0, 1)$ .

### Definition 1.11 ideals

Designate by  $\mathcal{O}_{\mathbb{K}}$  the ring of integers of an algebraic number field  $\mathbb{K}$  of degree  $n$ . An **ideal**  $I$  is a sub- $\mathbb{Z}$ -module of  $\mathcal{O}_{\mathbb{K}}$  such that  $\forall a \in I, \forall b \in \mathcal{O}_{\mathbb{K}}, ab \in I$ . An ideal  $I \neq \mathcal{O}_{\mathbb{K}}$  is **prime** if whenever  $I|AB$ , a product of two ideals, then  $I|A$  or  $I|B$ . The **norm** of an ideal  $I$  is defined as the cardinality of the quotient ring  $\mathcal{O}_{\mathbb{K}}/I$ . An ideal is **principal** if it can be written as:  $I = \alpha \mathcal{O}_{\mathbb{K}}$  for some algebraic integer  $\alpha$ . In this case,  $N_{\mathbb{K}}(I) = N_{\mathbb{K}}(\alpha)$ . Any element  $a \in I$  can be expressed as:  $a = \sum_{j=0}^{n-1} a_j \gamma_j$  where  $a_0, \dots, a_{n-1} \in \mathbb{Z}$  and  $\{\gamma_0, \dots, \gamma_{n-1}\}$  is a  $\mathbb{Z}$ -basis of  $I$ .

### Definition 1.12 lattices, generator matrix and fundamental parallelopope

Let  $l_1, \dots, l_m \in \mathbb{R}^n$  be  $\mathbb{R}$ -linearly independent vectors ( $m, n \in \mathbb{N}, m \leq n$ ). If:

$$\Lambda_L = \{b \in \mathbb{R}^n ; b = \sum_{j=1}^m z_j l_j ; z_1, \dots, z_m \in \mathbb{Z}\} = L\mathbb{Z} \quad (1.11)$$

then  $\Lambda_L$  is called an *m-dimensional lattice* of  $\mathbb{R}^n$ . The  $n \times m$  matrix  $\mathcal{L} = [l_1 \dots l_m]$  is called the **generator matrix** of  $\Lambda_L$ . If  $n = m$ ,  $\Lambda_L$  is called a **full-rank lattice**. The set  $\mathcal{P}$  defined by:

$$\mathcal{P} = \left\{ \sum_{j=1}^n r_j l_j ; r_j \in \mathbb{R} ; 0 \leq r_j < 1 ; j = 1, \dots, n \right\} \quad (1.12)$$

is called the **fundamental parallelotope** of  $\Lambda_L$ . An invariant of  $\Lambda_L$  is:

$$\text{vol}(\Lambda_L) = |\det(\mathcal{L})| \quad (1.13)$$

and it is called the **volume** of the fundamental parallelotope of  $\Lambda_L$ .

### Definition 1.13 lattices and ideals

After applying the canonical embedding  $\sigma$  to an ideal  $I$ , we obtain the lattice  $\Lambda_I = \sigma(I)$ . The generator matrix of  $\Lambda_I$  can be expressed as:

$$G_I = \begin{bmatrix} \sigma^0(\gamma_0) & \sigma^0(\gamma_1) & \cdots & \sigma^0(\gamma_{n-1}) \\ \vdots & \vdots & \ddots & \vdots \\ \sigma^{r_1-1}(\gamma_0) & \sigma^{r_1-1}(\gamma_1) & \cdots & \sigma^{r_1-1}(\gamma_{n-1}) \\ \Re(\sigma^{r_1}(\gamma_0)) & \Re(\sigma^{r_1}(\gamma_1)) & \cdots & \Re(\sigma^{r_1}(\gamma_{n-1})) \\ \Im(\sigma^{r_1}(\gamma_0)) & \Im(\sigma^{r_1}(\gamma_1)) & \cdots & \Im(\sigma^{r_1}(\gamma_{n-1})) \\ \vdots & \vdots & \ddots & \vdots \\ \Re(\sigma^{r_1+r_2-1}(\gamma_0)) & \Re(\sigma^{r_1+r_2-1}(\gamma_1)) & \cdots & \Re(\sigma^{r_1+r_2-1}(\gamma_{n-1})) \\ \Im(\sigma^{r_1+r_2-1}(\gamma_0)) & \Im(\sigma^{r_1+r_2-1}(\gamma_1)) & \cdots & \Im(\sigma^{r_1+r_2-1}(\gamma_{n-1})) \end{bmatrix} \quad (1.14)$$

where  $\{\gamma_0, \dots, \gamma_{n-1}\}$  is a  $\mathbb{Z}$ -basis of  $I$ . The volume of the fundamental parallelotope of  $\Lambda_I$  is:

$$\text{vol}(\Lambda_I) = |\det(G_I)| = 2^{-r_2} \sqrt{d_{\mathbb{K}}} N_{\mathbb{K}}(I) \quad (1.15)$$

For the ring of integers  $\mathcal{O}_{\mathbb{K}}$ , the generator matrix  $G$  of  $\Lambda = \sigma(\mathcal{O}_{\mathbb{K}})$  is obtained by applying eq. (1.14) on the integral basis. In this case:

$$\text{vol}(\mathcal{O}_{\mathbb{K}}) = 2^{-r_2} \sqrt{d_{\mathbb{K}}} \quad (1.16)$$

For totally real fields, the  $n$ -dimensional lattice  $\Lambda_I$  has a diversity order of  $n$ . The **minimum product distance** of the generated lattice verifies [36]:

$$d_{\min} = \min_{x \in \Lambda_I ; x \neq 0_n} \prod_{j=1}^n |x_j| = \frac{1}{\sqrt{d_{\mathbb{K}/\mathbb{Q}}}} \quad (1.17)$$

Moreover, the lattice  $\Lambda_I$  is equivalent to  $\mathbb{Z}^n$  if the generator matrix  $G_I$  is unitary.

For example, let  $\mathbb{K} = \mathbb{Q}(\theta)$  where  $\theta$  is the Golden number. If there exists a totally positive element  $\alpha \in \mathbb{K}$  verifying  $N_{\mathbb{K}/\mathbb{Q}}(\alpha) = \frac{1}{d_{\mathbb{K}/\mathbb{Q}}} = \frac{1}{5}$ , then the matrix:

$$G_I = \text{diag} \left( \sqrt{\alpha} \quad \sqrt{\bar{\alpha}} \right) \mathcal{D} = \begin{bmatrix} \sqrt{\alpha} & 0 \\ 0 & \sqrt{\bar{\alpha}} \end{bmatrix} \begin{bmatrix} 1 & \theta \\ 1 & \bar{\theta} \end{bmatrix}$$

generates a rotated square lattice since  $\mathcal{D} \mathcal{D}^T$  is a diagonal matrix. We can choose  $\alpha = \frac{3-\theta}{5}$  since both  $\alpha$  and  $\bar{\alpha} = \sigma(\alpha)$  are positive and  $N_{\mathbb{K}/\mathbb{Q}}(\alpha) = \frac{N_{\mathbb{K}/\mathbb{Q}}(3-\theta)}{5^2} = \frac{1}{5} = d_{\mathbb{K}/\mathbb{Q}}^{-1}$ .

**Definition 1.14** *lattice reduction*

The generator matrix  $G_I$  of a lattice  $\Lambda_I$  is not unique. In particular, any matrix  $\tilde{G}_I = G_I T$  generates the same lattice  $\Lambda_I$  if the matrix  $T$  is unimodular, that is,  $T \in \mathbb{Z}^{n \times n}$  and  $\det(T) = \pm 1$ . In the same way,  $G_I = \tilde{G}_I T^{-1}$  and  $T^{-1}$  is unimodular. Since  $|\det(T)| = 1$ , then  $\text{vol}(\Lambda_I)$  is independent from the choice of the generator matrix. The aim of the lattice reduction is to transform the basis composed from the columns of  $G_I$  into a new basis (composed from the columns of  $\tilde{G}_I$ ) whose components have shorter length. In an equivalent manner, the lattice reduction corresponds to the best choice of  $T$  that enhances the orthogonality between the columns of  $\tilde{G}_I$ .

Among the different lattice reduction techniques, the Lenstra, Lenstra and Lovász (LLL) algorithm [37] is appealing because it has a polynomial complexity. Writing the QR decomposition of  $\tilde{G}_I$  as  $\tilde{G}_I = \tilde{Q}\tilde{R}$ , then  $\tilde{G}_I$  is said to be LLL-reduced with parameter  $\delta$  ( $1/4 < \delta \leq 1$ ) if:

$$\begin{cases} |\tilde{r}_{i,j}| \leq \frac{1}{2} |\tilde{r}_{i,i}| & \text{for } 1 \leq i < j \leq n \\ \delta \tilde{r}_{i-1,i-1}^2 \leq \tilde{r}_{i,i}^2 + \tilde{r}_{i-1,i}^2 & \text{for } i = 2, \dots, n \end{cases} \quad (1.18)$$

where the parameter  $\delta$  influences the quality of the reduced basis. In some situations and depending on the structure of  $G_I$ , applying the LLL algorithm results in an orthogonal basis. The pseudo-code for a possible implementation of the LLL algorithm can be found in [38].

**Definition 1.15** *cyclic division algebras*

Let  $\mathbb{K}/\mathbb{L}$  be a Galois extension of degree  $n$  with Galois group  $\text{Gal}(\mathbb{K}/\mathbb{L}) = \langle \sigma \rangle$  with  $\sigma^n = 1$ . We choose a non-zero element  $\gamma$  in  $\mathbb{L}$  and construct a right  $\mathbb{K}$ -vector space with formal basis  $\{1, z, \dots, z^{n-1}\}$ :

$$\mathcal{A} = \mathbb{K} \oplus z\mathbb{K} \oplus \dots \oplus z^{n-1}\mathbb{K} \quad (1.19)$$

where the multiplication over  $\mathcal{A}$  satisfies  $z^n = \gamma$  and  $kz = z\sigma(k) \forall k \in \mathbb{K}$ .  $\mathcal{A}$  is a **cyclic algebra** denoted by  $\mathcal{A}(\mathbb{K}/\mathbb{L}, \sigma, \gamma)$ . An element  $k = \sum_{j=0}^{n-1} z^j k_j \in \mathcal{A}$  can be associated with the following  $n \times n$  matrix:

$$C(k_0, \dots, k_{n-1}) = \begin{bmatrix} k_0 & k_1 & k_2 & \cdots & k_{n-1} \\ \gamma\sigma(k_{n-1}) & \sigma(k_0) & \sigma(k_1) & \cdots & \sigma(k_{n-2}) \\ \gamma\sigma^2(k_{n-2}) & \gamma\sigma^2(k_{n-1}) & \sigma^2(k_0) & \cdots & \sigma^2(k_{n-3}) \\ \vdots & \vdots & \vdots & \vdots & \vdots \\ \gamma\sigma^{n-1}(k_1) & \gamma\sigma^{n-1}(k_2) & \gamma\sigma^{n-1}(k_3) & \cdots & \sigma^{n-1}(k_0) \end{bmatrix} \quad (1.20)$$

**Proposition 1.1** [39]:  $\det(C(k_0, \dots, k_{n-1})) \in \mathbb{L} \forall k_0, \dots, k_{n-1} \in \mathbb{K}$ .

**Proposition 1.2** [39]: Let  $\mathbb{K}/\mathbb{L}$  be a degree- $n$  Galois extension with  $\text{Gal}(\mathbb{K}/\mathbb{L}) = \langle \sigma \rangle$  and  $\gamma \in \mathbb{L}^* = \mathbb{L} \setminus \{0\}$ . If there are no elements in  $\mathbb{K}$  whose norms are equal to  $\gamma^t$  for  $t = 1, \dots, n-1$ , then the cyclic algebra  $\mathcal{A}(\mathbb{K}/\mathbb{L}, \sigma, \gamma)$  is a cyclic division algebra (CDA).

## 1.3 Multiple-Input-Multiple-Output communications

### 1.3.1 Introduction

MIMO processing has emerged as a promising technique for improving the performance of wireless systems [40,41]. The limited resources of a communication system, such as spectrum and power, can be efficiently used to provide sufficient quality and capacity to a wide range of high data rate systems.

In the literature, the basic MIMO system model consisted of a quasi-static and frequency-flat Rayleigh fading channel. Consider a system with  $P$  transmit antennas and  $Q$  receive antennas. The complex baseband channel, within a single fading block of  $T$  symbol durations, can be expressed as:

$$Y_{Q \times T} = \sqrt{\frac{SNR}{P}} H_{Q \times P} C_{P \times T} + N_{Q \times T} \quad (1.21)$$

where the subscripts indicate the corresponding matrices' dimensions and the term  $SNR$  corresponds to the signal-to-noise ratio per receive antenna. The  $(q, p)$ -th term of the channel matrix  $H$  corresponds to the channel between the  $p$ -th transmit and the  $q$ -th receive antenna and it is modeled as a complex Gaussian random variable. The matrix  $N$  corresponds to the additive white noise whose entries  $N_{q,t} \sim \mathcal{CN}(0, 1)$  (complex normal random variables with zero mean and unit variance). The  $(p, t)$ -th entry of  $C$  corresponds to the symbol transmitted from the  $p$ -th antenna during the  $t$ -th symbol duration.

For this kind of channels, the capacity at high SNRs was found to scale with  $\min\{P, Q\}$  [41]:

$$C(P, Q, SNR) \simeq \min\{P, Q\} \log(SNR) \quad (1.22)$$

In the case of sufficiently-spaced transmit and receive antenna arrays, the  $PQ$  sub-channels are independent resulting in a well-conditioned channel matrix. In other words, the additional spatial degrees of freedom permit to transmit independent data flows through the channel and to separate these flows at the receiver side. Equation (1.22) indicates that there are approximately  $\min\{P, Q\}$  parallel spatial channels between the transmitter and the receiver. From this point of view, MIMO techniques permit to increase the data rate of wireless systems. Several schemes were proposed to profit from this spatial multiplexing phenomenon [42, 43].

MIMO techniques can be also used to combat fading. Different independently faded replicas of the information symbols that have propagated through different channels are available at the receiver side. In other words, the signal is lost if all these replicas are lost implying a better immunity against multi-path fading. A maximum diversity advantage of  $PQ$ , corresponding to the number of channels between the transmitter and the receiver, can be achieved. For exploiting the diversity at the transmitter side, several space-time (ST) codes were proposed in the literature [44–47]. In general, we can distinguish between ST trellis codes and ST block codes (STBC). In this work, we are interested in STBCs.

### 1.3.2 Diversity and Multiplexing Tradeoff

In [48] Zheng and Tse observed that both the diversity and multiplexing gains can be achieved simultaneously, but there is a fundamental tradeoff between them over Rayleigh fading channels. A scheme  $\{C(SNR)\}$  is defined as a family of ST codes, one for each SNR. A scheme is said to achieve a spatial multiplexing gain  $r$  and a diversity gain  $d$  if:

$$\lim_{SNR \rightarrow \infty} \frac{R(SNR)}{\log(SNR)} = r ; \quad \lim_{SNR \rightarrow \infty} \frac{\log(P_e)}{\log(SNR)} = -d \quad (1.23)$$

where  $R(SNR)$  is the data rate in bits per channel use (PCU) and  $P_e$  is the probability of error.

**Lemma 1.1** [48] If  $T \geq P + Q - 1$ , the maximum achievable diversity gain is given by the piece-wise linear function connecting the points  $(r, d(r))$  for  $r = 0, \dots, \min\{P, Q\}$  where:

$$d(r) = (P - r)(Q - r) \quad (1.24)$$

From eq. (1.24), the maximum multiplexing gain  $r_{max} = \min\{P, Q\}$  comes at the expense of sacrificing the diversity gain ( $d = 0$ ). In the same way, the maximal diversity gain is  $d_{max} = PQ$ . In [49], it was shown that the tradeoff for  $T = P$  is the same as in eq. (1.24) for all values of  $P$  and  $Q$ .

### 1.3.3 Design criteria of Space-Time codes

Designate by  $\mathcal{C}$  a codebook whose cardinality is equal to  $|\mathcal{C}|$ . In [50], Tarokh *et al.* derived the design criteria of ST codes over slow flat fading channels. The average codeword error probability can be bounded by:

$$P_e \leq \frac{1}{|\mathcal{C}|} \sum_{c \in \mathcal{C}} \sum_{c' \in \mathcal{C} \setminus \{c\}} E [P(c \rightarrow c'|H)] \quad (1.25)$$

where  $P(c \rightarrow c'|H)$  is the conditional pairwise error probability (PEP) defined as the probability of deciding in the favor of the codeword  $c'$  when the codeword  $c$  was transmitted. From eq. (1.21), it can be expressed as:

$$P(c \rightarrow c'|H) = Q\left(\frac{\sqrt{E_s}\|H(c - c')\|}{\sqrt{2N_0}}\right) \quad (1.26)$$

$$\leq \exp\left(-\frac{E_s\|H(c - c')\|^2}{4N_0}\right) \quad (1.27)$$

where  $E_s$  is the average energy per symbol and  $N_0$  is the noise spectral density.  $Q(x) = \frac{1}{\sqrt{2\pi}} \int_x^\infty \exp(-\frac{t^2}{2}) dt$  is the Gaussian tail function. After some manipulations, eq. (1.27) takes the form:

$$P(c \rightarrow c'|H) \leq \prod_{q=1}^Q \prod_{p=1}^P \exp\left(-\frac{E_s}{4N_0} \lambda_p |\beta_{q,p}|^2\right) \quad (1.28)$$

where  $\beta_{q,p} = \sum_{p'=1}^P h_{q,p'} v_{p,p'}$ .  $h_{q,p}$  is the  $(q, p)$ -th entry of the channel matrix  $H$ ,  $\lambda_p$  is the  $p$ -th eigenvalue of the matrix  $B(c, c') = (c - c')(c - c')^H$  and  $v_{i,j}$  is the  $(i, j)$ -th entry of the unitary matrix  $V$  composed of the eigenvectors of the Hermitian matrix  $B(c, c')$ .

When the channel coefficients are complex Gaussian random variables,  $\beta_{q,p}$  is Gaussian. In this case, integrating eq. (1.28) over a Rayleigh distribution results in the following upper bound on the average pairwise error probability [50]:

$$P(c \rightarrow c') \leq \left( \prod_{p=1}^r \lambda_p \right)^{-Q} \left( \frac{E_s}{4N_0} \right)^{-rQ} \quad (1.29)$$

where  $r$  is the rank of  $B(c, c')$ . The design criteria, namely the rank criterion and determinant criterion, follow from eq. (1.29) as follows [50]:

#### Definition 1.16 Rank Criterion

The number of non-zero eigenvalues of the matrix  $B(c, c')$  must be maximized over the set of all distinct codewords  $c$  and  $c'$ . If the rank of  $B(c, c')$  is equal to  $r$ , then a diversity gain of  $rQ$  is achieved. Note that on a log-log plot,  $rQ$  corresponds to the slope of the PEP at high SNRs. A code is said to achieve full diversity when  $B(c, c')$  has full rank ( $r = P$ ).

**Definition 1.17 Determinant Criterion**

The coding gain is equal to  $(\prod_{p=1}^r \lambda_p)^{\frac{1}{r}}$  and it must be maximized. Note that for a given diversity gain, the coding gain corresponds to a simple translation of the PEP curve on a log-log scale. When  $r = P$ , maximizing the coding gain is equivalent to maximizing:

$$\min_{c, c' \in \mathcal{C}; c \neq c'} |\det(c - c')| \quad (1.30)$$

When the product  $PQ$  is large, an additional criterion referred to as the trace criterion was proposed in [51]:

**Definition 1.18 Trace Criterion**

Maximize the minimum Euclidean distance between all pairs of distinct codewords. This is equivalent to maximizing the trace of the matrix  $B(c, c')$ .

As observed in [52], the previous design criteria constitute an upper bound for different kinds of channels under the condition of independent fading. If the entries of the channel matrix  $H$  are independent, the average PEP from eq. (1.28) can be expressed as:

$$P(c \rightarrow c') = \prod_{q=1}^Q \prod_{p=1}^P \int \exp \left( -\frac{E_s}{4N_0} \lambda_p |\beta_{q,p}|^2 \right) p(\beta_{q,p}) d\beta_{q,p} \quad (1.31)$$

Applying the Cauchy-Schwartz inequality, eq. (1.31) can be upper-bounded by:

$$P(c \rightarrow c') \leq \prod_{q=1}^Q \prod_{p=1}^P \left[ \int p^2(\beta_{q,p}) d\beta_{q,p} \right]^{\frac{1}{2}} \left[ \int \exp \left( -\frac{E_s}{2N_0} \lambda_p |\beta_{q,p}|^2 \right) d\beta_{q,p} \right]^{\frac{1}{2}} \quad (1.32)$$

$$\leq k \left( \prod_{p=1}^r \lambda_p \right)^{-\frac{Q}{4}} \left( \frac{2 E_s}{\pi N_0} \right)^{-\frac{rQ}{4}} \quad (1.33)$$

where  $k$  is a constant and the last equation follows from the fact that for physical channels  $p^2(\beta_{q,p})$  is finite and integrable.

In the literature, the rank and determinant criteria were widely used for constructing ST codes over different kinds of fading channels. In [53], it was shown that these criteria still hold with Rician-fading channels in the presence of lognormal shadowing on the line-of-sight component. In fact, this shadowing results in multiplying eq. (1.29) by a term that depends uniquely on the parameters of the shadowing. Similar results were observed with Rician-Nakagami channels [54].

### 1.3.4 Space-Time Block Codes

The literature of ST coding is huge. In this section, we present some existing ST codes. A special attention is paid to the codes constructed from cyclic division algebras. In what follows, ST codes that transmit  $P$  symbols PCU ( $P$  is the number of transmit antennas) are referred to as full-rate codes.

#### Orthogonal Space-Time codes

A ST block codes is said to be orthogonal if the different information symbols contained in each codeword can be decoded separately. In other words, Maximum Likelihood (ML) decoding is possible with

linear combining at the receiver side. The first ST block code was proposed by Alamouti in [44] for 2 transmit antennas and was later generalized to larger number of transmit antennas [45]. The  $2 \times 2$  Alamouti code is given by:

$$C = \begin{bmatrix} s_1 & -s_2^* \\ s_2 & s_1^* \end{bmatrix} \quad (1.34)$$

where  $s_1$  and  $s_2$  are the information symbols that belong to a PSK or QAM constellation and  $s^*$  stands for the complex conjugate of  $s$ . This code achieves full diversity while transmitting at a rate of 1 symbol PCU. The coding gain is given by:

$$\delta_C = \min_{(s_1, s_2) \neq (s'_1, s'_2)} (|s_1 - s'_1|^2 + |s_2 - s'_2|^2) > 0 \quad (1.35)$$

It was shown in [49] that the Alamouti code achieves the optimal diversity-multiplexing tradeoff with  $Q = 1$  receive antenna. However, this optimality is lost for  $Q > 1$  and the Alamouti code is not information-lossless in this case [47].

For larger number of transmit antennas, full diversity can be always achieved. However, this may be obtained at the expense of a data rate loss (rate  $< 1$  symbol PCU). For example, rate-1 real orthogonal designs exist only with  $P = 2, 4$  and  $8$  transmit antennas. For complex orthogonal designs, the maximum achievable data rate depends on  $P$  and it is equal to  $3/4$  symbols PCU for  $3$  and  $4$  transmit antennas.

### Space-Time codes for PSK modulations

The construction of the majority of ST codes in the literature was based on the rank criterion (Section 1.16) which applies to the difference between the complex-valued baseband versions of the codewords. In [55], Hammons *et al.* proposed an equivalent binary rank criterion that depends on the unmodulated signals. This approach simplifies the design of the ST codes and relates this design to the well understood results from the coding theory over finite fields. For BPSK, the binary rank criterion states simply that the ST code is fully diverse if every non-zero codeword has full rank over the binary field. Denote by  $\mathbb{F}$  the field of integers modulo 2 and by  $\oplus$  the modulo 2 addition. Based on the binary rank criterion, the authors of [55] proposed a simple stacking construction for  $P \times T$  ( $T \geq P$ ) ST block codes given by:

$$C(\bar{x}) = \begin{bmatrix} \bar{x}M_1 \\ \vdots \\ \bar{x}M_P \end{bmatrix} \quad (1.36)$$

where  $\bar{x}$  denotes a  $k$ -tuple of information bits.  $M_1, \dots, M_P$  are binary  $k \times T$  matrices.  $C(\bar{x})$  in eq. (1.36) achieves full diversity if  $\forall a_1, \dots, a_P \in \mathbb{F}$ , the matrix  $M = a_1M_1 \oplus \dots \oplus a_P M_P$  is nonsingular unless when  $a_1 = \dots = a_P = 0$ .

While the orthogonal design [45] results in a rate of  $3/4$  with 3 transmit antennas, the authors proposed a new rate-1  $3 \times 3$  code that is fully diverse with BPSK and QPSK modulations based on the stacked construction. This code is obtained by setting  $P = T = K = 3$  in eq. (1.36). Denote by  $s_1, \dots, s_3$  the BPSK or QPSK signals, the  $3 \times 3$  codewords are given by:

$$C = \begin{bmatrix} s_1 & s_2 & s_3 \\ s_2 & s_3 & s_1 + s_2 \\ s_3 & s_1 + s_2 & s_2 + s_3 \end{bmatrix} \quad (1.37)$$

### Tilted-QAM design

In [56], Yao *et al.* proposed a  $2 \times 2$  code that has been referred to as the tilted-QAM in the literature. Designate by  $s_1, \dots, s_4$  the information symbols that are taken from a QAM constellation and define the two 2-dimensional vectors  $x$  and  $y$  as follows:

$$x = M_{\theta_1} [s_1 \ s_2]^T ; \quad y = M_{\theta_2} [s_3 \ s_4]^T \quad (1.38)$$

where  $M_{\theta_1}$  and  $M_{\theta_2}$  are two rotation matrices given by:

$$M_{\theta_i} = \begin{bmatrix} \cos(\theta_i) & -\sin(\theta_i) \\ \sin(\theta_i) & \cos(\theta_i) \end{bmatrix} \quad (1.39)$$

The codeword associated with the symbols  $s_1, \dots, s_4$  is given by:

$$C = \begin{bmatrix} x_1 & y_2 \\ y_1 & x_2 \end{bmatrix} \quad (1.40)$$

where  $x_i$  and  $y_i$  are the  $i$ -th components of vectors  $x$  and  $y$  respectively.

The authors found that there is one pair of rotation angles that maximizes the coding gain for all constellation sizes. This pair is given by:  $(\theta_1, \theta_2) = (\frac{1}{2} \arctan(\frac{1}{2}), \frac{1}{2} \arctan(2))$  and the corresponding coding gain is equal to  $\frac{1}{2\sqrt{5}}$ .

### A $2 \times 2$ code based on number theory ( $B_{2,\phi}$ )

In [47], Damen *et al.* proposed the following  $2 \times 2$  ST code that can be associated with constellations carved from  $\mathbb{Z}[i]$  (QAM or PAM):

$$B_{2,\phi} = \frac{1}{\sqrt{2}} \begin{bmatrix} s_1 + \phi s_2 & \theta(s_3 + \phi s_4) \\ \theta(s_3 - \phi s_4) & s_1 - \phi s_2 \end{bmatrix} \quad (1.41)$$

where  $\phi = \theta^2$ . It is clear that  $B_{2,\phi}$  has a full rate since it transmits 4 information symbols during 2 symbol durations.

The determinant of eq. (1.41) is given by:

$$d(s, \phi) = \sum_{j=0}^3 a_j \phi^j \quad (1.42)$$

where  $[a_0, a_1, a_2, a_3] = [s_1^2, -s_2^2, -s_3^2, s_4^2] = a \in \mathbb{Z}[i]^4$ . Let  $s = [s_1, \dots, s_4]$ , it is clear that for  $s \neq \mathbf{0}_{1 \times 4}$ ,  $d(s, \phi) \neq 0$  if  $\{1, \phi, \phi^2, \phi^3\}$  forms a free set over  $\mathbb{Z}[i]$ . Therefore, choosing  $\phi$  to be an algebraic number of degree  $\geq 4$  results in a fully-diverse code. In the same way,  $\phi$  can be chosen to be any transcendental number. For this particular construction, any algebraic element of degree 2 over  $\mathbb{Q}[i]$  achieves full diversity if  $\phi^2 \in \mathbb{Q}[i]$ . This follows from the fact that the components of  $a$  are perfect squares in  $\mathbb{Z}[i]$  and  $\phi$  can not be a perfect square in  $\mathbb{Q}[i]$  since its degree is greater than 1.

For 4-QAM and 16-QAM constellations, the value of  $\phi$  that maximizes the coding gain can be obtained by performing a computer search. This approach can not be adopted for high order constellations that generate a very large number of codewords. Finally, the coding gain of  $B_{2,\phi}$  decreases with the size of the constellation.

### Threaded Algebraic Space Time (TAST) codes

The approach used for constructing  $B_{2,\phi}$  in [47] was extended by El Gamal *et al.* in [57] for  $P \geq 2$  transmit antennas. A  $P \times P$  TAST code with  $L$  layers ( $L \leq P$ ) is denoted by  $\mathcal{T}_{P,L}$  and it achieves a rate of  $L$  symbols PCU. The codewords are given by:

$$\mathcal{T}_{P,L} = \begin{bmatrix} s_{1,1} & s_{2,1} & \cdots & s_{P,1} \\ s_{P,2} & s_{1,2} & \ddots & \vdots \\ \vdots & \ddots & \ddots & s_{2,P-1} \\ s_{2,P} & \cdots & s_{P,P} & s_{1,P} \end{bmatrix} \quad (1.43)$$

where:

$$\begin{bmatrix} s_{p,1} & \cdots & s_{p,P} \end{bmatrix}^T = \begin{cases} \phi_p \mathcal{M}_p \begin{bmatrix} a_{(p-1)P+1} & \cdots & a_{pP} \end{bmatrix}^T & ; p = 1, \dots, L \\ \begin{bmatrix} 0 & \cdots & 0 \end{bmatrix}^T & ; p = L+1, \dots, P \end{cases} \quad (1.44)$$

where  $\phi_p = \phi^{\frac{p-1}{P}}$ ,  $a_1, \dots, a_{PL}$  are the information symbols carved from  $\mathbb{Z}[i]$  and  $\mathcal{M}_1, \dots, \mathcal{M}_P$  are  $P \times P$  rotation matrices that achieve full modulation diversity [36, 58].

The TAST code is based on the following principle. Let  $s = \mathcal{M} a$  where  $s$  and  $a$  are  $P$ -dimensional vectors and  $\mathcal{M}$  is a  $P \times P$  matrix. Suppose that the  $P$  components of  $s$  are transmitted over  $P$  parallel channels (for example on the  $l$ -th thread of  $\mathcal{T}_{P,L}$  that is composed from the entries of the  $l$ -th upper diagonal and  $(P-l)$ -th lower diagonal of  $\mathcal{T}_{P,L}$ ). If  $\mathcal{M}$  is a  $P \times P$  real or complex rotation matrix that achieves full modulation diversity, then the components of  $a$  can be recovered unless when all the components of  $s$  are lost (because of deep fades on the  $P$  channels). In eq. (1.43),  $L$  threads are transmitted simultaneously (over  $P$  symbol durations). In this case, the scalars  $\{\phi_1, \dots, \phi_L\}$  are introduced in order to render the  $L$  threads transparent to each other. The code is said to be symmetric when the same rotation matrix is applied on the  $L$  threads ( $\mathcal{M}_1 = \dots = \mathcal{M}_L \triangleq \mathcal{M}$ ).

$\mathcal{T}_{P,L}$  achieves full diversity if  $\phi$  is an algebraic integer such that the elements of the set  $\{\phi_l\}_{l=1}^L$  are algebraically independent over the algebraic number field used to construct the rotation matrix  $\mathcal{M}$ . In the same way, any transcendental element results in a fully diverse code; in particular,  $\phi = \exp(i\lambda)$  with  $\lambda \neq 0$  being any algebraic number.

The authors of [57] related the coding gain of the TAST code to the Diophantine approximation of  $\phi$  by algebraic numbers. Increasing the size of the constellation enhances this approximation and, consequently, decreases the coding gain. On the other hand, the algebraic numbers are not very well approximated by other algebraic numbers and choosing  $\phi$  to be algebraic results in better coding gains.

### Space-Time codes from field extensions

This construction was proposed by Sethuraman *et al.* in [39]. Designate by  $n$  the number of transmit antennas. Let  $\mathbb{K} = \mathbb{F}(\gamma)$  be a field extension with minimal polynomial  $x^n - \gamma \in \mathbb{F}[x]$ . Designate by  $M_n(\mathbb{F})$  the set of  $n \times n$  matrices whose entries belong to  $\mathbb{F}$ . It is simple to show that there exists an embedding of  $\mathbb{K}$  into  $M_n(\mathbb{F})$  where an element  $k = \sum_{j=0}^{n-1} f_j \gamma^j \in \mathbb{K}$  is mapped onto the  $n \times n$  matrix given by:

$$C(f_0, \dots, f_{n-1}) = \begin{bmatrix} f_0 & f_1 & \cdots & f_n \\ \gamma f_n & f_0 & \ddots & \vdots \\ \vdots & \ddots & \ddots & f_1 \\ \gamma f_1 & \cdots & \gamma f_n & f_0 \end{bmatrix} \quad (1.45)$$

Since  $\mathbb{K}$  is a field (its non-zero elements are invertible), then the difference between any two distinct matrices, having the form given in eq. (1.45), has full rank. This motivates the construction of ST codes based on field extensions. The problem can be stated as follows. Given a certain constellation  $\mathcal{S}$ , designate by  $\mathbb{F}$  the infinite field containing all the elements of  $\mathcal{S}$ . For example, for  $m$ -PSK constellations,  $\mathbb{F} = \mathbb{Q}(\omega_m)$  where  $\omega_m = \exp(\frac{2\pi i}{m})$  is the  $m$ -th root of unity. The construction of the ST code reduces to finding an element  $\gamma \in \mathbb{F}$  such that  $x^n - \gamma$  is irreducible over  $\mathbb{F}[x]$  (so that  $\mathbb{K}$  is a  $n$ -dimensional field extension of  $\mathbb{F}$ ).

The authors of [39] proposed the following method for choosing  $\gamma$ . For  $m$ -PSK signals with  $n$  transmit antennas, designate by  $M$  the integer containing all the primes of both  $m$  and  $n$ . Then the polynomial  $x^n - \omega_M^l$  is irreducible over  $\mathbb{Q}(\omega_M)$  (and consequently over  $\mathbb{Q}(\omega_m)$ ) for any integer  $l$  that is relatively prime with  $M$ . Note that when all the primes that appear in the prime factorization of  $n$  appear also in the factorization of  $m$ , then  $M$  can be chosen to be equal to  $m$ . In this case,  $\gamma\mathcal{S} = \mathcal{S}$  and the coding scheme does not introduce any constellation expansion. For example, for 4-PSK constellations with  $n = 2$  transmit antennas,  $M = 4$  and  $\gamma = \omega_4 = \sqrt{-1}$ . In this case, the 16 generated codewords turn out to be the same as those corresponding to the Alamouti code [44].

Full diversity can be also achieved by choosing  $\gamma$  to be transcendental. In this case,  $\mathbb{F}(\gamma)$  is the set of quotients of polynomials in  $\gamma$  with entries in  $\mathbb{F}$ . This approach results in constructing ST codes for any constellation and for an arbitrary number of antennas since  $x^n - \gamma$  is irreducible over  $\mathbb{F}(\gamma)[x]$  for all integers  $n \geq 1$  and for any transcendental number  $\gamma$ .

### Space-Time codes from cyclic division algebras

Cyclic division algebras are powerful tools for constructing full rate and fully diverse ST codes [39, 49, 59–65]. Suppose that we want to construct a minimal-delay  $n \times n$  ST code for a system equipped with  $n$  transmit antennas. From eq. (1.20), the codebook associated with a signal constellation  $\mathcal{S}$  can be determined from a cyclic division algebra  $\mathcal{A}(\mathbb{K}/\mathbb{F}, \sigma, \gamma)$  as follows:

$$\mathcal{C}_{\mathcal{S}} = \left\{ C(s_1, \dots, s_{n^2}) ; (s_1, \dots, s_{n^2}) \in \mathcal{S}^{n^2} \right\} \quad (1.46)$$

where the codeword associated with the symbols  $s_1, \dots, s_{n^2}$  is given by:

$$C(s_1, \dots, s_{n^2}) = \begin{bmatrix} \sum_{j=0}^{n-1} s_{j+1} \theta^j & \sum_{j=0}^{n-1} s_{n+j+1} \theta^j & \cdots & \sum_{j=0}^{n-1} s_{n(n-1)+j+1} \theta^j \\ \gamma \sum_{j=0}^{n-1} s_{n(n-1)+j+1} \theta_1^j & \sum_{j=0}^{n-1} s_{j+1} \theta_1^j & \ddots & \vdots \\ \vdots & \ddots & \ddots & \sum_{j=0}^{n-1} s_{n+j+1} \theta_{n-2}^j \\ \gamma \sum_{j=0}^{n-1} s_{n+j+1} \theta_{n-1}^j & \cdots & \gamma \sum_{j=0}^{n-1} s_{n(n-1)+j+1} \theta_{n-1}^j & \sum_{j=0}^{n-1} s_{j+1} \theta_{n-1}^j \end{bmatrix} \quad (1.47)$$

The procedures of constructing a ST code from cyclic division algebras can be summarized by the following steps:

- In order to construct a ST code over a complex alphabet, the first step consists of the choice of a quadratic field extension  $\mathbb{F}$  of  $\mathbb{Q}$  such that  $\mathcal{S} \subset \mathbb{F}$ .  $\mathbb{F}$  constitutes the center of the algebra  $\mathcal{A}$ .
- Choose the maximal subfield  $\mathbb{K}$  of degree  $n$  over  $\mathbb{F}$  such that  $\mathbb{K}$  is Galois over  $\mathbb{F}$  and  $Gal(\mathbb{K}/\mathbb{F})$  is cyclic.
- Choose a value of  $\gamma$  that verifies proposition 1.2. Such an element will be referred to as a “non-norm” element in the sequential.

The constructed ST block-code will have the following properties:

- The constructed code has a full rate. From eq. (1.47),  $n^2$  symbols are included in a codeword occupying  $n$  symbol durations resulting in a rate of  $n$  symbols PCU.
- The constructed code is fully diverse. This results from the fact that a non-norm element  $\gamma$  results in a division algebra and thus the difference between any two distinct codewords (which is always isomorphic to an element of  $\mathcal{A}$ ) has full rank.

In [39, 59], a family of ST codes based on transcendental extensions and respecting the three above mentioned construction constraints was proposed. In this work,  $\mathbb{F}$  was chosen as:  $\mathbb{F} = \mathbb{Q}(s, t, \omega_n)$ . The authors proved that the extension  $\mathbb{K} = \mathbb{F}(t_n = t^{\frac{1}{n}})$  is cyclic for any transcendental number  $t$ . As for the choice of  $\gamma$ , any transcendental number can be chosen. The generator of the Galois group is given by  $\sigma : t_n \rightarrow \omega_n t_n$ . The code  $B_{2,\phi}$  in eq. (1.41) follows as a special case of this generic construction procedure when  $n = 2$ . The  $2 \times 2$  codewords constructed from [39, 59] can be expressed as ( $\sigma(t_2) = -t_2$ ):

$$C = \frac{1}{\sqrt{2}} \begin{bmatrix} s_1 + t^{\frac{1}{2}}s_2 & s_3 + t^{\frac{1}{2}}s_4 \\ \gamma(s_3 - t^{\frac{1}{2}}s_4) & s_1 - t^{\frac{1}{2}}s_2 \end{bmatrix} \equiv \frac{1}{\sqrt{2}} \begin{bmatrix} s_1 + t^{\frac{1}{2}}s_2 & \gamma^{\frac{1}{2}}(s_3 + t^{\frac{1}{2}}s_4) \\ \gamma^{\frac{1}{2}}(s_3 - t^{\frac{1}{2}}s_4) & s_1 - t^{\frac{1}{2}}s_2 \end{bmatrix} \quad (1.48)$$

where  $\gamma$  and  $t$  are any transcendental numbers and the equivalence follows from the fact that the two matrix forms have the same determinant. Fixing  $t = \gamma^2$  results in  $B_{2,\phi}$  given in eq. (1.41) (with  $\phi = t^{\frac{1}{2}} = \gamma$ ). Among all transcendental numbers, the ones verifying  $t = \exp(i\lambda)$  with  $\lambda$  algebraic are appealing since in this case  $|t| = 1$  resulting in the same average energy per transmit antenna.

While all transcendental elements can be associated with any cyclic field  $\mathbb{K}$ , it was pointed out in [60] that it is more interesting to choose  $\gamma$  to be an algebraic integer. In fact, if  $\gamma$  and the information symbols are taken from the ring of integers of  $\mathbb{F}$  (for example  $\mathbb{Z}[i]$  for QAM constellations and  $\mathbb{Z}(\omega_3)$  for HEX constellations). Then, from proposition 1.1, it follows that the set  $\{\det(C) ; C \in \mathcal{C}_S\}$  is a discrete set of  $\mathcal{O}_{\mathbb{F}}$ . Therefore,  $\min_{C \neq \mathbf{0}_{n \times n}} |\det(C)| \geq 1$ . This results in a non-vanishing determinant (NVD). In other words, the coding gain does not decrease with the size of the constellation. Moreover, since the information vector  $[1, \mathbf{0}_{1 \times (n^2-1)}] \in \mathcal{O}_{\mathbb{F}}^{n^2}$  for different constellation sizes and since for this information vector  $\det(C) = 1$ , then the NVD property implies that:

$$\delta_C = \min_{C \in \mathcal{C}_S ; C \neq \mathbf{0}_{n \times n}} |\det(C)| = 1 \quad \forall S \subset \mathcal{O}_{\mathbb{F}} \quad (1.49)$$

The NVD is a very interesting property over Rayleigh fading channels. In fact, codes with a NVD achieve the optimal diversity-multiplexing tradeoff of the underlying multi-antenna channel [49].

In some cases,  $\mathbb{F}$  can be simply the infinite field containing  $s$ . For example,  $\mathbb{F} = \mathbb{Q}(i)$  if  $S$  is a QAM constellation and  $\mathbb{F} = \mathbb{Q}(\omega_3)$  if  $S$  is a HEX constellation.

For example, with  $n = 2$  transmit antennas and QAM constellations [60],  $\mathbb{F} = \mathbb{Q}(i)$  and  $\mathbb{K} = \mathbb{Q}(\omega_8)$  is cyclic over  $\mathbb{F}$  (with degree 2). Any transcendental number  $\gamma$  results in a fully diverse code. However,  $\gamma = 2 + i \in \mathcal{O}_{\mathbb{F}} = \mathbb{Z}[i]$  is a non-norm element and it results in a NVD. In fact, the ideal  $5\mathcal{O}_{\mathbb{K}}$  factorizes as  $5\mathcal{O}_{\mathbb{K}} = I_1 I_2$  where  $I_1$  and  $I_2$  are the principal ideals generated by  $2 + i$  and  $2 - i$  respectively showing that the ideal  $I_1$  is prime and consequently there is no element in  $\mathbb{K}$  whose norm is equal to  $\gamma = 2 + i$ . The same procedure was generalized in [61] for  $n = 2^k$  and  $n = 3 \cdot 2^k$  transmit antennas with QAM constellations where it was shown that the extension  $\mathbb{Q}(\omega_{2^{k+2}})/\mathbb{Q}(i)$  is always cyclic and  $\gamma = 2 + i$  is a non-norm element. In the same way, systems with  $n = 3^k$  or  $n = 2 \cdot 3^k$  transmit antennas were associated

with HEX constellations [60, 61]. In this case, the field extension  $\mathbb{Q}(\omega_{3^{k+1}})/\mathbb{Q}(\omega_3)$  is always cyclic and  $\gamma = 3 + \omega_3$  is a non-norm element.

In other cases,  $\mathbb{F}$  must be obtained by adjoining an algebraic element to the infinite field containing  $s$  in order to have a cyclic extension (this element does not belong to the infinite field containing  $s$ ). For example, for  $n = 3$  transmit antennas with QAM constellations,  $\omega_3$  must be adjoined to  $\mathbb{Q}(i)$  resulting in  $\mathbb{F} = \mathbb{Q}(i, \omega_3)$ . In this case,  $\mathbb{F}(\omega_9)/\mathbb{Q}(i)$  is cyclic [39].

In [49], cyclic extensions of QAM (or HEX) constellations were proposed for different numbers of transmit antennas. Moreover, finding a non-norm element was shown to be equivalent to finding a prime ideal of  $\mathcal{O}_{\mathbb{F}}$  that remains inert in  $\mathcal{O}_{\mathbb{K}}$ . Non-norm elements were found for all values of  $n$ .

## Perfect Codes

The perfect codes [63, 64] are based on cyclic division algebras. However, two additional constructing constraints are added to the constraints of codes from cyclic division algebras. Namely:

- $\mathbb{K}/\mathbb{F}$  must be cyclic (refer to the previous subsection).
- $\gamma$  must be an algebraic non-norm integer (refer to the previous subsection).
- $|\gamma|$  must be equal to 1 in order to have a uniform average transmitted energy per antenna.
- Good shaping of the constellation. This means that the transmitted entries on each layer of the codeword must be a rotation of the initial (QAM or HEX) signal set. In eq. (1.47), the elements of each layer can be viewed as taken from a lattice  $R\mathbb{Z}[i]^n$  (or  $R\mathbb{Z}(\omega_3)^n$ ). In order not to introduce any shaping losses, this lattice must be isometric to  $\mathbb{Z}[i]^n$  (or  $\mathbb{Z}(\omega_3)^n$ ). In other words, the generator matrix  $R$  must be unitary.

The perfect codes were constructed for  $n = 2, 3, 4, 6$  transmit antennas and were associated with QAM for  $n = 2, 4$  and HEX for  $n = 3, 6$  [64]. These codes satisfy a large number of hard to achieve criteria and show the best performance among all the existing ST block codes. The  $2 \times 2$  perfect code is also known as the Golden code and it is based on the Golden number  $\frac{1+\sqrt{5}}{2}$  [63].

The codewords of a  $n \times n$  perfect code can be expressed as [64]:

$$P = DC(s_1, \dots, s_{n^2}) \quad (1.50)$$

$$= \text{diag}(\alpha, \sigma(\alpha), \dots, \sigma^{n-1}(\alpha)) C(s_1, \dots, s_{n^2}) \quad (1.51)$$

where  $D$  is a  $n \times n$  diagonal matrix and  $C(s_1, \dots, s_{n^2})$  is the codeword constructed from cyclic division algebras in eq. (1.47).  $\alpha \in \mathcal{O}_{\mathbb{F}}$  and the volume of the fundamental parallelopiped of the lattice  $\Lambda(I = \alpha \mathcal{O}_{\mathbb{K}})$  must verify:

$$\text{vol}(\Lambda(I)) = 2^{-n} \sqrt{|d_{\mathbb{K}/\mathbb{Q}}|} N_{\mathbb{K}/\mathbb{Q}}(I) = \begin{cases} c^n, & \text{for QAM constellations} \\ c^n \left(\frac{\sqrt{3}}{2}\right)^n, & \text{for HEX constellations} \end{cases} \quad (1.52)$$

where  $d_{\mathbb{K}/\mathbb{Q}}$  is the absolute discriminant of  $\mathbb{K}$ . Based on eq. (1.50) and eq. (1.52), the coding gain of the perfect codes with any QAM or HEX constellation can be expressed as:

$$\delta_P = \min_{P \neq \mathbf{0}_{n \times n}} |\det(D) \det(C)| = |\det(D)| = |N_{\mathbb{K}/\mathbb{F}}(\alpha)| = |N_{\mathbb{K}/\mathbb{Q}}(\alpha)|^{\frac{1}{2}} = d_{\mathbb{K}/\mathbb{F}}^{-\frac{1}{2}} \quad (1.53)$$

Multiplying the codewords constructed from cyclic division algebras by the diagonal matrix  $D$  in eq. (1.50) is equivalent to limiting the construction in the ideal  $I = \alpha\mathcal{O}_{\mathbb{K}}$ . In this case, the integral basis  $\{\theta^j\}_{j=0}^{n-1}$  is replaced by the  $\mathbb{F}$ -basis of  $I$  given by  $\{\alpha\theta^j\}_{j=0}^{n-1}$ . If this basis is not unitary, an appropriate change of basis is performed in order to construct a new orthogonal basis  $\{v_j\}_{j=0}^{n-1}$ . The new codewords are obtained by replacing  $\{\theta^j\}_{j=0}^{n-1}$  with  $\{v_j\}_{j=0}^{n-1}$  in eq. (1.47).

For example, the Golden code is constructed over the integral basis of  $\mathbb{Q}(i, \sqrt{5})/\mathbb{Q}$  given by  $\mathcal{O}_{\mathbb{K}} = \mathbb{Z}(i, \theta)$  where  $\theta$  is the Golden number. For QAM constellations, the codewords are given by [63]:

$$G = \frac{1}{\sqrt{5}} \begin{bmatrix} \alpha & 0 \\ 0 & \sigma(\alpha) \end{bmatrix} \begin{bmatrix} s_1 + \theta s_2 & s_3 + \theta s_4 \\ \gamma(s_3 + \theta_1 s_4) & s_1 + \theta_1 s_2 \end{bmatrix} \quad (1.54)$$

where  $\theta_1 = \sigma(\theta) = \frac{1-\sqrt{5}}{2}$  and  $\alpha = 1 + i(1 - \theta)$ . The elements of each layer belong to the lattice  $R\mathbb{Z}[i]$  where the generator matrix  $R$  is given by:

$$R = \begin{bmatrix} \alpha & \alpha\theta \\ \sigma(\alpha) & \sigma(\alpha)\theta_1 \end{bmatrix} \quad (1.55)$$

Since  $RR^H = I_2$ , the code has good shaping. The uniform average transmitted energy per antenna is assured by choosing  $\gamma = i$  (which is a non-norm element over  $\mathcal{O}_{\mathbb{K}}$ ). An equivalent version of the Golden code was proposed in [66]. This code can be related to the Golden code by  $D_1GD_2$  for two diagonal and unitary matrices  $D_1$  and  $D_2$ . The code in [66] was obtained by numerically optimizing the coding gain and it shows the same performance as the Golden code.

Since  $\gamma$  must belong to  $\mathbb{Z}[i]$  or  $\mathbb{Z}(\omega_3)$  with  $|\gamma| = 1$ , then  $\gamma$  can take one of the values in the set  $\{-1, \pm i, \pm\omega_3, \pm\omega_3^2\}$ . The authors of [64] observed that none of the elements of this set results in a cyclic division algebra for  $n = 5$  showing the non-existence of perfect codes with 5 transmit antennas. Moreover, let  $x$  be any element of this set, we have  $x^6 = 1$  showing the non-existence of perfect codes for  $n > 6$  antennas.

Recently, perfect ST codes with any number of transmit antennas were proposed by Elia *et al.* in [65]. In a previous work [49], the authors were able to find appropriate cyclic extensions of  $\mathbb{Q}(i)$  (or  $\mathbb{Q}(\omega_3)$ ) and appropriate non-norm elements in these fields for all values of  $n$ . Writing this non-norm element as  $a + bi$  (or  $a + \omega_3 b$ ). In [65], the authors showed that  $\gamma = \frac{a+bi}{b+ai}$  (or  $\frac{a+b\omega_3}{b+a\omega_3}$ ) is also a non-norm element. Since  $|\gamma| = 1$ , this choice along with an appropriate construction of a unitary ideal generator matrix results in perfect codes.

### Lattice Space-Time codes

In [67], El Gamal *et al.* proposed a lattice-based construction for full-rate ST block codes. This construction is referred to as the generalized mod- $\Lambda$  scheme. Unlike the above mentioned coding constructions that are based on optimizing the coding gain, the mod- $\Lambda$  scheme has no space-time structure. Designate by  $x$  a  $m = 2PT$ -dimensional vector obtained from the vertical concatenation of the real and imaginary parts of the columns of the  $P \times T$  codewords. Let  $\Lambda_c$  be a lattice in  $\mathbb{R}^m$  and  $\Lambda_s$  a sublattice of  $\Lambda_c$ . The transmitted vectors  $x$  are determined from a dither vector  $u$  and from vectors  $c$  that belong to the nested lattice defined by the partition of  $\Lambda_c/\Lambda_s$  and given by  $\mathcal{C} = \Lambda_c \cap \mathcal{V}_s$  where  $\mathcal{V}_s$  is the fundamental Voronoi cell of  $\Lambda_s$ . The nested lattice  $\Lambda_s \subset \Lambda_c$  is drawn from an ensemble of lattices that are good for covering

and consequently good for MSE quantization. The encoding scheme is defined by:

$$x = (c - u) \mod \Lambda_s \quad (1.56)$$

$$= (c - u) - \operatorname{argmin}_{\lambda \in \Lambda_s} |(c - u) - \lambda| \quad (1.57)$$

where  $c$  is randomly selected from  $\mathcal{C}$  and  $u$  is known at the receiver side. The receiver consists of a MMSE-DFE estimator followed by a lattice decoder where the boundaries of the lattice are disregarded when determining the closest lattice point to a certain received point. Designate by  $F$  and  $B$  the forward and feedback filter matrices respectively, the decoder decides in the favor of  $\hat{c}$  such that:

$$\hat{c} = G\hat{z} \mod \Lambda_s ; \hat{z} = \operatorname{argmin}_{z \in \mathbb{Z}^m} |Fy + Bu - BGz|^2 \quad (1.58)$$

where  $y$  is the received vector and  $G$  is the generator matrix of the lattice  $\Lambda_c$ . The authors showed that the association of the nested-lattice structure, the random dither and the MMSE-DFE lattice decoding permits to achieve the optimal diversity-multiplexing tradeoff for  $T \geq P + Q - 1$  ( $Q$  is the number of receive antennas). In comparison with the Gaussian coding ensembles (that achieve the D-MG tradeoff for  $T \geq P + Q - 1$  as shown in [49]), the mod- $\Lambda$  scheme has a simple encoding and decoding structure. Moreover, storing the whole codebook is not required at the transmitter side and the exhaustive search at the receiver is replaced by a lattice decoder.

### 1.3.5 Cooperative Diversity

In many situations, profiting from the spatial diversity by employing antenna arrays can be infeasible especially for small mobile or sensor nodes. In such situations, the terminals of a wireless network can cooperate with each other in order to profit from the spatial diversity in a distributed manner by forming a virtual antenna array [68–74]. Consider a wireless network composed of a certain number of half-duplex terminals that can either transmit or receive at a certain time (but not both). Moreover, suppose that each terminal is equipped with a single antenna. In cooperative networks, the neighboring nodes can help a certain source in delivering its message to its corresponding destination. Such nodes behave as relays for the communication between the source and the destination.

In general, the cooperation protocols can be classified as amplify-and-forward (AF) or decode-and-forward (DF). In the first case, the relays simply transmit scaled versions of their corresponding received signals. In the DF mode, each relay can decode the messages of the source and then re-encodes them with a possibly different codebook. In general, the DF schemes outperform the AF schemes at the expense of an increased complexity [73]. In many situations, the quality of the channel between the source and a certain relay can be bad. In this case, it might be better for the source to continue its direct transmission with no relaying. This is referred to as selective-relaying [70] where a relay cooperates with the source only if the quality of the channel between the source and this relay falls above a certain threshold. The quality of this channel can be measured by the magnitude of the channel coefficient [70] or by the mutual information between the source and the relay [73].

In [70], AF and DF schemes were proposed where the source and the relay transmit on orthogonal subspaces. These subspaces can be the different time slots in a TDMA network or the orthogonal spreading sequences in a CDMA network. Later this DF strategy was extended to the case of more than one relay in [71]. Another protocol, referred to as a space-time coded protocol, was also proposed in [71]. In this case, all the relays can transmit simultaneously but their transmissions take place over a signal

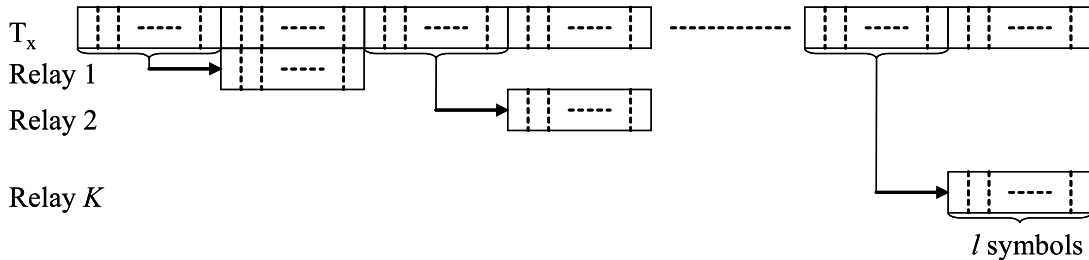


Figure 1.3: The NAF protocol with  $K$  relays.

subspace that is orthogonal to the signal subspace of the source. The non-orthogonal AF protocol (NAF) proposed in [73] outperforms all of the existing AF protocols [70, 71]. The superiority of the NAF protocol follows from the fact that the transmissions of the source and the cooperating relays take place in the same signal subspace. In this case, the continuous transmission of the source enhances the multiplexing gain of the NAF protocol while the cooperation enhances the diversity advantage [73].

The NAF protocol with  $K$  relays is described in Fig. 1.3. The cooperation is periodic with a period of  $2Kl$  symbol durations. The cooperation period is divided into  $2K$  frames each composed of  $l$  symbols. The  $k$ -th relay retransmits an amplified version of the  $(2k-1)$ -th frame during the  $2k$ -th frame duration (Fig. 1.3). The diversity-multiplexing tradeoff of the NAF scheme with  $K$  relays is given by [73]:

$$d(r) = (1 - r) + K \max\{0, (1 - 2r)\} \quad (1.59)$$

Equation (1.59) shows that the NAF protocol achieves full diversity ( $d(0) = K + 1$  corresponds to the diversity advantage of an antenna array with  $K + 1$  antennas). The authors of [73] showed that the diversity-multiplexing tradeoff in eq. (1.59) can be achieved by using random Gaussian codebooks with a sufficiently large codeword length.

Block codes for the NAF protocol were proposed in [74] and were shown to achieve the D-MG tradeoff given in eq. (1.59). For these minimal-delay codes, the length of each frame in the NAF scheme is  $l = 2$ . This construction is based on cyclic division algebras. Let  $\mathbb{P} = \mathbb{Q}(i)$  and  $\mathbb{P} = \mathbb{Q}(j)$  for QAM and HEX constellations respectively. Designate by  $\mathbb{K} = \mathbb{P}(\theta)$  a  $K$ -dimensional field extension of  $\mathbb{P}$  whose Galois group is  $\text{Gal}(\mathbb{K}/\mathbb{P}) = \langle \sigma \rangle$  with  $\sigma^K = 1$ . In the same way, let  $\mathbb{F} = \mathbb{K}(\phi) = \mathbb{P}(\theta, \phi)$  whose Galois group is  $\langle \tau \rangle$ . Designate by  $C_1, \dots, C_K$  the  $2 \times 2$  matrices given by:

$$C_k = \sigma^{k-1} \begin{bmatrix} \sum_{j=0}^{K-1} (s_j + \phi s_{K+j}) \theta^j & \sum_{j=0}^{K-1} (s_{2K+j} + \phi s_{3K+j}) \theta^j \\ \gamma \sum_{j=0}^{K-1} (s_{2K+j} + \tau(\phi) s_{3K+j}) \theta^j & \sum_{j=0}^{K-1} (s_j + \tau(\phi) s_{K+j}) \theta^j \end{bmatrix} \quad (1.60)$$

where  $s_0, \dots, s_{4K-1}$  are the information symbols and  $\gamma \in \mathbb{K}$  verifies the condition that there are no elements in  $\mathbb{F}$  whose norm are equal to  $\gamma^t$  for  $t = 1, \dots, 2K - 1$  resulting in a cyclic division algebra.

The first and second rows of  $C_k$  in eq. (1.60) correspond to the signals transmitted from the source during the  $2k$ -th and the  $(2k-1)$ -th frames respectively. The  $k$ -th relay transmits an amplified version of the received signal corresponding to the second row of  $C_k$  for  $k = 1, \dots, K$ . Note that all of the  $4K$  information symbols must be included in  $C_k$  for all values of  $k$  in order to achieve full diversity. Moreover,  $4K$  symbols are transmitted during  $2K$  frames each consisting of  $l = 2$  symbols resulting in no data rate loss with respect to non-cooperative systems.

As in [64], since  $s_j \in \mathcal{O}_{\mathbb{P}}$  for  $j = 0, \dots, 4K - 1$  (QAM or HEX symbols), limiting  $\gamma \in \mathcal{O}_{\mathbb{K}}$  results in a non-vanishing determinant. Moreover,  $\gamma$  is chosen to verify  $|\gamma| = 1$  resulting in a uniform energy per

relay. In the same way, the integral basis  $\{1, \dots, \theta^{K-1}, \phi, \dots, \phi\theta^{K-1}\}$  can be replaced by an orthogonal basis resulting in no shaping losses. For example, the Golden code [63] can be used with  $K = 1$  relay ( $\mathbb{K} = \mathbb{Q}(i)$  and  $\mathbb{F} = \mathbb{K}(\sqrt{5})$ ). For  $K = 2$  relays,  $\mathbb{P} = \mathbb{Q}(i)$ ,  $\mathbb{K} = \mathbb{P}(\omega_{16})$  and  $\mathbb{F} = \mathbb{K}(\sqrt{5})$  where  $\omega_m$  is the  $m$ -th root of unity. In this case,  $\gamma = \omega_{16}$  results in full diversity. Note that these codes are constructed based on the design criteria of ST codes with co-located antenna arrays. It was shown in [72] that these criteria still hold for virtual arrays.

## 1.4 MIMO-UWB communication systems

In the recent years, there was a great interest in beamforming with IR-UWB (refer to [75] and the references therein). In such systems, an adaptive antenna array can result in highly directive beam patterns. The very fine temporal resolution of the UWB pulses results in very narrow main lobes that are capable of limiting the interference even from radio terminals that are very close to the desired transmitter. For the positioning and imaging applications, the fine angular and temporal resolutions permit to differentiate between closely spaced targets [76].

Another active research area includes the multi-antenna UWB techniques. MIMO techniques can be a possible solution for overcoming the very low tolerated transmission levels [2] resulting in enhanced data rates, communication ranges and quality of service. MIMO-UWB systems profit from SNR improvements, higher channel capacities [77] and better interference rejection [78]. However, given the important multi-path diversity of the UWB channels, the utility of an additional spatial diversity may be questionable. In fact, the large frequency band occupied by the UWB signals makes them not very sensitive to deep notches that can occur in any part of the spectrum. Deeper discussions on the utility of the multi-antenna techniques with UWB systems will be the main subject of the next chapter.

The absence of a carrier frequency is the very fundamental character that differentiates impulse radio from narrow-band applications, wideband DSSS-CDMA, MC-CDMA and OFDM. This has a direct impact on the design and the performance of the ST codes that must be used in conjunction with IR-UWB. Given that IR-UWB transmissions must be totally-real, the complex-valued ST codes can not be applied with IR-UWB (in particular the Golden code and the perfect codes). This is a very limiting constraint. In fact, except for [79] (to the author's knowledge), full-rate and fully diverse ST coding with IR-UWB was never considered elsewhere. In the literature of UWB, multi-antenna systems were used exclusively to enhance the overall diversity with no data rate enhancement [80–83]. Another approach was the spatial multiplexing where independent data flows are transmitted simultaneously from the transmit antennas resulting in enhanced data-rates with no transmit diversity advantage [84, 85]. In the remaining parts of this section, we will briefly discuss the most relevant contributions in MIMO-UWB communications.

### 1.4.1 Space-Hopping with IR-UWB

In [79], a space-hopping (SH) scheme was proposed for IR systems. For a system equipped with  $P$  transmit antennas, different TH sequences are associated with each one of the transmit antennas. In order to achieve a rate of  $P$  symbols PCU,  $P$  PPM modulated symbols are transmitted during one symbol duration which is composed of  $N_f$  time frames (eq. (1.9)). Suppose that  $P$  divides  $N_f$  and let  $P' = \frac{N_f}{P}$ . Designate by  $d_1, \dots, d_P \in \{0, \dots, M - 1\}$  the positions of the  $P$  symbols taken from a  $M$ -ary PPM

constellation. The coding scheme can be determined from the following  $P \times P$  matrix:

$$C_{p'} = \begin{pmatrix} w(t - d_1) & w(t - d_2) & \cdots & w(t - d_P) \\ w(t - d_P) & w(t - d_1) & \ddots & \vdots \\ \vdots & \ddots & \ddots & w(t - d_2) \\ w(t - d_2) & \cdots & w(t - d_P) & w(t - d_1) \end{pmatrix} \quad (1.61)$$

where  $w(t)$  is the pulse waveform and the  $(i, j)$ -th element of  $C_{p'}$  corresponds to the pulse transmitted from the  $i$ -th transmit antenna during the  $((p' - 1)P' + j)$ -th frame duration for  $p' = 1, \dots, P'$ . In other words, the coding scheme is determined from the  $P \times N_f$  matrix  $C = [C_1 \ \cdots \ C_{P'}]$ . In order to avoid the interference between the elements of the same column of  $C_{p'}$ , different TH sequences are associated with the transmit antennas. Moreover, for a given time frame, the time shifts introduced at the different antennas must be all different. From eq. (1.61), the information symbols are interleaved over the transmit antennas resulting in a full diversity advantage.

However, SH was considered uniquely over flat fading channels [79]. The advantages of this scheme are exclusive to this kind of channels. In fact, for flat-fading channels, the orthogonality between the received signals is assured by having at least  $P$  chips of duration  $T_c$  in each time frame ( $T_f \geq PT_c$  in eq. (1.9)). On the other hand, over frequency selective channels, we must have  $T_f \geq P\Gamma$  where  $\Gamma$  is the channel delay spread of the UWB channels. Given that  $\Gamma \gg T_c$ , the orthogonality over UWB channels can be achieved at the expense of larger time frames (approximately  $P$  times larger than that of single-antenna systems). As a conclusion, the proposed system performs well over flat fading channels while the diversity advantage can be lost over frequency selective channels because the multi-path propagation can break down the orthogonality between the transmitted data streams.

### 1.4.2 Coherent Rate-1 Space-Time codes for IR-UWB

In [81], Giannakis *et al.* introduced a diversity scheme that achieves full spatial and multi-path diversity with two transmit antennas while transmitting at a rate of 1 symbol PCU. Unlike the Alamouti code [44] that encodes two adjacent symbols, the proposed scheme encodes the  $N_f$  pulses of the same information symbol.

For a peer-to-peer communication with 2-PAM constellations, the transmitted signals corresponding to the information symbol  $s$  are given by [81]:

$$s_1(t) = s \sqrt{\frac{E_s}{2N_f}} \sum_{n=0}^{N_f-1} (-1)^n w(t - nT_f) \quad (1.62)$$

$$s_2(t) = s \sqrt{\frac{E_s}{2N_f}} \sum_{n=0}^{N_f-1} w(t - nT_f) \quad (1.63)$$

where  $s_p(t)$  corresponds to the signal transmitted from the  $p$ -th antenna and  $s \in \{\pm 1\}$  is the information symbol.

For a system with one receive antenna, designate by  $g_p(t)$  the impulse response of the channel from the  $p$ -th transmit antenna. Define  $h_p(t)$  as the convolution of  $g_p(t)$  with  $w(t)$ . The conditional bit error rate using a  $L$ -th order Rake receiver can be expressed as:

$$P(e | \{\alpha_1(l), \alpha_2(l)\}_{l=1}^L) = Q \left( \left[ \frac{\rho}{2} \sum_{l=1}^L (\alpha_1^2(l) + \alpha_2^2(l)) \right]^{\frac{1}{2}} \right) \quad (1.64)$$

where  $\rho$  is the signal to noise ratio.  $\alpha_p(l) = \int h_p(t)w(t - \Delta(l))dt$  and  $\{\Delta(l)\}_{l=1}^L$  are the delays of the Rake fingers chosen to verify  $|\Delta(l) - \Delta(l-1)| \geq 2T_w$  resulting in  $E [\alpha_p(l)\alpha_{p'}(l')] = \beta_l\delta(l-l')\delta(p-p')$ .  $\beta_l = E [\alpha_p^2(l)]$  and it is independent from  $p$  for independent and identically distributed channel impulse responses.

The channel model considered in [81] is the SV model [21] with Rayleigh fading on the multi-path components. Given the nature of the carrier-less transmissions and the associated homodyne receivers, only the real parts of the multi-path components (which have a Gaussian distribution) are considered. Based on this model, the impulse responses can be expressed as:  $g_p(t) = \sum_{l'=0}^{L_p-1} a_{p,l'}\delta(t - \tau_{p,l'})$  where  $L_p$  is the total number of multi-path components of  $g_p(t)$ .  $\tau_{p,l'}$  and  $a_{p,l'}$  are the arrival times and the amplitudes of the multi-path components of the  $p$ -th channel with  $a_{p,l'}$  having a Gaussian distribution. Now  $\alpha_p(l)$  is given by:

$$\alpha_p(l) = \sum_{l'=0}^{L_p-1} a_{p,l'}R_w(\Delta(l) - \tau_{p,l'}) \quad (1.65)$$

where  $R_w(t)$  is the autocorrelation function of  $w(t)$ .

Being the sum of Gaussian random variables,  $\alpha_p(l)$  is also a Gaussian random variable for  $p = 1, 2$  and  $l = 1, \dots, L$ . In this case, the Chernoff bound can be determined from the conditional error probability in eq. (1.64) as follows [81]:

$$P(e) \leq \left[ \frac{\rho}{2} \left( \prod_{l=1}^L \beta_l \right)^{\frac{1}{L}} \right]^{-L} \quad (1.66)$$

On the other hand, the BER of a single-antenna system verifies  $P(e) \leq \left( \rho \left( \prod_{l=1}^L \beta_l \right)^{\frac{1}{L}} \right)^{-\frac{L}{2}}$ . Therefore, the proposed system achieves full diversity since the diversity advantage is doubled (it passes from  $\frac{L}{2}$  to  $L$ ). Note that, for  $L = 1$ , the BER with Gaussian fading decays as  $\rho^{-\frac{1}{2}}$  (for large values of  $\rho$ ) unlike the Rayleigh channels where the BER decays as  $\rho^{-1}$ .

Note that the proposed system is equivalent to the Alamouti code [44]. While the Alamouti code is an orthogonal design that encodes adjacent symbols, the system in [81] takes advantage of the pulse repetitions in order to introduce orthogonality among the transmitted data streams. A similar encoding and decoding scheme was proposed in [80] for  $M$ -PPM modulations over flat fading channels.

In an independent work, the authors of [82, 83] determined the performance of TH and DSSS multi-antenna systems using the Alamouti code over Nakagami-faded multi-path channels. It was shown in [83] that for independent Nakagami- $m$  fading coefficients with  $P$  transmit antennas,  $Q$  receive antennas and a  $L$ -finger Rake, the total diversity advantage is equal to  $\tilde{m}PQL$  where  $\tilde{m} = Pm(Pm - m + 1)^{-1}$ . Note that for Gaussian (resp. Rayleigh) fading channels the maximal diversity order is  $\frac{1}{2}PQL$  (resp.  $PQL$ ).

### 1.4.3 Non-coherent Rate-1 Space-Time codes for IR-UWB

As an extension of their coherent rate-1 ST code, Giannakis *et al.* [81] proposed a non-coherent multi-antenna scheme that can be associated with 2-PPM modulations. The proposed system is based on energy integration and does not require any channel estimation procedure. Keeping the same notations

as in Section 1.4.2, the transmitted signals take the form:

$$s_1(t) = \sqrt{\frac{E_s}{2N_f}} \sum_{n=0}^{N_f-1} (-1)^n w(t - nT_f - s\delta) \quad (1.67)$$

$$s_2(t) = \sqrt{\frac{E_s}{2N_f}} \sum_{n=0}^{N_f-1} w(t - nT_f - s\delta) \quad (1.68)$$

where  $s \in \{0, 1\}$  indicates the position of the modulated symbol and  $\delta$  is chosen to be larger than the channel delay spread in order to avoid the interference among the modulation positions (this interference can not be mitigated with energy detectors).

Designate by  $x_e^{(m)}(l)$  (resp.  $x_o^{(m)}(l)$ ) the sum over the  $\frac{N_f}{2}$  even (resp. odd) time frames of the outputs of the  $l$ -th Rake finger during the  $m$ -th position. The corresponding decision vector is given by:

$$x^{(m)}(l) = \begin{bmatrix} x_e^{(m)}(l) \\ x_o^{(m)}(l) \end{bmatrix} = \sqrt{\frac{N_f E_s}{8}} \begin{bmatrix} \alpha_1(l) + \alpha_2(l) \\ \alpha_1(l) - \alpha_2(l) \end{bmatrix} \delta(s-m) + \begin{bmatrix} n_e(l) \\ n_o(l) \end{bmatrix} \quad (1.69)$$

Let  $z^{(m)} = \sum_{l=1}^L (x^{(m)}(l))^T x^{(m)}(l)$ , the receiver decides in the favor of the position  $\hat{m}$  such that:

$$\hat{m} = \arg \max_{m \in \{0,1\}} (z^{(m)}) \quad (1.70)$$

In the absence of noise,  $z^{(m)} = \frac{N_f E_s}{2} \sum_{l=1}^L (\alpha_1^2(l) + \alpha_2^2(l)) \delta(s-m)$  has the same value as with coherent systems implying that the non-coherent ST scheme still profits from full transmit and multi-path diversity.

#### 1.4.4 Spatial Multiplexing with IR-UWB

For a system equipped with  $P$  transmit antennas, spatial multiplexing (SM) is a simple way for multiplying the data-rate by  $P$  without profiting from any transmit diversity. SM for IR-UWB was considered in [84] with 2-PAM constellations and correlation receivers (refer to Section 1.1.6). The considered channel model was the Kunisch-Pamp model [22, 23]. As explained in Section 1.1.5, the cross-correlations between the entire channel impulse responses are very small. In other words, correlation receivers using filters matched to the entire channel response result in very limited co-channel interference. This results in better performance with respect to narrow band systems [84].

A similar approach was adopted in [85] with 2-PAM constellations, Rake receivers and MMSE detectors. A tapped delay line channel model was adopted. For a  $P \times Q$  MIMO system, the  $PQ$  channels are drawn randomly according to the IEEE channel model recommendation [17]. At a second time, correlations between the antennas are introduced by applying the Kronecker model where the MIMO channel covariance matrix is determined from the Kronecker product of the channel covariance matrices at the transmitter and the receiver sides. Even though a tapped delay line model is not accurate for UWB channels (refer to Section 1.1.5), this formulation gives more insights on the effect of spatial correlation on the system performance. Results showed that, at high data rates, TH-UWB systems have better performance than DSSS-UWB systems that suffer from excessive inter-chip interference. Moreover, a spatial correlation factor of 0.5 (at both the transmitter and the receiver) introduces a limited performance loss of about 0.5 dB at a BER of  $10^{-4}$  with a  $2 \times 2$  MIMO-TH-UWB system having a data rate of 748.5 Mbps.

### 1.4.5 MIMO-UWB systems using orthogonal pulses

In IR-UWB, an additional degree of freedom resides in the possibility of transmitting several orthogonal pulses simultaneously. An example of a family of orthogonal pulses is the modified Hermite pulses (refer to Section 1.1.2). For single-antenna systems, associating position, amplitude and shape modulations results in high data rates [86]. For MIMO systems where the channel estimation is more challenging, orthogonal pulses were used for enhancing the channel estimation and detection [87, 88]. In particular, two orthogonal pulses (the Gaussian pulse and its first derivative), destined for the channel estimation and data transmissions, are transmitted simultaneously.

## 1.5 Thesis outline and contributions

The remaining part of this work is organized as follows:

- In chapter 2, we present a generic system model for multi-antenna TH-UWB systems. This model takes into account the possibility of having inter symbol interference (ISI) and multi-user interference (MUI). Moreover, this system model, that will be considered throughout the remaining parts of this work, is associated with different kinds of practical receivers that achieve different compromises between performance and complexity. We then propose a new rate-1 ST coding scheme that is based on inter pulse coding and that can be associated with any number of transmit antennas. The performance of this coded system as well as that of uncoded MIMO systems is then determined over the IEEE 802.15.3a channel model recommendations [17]. The performance is measured by the achieved error rates as well as the achieved diversity-multiplexing tradeoffs. Finally, we present a new design of the low-dimensional amplitude spreading matrices that are associated with the pulses used to transmit a given information symbol. This design permits to reduce the level of MUI in multiple access channels.
- In chapter 3, we present new full rate ST coding constructions that can be associated with carrier-less TH-UWB systems. While carrier-less UWB systems were considered uniquely with rate -1 totally-real ST codes in the literature, the proposed ST codes are the first proposed schemes that have full rate and that satisfy a large number of constraints that are difficult to achieve. Different families of codes are presented. We discuss the constructions from cyclic division algebras, intra-symbol coding, joint inter-symbol and intra-symbol coding. We also present novel diversity schemes that follow from the association of Hermite pulses with modulation diversity. For the first time, we introduce new families of ST codes that can be exclusive to PPM and to PPAM and that outperform all “classical” constructions based on cyclic division algebras.
- In chapter 4, the principles used in chapter 3 for the construction of ST codes are extended to the cooperative TH-UWB systems. While cooperation was never studied in the UWB context, the proposed schemes turn out to be very beneficial for UWB ad hoc and sensor networks. In particular, we present new totally-real constructions for the non-orthogonal amplify-and-forward scheme. All of the proposed codes are totally-real and they permit to achieve full rate and full diversity. Because of the totally-real constraint, some families present the advantage of having a non-vanishing determinant at the expense of not being information lossless. Other families of codes are information lossless and have a uniform average transmitted energy per antenna at the expense of having a coding gain that decreases with the spectral efficiency. For given constellation dimensions (number of

modulation positions), the non-vanishing determinant and the energy efficiency can be obtained simultaneously. We also present novel coherent, non-coherent, and differential decode-and-forward strategies that take advantage of the pulse repetitions that are intrinsic to TH-UWB systems. Some practical issues related to timing errors are also discussed.

- In chapter 5, we consider the problem of decoding the multi-dimensional PPM and PPAM constellations. Unlike QAM and PAM constellations where all the components of the transmitted information vectors are independent from each other, PPM and PPAM are sparse constellations where only one position (among the  $M$  modulation positions) is occupied. The sphere decoder as well as other sub-optimal decoders (such as the V-BLAST decoder) are modified to efficiently decode these constellations.

Finally, concluding remarks and future work perspectives are given. The appendices are dedicated for the complementary material and for the proof of the different lemmas and propositions.



## Chapter 2

# Receiver Design and Performance Analysis

In this chapter, we present the system model of MIMO-IR-UWB systems. An accurate model must take the impulsive nature of time domain UWB systems into consideration. Moreover, the effects of the high frequency selectivity of the UWB channels must be considered for accurate transceiver design. At the receiver side, practical implementations based on Rake receivers and correlation receivers are considered (Section 1.1.6). At a second time, we present analytical, semi-analytical as well as numerical analysis on the performance of MIMO-UWB systems over realistic multi-path indoor channels. Throughout the analysis, we try to answer the question about the utility of spatial diversity in UWB systems.

Throughout this work, the considered system model is based on the following assumptions that are commonly used in the wireless communications literature.

- **Channel State information:** In this work, we consider the case where the CSI is available only at the receiver side. In some situations, we also consider differential systems where the CSI is not available at the communicating terminals.
- **Block Fading:** A block fading model is used to characterize the time varying nature of the wireless channels. In other words, we assume that the channel is invariant over a block composed of a certain number of symbol durations and then the channel parameters change independently from one fading block to another. In general, indoor channels are stationary and the duration of each fading block can be very large.
- **Perfect synchronization:** For peer-to-peer links, perfect synchronization is assumed between the communicating terminals. For multiuser systems, the proposed model takes the possible asynchronization between the different users into consideration.
- **Multi-path channels:** In the absence of an accurate and widely approved MIMO-UWB channel model, we adopt two different approaches for studying the performance of the proposed systems. The first approach consists of adopting the IEEE 802.15.3a single-antenna channel model recommendations [17]. In this case, the different sub-channels between the transmit and the receive antenna arrays are generated independently according to [17]. In other words, we assume that the antenna arrays are sufficiently spaced. In all cases, this approach constitutes an upper bound that quantifies the maximum performance improvements offered by multi-antenna techniques. The second approach consists of providing numerical results based on channel measurements. Even though an analytical analysis is not possible in this case, this approach is beneficial in giving more

insights on the system performance in realistic situations. In all cases, highly frequency-selective channels are considered.

- **Additive White Gaussian Noise at the receiver:** The noise at the receiver side is taken to be real AWGN with zero mean and double-sided spectral density  $\frac{N_0}{2}$ .

Recent work on the performance analysis of MIMO-UWB systems can be found in [89, 90]. In [89], the error rate of spatial multiplexing was evaluated over a multi-path lognormal-fading channel for the first time. This approach is interesting because the IEEE channel models [17, 18] are based on lognormal fading. The receiver performed zero-forcing and maximum ratio combining in order to separate the incoming data streams. However, the authors made the assumption that all the combined paths have the same average power, and the proposed model is valid only for limited number of combined multi-path components. Moreover, the ray arrival times were taken to occur at integer multiples of the pulse-width, and therefore, the proposed calculations can not be applied on the channel models proposed in [17] where different multi-path components can arrive during the same pulse duration.

The performance of PPM constellations over multi-path Nakagami-fading channels was considered in [90]. The considered system transmits at a rate of 1 symbol PCU and the transmit diversity is achieved by antenna switching. For systems with  $P$  transmit antennas and  $N_f$  pulses per symbol, antenna switching is equivalent to transmitting  $\frac{N_f}{P}$  pulses from each transmit antenna where only one antenna transmits during each frame duration. For such systems, the authors showed that the diversity advantage, in the sense of having steeper BER-versus-SNR curves, is achievable for systems having a small number of Rake fingers. However, despite this contribution, the analysis proposed in [90] is exclusive to systems based on antenna switching (in other words MIMO systems that do not suffer from co-channel interference).

## 2.1 System Model

Consider a MIMO-TH-UWB system where the transmitter and the receiver are equipped with  $P$  and  $Q$  antennas respectively. We consider a  $M$ -PPM- $M'$ -PAM constellation that entails  $M$ -PPM and  $M'$ -PAM as special cases. Keeping the same notations as in Section 1.1.4, the signal transmitted from the  $p$ -th antenna can be obtained by slightly modifying eq. (1.9):

$$s_p^{(k)}(t) = \sqrt{\frac{E_s \mathcal{E}_k}{PN_f}} \sum_{j=-\infty}^{\infty} a_{p,j}^{(k)} \sum_{n=0}^{N_f-1} b_{p,j,n}^{(k)} w(t - jT_s - nT_f - c_{p,j,n}^{(k)} T_c - d_{p,j}^{(k)} \delta) \quad (2.1)$$

where the multiplying factor  $\frac{1}{\sqrt{P}}$  was introduced in order to have the same total transmitted energy as in the case of single-antenna systems. In what follows, the amplitude spreading sequence  $\{b_{p,j,n}^{(k)}\}$  and the TH sequence  $\{c_{p,j,n}^{(k)}\}$  are taken to be periodic with period  $N_f$  and therefore the subscript  $j$  can be dropped down. Moreover, the antennas of a given user will share the same pseudo-random TH sequence and the subscript  $p$  can be dropped down from the TH sequence. The amplitude and position of the symbol transmitted from the  $p$ -th antenna of the  $k$ -th user during the  $j$ -th symbol duration are given by  $a_{p,j}^{(k)}$  and  $d_{p,j}^{(k)}$  respectively. Let:

$$a_{p,j,m}^{(k)} = a_{p,j}^{(k)} \delta(d_{p,j}^{(k)} - m) \quad ; \quad m = 0, \dots, M-1 \quad (2.2)$$

Equation (2.1) can now be expressed as [6, 8]:

$$s_p^{(k)}(t) = \sqrt{\frac{E_s \mathcal{E}_k}{PN_f}} \sum_{j=-\infty}^{\infty} \sum_{n=0}^{N_f-1} \sum_{m=0}^{M-1} a_{p,j,m}^{(k)} b_{b,n}^{(k)} w(t - jT_s - nT_f - c_n^{(k)} T_c - m\delta) \quad (2.3)$$

Designate by  $g_{q,p}^{(k)}(t)$  the impulse response of the frequency selective channel between the  $p$ -th transmit antenna of the  $k$ -th user and the  $q$ -th receive antenna. In a system comprising  $K$  interfering users, the received signal at the  $q$ -th receive antenna can be expressed as:

$$r_q(t) = \sum_{k=0}^K \sum_{p=1}^P s_p^{(k)}(t) * g_{q,p}^{(k)}(t - \tau^{(k)} - \epsilon_{q,p}^{(k)}) + n_q(t) \quad (2.4)$$

where  $n_q(t)$  is the noise at the  $q$ -th antenna and it is assumed to be real AWGN with variance  $N_0/2$ .  $\tau^{(k)}$  corresponds to the propagation delay of the  $k$ -th user with respect to the first user ( $\tau^{(0)} = 0$ ).

$\epsilon_{q,p}^{(k)}$  corresponds to the arriving time of the first multi-path component of  $g_{q,p}^{(k)}(t)$ . The spacing between the antennas of a given array results in different arrival times that are not negligible with respect to the very short duration of the UWB pulses. These additional delays are calculated with respect to the first arriving ray of the first user. In other words,  $\min_{p,q}(\epsilon_{q,p}^{(0)}) = 0$ . In what follows, we fix:

$$h_{q,p}^{(k)}(t) = w(t) * g_{q,p}^{(k)}(t - \epsilon_{q,p}^{(k)}) \quad (2.5)$$

implying that the receiver is synchronized to the first multi-path component between the transmit and the receive arrays.

Following these notations and dropping the superscript  $k$  for the desired user and the subscript  $j$  for the desired symbol duration (the period during which the decision variables are collected), eq. (2.3) and eq. (2.4) can now be combined together resulting in:

$$\begin{aligned} r_q(t) &= \sqrt{\frac{E_s}{PN_f}} \left\{ \sum_{p=1}^P \sum_{n=0}^{N_f-1} \sum_{m=0}^{M-1} a_{p,m} b_{p,n} h_{q,p}(t - nT_f - c_n T_c - m\delta) \right. \\ &\quad \left. + \underbrace{\sum_{k=1}^K \sqrt{\mathcal{E}_k} \sum_{j=-\infty}^{+\infty} \sum_{p=1}^P \sum_{n=0}^{N_f-1} \sum_{m=0}^{M-1} a_{p,j,m}^{(k)} b_{b,n}^{(k)} h_{q,p}^{(k)}(t - jT_s - nT_f - \tau^{(k)} - c_n^{(k)} T_c - m\delta)}_{r_q^{(mui)}(t)} \right. \\ &\quad \left. + \underbrace{\sum_{0 \neq j=-\infty}^{+\infty} \sum_{p=1}^P \sum_{n=0}^{N_f-1} \sum_{m=0}^{M-1} a_{p,j,m} b_{p,n} h_{q,p}(t - jT_s - nT_f - c_n T_c - m\delta)}_{r_q^{(isi)}(t)} \right\} + n_q(t) \quad (2.6) \end{aligned}$$

In what follows, we ignore the impact of inter symbol interference (ISI) and multi user interference (MUI) that will be discussed in Section 2.4. Denote by  $\Gamma$  the maximum delay spread of the underlying channel ( $\Gamma \gg T_w$ ), ISI can be eliminated by choosing:

$$T_f \geq \Gamma + N_c T_c + (M-1)\delta + T_w \quad (2.7)$$

### 2.1.1 Rake receivers

We first consider the case where a  $L$ -th order Rake is used after each receive antenna. At each arm of the Rake receiver, a bank of  $M$  correlators is needed to detect the  $M$ -dimensional signals. For a  $L$ -th order Rake, designate by  $\Delta_{q,p,l}$  the delay of the  $l$ -th finger associated with the channel from the  $p$ -th transmit to the  $q$ -th receiver antenna for  $l = 0, \dots, L - 1$ . In general, we can differentiate between Partial Rakes (PRakes) and Selective Rakes (SRakes) (refer to Section 1.1.6). For PRakes that combine the first  $L$  arriving multi-path components, we fix  $\Delta_{q,p,l} = \Delta_l = lMT_w$  for all values of  $p$  and  $q$ . For SRakes,  $\Delta_{q,p,l}$  corresponds to the arrival time of the  $l$ -th strongest multi-path component between the  $p$ -th transmit and the  $q$ -th receive antenna. In general, the receiver can not resolve multi-path components separated by a duration less than  $T_w$  and therefore,  $\Delta_{q,p,l}$  is always chosen to be a multiple of  $T_w$ . The signal at each receive antenna is correlated with the following reference signals:

$$\tilde{w}_{q,l,p,n,m}(t) = w(t - nT_f - c_n T_c - \Delta_{q,p,l} - m\delta) \quad (2.8)$$

This results in *QPLM* decision variables collected during each frame duration ( $T_f$ ). From eq. (2.6) and eq. (2.8), the output of the correlator matched to the  $l$ -th multi-path component of  $h_{q,p}(t)$  during the  $m$ -th modulation position of the  $n$ -th frame is given by:

$$x_{q,l,p,n,m} = \int_{nT_f}^{(n+1)T_f} r_q(t) \tilde{w}_{q,l,p,n,m}(t) dt \quad (2.9)$$

$$= \sqrt{\frac{E_s}{PN_f}} \sum_{p'=1}^P \sum_{m'=0}^{M-1} a_{p',m'} b_{p',n} r_{q,p'}((m-m')\delta + \Delta_{q,p,l}) + n_{q,l,p,n,m} \quad (2.10)$$

where:

$$r_{q,p}(\tau) = \int_0^{T_f} h_{q,p}(t) w(t - \tau) dt \quad (2.11)$$

and the noise term  $n_{q,l,p,n,m}$  is given by:

$$n_{q,l,p,n,m} = \int_{nT_f}^{(n+1)T_f} n_q(t) \tilde{w}_{q,l,p,n,m}(t) dt \quad (2.12)$$

Given that the reference signals are different from zero only over a limited time interval (of duration  $T_w$ ) and are equal to zero elsewhere, the correlation between the noise samples verifies:

$$\begin{aligned} E[n_{q,l,p,n,m} n_{q',l',p',n',m'}] &= E \left[ \int_{-\infty}^{+\infty} n_q(t) \tilde{w}_{q,l,p,n,m}(t) dt \int_{-\infty}^{+\infty} n_{q'}(\tau) \tilde{w}_{q',l',p',n',m'}(\tau) d\tau \right] \\ &= \int_{-\infty}^{+\infty} \int_{-\infty}^{+\infty} \tilde{w}_{q,l,p,n,m}(t) \tilde{w}_{q',l',p',n',m'}(\tau) E[n_q(t) n_{q'}(\tau)] dt d\tau \end{aligned} \quad (2.13)$$

Since the noise terms  $n_q(t)$  are AWGN,  $E[n_q(t) n_{q'}(\tau)] = \frac{N_0}{2} \delta(q - q') \delta(t - \tau)$  and the double integral in eq. (2.13) simplifies to a simple integral:

$$\begin{aligned} E[n_{q,l,p,n,m} n_{q',l',p',n',m'}] &= \frac{N_0}{2} \delta(q - q') \int_{-\infty}^{+\infty} \tilde{w}_{q,l,p,n,m}(t) \tilde{w}_{q',l',p',n',m'}(t) dt \\ &= \frac{N_0}{2} \gamma_w ((n' - n)T_f + (c_{n'} - c_n)T_c + (m' - m)\delta + \Delta_{q',l',p'} - \Delta_{q,l,p}) \delta(q - q') \end{aligned} \quad (2.14)$$

where  $\gamma_w(t)$  is the autocorrelation function of  $w(t)$ .

Suppose that the time support of each matched filter does not exceed the frame duration. In other words,  $\max_{q,p,l}(\Delta_{q,p,l}) \leq T'_g$  where  $T'_g$  is given in given by:

$$T'_g = T_f - N_c T_c - (M-1)\delta - T_w \quad (2.15)$$

In this case, eq. (2.14) simplifies to:

$$E[n_{q,l,p,n,m} n_{q',l',p',n',m'}] = \frac{N_0}{2} \gamma_w((m'-m)\delta + \Delta_{q',p',l'} - \Delta_{q,p,l}) \delta(q-q') \delta(n-n') \quad (2.16)$$

For PRakes, we fix  $\Delta_{q,p,l} = \Delta_l = lMT_w$  for  $l = 0, \dots, L-1$  and for all values of  $p$  and  $q$ . From eq. (2.16), it is easy to show that this choice along with  $\delta \geq T_w$  result in white noise terms since  $\gamma_w(kT_w) = 0$  for  $k \in \mathbb{Z} \setminus \{0\}$ . For SRakes, the correlation between the noise terms depends on the channel. For the  $q$ -th receive antenna and for a given modulation positions ( $m$ ), if the  $l$ -th strongest path of  $h_{q,p}(t)$  coincides with the  $l'$ -th strongest path of  $h_{q,p'}(t)$ , then the corresponding integrated noise terms are correlated.

From eq. (2.10), designate by  $X_{q,l}$  the vector of length  $PN_f M$  whose  $((p-1)N_f M + nM + m+1)$ -th component is equal to  $x_{q,l,p,n,m}$  for  $p = 1, \dots, P$ ,  $n = 0, \dots, N_f - 1$  and  $m = 0, \dots, M-1$ .  $X_{q,l}$  can be expressed as:

$$X_{q,l} = \sqrt{\frac{E_s}{PN_f}} R_{q,l} (\mathcal{B} \otimes I_M) A + N_{q,l} \quad (2.17)$$

where:

- $N_{q,l}$  is the noise vector that is constructed in the same way as  $X_{q,l}$ .
- $A$  is the  $PM$ -dimensional information vector. It can be expressed as:  $A = [A_1^T \cdots A_P^T]^T$  where  $A_p$  is the  $M$ -dimensional vector representation of the symbol that is transmitted from the  $p$ -th antenna. For example, for  $M$ -PPM- $M'$ -PAM constellations  $A_p \in \mathcal{C}$  given in eq. (1.8). For PAM constellations,  $A_p$  is a scalar for all values of  $p$ .
- Designate by  $B$  the  $P \times N_f$  amplitude spreading matrix whose  $(p, n+1)$ -th entry is equal to  $b_{p,n}$  for  $p = 1, \dots, P$  and  $n = 0, \dots, N_f - 1$ . Then  $\mathcal{B}$  is the  $PN_f \times P$  matrix given by:  $\mathcal{B} = \text{diag}(B_1^T \cdots B_P^T)$  where  $B_p$  designates the  $p$ -th row of  $B$ .
- $R_{q,l}$  is a  $PN_f M \times PN_f M$  matrix given by:

$$R_{q,l} = \begin{bmatrix} I_{N_f} \otimes R_{q,l,1,1} & \cdots & I_{N_f} \otimes R_{q,l,1,P} \\ \vdots & \ddots & \vdots \\ I_{N_f} \otimes R_{q,l,P,1} & \cdots & I_{N_f} \otimes R_{q,l,P,P} \end{bmatrix} \quad (2.18)$$

where  $R_{q,l,p,p'}$  is a  $M \times M$  toeplitz matrix whose  $(m, m')$ -th element is given by:

$$R_{q,l,p,p'}(m, m') = r_{q,p'}((m-m')\delta + \Delta_{q,p,l}) \quad (2.19)$$

and it corresponds to the impact of the pulse (if any) transmitted by the  $p'$ -th antenna at the  $m'$ -th modulation position on the filter matched to the  $l$ -th ray of  $h_{q,p}(t)$  (the delay of this filter is further translated by a duration corresponding to the  $m$ -th position). Note that for PAM,  $R_{q,l,p,p'}$  is a scalar that corresponds to the amplitude of the multi-path component of  $h_{q,p'}(t)$  whose arrival coincides with that of the  $l$ -th path of  $h_{q,p}(t)$ . A schematic representation of a MIMO-UWB SRake receiver is given in Fig. 2.1.

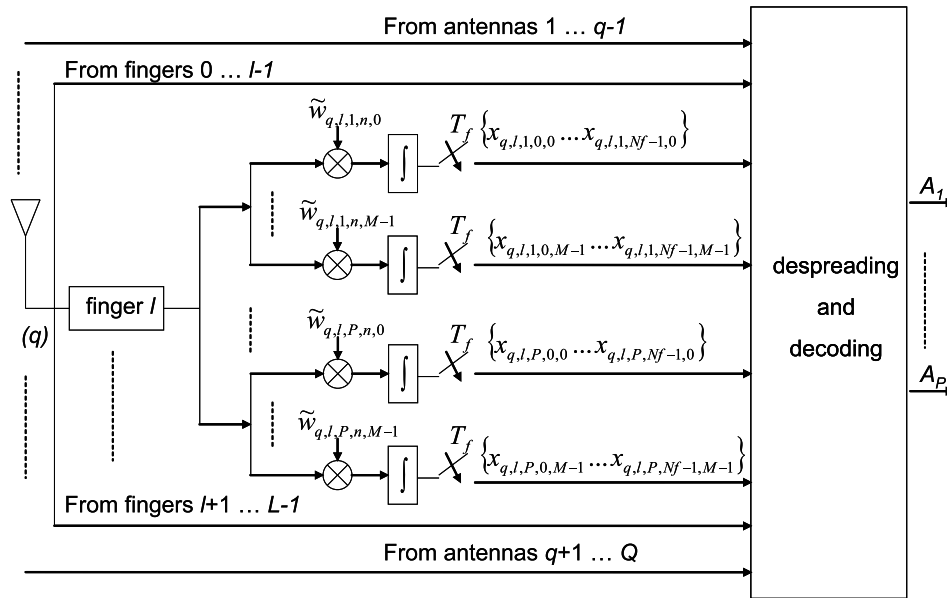


Figure 2.1: Schematic representation of a MIMO-UWB SRake receiver.

In what follows, and for notational simplicity, the multiplying factor  $\sqrt{\frac{E_s}{PN_f}}$  is removed from eq. (2.17) since this term can be included in the expression of the noise variance.

From eq. (2.17), designate by  $X_q = [X_{q,0}^T \cdots X_{q,L-1}^T]^T$  the vector of length  $LPN_fM$ . The  $QLPN_fM$ -dimensional decision vector is given by:  $X = [X_1^T \cdots X_Q^T]^T$ . In the same way, we denote by  $R_q$  the  $LPN_fM \times PN_fM$  channel matrix corresponding to the  $q$ -th receive antenna and that is given by:  $R_q = [R_{q,0}^T \cdots R_{q,L-1}^T]^T$ . Finally, the  $QLPN_fM \times PN_fM$  channel matrix  $R$  is given by:  $R = [R_1^T \cdots R_Q^T]^T$ . Following these notations, the input-output relation can be expressed as:

$$X_{(QLPN_fM \times 1)} = R_{(QLPN_fM \times PN_fM)} \left( \mathcal{B}_{(PN_f \times P)} \otimes I_{(M \times M)} \right) A_{(PM \times 1)} + N_{(QLPN_fM \times 1)} \quad (2.20)$$

where  $N$  is the noise vector that is constructed in the same way as  $X$  and the subscripts in eq. (2.20) indicate the matrices' dimensions. Note that the noise term  $N$  is not white. The components of the covariance matrix  $\Sigma_n$  of  $N$  are obtained by multiplying eq. (2.16) by  $\frac{PN_f}{E_s}$ .

For PRakes, the matrix  $R_{q,l}$  in eq. (2.18) will have dimensions  $N_fM \times PN_fM$ . In this case, eq. (2.18) can be written as:

$$R_{q,l} = \begin{bmatrix} I_{N_f} \otimes R_{q,l,1} & \cdots & I_{N_f} \otimes R_{q,l,P} \end{bmatrix} \quad (2.21)$$

where  $R_{q,l,p}$  is a  $M \times M$  toeplitz matrix whose  $(m, m')$ -th element is given by the following relation:  $R_{q,l,p}(m, m') = r_{q,p}((m - m')\delta + lMT_w)$ .

Equation (2.20) can be written in a more general form as:

$$X_{(QLP'N_fM \times 1)} = R_{(QLP'N_fM \times PN_fM)} \left( \mathcal{B}_{(PN_f \times P)} \otimes I_{(M \times M)} \right) A_{(PM \times 1)} + N_{(QLP'N_fM \times 1)} \quad (2.22)$$

where  $P' = P$  for SRakes and  $P' = 1$  for PRakes. For PRakes, the noise vector  $N$  is white with variance  $\frac{PN_fN_0}{2E_s}$ .

For 2-PPM modulations, the reference signals in eq. (2.8) can be replaced by:

$$\tilde{w}_{q,l,p,n}(t) = w(t - nT_f - c_n T_c - \Delta_{q,p,l}) - w(t - nT_f - c_n T_c - \Delta_{q,p,l} - \delta) \quad (2.23)$$

In this case, the  $M \times M$  matrix  $R_{q,l,p,p'}$  in eq. (2.19) reduces to the scalar:

$$R_{q,l,p,p'} = r_{q,p'} (\Delta_{q,p,l}) - r_{q,p'} (\delta + \Delta_{q,p,l}) \quad (2.24)$$

In the same way, for PRakes with 2-PPM, the matrix  $R_{q,l,p}$  reduces to the scalar:  $R_{q,l,p} = r_{q,p} (2lT_w) - r_{q,p} (\delta + 2lT_w)$ .

### 2.1.2 Correlation receivers

For correlation receivers, the signal received at the  $q$ -th receive antenna is correlated with  $P$  reference signals corresponding to the filters matched to the channels  $h_{q,1}, \dots, h_{q,P}$ . In the case of perfect channel estimation, the reference signals are given by:

$$\tilde{h}_{q,p,n,m}(t) = h_{q,p}(t - nT_f - c_n T_c - m\delta) \quad (2.25)$$

The decision variables at the receiver side are given by:

$$x_{q,p,n,m} = \int_0^{T_i} r_q(t) \tilde{h}_{q,p,n,m}(t) dt \quad (2.26)$$

$$= \sqrt{\frac{E_s}{PN_f}} \sum_{p'=1}^P \sum_{m'=0}^{M-1} a_{p',m'} b_{p',n} r_{q,p,p'} ((m-m')\delta) + n_{q,p,n,m} \quad (2.27)$$

where:

$$r_{q,p,p'}(\tau) = \int_0^{T_i} h_{q,p'}(t) h_{q,p}(t-\tau) dt \quad (2.28)$$

and  $T_i$  is the integration time. When  $T_i = \Gamma$  (the maximum channel delay spread), then the above receiver is equivalent to an All-Rake (ARake) that combines all of the multi-path components. The correlations between the noise terms verify:

$$E[n_{q,p,n,m} n_{q',p',n',m'}] = \frac{N_0}{2} r_{q,p',p} ((n'-n)T_f + (c_{n'} - c_n)T_c + (m'-m)\delta) \delta(q-q') \quad (2.29)$$

which simplifies to:

$$E[n_{q,p,n,m} n_{q',p',n',m'}] = \frac{N_0}{2} r_{q,p',p} ((m'-m)\delta) \delta(q-q') \delta(n-n') \quad (2.30)$$

when  $T_i \leq T_f$ . Equation (2.27) can be expressed in matrix form as:

$$X = \sqrt{\frac{E_s}{PN_f}} R (\mathcal{B} \otimes I_M) A + N \quad (2.31)$$

where  $R = [R_1^T \cdots R_Q^T]^T$  has dimensions  $QPN_f M \times PN_f M$ . In a way similar to eq. (2.18),  $R_q$  is given by:  $R_q = [(I_{N_f} \otimes R_{q,p,p'})]_{p,p'=1}^P$  where the  $(m,m')$ -th element of the  $M \times M$  toeplitz matrix  $R_{q,p,p'}$  is given by:

$$R_{q,p,p'}(m, m') = r_{q,p,p'} ((m-m')\delta) \quad (2.32)$$

Finally, as in Section 2.1.1, the multiplying factor  $\sqrt{\frac{E_s}{PN_f}}$  is removed from eq. (2.31) and included in the noise variance.

There is a big similarity between PRakes and correlation receivers. In fact, a correlation receiver with integration time  $T_i$  collects the same energy as a  $L$ -th order PRake with  $L = \frac{T_i}{MT_w}$ . However, from eq. (2.8) and eq. (2.25), it can be seen that the correlation receivers do not suffer from intra-pulse interference since they can resolve the multi-path components separated by a duration less than  $T_w$ .

### 2.1.3 Despread

In order to simplify the structure of the receivers, we choose to combine the decision variables corresponding to the  $N_f$  pulses of the same transmitted symbol prior to decoding. This corresponds to multiplying by a despreading matrix  $D$ . In this case, the new decision vector  $Y$  at the receiver can be expressed as:

$$Y = DX = \underbrace{DR(\mathcal{B} \otimes I_M)}_{\mathcal{H}} A + N \quad (2.33)$$

The length of  $Y$  is equal to  $QLP'M$  for Rake receivers and  $QPM$  for correlation receivers. In particular, spatial multiplexing follows as a special case of this generic model. In this case, independent data flows are transmitted simultaneously and the same spreading sequence is associated with all transmit antennas. In particular, we can choose  $B = \mathbf{1}_{P \times N_f}$ . The despreading matrix  $D$  is given by  $D = I_{QLP'} \otimes (B_1 \otimes I_M)$  for Rake receivers and  $D = I_{QP} \otimes (B_1 \otimes I_M)$  for correlation receivers where  $B_1 = \mathbf{1}_{1 \times N_f}$  is the first row of  $B$ . For example, when associating spatial multiplexing with correlation receivers, eq. (2.33) simplifies to:

$$Y = HA + N = \begin{bmatrix} R_{1,1,1} & \cdots & R_{1,1,P} \\ \vdots & \ddots & \vdots \\ R_{1,P,1} & \cdots & R_{1,P,P} \\ \vdots & \vdots & \vdots \\ R_{Q,1,1} & \cdots & R_{Q,1,P} \\ \vdots & \ddots & \vdots \\ R_{Q,P,1} & \cdots & R_{Q,P,P} \end{bmatrix} A + N \quad (2.34)$$

where the  $(m, m')$ -th element of the matrix  $R_{q,p,p'}$  is given in eq. (2.32). Since  $D$  is unitary, the covariance matrix of the zero-mean noise term  $N$  verifies:  $\Sigma_n = E[NN^T] = \frac{PN_0}{2E_s} H$ .

## 2.2 Rate-1 coherent ST-coded systems

### 2.2.1 Transceiver Structure

In this case, the same information symbol is transmitted from the  $P$  antennas and orthogonal amplitude spreading sequences are associated with the different transmit antennas. While orthogonal codes achieve a rate of 1 symbol PCU for some specific values of  $P$  ( $P = 2, 4, 8$ ) [45], the proposed scheme profits from the pulse repetitions in order to introduce orthogonality among the transmitted data streams. It can be associated with any number of transmit antennas verifying  $P \geq N_f$ . Given that  $N_f$  can be in the order of 10 in IR-UWB systems, this approach is feasible with practical systems having a limited number of antennas. The considered scheme can be seen as an extension of the ST code (“STC1”) proposed in [81] for  $P > 2$ . While [81] was limited to 2-PAM constellations and PRakes, the considered scheme is generalized for all constellations associated with PRakes, SRakes or correlation receivers.

More explicitly, the  $P \times N_f$  amplitude-spreading matrix  $B$  is chosen to verify  $BB^T = N_f I_P$ . The despreading matrix  $D$  in eq. (2.33) is given by  $D = I_{QLP'} \otimes (B \otimes I_M)$  for Rake receivers and  $D = I_{QP} \otimes (B \otimes I_M)$  for correlation receivers. In what follows, the performance analysis is limited to correlation receivers.

For the rate-1 ST coded systems, it can be easily seen that eq. (2.33) can be written in an equivalent way as:

$$Y = HA + N = \begin{bmatrix} \text{diag}(R_{1,1} \dots R_{1,P}) \\ \vdots \\ \text{diag}(R_{Q,1} \dots R_{Q,P}) \end{bmatrix} A + N \quad (2.35)$$

where  $R_{q,p}$  is a  $M \times M$  matrix for  $q = 1, \dots, Q$  and  $p = 1, \dots, P$ . Its  $(m, m')$ -th element is given by  $r_{q,p}((m - m')\delta)$  where  $r_{q,p}(\tau) = \int_0^{T_i} h_{q,p}(t)h_{q,p}(t - \tau)dt$ . Since the same symbol is transmitted from all antennas,  $A$  can be written as  $A = \mathbf{1}_{P \times 1} \otimes S$  where  $S$  denotes the  $M$ -dimensional vector representation of the transmitted symbol ( $A_1 = \dots = A_P = S$ ).  $N$  is a colored noise:

$$E[NN^T] = \frac{PN_0}{2E_s} \text{diag} \left( \begin{array}{ccc} R_{1,1} \dots R_{1,P} & \dots & R_{Q,1} \dots R_{Q,P} \end{array} \right) \quad (2.36)$$

Since this orthogonal scheme is equivalent to creating  $PQ$  parallel channels between the transmitter and the receiver, the outputs of the  $PQ$  matched filters corresponding to a given position  $m$  can be added up. Therefore, eq. (2.35) can be written in an equivalent way as:

$$\begin{aligned} x_m &= \sum_{q=1}^Q \sum_{p=1}^P Y_{(q-1)PM+(p-1)M+m} \\ &= \sum_{q=1}^Q \sum_{p=1}^P \sum_{m'=0}^{M-1} r_{q,p}((m - m')\delta) s_{m'} + n_m \end{aligned} \quad (2.37)$$

where  $s_m$  is the  $m$ -th component of  $S$ . From eq. (2.36), the correlation between  $n_m$  and  $n_{m'}$  is given by:

$$\rho_{m,m'} = \frac{E[n_m n_{m'}]}{\sqrt{E[n_m^2]E[n_{m'}^2]}} = \frac{\sum_{q,p} \alpha_{q,p,m-m'}}{\sum_{q,p} \alpha_{q,p,0}} \quad (2.38)$$

where  $\alpha_{q,p,m} \triangleq r_{q,p}(m\delta) = \alpha_{q,p,-m}$ .

## 2.2.2 Conditional Error probability with bi-orthogonal PPAM

The bi-orthogonal PPAM corresponds to hybrid  $M$ -PPM-2-PAM constellations. Suppose that a pulse whose amplitude verifies  $s_m \in \{\pm 1\}$  was transmitted at the  $m$ -th position ( $0 \leq m \leq M - 1$ ). The  $M$  decision variables in eq. (2.37) can be expressed as:

$$x_{m'} = s_m \sum_{q,p} \alpha_{q,p,m'-m} + n_{m'} \quad (2.39)$$

for  $m' = 0, \dots, M - 1$ .

We show in Appendix B that the conditional error probability verifies:

$$P_{e/H} \leq Q \left( \sqrt{\frac{2E_s \sum_{q,p} \alpha_{q,p,0}}{PN_0}} \right) + \frac{2}{M} \sum_{m=1}^{M-1} (M - m) \left( \mathcal{P}_m^{(1)} + \mathcal{P}_m^{(2)} - 2\mathcal{P}_m^{(1)}\mathcal{P}_m^{(2)} \right) \quad (2.40)$$

where  $\mathcal{P}_m^{(1)}$  and  $\mathcal{P}_m^{(2)}$  are given by:

$$\mathcal{P}_m^{(i)} = Q \left( \sqrt{\frac{E_s \sum_{q,p} (\alpha_{q,p,0} + (-1)^{i-1} \alpha_{q,p,m})}{PN_0}} \right) \quad (2.41)$$

The error probability of PPM constellations follows as a special case by setting  $\mathcal{P}_m^{(2)}$  and the first term of the right hand side of eq. (2.40) to zero.

### 2.2.3 Error probability with PAM

For 2-PAM constellations,  $\alpha_{q,p,0} = \int_0^{T_i} h_{q,p}(t)^2 dt$  corresponds to the total energy contained in the channel impulse response for  $T_i = \Gamma$ . From [17],  $\alpha_{q,p,0} = \exp(\mathcal{N})$  where  $\mathcal{N}$  is a zero-mean normal random variable with standard deviation  $\sigma_{\mathcal{N}} = \frac{\ln(10)}{10} \sigma_x$ .  $\sigma_x = 3\text{dB}$  is the standard deviation of the lognormal shadowing that affects all multi-path components [17]. Therefore, the average error probability with 2-PAM constellations can be expressed as:

$$P_e = \int_0^{\infty} \cdots \int_0^{\infty} Q\left(\sqrt{\frac{2E_s \sum_i^{PO} x_i}{PN_0}}\right) \left(\prod_{i=1}^{PQ} p(x_i)\right) dx_1 \cdots dx_{PQ} \quad (2.42)$$

where  $x_1, \dots, x_{PQ}$  are independent and identically distributed lognormal random variables that can be written as  $x_i = \exp(\mathcal{N}_i)$  where  $\mathcal{N}_i$  is a Gaussian random variables with mean  $u = 0$  and variance  $v = \sigma_{\mathcal{N}}^2$  for  $i = 1, \dots, PQ$ .  $p(x_i)$  is the probability density function of  $x_i$ .

Let  $x = \sum_{i=1}^N x_i$  where  $N = PQ$ . Being a sum of lognormal random variables,  $x$  can be well approximated by a lognormal distribution [91, 92]. Designate by  $u$  and  $v$  the parameters of the lognormal approximation of the distribution of  $x$ , then eq. (2.42) can be approximated by:

$$P_e \simeq \int_0^{\infty} Q\left(\sqrt{\frac{2E_s x}{PN_0}}\right) \frac{1}{x \sqrt{2\pi v}} \exp\left(-\frac{(\ln(x) - u)^2}{2v}\right) dx \quad (2.43)$$

Several approaches have been proposed for determining the values of  $u$  and  $v$  from the parameters of the constituent random variables  $x_1, \dots, x_N$ . For example, we can cite Wilkinson's approach, Farley's approach and Schleher's cumulants matching approach [92]. In particular, Wilkinson's method is based on matching the first two moments of a lognormal random variable  $x$  to the moments of the sum  $\sum_i x_i$ . In this case,  $u$  and  $v$  are given by:

$$\begin{aligned} u &= \ln\left(\frac{u_1^2}{\sqrt{u_2}}\right); v = \ln\left(\frac{u_2}{u_1^2}\right); u_1 = N \exp\left(\frac{\sigma_{\mathcal{N}}^2}{2}\right) \\ u_2 &= N \exp(2\sigma_{\mathcal{N}}^2) + N(N-1) \exp(\sigma_{\mathcal{N}}^2) \end{aligned} \quad (2.44)$$

### 2.2.4 Achieved diversity order over the IEEE 802.15.3a channel models

Using the Chernoff bound, eq. (2.43) can be upper bounded by:

$$P_e \simeq \frac{1}{2} \int_0^{\infty} \exp\left(-\frac{E_s x}{PN_0}\right) \frac{1}{x \sqrt{2\pi v}} \exp\left(-\frac{(\ln(x) - u)^2}{2v}\right) dx \quad (2.45)$$

Equation (2.45) corresponds to the moment generating function of the lognormal distribution that doesn't have a closed form expression. The numerical evaluation of eq. (2.45) shows that the curve  $P_e$  versus  $E_s N_0^{-1}$  (or versus SNR) becomes steeper when the value of  $v$  decreases. This is equivalent to the rank criterion [50] and therefore the diversity advantage over the IEEE 802.15.3a channel models is related to the value of  $v$ . From eq. (2.44), since  $v$  is a decreasing function of  $N$ , then the proposed orthogonal ST coding scheme is equivalent to transforming the SISO channel into another channel having the same distribution but with a lower variation in the captured energy (and hence lower fading margins).

On the other hand, for a fixed value of  $v$ , increasing the value of  $u$  results in a simple translation of these curves. This is equivalent to the coding gain achieved by ST codes [50]. The interest of ST coding over the considered channels is evident since  $u$  is an increasing function of  $N$ .

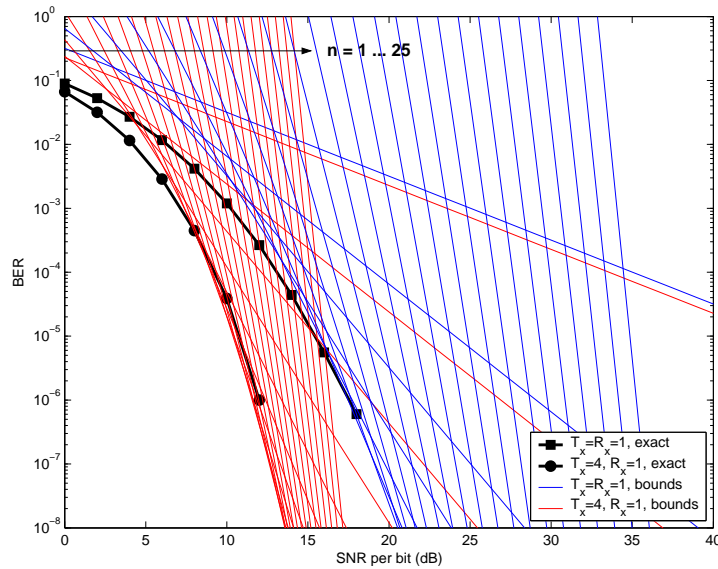


Figure 2.2: Bounds on the performance of single antenna systems and of the  $(4 \times 1)$  orthogonal code over the IEEE 802.15.3a CM2 channel model.

Note that  $P$  and  $Q$  have the same impact on the performance curves since, from eq. (2.44),  $u$  and  $v$  depend uniquely on the product  $N = PQ$  (without mentioning the energy capture enhanced by increasing  $Q$ ). Since the receive diversity is assured by this kind of coherent receivers, this proves that, in an equivalent way, the proposed system profits from full transmit diversity.

In order to determine the achieved diversity order over the considered channels (the slope of the log-log plot of  $P_e$  versus  $E_s N_0^{-1}$ ), we try to conveniently upper bound eq. (2.45). Since  $\exp(-x) = (\sum_{n=0}^{+\infty} \frac{x^n}{n!})^{-1} \leq \frac{n!}{x^n} \forall n \in \mathbb{N}$ , then eq. (2.45) can be bounded by:

$$\begin{aligned} P_e &\leq \frac{1}{2} n! \int_0^{+\infty} t^{-n} \frac{1}{t \sqrt{2\pi v}} \exp\left(-\frac{[\ln(t) - (u + \ln(E_s) - \ln(PN_0))]^2}{2v}\right) dt \\ &\leq \frac{1}{2} n! E[t^{-n}] = \frac{n!}{2 \left( \exp(u) \exp(-\frac{mv}{2}) E_s (PN_0)^{-1} \right)^n} \quad \forall n \in \mathbb{N} \end{aligned} \quad (2.46)$$

From eq. (2.46), it can be seen that the considered channels profit from an infinite diversity order as  $SNR \rightarrow +\infty$ . For example, unlike the Rayleigh fading channels that behave asymptotically as  $(SNR)^{-PQ}$ , the slope of  $P_e(SNR)$  over the channels in [17] has an infinite value for large SNRs. It can be also seen from eq. (2.46) that unlike  $u, v$  has an impact on the achieved diversity order since it is multiplied by  $n$ .

Because of this infinite diversity order at asymptotic values of the SNR, the utility of an additional spatial diversity over the IEEE 802.15.3a channels is questionable. However, even though the bound in eq. (2.46) gives a clear idea on the slope of  $P_e(SNR)$  as  $SNR \rightarrow +\infty$ , it becomes looser with increasing values of  $n$  especially at practical SNRs. The bound in eq. (2.46) for different values of  $n$  as well as the error probability in eq. (2.43) are plotted in Fig. 2.2. This figure shows that despite the infinite diversity order achieved at infinite SNRs, the diversity advantage can be enhanced at practical values of the SNR.

Note that the above calculations were limited to the case  $T_i = \Gamma$ . However, as will be shown later in Section 2.3.1, the integrated energy can be well approximated by a lognormal distribution for different values of the integration time. Therefore, the proposed approach can be applied with different values of

$T_i$  and an infinite diversity order can be achieved at infinite SNRs. However, since  $u$  (resp.  $v$ ) in eq. (2.46) decreases (resp. increases), this asymptotic regime is achieved for higher SNRs and the enhancements introduced by ST coding for practical values of the SNR become more pronounced.

In a similar way, the conditional error probability of the considered coding scheme with Rake receivers and 2-PAM constellations can be expressed as:

$$P_e = Q \left( \sqrt{\frac{2E_s \sum_{q=1}^Q \sum_{p=1}^P \sum_{l=0}^{L-1} r_{q,p,l}^2}{PN_0}} \right) \quad (2.47)$$

where  $r_{q,p,l} = r_{q,p}(\Delta_{q,p,l})$  and  $r_{q,p}(\tau)$  is given in eq. (2.11).  $h_{q,p}(t)$  can be expressed as:

$$h_{q,p}(t) = \sum_{l=0}^{L_{q,p}-1} \alpha_{q,p,l} w(t - \tau_{q,p,l}) \quad (2.48)$$

where  $L_{q,p}$  is the number of multi-path components.  $\alpha_{q,p,l}$  and  $\tau_{q,p,l}$  correspond to the amplitudes and the arrival times of these multi-path components respectively.  $\alpha_{q,p,l} = \theta_{q,p,l} \eta_{q,p,l}$  where  $\theta_{q,p,l} = \pm 1$  with equal probability and it accounts for the random pulse inversion that can occur due to reflections. The magnitude term  $\eta_{q,p,l}$  is a lognormally distributed random variable and it corresponds to the ray, cluster and overall energy shadowing [17]. From eq. (2.11) and eq. (2.48), it follows that:

$$r_{q,p,l} = \sum_{l'=0}^{L_{q,p}-1} \theta_{q,p,l'} \eta_{q,p,l'} \gamma_w(\tau_{q,p,l'} - \Delta_{q,p,l}) = r_{q,p,l}^+ - r_{q,p,l}^- \quad (2.49)$$

where:

$$r_{q,p,l}^\pm = \sum_{l' \in \mathcal{A}^\pm} |\gamma_w(\tau_{q,p,l'} - \Delta_{q,p,l})| \eta_{q,p,l'} \quad (2.50)$$

and  $\mathcal{A}^\pm$  is the set of values of  $l'$  verifying  $\theta_{q,p,l'} \gamma_w(\tau_{q,p,l'} - \Delta_{q,p,l}) \geq 0$ .

Being the sum of lognormal random variables,  $r_{q,p,l}^+$  and  $r_{q,p,l}^-$  can be approximated by lognormal distributions. Therefore  $r_{q,p,l}$  is equivalent to the difference between two lognormal distributions. To the author's knowledge, there are no valid approximations for the distribution of  $r_{q,p,l}$  and therefore an analytical analysis of the average probability of error with Rake receivers is not possible.

However, if the receiver uses a very high resolution fractionally-sampled (FS) Rake receivers that can resolve multi-path components whose temporal separation is less than  $T_w$  [93], then  $r_{q,p,l}^+$  and  $r_{q,p,l}^-$  can be coherently combined and  $r_{q,p,l}$  can be approximated by a lognormal random variable. Therefore, these receivers are equivalent to the correlation receivers and they achieve an infinite diversity order at large SNRs.

Concerning the construction of ST coding schemes over the UWB channels [17] that do not lend themselves to an analytical characterization, we have no choice except adopting the design criteria given in definitions 1.16 and 1.17. In all cases, these criteria constitute an upper bound (even if it may be loose) for constructing "good" ST codes as shown in eq. (1.33).

## 2.3 Diversity-Multiplexing Tradeoff over the 802.15.3a channel models

In this section, we evaluate the diversity-multiplexing gain (D-MG) tradeoff of single-antenna and multi-antenna UWB channels in [17]. This formulation which is a very powerful tool for evaluating the underlying communication channel was never considered in the UWB context. Evaluating the D-MG tradeoff

gives more insights on the true utility of merging MIMO techniques with UWB independently from any calculation approximations and receiver structure. Given the high frequency selectivity of the considered channels, the entries of the channel matrices (in eq. (2.34) for example) have no closed form distributions.

Our approach consists of evaluating the statistical behavior of some significant parameters of the channels in [17]. At a second time, the distribution of these parameters is used to derive lower and upper bounds as well as approximate values of the achieved D-MG tradeoffs.

### 2.3.1 Statistical characterization

Consider, for simplicity, the case of a correlation receiver equipped with  $Q = 1$  receive antenna. For PAM, multiplying eq. (2.34) by  $H^{-\frac{1}{2}}$  in order to whiten the noise results in:

$$Y' = H^{-\frac{1}{2}}Y = H^{\frac{1}{2}}A + N \quad (2.51)$$

where  $N$  is white with variance  $\frac{PN_0}{2E_s} \triangleq P\rho^{-1}$  where  $\rho$  is the signal-to-noise ratio.  $H$  is a  $P \times P$  matrix whose  $(p, p')$ -th element is  $H_{p,p'} = H_{p',p} = \int_0^{T_i} h_p(t)h_{p'}(t)dt$  where  $h_p(t)$  corresponds to the channel between the  $p$ -th transmit antenna and the receive antennas.  $\lambda_p = H_{p,p}$  corresponds to the energy received in an integration window of duration  $T_i$ .

#### Statistical model of the integrated energy

We suppose that the channel responses are uncorrelated and we denote by  $\lambda$  the random variable describing the behavior of the independent and identically distributed random variables  $\lambda_p$  for all values of  $p$ . For example, it was seen in Section 2.2.3 that when  $T_i = \Gamma$ ,  $\lambda$  is a lognormal random variable with parameters  $u = 0$  and  $\sigma = 3\frac{\ln(10)}{10}$ .

In what follows  $w(t)$  is taken to be the second derivative of the Gaussian pulse with a duration of 0.5 ns. We found that  $\lambda$  can be well approximated by a lognormal distribution for all integration times and channel profiles [17]. For CM2 that corresponds to NLOS conditions, the complementary density function (CDF) of  $\lambda$  and that of its lognormal approximation are presented in Fig. 2.3 for different values of  $T_i$ . Similar results are obtained for the other profiles CM1, CM3 and CM4.

#### Statistical model of the maximal eigenvalue of the channel matrix

Studying the D-MG tradeoff for any number of transmit antennas necessitates the knowledge of the joint probability density function of the eigenvalues of the channel matrix in eq. (2.51). While this distribution is known in the case of Gaussian random matrices [48], such an analytical characterization is impossible for the channel matrices in eq. (2.51). In this section, we present a statistical approximation of the distribution of the maximal eigenvalue of the channel matrix denoted by  $\alpha_{max}$ . This characterization is useful in determining lower and upper bounds on the D-MG tradeoffs over the MIMO-UWB channels.

$\alpha_{max}$  is also found to be well approximated by a lognormal distribution. The probability density function (PDF) over CM2 is shown in Fig. 2.4 for different number of transmit antennas and integration times. Similar results are obtained over the other channel profiles.

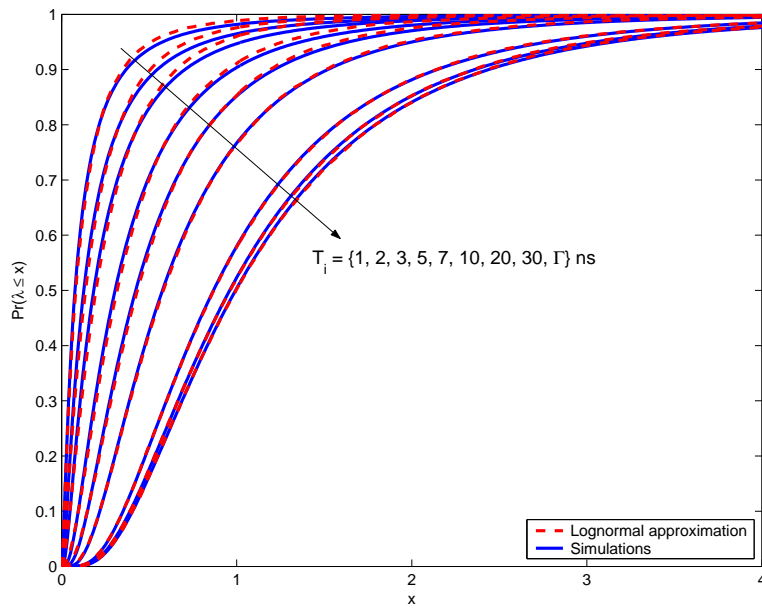


Figure 2.3: Exact and approximated CDF of the energy integrated in a duration of  $T_i$  over CM2.  $\Gamma$  corresponds to the maximum channel delay spread.

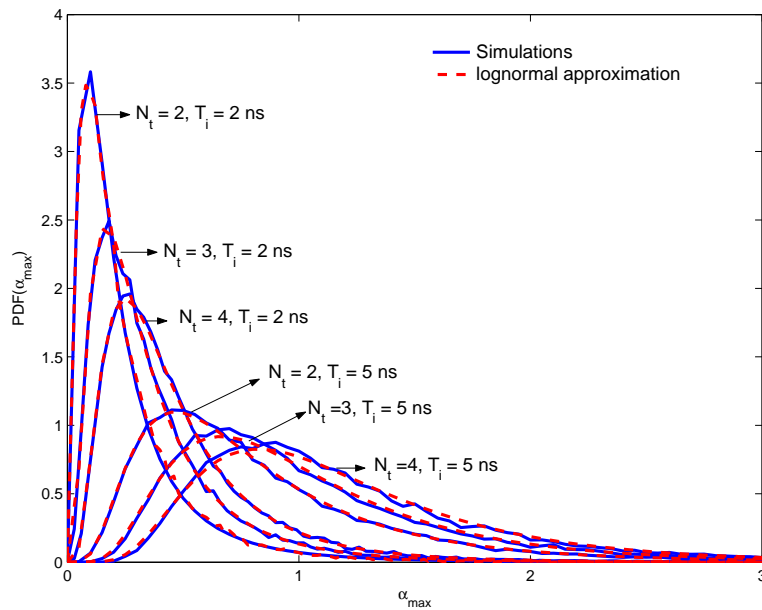


Figure 2.4: PDF of  $\alpha_{max}$  over CM2. Solid and dashed lines correspond to the simulated distributions and their lognormal approximations respectively.

### 2.3.2 Achieved Tradeoffs

Rather than studying the D-MG tradeoffs at asymptotic values of the SNR as in [48], we choose to apply the framework proposed in [94] for determining the D-MG tradeoffs at finite values of the SNR ( $\rho$ ). The multiplexing gain  $r$  is defined as the ratio of the spectral efficiency  $R$  (bps/Hz) to the capacity of an AWGN channel:

$$r = \frac{R}{\log_2(1 + \rho)} \quad (2.52)$$

As in [48], this definition implies that for a constant multiplexing gain, the spectral efficiency increases with the SNR. The diversity gain  $d(r, \rho)$  is the negative slope of the log-log plot of the outage probability  $P_{out}(r, \rho)$  [94]:

$$d(r, \rho) = -\frac{\rho}{P_{out}(r, \rho)} \cdot \frac{\partial P_{out}(r, \rho)}{\partial \rho} \quad (2.53)$$

At a fixed SNR,  $d(r, \rho)$  provides an indication on the additional power required to decrease the outage probability by a specified quantity.

#### Single-antenna systems

From eq. (2.51), the outage probability at a given SNR ( $\rho$ ), multiplexing gain  $r$  and channel realization (determined by  $\lambda$ ) is given by:

$$P_{out}(r, \rho) = \Pr\{I = \log_2(1 + \rho\lambda) < R = r\log_2(1 + \rho)\} \quad (2.54)$$

From Section 2.3.1,  $\lambda$  can be approximated by a lognormal random variable and eq. (2.54) can be written as:

$$P_{out}(r, \rho) = \Pr\{\lambda < \rho^{-1}[(1 + \rho)^r - 1]\} \quad (2.55)$$

$$= Q\left(\frac{u + \ln(\rho) - \ln((1 + \rho)^r - 1)}{\sigma}\right) \quad (2.56)$$

where  $u$  and  $\sigma$  are the mean and the standard deviation of  $\ln(\lambda)$  respectively.

From eq. (2.53) and eq. (2.56), we obtain:

$$d(r, \rho) = \frac{1}{\sqrt{2\pi}\sigma Q(x)} \exp\left(-\frac{x^2}{2}\right) \left[1 - r\rho \frac{(1 + \rho)^{r-1}}{(1 + \rho)^r - 1}\right] \quad (2.57)$$

where  $\sigma x = [u + \ln(\rho) - \ln((1 + \rho)^r - 1)]$ .

Two remarks follow from eq. (2.57):

1.  $\lim_{\rho \rightarrow \infty} d(r, \rho) = \infty$ . This shows that at very high SNR, the UWB channels in [17] behave in the same way as the Gaussian channel. In other words, an infinite diversity gain can be obtained even in single antenna situations. This is in coherence with the observation made in Section 2.2.3. At a first glance, this shows that there is no interest in profiting from the spatial diversity at high SNR by the use of space-time coding techniques.
2. For large values of the SNR, eq. (2.57) behaves as  $\ln(\rho)$ . This implies that the asymptotic behavior (with an infinite diversity gain) is reached at very high SNRs. These SNRs can not be obtained in practical systems implying that the asymptotic regime can never be reached in some situations. For

example,  $\rho = 30$  dB results in an asymptotic behavior over the Rayleigh-fading channel. However,  $\ln(\rho) = 8.3$  dB may not be in the asymptotic region (which is the case for practical values of  $u$  and  $\sigma$  as shown later). The interest of using multi-antenna systems arises from this remark. In other words, for practical SNRs, MIMO techniques introduce an additional diversity advantage.

### Rate-1 ST coded systems

In order to avoid redundancy, we introduce the following notations:

$$\begin{aligned} P_{ref}(r, \rho, u, v, n', n) &= \Pr \left\{ n' \log_2 \left( 1 + \frac{\rho}{n} \lambda \right) < r \log_2 (1 + \rho) \right\} \\ &= Q \left( \frac{u + \ln(\rho/n') - \ln((1+\rho)^{\frac{r}{n}} - 1)}{\sqrt{v}} \right) \end{aligned} \quad (2.58)$$

where  $u$  and  $v$  are the mean and variance of  $\ln(\lambda)$  respectively and  $\lambda$  is a lognormal random variable. Applying eq. (2.53) on eq. (2.58), we obtain:

$$\begin{aligned} d_{ref}(r, \rho, u, v, n', n) &= \frac{1}{Q \left( \frac{u + \ln(\rho/n') - \ln((1+\rho)^{\frac{r}{n}} - 1)}{\sqrt{v}} \right)} \\ &\quad \frac{1}{\sqrt{2\pi v}} \exp \left[ -\frac{1}{2} \left( u + \ln \left( \frac{\rho}{n'} \right) - \ln((1+\rho)^{\frac{r}{n}} - 1) \right)^2 \right] \left[ 1 - \frac{r\rho}{n} \frac{(1+\rho)^{\frac{r}{n}-1}}{(1+\rho)^{\frac{r}{n}} - 1} \right] \end{aligned} \quad (2.59)$$

For the rate-1 coded systems described in Section 2.2, the mutual information between the input and the output of the channel defined in eq. (2.35) with PAM and one receive antenna is given by:

$$I^{(c)} = r_s \log_2 \left( 1 + \frac{\rho}{P} H^{\frac{1}{2}T} H^{\frac{1}{2}} \right) = r_s \log_2 \left( 1 + \frac{\rho}{P} \sum_{p=1}^P \lambda_p \right) \quad (2.60)$$

where  $r_s = 1$  is the number of symbols transmitted per channel use.

Since  $\lambda_1, \dots, \lambda_P$  are lognormal random variables,  $\lambda = \sum_{p=1}^P \lambda_p$  can be well approximated by a lognormal random process [92]. As in Section 2.2.3, the mean  $U$  and the variance  $V$  of  $\ln(\lambda)$  can be obtained from the parameters  $u$  and  $\sigma$  of the constituent distributions by applying Wilkinson's method:

$$\begin{aligned} U &= \ln \left( \frac{u_1^2}{\sqrt{u_2}} \right); V = \ln \left( \frac{u_2}{u_1^2} \right); u_1 = P \exp \left( u + \frac{\sigma^2}{2} \right) \\ u_2 &= P \exp (2u + \sigma^2) (P - 1 + \exp (\sigma^2)) \end{aligned} \quad (2.61)$$

Finally, the outage probability and the diversity gain of the rate-1 coded systems can be expressed as:

$$P_{out}^{(c)}(r, \rho) \simeq P_{ref}(r, \rho, U, V, P, 1) \quad (2.62)$$

$$d^{(c)}(r, \rho) \simeq d_{ref}(r, \rho, U, V, P, 1) \quad (2.63)$$

### Spatial Multiplexing

The D-MG tradeoff of uncoded systems (spatial multiplexing) is equivalent to that of the underlying multi-antenna channel. The mutual information of eq. (2.51) is given by:

$$I^{(SM)} = P \log_2 \det \left( I_P + \frac{\rho}{P} H \right) = P \log_2 \left( \prod_{p=1}^P \left( 1 + \frac{\rho}{P} \alpha_p \right) \right) \quad (2.64)$$

where  $\alpha_p$  is the  $p$ -th eigenvalue of  $H$ .

$H$  is a positive semi-definite Hermitian matrix, this implies that  $\alpha_p \geq 0$  for all values of  $p$ . Therefore, eq. (2.64) verifies:

$$I^{(SM)} \leq P \log_2 \left( \prod_{p=1}^P \left(1 + \frac{\rho}{P} \alpha_{max}\right) \right) = P^2 \left(1 + \frac{\rho}{P} \alpha_{max}\right) \quad (2.65)$$

where  $\alpha_{max}$  is the maximum eigenvalue of  $H$ . In the same way:

$$I^{(SM)} = P \sum_{p=1}^P \log_2 \left(1 + \frac{\rho}{P} \alpha_p\right) \geq P \left(1 + \frac{\rho}{P} \alpha_{max}\right) \quad (2.66)$$

From Section 2.3.1,  $\alpha_{max}$  can be approximated by a lognormal distribution. Therefore, equations (2.65) and (2.66) imply that:

$$P_{ref}(r, \rho, u, v, P, P^2) \leq P_{out}^{(SM)}(r, \rho) \leq P_{ref}(r, \rho, u, v, P, P) \quad (2.67)$$

$$d_{ref}(r, \rho, u, v, P, P) \leq d^{(SM)}(r, \rho) \leq d_{ref}(r, \rho, u, v, P, P^2) \quad (2.68)$$

$u$  and  $v$  being the mean and variance of  $\ln(\alpha_{max})$  respectively.

When  $P = 2$ , better bounds can be obtained without the knowledge of the distribution of the maximal eigenvalue of the channel matrix. In this case, eq. (2.64) can be expressed as:

$$I^{(SM)} = 2 \log_2 \left(1 + \frac{\rho}{2} \lambda_1 + \frac{\rho}{2} \lambda_2 + \frac{\rho^2}{4} (\lambda_1 \lambda_2 - H_{1,2}^2)\right) \quad (2.69)$$

From the Cauchy-Schwartz inequality we have:

$$\lambda_1 \lambda_2 - H_{1,2}^2 = \int_0^{T_i} h_1^2(t) dt \int_0^{T_i} h_2^2(t) dt - \left( \int_0^{T_i} h_1(t) h_2(t) dt \right)^2 \geq 0$$

This implies that:

$$I^{(2)} \geq 2 \log_2 \left(1 + \frac{\rho}{2} (\lambda_1 + \lambda_2)\right) \quad (2.70)$$

In a similar way, eq. (2.69) can be upper bounded by:

$$2^{I^{(SM)}} \leq \left(1 + \frac{\rho}{2} \lambda_1\right) \left(1 + \frac{\rho}{2} \lambda_2\right) \leq \frac{1}{2} \left(2 + \frac{\rho}{2} (\lambda_1 + \lambda_2)\right)^2 \leq \left(1 + \frac{\rho}{2} (\lambda_1 + \lambda_2)\right)^2 \quad (2.71)$$

Finally, eq. (2.70) and eq. (2.71) result in:

$$P_{ref}(r, \rho, U, V, 2, 4) \leq P_{out}^{(SM)}(r, \rho) \leq P_{ref}(r, \rho, U, V, 2, 2) \quad (2.72)$$

$$d_{ref}(r, \rho, U, V, 2, 2) \leq d^{(SM)}(r, \rho) \leq d_{ref}(r, \rho, U, V, 2, 4) \quad (2.73)$$

where  $U$  and  $V$  are obtained by setting  $P = 2$  in eq. (2.61). Equations (2.63) and (2.73) show that the D-MG tradeoff achieved by the orthogonal rate-1 codes is less than the maximum achievable tradeoff over the considered channel. This shows that these codes that are not optimal over the Rayleigh fading channels [48] are also not optimal over the UWB channels in [17].

Fig. 2.5 shows the achieved D-MG tradeoff over CM1 at  $\rho = 15$  dB and  $\rho = 30$  dB with  $T_i = 5$  ns. Results show that single-antenna and multi-antenna UWB systems achieve an infinite diversity gain at  $r = 0$ . However, the superiority of the multi-antenna systems is evident in all cases. This figure also shows the non-optimality of the simple rate-1 orthogonal coding schemes.

Fig. 2.6 shows the achieved D-MG tradeoffs over CM4 at  $\rho = 20$  dB with  $T_i = 1$  ns. For comparison reasons, we also show the D-MG tradeoff of the single-antenna systems with  $T_i = \Gamma$  (which is equivalent to an All-Rake). The derived bounds permit to have more insights on the D-MG tradeoff especially for large number of antennas and high SNRs because, in these cases, the simulation results are not exact because the outage probability curves are very steep. Results show that for high data rates, it is more beneficial to increase the number of transmit antennas rather than the integration time (or the number of Rake fingers). For example, a 2-antenna (or 4-antenna) system combining only the first 2 arriving multi-path components has a much better D-MG tradeoff than a single antenna system that profits from the full multi-path diversity (for  $r > 1$ ). It is worth noting that this diversity advantage is not associated with an increased complexity because in practice a multi-antenna system with limited number of Rake fingers is simpler to implement than a single-antenna All-Rake receiver that necessitates the estimation of the amplitudes of a very large number of multi-path components.

## 2.4 Interference model

### 2.4.1 Inter Symbol Interference

Each symbol can interfere with  $N_{isi}$  symbols such that:

$$N_{isi} = \left\lceil \frac{\Gamma - T_g'}{N_f T_f} \right\rceil \quad (2.74)$$

where  $T_g'$  is given in eq. (2.15). For Rake receivers, the ISI on the decision variable  $x_{q,l,p,n,m}$  in eq. (2.10) is given by:

$$x_{q,l,p,n,m}^{(isi)} = \int_{nT_f}^{(n+1)T_f} r_q^{(isi)}(t) \tilde{w}_{q,l,p,n,m}(t) dt \quad (2.75)$$

where  $\tilde{w}_{q,l,p,n,m}(t)$  is given in eq. (2.8) and  $r_q^{(isi)}(t)$  is given in eq. (2.6). Denote by  $X_{isi}$  the vector of length  $QLP'N_fM$  constructed from  $x_{q,l,p,n,m}^{(isi)}$  in eq. (2.75) in the same way as the vector  $X$  was constructed from the decision variables  $x_{q,l,p,n,m}$  in eq. (2.22).  $X_{isi}$  can be expressed as:

$$X_{isi} = R_{isi} (I_{N_{isi}} \otimes (\mathcal{B} \otimes I_M)) A_{isi} \quad (2.76)$$

where:

- $A_{isi}$  is a  $N_{isi}PM$  vector. For the given symbol duration,  $A_{isi}$  corresponds to the symbols that will interfere with the considered transmitted vector. If  $A(j)$  corresponds to the  $PM$ -dimensional information vector transmitted from the  $P$  antennas during the  $j$ -th symbol duration, then  $A_{isi} = [A^T(j-N_{isi}) \cdots A^T(j-1)]^T$ .
- $R_{isi}$  is a  $QLP'N_fM \times N_{isi}PN_fM$  given by:  $R_{isi} = [R(1) \cdots R(N_{isi})]$  where  $R(j)$  is a  $QLP'N_fM \times PN_fM$  matrix for  $j = 1, \dots, N_{isi}$ .  $R(j) = [R_1^T(j) \cdots R_Q^T(j)]^T$  where  $R_q(j)$  is a  $LP'N_fM \times PN_fM$  matrix for  $q = 1, \dots, Q$ .  $R_q(j) = [R_{q,0}^T(j) \cdots R_{q,L-1}^T(j)]^T$  where  $R_{q,l}(j)$  is a  $P'N_fM \times PN_fM$  matrix for  $l = 0, \dots, L-1$ .  $R_{q,l}(j)$  is given by:

$$R_{q,l}(j) = \begin{bmatrix} R_{q,l,1,1}(j) & \cdots & R_{q,l,1,P}(j) \\ \vdots & \ddots & \vdots \\ R_{q,l,P',1}(j) & \cdots & R_{q,l,P',P}(j) \end{bmatrix} \quad (2.77)$$

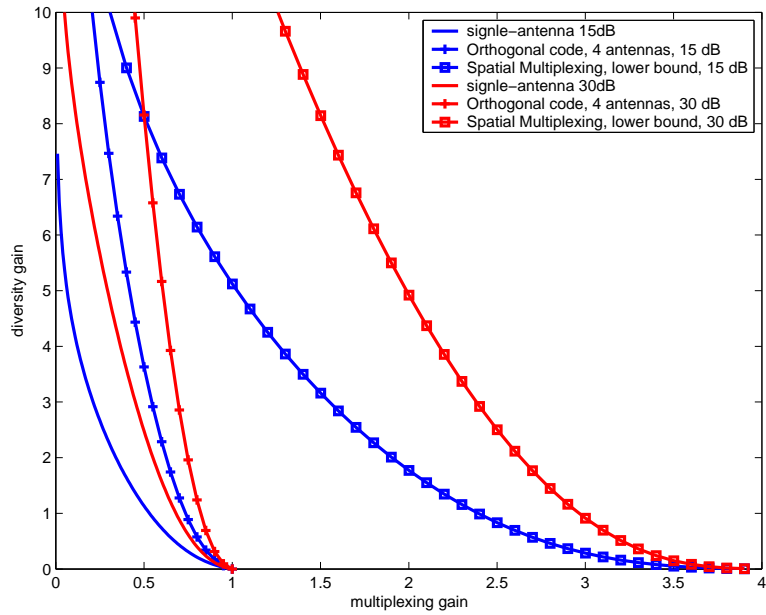


Figure 2.5: D-MG tradeoffs over CM1 at a SNR of 15 dB and 30 dB with  $T_i = 5$  ns.

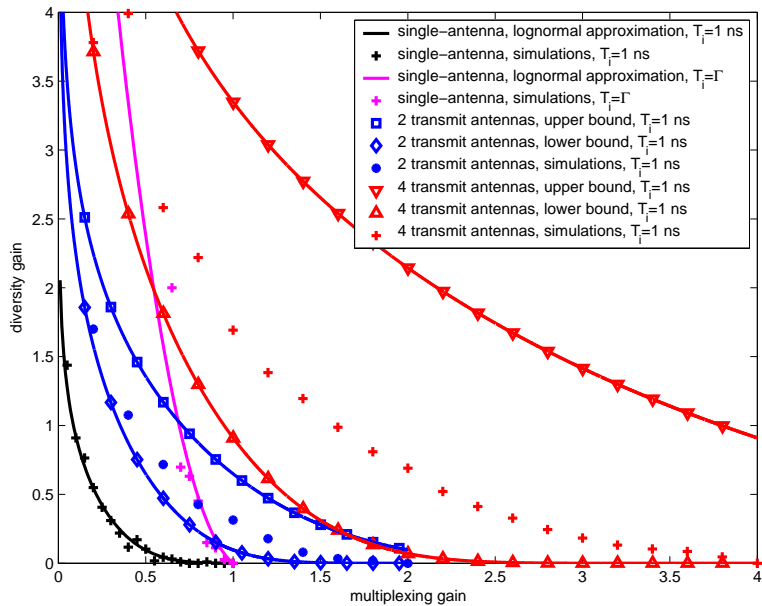


Figure 2.6: D-MG tradeoffs over CM4 at a SNR of 20 dB.

where  $R_{q,l,p,p'}(j)$  is a  $N_f M \times N_f M$  matrix whose  $(nM + m + 1, n'M + m' + 1)$ -th element is given by:

$$r_{q,p'} (\Delta_{q,p,l} + (m - m')\delta + (c_n - c_{n'})T_c + (n - n' + jN_f)T_f) \quad (2.78)$$

for  $n, n' \in \{0, \dots, N_f - 1\}$  and  $m, m' \in \{0, \dots, M - 1\}$ .

For correlation receivers,  $R(j)$  is obtained by the vertical concatenation of  $R_q(j) = [R_{q,p,p'}(j)]_{p,p'=1}^P$ . The  $(nM + m + 1, n'M + m' + 1)$ -th element of the  $N_f M \times N_f M$  matrix  $R_{q,p,p'}(j)$  is given by:

$$r_{q,p,p'} ((m - m')\delta + (c_n - c_{n'})T_c + (n - n' + jN_f)T_f) \quad (2.79)$$

## 2.4.2 Multi User Interference

We suppose that the users are symbol-synchronous. This is a generally accepted approximation given that the symbol duration is very large with respect to the pulse width. In other words,  $\tau^{(k)}$  in eq. (2.4) is written as  $\tau^{(k)} = \tau_1^{(k)} T_f + \tau_2^{(k)}$  where  $\tau_1^{(k)}$  is uniformly distributed over  $[-\frac{N_f}{2}, \frac{N_f}{2}]$  and  $\tau_2^{(k)}$  is uniformly distributed over  $[-\frac{T_f}{2}, \frac{T_f}{2}]$ . The  $n$ -th frame of the  $(j - x)$ -th symbol interferes with the first frame of the  $j$ -th symbol if  $(x, j, n \in \mathbb{N})$ :

$$\Gamma - T_g' \geq xN_f T_f - nT_f - \tau^{(k)} \quad (2.80)$$

We first consider the case  $\tau^{(k)} < 0$ . Given that  $n \leq N_f - 1$  and  $\tau^{(k)} < 0$ , the maximum value of  $x$  in eq. (2.80) is denoted by  $N_{mui}^-$  and is given by:

$$N_{mui}^- = \left\lceil \frac{\Gamma - T_g'}{N_f T_f} + \frac{N_f - 1}{N_f} \right\rceil + 1 \quad (2.81)$$

where the first part of the right hand-side of eq. (2.81) corresponds to the causal interference caused by the symbols of the  $k$ -th user that precede the  $j$ -th symbol of the desired user ( $x \in \mathbb{N}$ ). The coefficient 1 was added since  $\tau^{(k)} < 0$  results in anti-causal interference. In other words, the  $(j + 1)$ -th symbol of the  $k$ -th user always interferes with the  $j$ -th symbol of the desired user when  $\tau^{(k)} < 0$ .

For  $\tau^{(k)} > 0$ , given that  $\tau^{(k)} \leq \frac{N_f}{2} T_f + \frac{T_f}{2}$  and  $n \leq N_f - 1$ , the maximum value of the symbol index  $x$  in eq. (2.80) is equal to:

$$N_{mui}^+ = \left\lceil \frac{\Gamma - T_g'}{N_f T_f} + \frac{3N_f - 1}{2N_f} \right\rceil \quad (2.82)$$

Note that for synchronous user,  $N_{mui} = N_{isi} + 1$  since the  $j$ -th symbol is interfered on by  $N_{isi}$  preceding symbols and by the  $j$ -th symbol of the  $k$ -th user ( $N_{isi}$  is given in eq. (2.74)). On the other hand, for systems that do not suffer from ISI,  $N_{isi} = 0$  and  $N_{mui}^- = N_{mui}^+ = 2$  for asynchronous users. In other words, the  $j$ -th and the  $(j + 1)$ -th (resp.  $(j - 1)$ -th) symbols of the  $k$ -th user interfere on the  $j$ -th symbol of the desired user for  $\tau^{(k)} < 0$  (resp.  $\tau^{(k)} > 0$ ).

The additional multi-user interference can be included in the vector  $X_{mui}$  of length  $QLP'N_f M$ :

$$X_{mui} = \sum_{k=1}^K \sqrt{\varepsilon_k} X^{(k)} \quad (2.83)$$

The interference from the  $k$ -th user is given by:

$$X^{(k)} = R^{(k)} \left( I_{N_{mui}^{(k)}} \otimes \left( \mathcal{B}^{(k)} \otimes I_M \right) \right) A_{mui}^{(k)} \quad (2.84)$$

where  $N_{mui}^{(k)} = N_{mui}^-$  given in eq. (2.81) for  $\tau^{(k)} < 0$  and  $N_{mui}^{(k)} = N_{mui}^+$  given in eq. (2.82) for  $\tau^{(k)} > 0$ .

- If  $A^{(k)}(j)$  corresponds to the  $PM$ -dimensional vector transmitted from the  $k$ -th user during the  $j$ -th symbol duration, then  $A_{mui}^{(k)}$  is the  $N_{mui}^{(k)}PM$  vector given by:

$$A_{mui}^{(k)} = \left[ A^{(k)T} \left( j - \mathcal{J}^{(k)}(1) \right) \cdots A^{(k)T} \left( j - \mathcal{J}^{(k)}(N_{mui}^{(k)}) \right) \right]^T \quad (2.85)$$

where  $\mathcal{J}^{(k)}$  is the set composed of  $N_{mui}^{(k)}$  integers and it is given by:

$$\mathcal{J}^{(k)} = \begin{cases} \{-(N_{mui}^- - 2), \dots, 1\}, & \tau^{(k)} < 0 \\ \{-(N_{mui}^+ - 1), \dots, 0\}, & \tau^{(k)} \geq 0 \end{cases} \quad (2.86)$$

- For Rake receivers,  $R^{(k)}$  is a  $QLP'N_fM \times N_{mui}^{(k)}PN_fM$  matrix given by:  $R^{(k)} = [R^{(k)}(1) \cdots R^{(k)}(N_{mui}^{(k)})]$  where the constituent matrices are obtained from the vertical concatenation of the matrices  $R_{q,l}^{(k)}(j)$  of dimensions  $P'N_fM \times PN_fM$  for  $l = 0, \dots, L-1$ ,  $q = 1, \dots, Q$  and  $j = 1, \dots, N_{mui}^{(k)}$ .  $R_{q,l}^{(k)}(j)$  has the same structure as in eq. (2.77) but now the  $(nM + m + 1, n'M + m' + 1)$ -th element of the constituent matrix  $R_{q,l,p,p'}^{(k)}(j)$  is given by:

$$r_{q,p'}^{(k)} \left( \Delta_{q,p,l} + (m - m')\delta + \left( c_n - c_{n'}^{(k)} \right) T_c + \left( n - n' - \mathcal{J}^{(k)}(j)N_f \right) T_f - \tau^{(k)} \right) \quad (2.87)$$

for  $n, n' \in \{0, \dots, N_f - 1\}$  and  $m, m' \in \{0, \dots, M - 1\}$ .

For synchronous users that do not suffer from ISI:

$$X^{(k)} = R^{(k)} \left( \mathcal{B}^{(k)} \otimes I_M \right) A_{mui}^{(k)} \quad (2.88)$$

where  $A_{mui}^{(k)} = A^{(k)}(j)$  for the  $j$ -th symbol duration. In this case,  $R^{(k)}$  is a  $QLP'N_fM \times PN_fM$  matrix constructed from the vertical concatenation of the matrices  $R_{q,l}^{(k)}$  of for  $l = 0, \dots, L-1$  and  $q = 1, \dots, Q$ . In this case,  $R_{q,l,p,p'}^{(k)}$  is a  $N_fM \times N_fM$  block-diagonal matrix given by:

$$R_{q,l,p,p'}^{(k)} = \text{diag} \left( R_{q,l,p,p',0}^{(k)} \cdots R_{q,l,p,p',N_f-1}^{(k)} \right) \quad (2.89)$$

where the  $(m, m')$ -th element of the constituent  $M \times M$  matrix  $R_{q,l,p,p',n}^{(k)}$  takes the form:

$$R_{q,l,p,p',n}^{(k)}(m, m') = r_{q,p'}^{(k)} \left( \Delta_{q,p,l} + (m - m')\delta + \left( c_n - c_n^{(k)} \right) T_c \right) \quad (2.90)$$

For correlation receivers, the term corresponding to MUI has the same expression as eq. (2.84). In this case,  $R^{(k)} = [R^{(k)}(1) \cdots R^{(k)}(N_{mui}^{(k)})]$ .  $R^{(k)}(j)$  is obtained from the vertical concatenation of  $R_q^{(k)}(j) = \left[ R_{q,p,p'}^{(k)}(j) \right]_{p,p'=1}^P$ . The  $(nM + m + 1, n'M + m' + 1)$ -th element of the matrix  $R_{q,p,p'}^{(k)}(j)$  is given by:

$$r_{q,p,p'}^{(k)} \left( (m - m')\delta + \left( c_n - c_{n'}^{(k)} \right) T_c + \left( n - n' - \mathcal{J}^{(k)}(j)N_f \right) T_f - \tau^{(k)} \right) \quad (2.91)$$

Finally, including the effect of ISI and MUI, eq. (2.33) generalizes to:

$$Y = HA + \underbrace{DR_{isi}(I_{N_{isi}} \otimes (\mathcal{B} \otimes I_M))}_{H_{isi}} A_{isi} + H_{mui} A_{mui} + N \quad (2.92)$$

where  $A_{mui}$  is given from the vertical concatenation of  $A_{mui}^{(k)}$  given in eq. (2.84) for  $k = 1, \dots, K$ .  $H_{mui}$  follows from eq. (2.83) and eq. (2.84):

$$H_{mui} = D\text{diag}\left(\sqrt{\mathcal{E}_1} \dots \sqrt{\mathcal{E}_K}\right) \left[R^{(1)} \dots R^{(K)}\right] \text{diag}\left(I_{N_{mui}^{(1)}} \otimes (\mathcal{B}^{(1)} \otimes I_M) \dots I_{N_{mui}^{(K)}} \otimes (\mathcal{B}^{(K)} \otimes I_M)\right) \quad (2.93)$$

For Rake receivers, the dimensions of  $H$ ,  $H_{isi}$  and  $H_{mui}$  are given by  $QLP'M \times PM$ ,  $QLP'M \times N_{isi}PM$  and  $QLP'M \times N_{mui}PM$  respectively where  $N_{mui} = \sum_{k=1}^K N_{mui}^{(k)}$  ( $P' = P$  for SRakes and  $P' = 1$  for PRakes). For correlation receivers, the number of rows of these matrices changes from  $QLP'M$  to  $QPM$ .

### 2.4.3 Performance with MMSE receivers

In order to eliminate the effect of ISI and MUI, a simple linear detector based on the minimum-mean-square-error (MMSE) criterion is implemented at the receiver side. A MMSE filter used for detecting the data vector  $A$  in eq. (2.92) is given by:

$$C_{MMSE} = H^T \left( HH^T + H_{isi}H_{isi}^T + H_{mui}H_{mui}^T + \frac{P}{E_s} \Sigma_n \right)^{-1} \quad (2.94)$$

where  $\Sigma_n$  is the noise covariance matrix whose elements can be determined from eq. (2.14) and eq. (2.29) for Rake and correlation receivers respectively. Since the receiver has no access to the CSI of the interfering users, the MMSE filter can be determined from  $C_{MMSE} = E[AY^T] (E[YY^T])^{-1}$  where the average is calculated over a training sequence.

Let  $Z = C_{MMSE}Y$ ,  $V = C_{MMSE}H$ ,  $V^{(isi)} = C_{MMSE}H_{isi}$ ,  $V^{(mui)} = C_{MMSE}H_{mui}$  and  $U = C_{MMSE}C_{MMSE}^T$ . For 2-PAM constellations, the conditional probability of detecting the symbols of the  $p$ -th transmit antenna erroneously is given by:

$$P_{e/H}^{(p)} = \frac{1}{2^{N_{isi}N_{mui}P^2(P-1)}} \sum_{A \in \{\pm 1\}^{P-1}} \sum_{A_{isi} \in \{\pm 1\}^{N_{isi}P}} \sum_{A_{mui} \in \{\pm 1\}^{N_{mui}P}} Q\left(\frac{V_{p,p} + \bar{V}_p A + V_p^{(isi)} A_{isi} + V_p^{(mui)} A_{mui}}{\sqrt{U_{p,p} PN_0 / 2E_s}}\right) \quad (2.95)$$

where  $X_i$  and  $X_{i,j}$  correspond to the  $i$ -th row and the  $(i, j)$ -th element of the matrix  $X$  respectively.  $\bar{V}_p$  is obtained by removing the  $p$ -th element from the  $p$ -th row of  $V$ .

Assuming that after applying the MMSE filter the co-channel interference, ISI and MUI are zero-mean Gaussian, eq. (2.95) can be approximated by:

$$P_{e/H}^{(p)} \approx Q\left(\frac{V_{p,p}}{\sqrt{U_{p,p} PN_0 / 2E_s + \bar{V}_p \bar{V}_p^T + V_p^{(isi)} V_p^{(isi)T} + V_p^{(mui)} V_p^{(mui)T}}}\right) \quad (2.96)$$

When it is possible to calculate eq. (2.95), i.e. for small values of  $P$ ,  $N_{isi}$  and  $N_{mui}$ , we realized that there is no difference between the values given by eq. (2.95) and eq. (2.96). This can be explained by the fact that the MMSE filter succeeds in suppressing co-channel interference, ISI and MAI [95].

Motivated by the fact that eq. (2.96) is a good indicator on the error performance, we now present an upper bound on the performance of  $M$ -PPM-2-PAM constellations. We keep the same notations as above and we denote by  $V^{(p)}$  the  $M \times M$  matrix obtained from the elements  $V_{(p-1)M+m, (p-1)M+m'}$  for  $p, p' = 1, \dots, P$  and  $m, m' = 0, \dots, M-1$  where, for notational simplicity,  $X_{i,j}$  is the  $(i+1, j+1)$ -th element of the matrix  $X$  in what follows. Suppose that a symbol  $s = \pm 1$  is transmitted at the  $m$ -th position

of the  $p$ -th transmit antenna, considering that co-channel interference, ISI and MAI are Gaussian, then the outputs of the  $M$  correlators corresponding to this antenna are given by:

$$y_{m'}^{(p)} = V_{m',m}^{(p)} s + n_{m'} \quad (2.97)$$

for  $m' = 0, \dots, M - 1$ . The term  $n_{m'}$  includes the effect of noise, co-channel interference, ISI and MAI. It will be considered as a zero-mean Gaussian random variable. In this case, its variance is given by:

$$\sigma_{m'}^2 = U_{m',m'}^{(p)} P N_0 / 2 E_s + \frac{1}{M} \{ \bar{V}_{(p-1)M+m'}^T \bar{V}_{(p-1)M+m'} + V_{(p-1)M+m'}^{(isi)} V_{(p-1)M+m'}^{(isi)T} + V_{(p-1)M+m'}^{(mui)} V_{(p-1)M+m'}^{(mui)T} \} \quad (2.98)$$

where  $U^{(p)}$  is constructed in the same way as  $V^{(p)}$  and  $\bar{V}_i$  (with  $i = (p-1)M + m'$ ) stands for removing the elements  $(p-1)M + 1, \dots, pM$  of the  $(i+1)$ -th row of the matrix  $V$ .

Applying an approach similar to that used in Appendix B, the conditional probability of detecting the pulse emitted at the  $m$ -th position of the  $p$ -th transmit antenna erroneously can be upper-bounded by:

$$P_{e/H}^{(p,m)} \leq Q_{p,m}^{(0)} + \sum_{m'=0; m' \neq m}^{M-1} Q_{p,m,m'}^{(1)} + Q_{p,m,m'}^{(2)} - 2Q_{p,m,m'}^{(1)} Q_{p,m,m'}^{(2)} \quad (2.99)$$

where  $Q_{p,m}^{(0)} = Q \left( \frac{V_{m,m}^{(p)}}{\sqrt{\sigma_m^2}} \right)$  and  $Q_{p,m,m'}^{(i)} = Q \left( \frac{V_{m,m}^{(p)} + (-1)^i V_{m',m}^{(p)}}{\sqrt{\sigma_m^2 + \sigma_{m'}^2}} \right)$  for  $i = 1, 2$ . The conditional error probability can be calculated from:

$$P_{e/H} = \frac{1}{M} \sum_{p=1}^P \sum_{m=0}^{M-1} P_{e/H}^{(p,m)} \quad (2.100)$$

For  $M$ -PPM,  $Q_{p,m}^{(0)}$  and  $Q_{p,m,m'}^{(2)}$  are set to zero. Since the performance is determined over the IEEE channel model [17] that does not lend itself to analytical solutions, the average error probability is evaluated by Monte Carlo simulations. More precisely, the error probability is determined by averaging  $P_{e/H}$  over different realizations of the channel, the interfering users' channels, the amplitude spreading matrices and the TH sequences.

#### 2.4.4 Designing the amplitude-spreading sequences

In [96], Poor *et al.* observed that randomizing the polarity of the pulses of a given information symbol resulted in a better immunity against MUI even in asynchronous single-antenna networks. In this section, we further investigate this point and propose a simplified construction of the randomizing sequences for single-antenna as well as multi-antenna systems. In particular, we consider the problem of designing the amplitude spreading matrices  $B^{(k)}$  for  $k = 0, \dots, K + 1$  where  $K$  is the number of interfering users. In what follows, these matrices are taken to be unitary.

The adopted approach consists of designing the amplitude-spreading sequences and the time-hopping sequences independently from each other. Without discussing neither the benefit nor even the feasibility of jointly designed sequences, the proposed approach results in a simple design criterion that can be readily exploited for designing interference-reducing amplitude-spreading sequences. So, the hopping sequences are designed as if there was no amplitude spreading and vice versa.

We consider the case of synchronous users. In the absence of ISI and TH, combining eq. (2.20), eq. (2.83) and eq. (2.88) we obtain:

$$X = R (\mathcal{B} \otimes I_M) A + \sum_{k=1}^K \sqrt{E_k} R^{(k)} \left( \mathcal{B}^{(k)} \otimes I_M \right) A_{mu}^{(k)} + N \quad (2.101)$$

Since no TH is used, the constituent elements of the matrix  $R^{(k)}$  given in eq. (2.90) have the same expression for all values of  $n$ . Therefore, eq. (2.101) can be written in a more convenient way as:

$$\chi = R\mathcal{A}B + \sum_{k=1}^K \sqrt{\mathcal{E}_k} R^{(k)} \mathcal{A}_{mui}^{(k)} B^{(k)} + \mathcal{N} \quad (2.102)$$

where the matrix  $\chi$  (of dimensions  $QLP'M \times N_f$ ) is obtained by rearranging the components of vector  $X$  whose length is equal to  $QLP'N_fM$ . If  $A$  is written as  $A = [A_1^T \cdots A_P^T]^T$ , then  $\mathcal{A} = \text{diag}(A_1^T \cdots A_P^T)$ .  $\mathcal{A}_{mui}^{(k)}$  is constructed in the same way.

Despread the components of eq. (2.102) is equivalent to multiplying by  $B^T$  resulting in:

$$\gamma = \chi B^T = R\mathcal{A} + \sum_{k=1}^K \sqrt{\mathcal{E}_k} R^{(k)} \mathcal{A}_{mui}^{(k)} B^{(k)} B^T + \mathcal{N} B^T \quad (2.103)$$

Based on eq. (2.103) and inspired from [97], we propose to construct the spreading matrices based on minimizing:

$$\max_{0 \leq k \leq K+1} \sum_{\substack{l=0 \\ l \neq k}}^{K+1} \det(B^{(k)^T} B^{(l)}) \quad (2.104)$$

This design criterion simply states that the spreading matrices of the different users must be chosen to be as orthogonal to each other as possible. Unlike the CDMA-like systems ( $N_f \gg 1$ ) where all the matrices  $B^{(k)}$  are chosen to be orthogonal to each other, the limited value of  $N_f$  and the potentially large number of users sharing the channel renders the totally orthogonal choice impossible. Equation (2.104) is equivalent to choosing the set  $\{B^{(0)}, \dots, B^{(K)}\}$  that maximizes:

$$d = \min_{0 \leq k \leq K+1} \sum_{\substack{l=0 \\ l \neq k}}^{K+1} \prod_{p=1}^P \sin^2 \theta_p^{(k,l)} \quad (2.105)$$

where  $(\theta_1^{k,l}, \dots, \theta_P^{k,l})$  are the principal angles (modulo  $\frac{\pi}{2}$ ) between the two subspaces generated from the rows of  $B^{(k)}$  and  $B^{(l)}$ .

From eq. (2.105), the construction of the spreading matrices depends on the number of interfering users. For example, a family of  $K+1$  matrices is designed for a network with  $K+1$  users. Now, if a user leaves the network, the matrices of the remaining  $K$  users must be changed since the optimal set of matrices for  $K$  users is not a subset of the set of optimal matrices for  $K+1$  users. In other words, all users must update their spreading matrices whenever a user joins or leaves the network. Taking this in consideration and observing that  $d \geq Kd_{min}$ , we propose to maximize:

$$d_{min} = \min_{0 \leq k \neq l \leq K+1} \prod_{p=1}^P \sin^2 \theta_p^{(k,l)} \quad (2.106)$$

In this way, the inclusion property is maintained and the family of matrices can be designed based on a single parameter that corresponds to the maximum number of users whose interference must be rejected. Maximizing eq. (2.106) is equivalent to reducing the interference between two particular users without taking other users in consideration. This simplification is similar to the classical approach of calculating the pairwise error probability in order to find a union bound on the performance. Another interpretation of eq. (2.106) is that it is the design under a worst-case scenario.

Equation (2.106) is nothing but the design criterion for the construction of non-coherent ST codes [98]. In what follows we fix  $N_f = 2P$  which, given the number of transmit antennas corresponds to low-dimensional spreading. Now, the approach used in [99] for the construction of such codes can be readily applied to the design of a family of matrices satisfying eq. (2.106).

$$B = I_{P \times 2P} \exp \begin{pmatrix} \mathbf{0}_{P \times P} & C^T \\ -C & \mathbf{0}_{P \times P} \end{pmatrix} \quad (2.107)$$

where  $C$  is any  $P \times P$  coherent ST code satisfying the design criteria of [50]. This code is scaled in order to insure that all principal angles in eq. (2.106) are smaller than  $\pi/2$ . In particular,  $C$  can be any full rate and fully diverse ST code. In this way, if  $C$  is constructed from the vectors  $s = [s_1, \dots, s_{P^2}]$  whose elements  $s_i \in \{\pm 1, \dots, \pm n_u\}$ , then  $(2n_u)^{P^2}$  users can share the same channel. To each one of these users is given a spreading matrix corresponding to a particular value of the vector  $s$ . Moreover, if  $C$  has a non-vanishing coding gain, then  $n_u$  can have large values without limiting the capability of reducing the interference level.

As in [96], when amplitude spreading is combined with TH, the resulting system is expected to suffer from less interference than systems using TH exclusively.

## 2.5 Numerical Results

### 2.5.1 All-digital systems based on direct sampling

We consider uncoded MIMO systems on CM2 with correlation receivers, MMSE decoders and 4-PPM-2-PAM constellations in the absence of ISI and MUI. We fix  $T_i = \Gamma$ . In particular, we compare simulation results with a semi-analytical approach based on the upper bound in eq. (2.99). Results presented in Fig. 2.7 show that the upper-bound is very close especially at high SNRs. The considered receivers combine the entire channel impulse responses that show low cross-correlations (refer to Section 1.1.5). Results show that a ML receiver shows practically the same performance as the MMSE linear receiver. Therefore, even though the fading margin is very low for  $T_i = \Gamma$ , the quasi-orthogonality of the constituent sub-channels results in higher rates with simple transceiver structures.

In Fig. 2.7, we also show the performance of a practical all-digital implementation of the correlation receivers. In this case, the reference and the received signals are sampled at 20 Gsample/s and quantized over 1 bit. Moreover, the reference signal is averaged over 100 symbol durations. The advantage of the MIMO techniques is evident with these practical systems.

### 2.5.2 Coded systems over realistic indoor channels

In this section we show the performance of PRake receivers with 1 receive antenna over the MIMO-UWB channel measurements given in Appendix A. We consider 2-PAM with the coded systems presented in Section 2.2. Fig. 2.8 shows the performance with different number of transmit antennas and Rake fingers. For a given number of transmit antennas, the difference between the error values at two different SNRs corresponds to the diversity gain. This difference increases with the number of transmit antennas showing the enhanced diversity order.

For a fixed diversity order given by the product  $PL$ , it seems more beneficial to increase the number of transmit antennas ( $P$ ) rather than the number of Rake fingers ( $L$ ). For example, for a diversity order

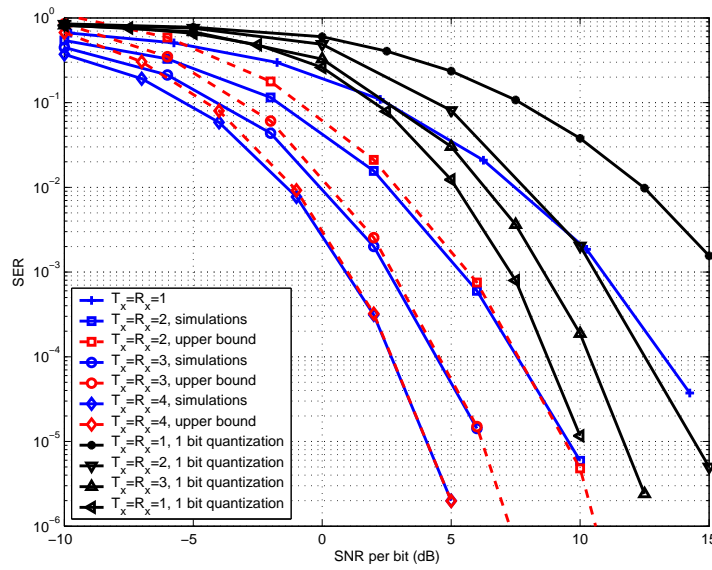


Figure 2.7: Performance of spatial multiplexing over CM2 with 4-PPM-2-PAM, correlation receivers and MMSE detectors.

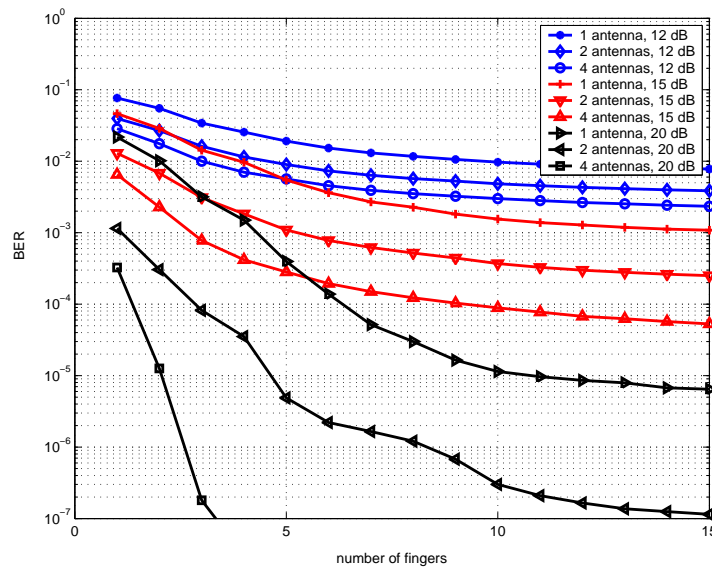


Figure 2.8: Performance of the rate-1 coded system over the measured channels with 2-PAM for different numbers of Rake fingers.

of 12 at 20 dB, the error rates with  $P = 1, 2$  and  $4$  ( $L = 12, 6$  and  $3$ ) are equal to  $9.10^{-6}$ ,  $2.10^{-6}$  and  $2.10^{-7}$  respectively. Note that this advantage is visible especially at high SNRs where the performance is dominated by fading. For low SNRs where the performance is dominated by the noise, increasing  $L$  may be more beneficial since this enhances the energy capture (that does not increase with  $P$ ).

### 2.5.3 Coverage extension offered by the MIMO techniques

Given the very low tolerated transmission levels [2], UWB systems often suffer from very limited communication ranges (especially for high data rate systems). In this context, the MIMO techniques can offer higher data rates at a given communication distance or, in an equivalent manner, they can extend the coverage of WPANs.

Designate by  $E_b$  and  $N_0$  the average energy per information bit and the noise spectral density respectively. The ratio  $E_b/N_0$  can be related to the communication distance ( $d$ ) by [17]:

$$\frac{E_b}{N_0} = EIRP + 10 \log_{10}(B) + G_t + G_r - 10\alpha \log_{10}\left(\frac{4\pi f_c d}{c}\right) - 10 \log_{10}(R_b) - (-173.83 + F) - I \quad (2.108)$$

where  $EIRP$  is the effective isotropic radiated power,  $B$  is the  $-10$  dB bandwidth of the transmitted pulses.  $G_t$  and  $G_r$  are the gains of the transmit and receive antennas respectively.  $\alpha$  is the path loss exponent. If  $f_{min}$  and  $f_{max}$  stand for the  $-10$  dB edges of the spectrum occupied by the waveforms, then  $f_c = \sqrt{f_{min}f_{max}}$ .  $F$  is the noise figure of the receiver and  $I$  is the implementation loss.  $R_b = \frac{P \log_2(MM')}{N_f T_f}$  is the transmission rate. In what follows, we consider FCC-compliant Gaussian pulses occupying the [3.1 5.1] GHz bandwidth (refer to Section 1.1.2). In this case,  $EIRP = -41.25$  dBm/MHz [2]. Moreover, we fix  $G_t = G_r = 0$  dB,  $F = 6$  dB,  $I = 5$  dB and  $\alpha = 2$  which corresponds to free-space propagation.

$R_b(d)$  is plotted in Fig. 2.9 for the channel models CM1 and CM2 [17]. A peer-to-peer spatial multiplexing system is used with 4-PPM-2-PAM constellations. We fix  $N_f = 4$  while  $T_f$  is varied from 2.5 ns to 100 ns. The receiver consists of a PRake equipped with  $L = 3$  fingers followed by a MMSE equalizer to eliminate the effect of ISI. Equations (2.99) and (2.100) are averaged over  $10^4$  channel realizations by Monte Carlo simulations. At a second time, the value of  $E_b/N_0$  corresponding to a target SER of  $10^{-3}$  is determined and  $d$  is calculated from eq. (2.108). Results in Fig. 2.9 show that MIMO-UWB systems are strong candidates for very high data rate systems. While a single antenna system can not deliver more than 10 Mbps at a distance of 10 m on CM1, the  $6 \times 6$  system achieves the data rate of about 160 Mbps (without any channel coding or transmit diversity techniques). In general, data rates in the order of 1 Gbps are possible for communications ranges that do not exceed 3 m.

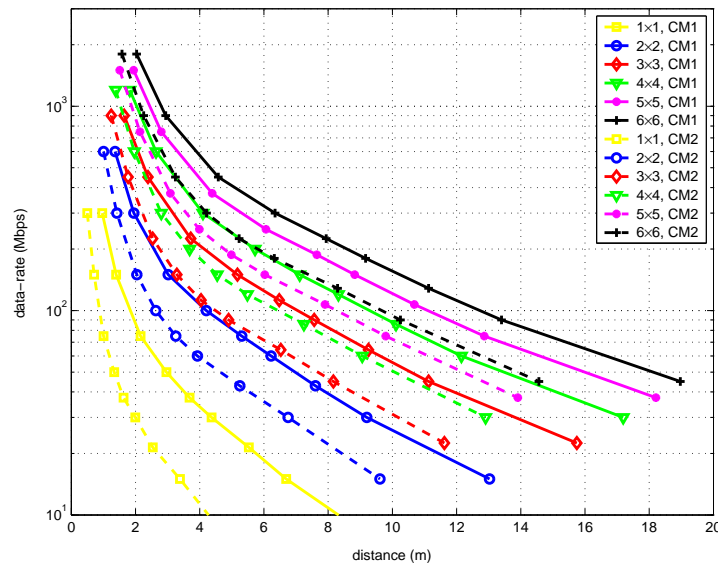


Figure 2.9: The achieved data rate vs. the communications distance at a SER of  $10^{-3}$  with 4-PPM-2-PAM, MMSE detectors and a 3-finger PRake.

# Chapter 3

## Full-Rate ST codes

In this chapter, we consider the construction of ST coding schemes with  $P$  transmit antennas. All of the considered codes will have a transmission rate of  $P$  symbols PCU. Since UWB is a baseband carrier-less technique, it can not be associated with any one of the full rate and fully diverse ST codes presented in Section 1.3.4 (except for the titled-QAM design which is a  $2 \times 2$  totally-real construction). This necessitates the construction of new totally-real ST codes. However, despite this limiting constraint, there is a number of additional degrees of freedom that can be exploited in designing full-rate coding schemes for IR-UWB systems:

- The first degree of freedom follows from the possibility of using different pulse shapes resulting in enhanced multiplexing gains.
- Another degree of freedom is the pulse repetitions that are intrinsic to TH-IR-UWB. While these repetitions mainly enhance the energy capture and the interference avoidance capabilities of TH-UWB systems, their presence is very beneficial in introducing new and simple transmit diversity schemes.
- Unlike the existing ST codes that were constructed for conventional QAM, PAM, PSK or HEX constellations, we can take advantage of the structure of the PPM and PPM-PAM constellations in order to propose new adapted coding schemes.

In this chapter, we first present a new partial-diversity scheme based on modified Hermite pulses associated with modulation diversity [36]. Then we propose three families of ST codes for TH-IR-UWB. The first family is based on the adaptation of the construction techniques based on cyclic division algebras [39, 62] to real-valued situations. At a second time, we take advantage of the pulse repetitions in order to propose a new coding scheme that encodes the pulses used to convey the same information symbol. Unlike the first families of codes that can be associated with PPM, PAM and PPM-PAM constellations, we propose a third family of codes that is exclusive to PPM or PPM-PAM constellations for some fixed values of the constellations' dimensions.

### 3.1 Partial Transmit Diversity Using Modified Hermite Pulses

In this case, the independent data streams transmitted from the different transmit antennas are rendered orthogonal by the use of modified Hermite pulses with different orders at each transmitter. More pre-

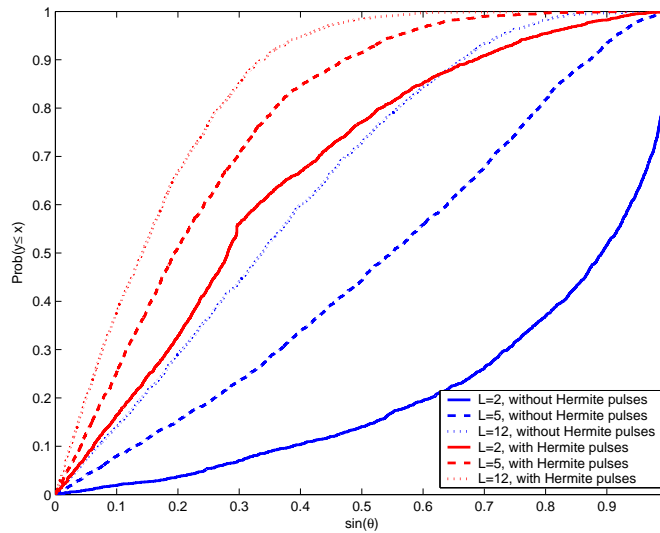


Figure 3.1: The orthogonality induced by the use of modified Hermite pulses over CM1.

cisely, the pulse waveform transmitted from the  $p$ -th antenna will consist of the modified Hermite polynomial of order  $p$  given in eq. (1.2). This waveform is denoted by  $w_p(t)$  in what follows. At the receiver side, each antenna is followed by  $P$  filters matched to  $w_p(t)$  for  $p = 1, \dots, P$ . For Rake receivers, the reference signal in eq. (2.8) will take the following form:

$$\tilde{w}_{q,l,p,n,m}(t) = w_p(t - nT_f - c_n T_c - \Delta_{q,p,l} - m\delta) \quad (3.1)$$

In this case the input-output relation in eq. (2.33) can be expressed as:

$$Y_{QLPM \times 1} = H_{QLPM \times PM} S_{PM \times 1} + N_{QLPM \times 1} \quad (3.2)$$

where  $H$  is the vertical concatenation of  $H_{q,l}$  for  $q = 1, \dots, Q$  and  $l = 0, \dots, L - 1$ .  $H_{q,l} = [R_{q,l,p,p'}]_{p,p'=1}^P$ . The expression of the  $(m, m')$ -th element of  $R_{q,l,p,p'}$  given in eq. (2.19) is now modified to:

$$R_{q,l,p,p'}(m, m') = r_{q,p,p'}((m - m')\delta + \Delta_{q,p,l}) \quad (3.3)$$

where  $r_{q,p,p'}(\tau) = \int h_{q,p'}(t) w_p(t - \tau) dt$  and in this case  $h_{q,p'}(t)$  is the convolution of the physical channel  $g_{q,p'}(t)$  with  $w_{p'}(t)$ . Note that when using modified Hermite pulses as signatures of the transmitted data streams, eq. (3.2) will have the same dimensionality with SRakes as well as PRakes. An expression similar to eq. (3.2) can be obtained with correlation receivers.

The vector  $S$  in eq. (3.2) is related to the information vector by:

$$S = (\mathcal{M} \otimes I_M) A \quad (3.4)$$

where  $\mathcal{M}$  can be any full-diversity  $P \times P$  rotation matrix [58, 100].

In eq. (3.4), a rotation is applied on the  $m$ -th components of the  $P$  information symbols for  $m = 1, \dots, M$ . After that, the rotated components are transmitted over the  $P$  signal subspaces determined by the different pulse forms. This strategy is similar to the one applied in [57]. In [57], rotations are applied between the  $P$  components of each layer of the codewords. At a second time, these layers are rendered orthogonal to each other by an appropriate choice of an algebraic or transcendental element.

In this section, we take advantage of the impulsive nature of the transmitted signal in order to introduce orthogonality by the use of modified Hermite pulses.

Because of the highly frequency selective UWB channel, multi-path components can arrive within the same pulse duration. This implies that the orthogonality is only partial at the receiver side. The orthogonality loss over CM1 is presented in Fig. 3.1 for a PRake with  $L = 2, 5$  and  $12$  fingers. We fix  $P = 2$  and  $Q = 1$  and the shown results correspond to the CDF of the sine of the principle angle between the columns of the channel matrix. Fig. 3.1 shows that co-channel interference is reduced despite the intra-pulse interference. We show later through simulations that the better conditioned channel matrix results in better performance. Moreover, the modulation diversity turns out to be robust against the mixing, caused by the channel, between the coordinates of the coded symbols that are mapped onto the different signal subspaces.

## 3.2 Inter-Symbol Coding (ISC)

In this case, the  $N_f$  pulses used to convey a given information symbol will all have the same amplitudes and positions. In other words, as with spatial multiplexing, we fix  $B = \mathbf{1}_{P \times N_f}$  (refer to Section 2.1.3). Extending eq. (2.33) over  $T$  symbol durations results in:

$$Y_{Q' \times T} = \mathcal{H}_{Q' \times PM} C_{PM \times T} + N_{Q' \times T} \quad (3.5)$$

where  $Q' = \{QLPM, QLM, QPM\}$  for SRakes, PRakes and correlation receivers respectively.  $Q$  is the number of receive antennas and  $M$  is the number of modulation positions of the  $M$ -PPM- $M'$ -PAM constellation.  $C$  is the ST codeword whose  $((p-1)M+m+1, t)$ -th entry corresponds to the amplitude of the pulse (if any) transmitted at the  $m$ -th position of the  $p$ -th transmit antenna during the  $t$ -th symbol duration for  $p = 1, \dots, P$ ,  $m = 0, \dots, M-1$  and  $t = 1, \dots, T$ .

In what follows, we limit ourselves to PAM constellations ( $M = 1$ ). The extension to the cases where  $M > 1$  will be discussed at the end of this section. Moreover, we consider minimal-delay codes and we fix  $P = T = n$ .

ISC is the construction based on totally-real cyclic division algebras (Definition 1.15). Since, we are limited to totally-real CDAs with PAM constellations, the center  $\mathbb{F}$  of the cyclic algebra  $\mathcal{A}(\mathbb{K}/\mathbb{F}, \sigma, \gamma)$  must be equal to  $\mathbb{Q}$ . In this case,  $\mathbb{K}$  can be any cyclic field extension of  $\mathbb{Q}$  with degree  $n$  and with Galois group  $Gal(\mathbb{K}/\mathbb{Q}) = \langle \sigma \rangle$  with  $\sigma^n = 1$ . Limiting the construction to the ring of integers  $\mathcal{O}_\mathbb{K}$  of  $\mathbb{K}$ , the  $n \times n$  codewords follow from eq. (1.20) as:

$$C_0 = \begin{bmatrix} k_0 & k_1 & k_2 & \cdots & k_{n-1} \\ \gamma\sigma(k_{n-1}) & \sigma(k_0) & \sigma(k_1) & \cdots & \sigma(k_{n-2}) \\ \gamma\sigma^2(k_{n-2}) & \gamma\sigma^2(k_{n-1}) & \sigma^2(k_0) & \cdots & \sigma^2(k_{n-3}) \\ \vdots & \vdots & \vdots & \vdots & \vdots \\ \gamma\sigma^{n-1}(k_1) & \gamma\sigma^{n-1}(k_2) & \gamma\sigma^{n-1}(k_3) & \cdots & \sigma^{n-1}(k_0) \end{bmatrix} \quad (3.6)$$

where  $k_i \in \mathcal{O}_\mathbb{K}$  for  $i = 0, \dots, n-1$ .  $n$  information symbols are contained in each value of  $k_i$  resulting in a full rate code. In other words,  $k_i = \sum_{j=0}^{n-1} a_{ni+j+1} \theta^j$  for  $i = 0, \dots, n-1$  where  $\{1, \theta, \dots, \theta^{n-1}\}$  is an integral basis of  $\mathcal{O}_\mathbb{K}$  and  $a_1, \dots, a_n$  are the information symbols that belong to a PAM constellation.

Consider the  $n$  information symbols  $a_{in+1}, \dots, a_{(i+1)n}$  for a given value of  $i \in \{0, 1, \dots, n-1\}$ . From

eq. (3.6), these symbols are contained uniquely in the conjugates of  $k_i$  according to:

$$\begin{bmatrix} k_i \\ \vdots \\ \sigma^{n-1}(k_i) \end{bmatrix} = \begin{bmatrix} 1 & \theta & \dots & \theta^{n-1} \\ \vdots & \vdots & \dots & \vdots \\ 1 & \sigma^{n-1}(\theta) & \dots & \sigma^{n-1}(\theta^{n-1}) \end{bmatrix} \begin{bmatrix} a_{in+1} \\ \vdots \\ a_{(i+1)n} \end{bmatrix} \triangleq \Gamma(\theta) \begin{bmatrix} a_{in+1} & \dots & a_{(i+1)n} \end{bmatrix}^T \quad (3.7)$$

Therefore, a modified version of the initial  $n$ -dimensional PAM constellation is transmitted. In order not to introduce any distortions on the PAM constellation, it is interesting that the transmitted and the original signal sets keep the same shape. This can be done by multiplying  $\Gamma(\theta)$  by a diagonal matrix  $D$  such that the matrix  $D' = D\Gamma(\theta)$  is unitary. In this case, the transmitted constellation is a rotated version of the initial signal set and no shaping losses are introduced. If  $D'$  is unitary, then  $\det(D) = \frac{1}{\sqrt{d_{\mathbb{K}}}}$  since  $\det(\Gamma(\theta)\Gamma(\theta)^T) \triangleq d_{\mathbb{K}}$  (the absolute discriminant of  $\mathbb{K}$ ).

When  $d_{\mathbb{K}}$  is a perfect square, we fix  $D = \text{diag}(\alpha, \dots, \sigma^{n-1}(\alpha))$  where  $\alpha \in \mathbb{K}$  verifying  $\det(D) = N_{\mathbb{K}/\mathbb{Q}}(\alpha) = \frac{1}{\sqrt{d_{\mathbb{K}}}}$ . In this case, the codewords are given by:

$$C = \text{diag}(\alpha, \sigma(\alpha), \dots, \sigma^{n-1}(\alpha)) C_0 \quad (3.8)$$

When  $d_{\mathbb{K}}$  is not a perfect square, we choose a totally positive element  $\alpha \in \mathbb{K}$  such that the diagonal matrix  $D$  is given by:  $D = \text{diag}(\sqrt{\alpha}, \dots, \sqrt{\sigma^{n-1}(\alpha)})$  and  $N_{\mathbb{K}/\mathbb{Q}}(\alpha) = \frac{1}{d_{\mathbb{K}}}$ . In this case the codewords take the form:

$$C = \text{diag}(\sqrt{\alpha}, \sqrt{\sigma(\alpha)}, \dots, \sqrt{\sigma^{n-1}(\alpha)}) C_0 \quad (3.9)$$

The above cases correspond to choosing an element  $\alpha$  such that:

$$\text{vol}(\alpha O_{\mathbb{K}}) = 1 \quad (3.10)$$

where  $\Lambda(\alpha O_{\mathbb{K}})$  is the lattice generated by the principal ideal  $\alpha O_{\mathbb{K}}$  and  $\text{vol}(\alpha O_{\mathbb{K}})$  stands for the volume of the fundamental parallelopiped of  $\Lambda(\alpha O_{\mathbb{K}})$ .

If  $\gamma \in \mathbb{Z}$  and  $\gamma$  is a non-norm element, then proposition 1.1 and proposition 1.2 imply that:

$$d_{\infty}(C) \triangleq \min_{a \in \mathbb{Z}^{n^2}, a \neq \mathbf{0}_{1 \times n^2}} |\det(C)| \quad (3.11)$$

$$= \det(D) \min_{a \in \mathbb{Z}^{n^2}, a \neq \mathbf{0}_{1 \times n^2}} |\det(C_0)| = \frac{1}{\sqrt{d_{\mathbb{K}}}} \quad (3.12)$$

since  $\det(C_0) \in \mathbb{Z}$  when  $\gamma \in \mathbb{Z}$  and  $\det(C_0) \neq 0$  for  $a \neq \mathbf{0}_{1 \times n^2}$  when  $\gamma$  is a non-norm element.

Equations (3.8) and (3.9) can be also expressed as:

$$C = \sum_{i=0}^{n-1} \text{diag}\left(\mathcal{M} \begin{bmatrix} a_{in+1}, \dots, a_{(i+1)n} \end{bmatrix}^T\right) \Omega^i \quad (3.13)$$

where  $\mathcal{M}$  is a  $n \times n$  matrix. Let  $\theta_0 = \theta$  and  $\theta_i = \sigma^i(\theta)$  for  $i = 1, \dots, n-1$ . When  $d_{\mathbb{K}}$  is a perfect square, the  $(i, j)$ -th element of  $\mathcal{M}$  is given by  $\sigma^{i-1}(\alpha \theta^{j-1}) = \sigma^{i-1}(\alpha) \theta_{i-1}^{j-1}$ . Otherwise,  $\mathcal{M}(i, j) = \sqrt{\sigma^{i-1}(\alpha)} \theta_{i-1}^{j-1}$ .

$\Omega$  is the  $n \times n$  matrix given by:

$$\Omega = \begin{bmatrix} 0 & 1 & \cdots & 0 \\ \vdots & 0 & \ddots & \vdots \\ 0 & \vdots & \ddots & 1 \\ \gamma & 0 & \cdots & 0 \end{bmatrix} \quad (3.14)$$

As a conclusion, ISC is based on eq. (3.13) and the design problem is reduced to the correct choice of the extension field  $\mathbb{K}$ , of a non-norm integer  $\gamma$  and of  $\alpha \in \mathbb{K}$  verifying eq. (3.10). ST codes constructed from eq. (3.13) will achieve full rate and full diversity with a non-vanishing minimum determinant and with no shaping losses.

As indicated in [63, 64], the choice  $|\gamma| = 1$  results in important performance gains. For totally-real codewords, transmitting a uniform average energy per antenna can be realized uniquely by  $\gamma = \pm 1$ . This implies that the constraint of having totally-real codewords results in energy non-efficient codes for  $n \geq 3$  since  $\gamma^2 = 1$  is always a norm in  $\mathbb{K}$  ( $N_{\mathbb{K}/\mathbb{Q}}(1) = 1$ ). Therefore, energy-efficient codes from CDAs are possible for  $n = 2$  transmit antennas uniquely. We will now present the construction of totally-real ST codes based on CDAs for  $n = 2, \dots, 6$ .

### 3.2.1 $2 \times 2$ codes

Since there are no 2-dimensional field extensions having a perfect square discriminant, the code is constructed from eq. (3.9). The matrix  $\mathcal{M}$  in eq. (3.13) takes the form:

$$\mathcal{M} = \begin{bmatrix} \sqrt{\alpha} & 0 \\ 0 & \sqrt{\sigma(\alpha)} \end{bmatrix} \begin{bmatrix} 1 & \theta \\ 1 & \sigma(\theta) \end{bmatrix} \quad (3.15)$$

It is possible to have a rotated version of the initial signal set if  $\mathcal{M}$  is unitary resulting in:

$$\begin{cases} \alpha(1 + \theta^2) = \sigma(\alpha)(1 + \sigma(\theta)^2) = 1 \\ \sqrt{\alpha\sigma(\alpha)}(1 + \theta\sigma(\theta)) = 0 \end{cases} \quad (3.16)$$

The second condition is verified if there exists an element  $\theta$  such that  $\theta\sigma(\theta) = N_{\mathbb{K}/\mathbb{Q}}(\theta) = -1$  and so  $\mathbb{K}$  must have an element whose norm is equal to  $-1$ . Therefore, for  $2 \times 2$  codes from CDAs energy efficiency comes at the expense of shaping losses and vice versa. In other words, totally-real perfect codes are not possible even with 2 transmit antennas. Therefore, for  $n = 2$  a compromise must be made between energy-efficient codes and shaping-lossless codes.

#### $2 \times 2$ energy-efficient code

The energy-efficient  $2 \times 2$  codewords can be expressed as:

$$C_{2,eq} = \begin{bmatrix} \frac{1}{\sqrt{1+\theta^2}} & 0 \\ 0 & \frac{1}{\sqrt{1+\theta_1^2}} \end{bmatrix} \begin{bmatrix} a_1 + a_2\theta & a_3 + a_4\theta \\ \gamma(a_3 + a_4\theta_1) & a_1 + a_2\theta_1 \end{bmatrix} \quad (3.17)$$

with  $\gamma = \pm 1$ . The first approach is to find numerically the value of  $(\gamma, \theta, \theta_1)$  that maximizes the coding gain over the set  $A = \{-1, 0, 1\}$ . By a computer search, varying the values of  $\theta$  and  $\theta_1$  from  $-4$  to  $4$  with a step size of  $0.001$ , we find that the choice  $\gamma = -1$ ,  $\theta = 1 + \sqrt{3}$  and  $\theta_1 = 1 - \sqrt{3}$  maximizes the value of the minimum determinant of eq. (3.17) over the set  $A^4$ . This maximum value is equal to:

$$d_\infty(C_{2,eq}) = \frac{1}{\sqrt{(1 + \theta^2)(1 + \theta_1^2)}} = \frac{1}{\sqrt{13}} \quad (3.18)$$

The interest of the above approach would have ended here if not for the following observation. Interestingly,  $\theta = 1 + \sqrt{3}$  and  $\theta_1 = 1 - \sqrt{3}$  are the roots of the equation  $x^2 - 2x - 2 = 0$ . Therefore,

eq. (3.17) corresponds to the matrix representation of the elements of the cyclic algebra  $\mathcal{A} = (\mathbb{K} = \mathbb{Q}(\theta), \sigma, \gamma = -1)$ . In Appendix C, we show that  $\gamma = -1$  is not a norm in  $\mathbb{Q}(1 + \sqrt{3})$  resulting in a cyclic division algebra and therefore the coding gain of  $\frac{1}{\sqrt{13}}$  can be achieved with all constellations carved from  $\mathbb{Z}$ .

### 2 × 2 shaping-lossless code

In this case, we construct a rotated constellation by choosing a field having units whose norms are equal to  $-1$ . For example, we can choose  $\mathbb{K} = \mathbb{Q}(\sqrt{5})$  whose ring of integers is given by  $\mathcal{O}_{\mathbb{K}} = \mathbb{Z}(\theta)$  where  $\theta = (1 + \sqrt{5})/2$ . Using KANT software [101], we find that the ideal  $2\mathcal{O}_{\mathbb{K}}$  is prime. This proves that there is no element in  $\mathbb{K}$  having a norm equal to  $2$ . Therefore, choosing  $\gamma = 2$  verifies Proposition 1.2. In this case, the codewords take the form:

$$C_{2,rot} = \begin{bmatrix} \sqrt{\alpha}(a_1 + a_2\theta) & \sqrt{\alpha}(a_3 + a_4\theta) \\ 2\sqrt{\alpha}(a_3 + a_4\theta_1) & \sqrt{\alpha}(a_1 + a_2\theta_1) \end{bmatrix} \quad (3.19)$$

The choice  $\alpha = \frac{1}{1+\theta^2} = \frac{3-\theta}{5}$  results in a unitary matrix  $\mathcal{M}$  in eq. (3.15). Since  $\alpha$  verifies eq. (3.10), then  $d_\infty(C_{2,rot}) = \frac{1}{\sqrt{d_{\mathbb{K}}}}$  with  $d_{\mathbb{K}} = 5$ .

### 3.2.2 3 × 3 code

The construction is performed in  $\mathbb{K} = \mathbb{Q}(\theta)$  with  $\theta = 2\cos(\frac{2\pi}{7})$  having a discriminant of  $d_{\mathbb{K}} = 7^2$ . The ideal  $2\mathcal{O}_{\mathbb{K}}$  is prime. This proves that the first power of  $2$  which is a norm of some elements in  $\mathbb{K}$  is  $2^n$ . Therefore, choosing  $\gamma = 2$  results in a division algebra. Choosing  $\alpha = \beta/7$  with  $\beta = 1 - \theta + 2\theta^2$  verifies eq. (3.10) since  $N_{\mathbb{K}/\mathbb{Q}}(\beta) = 7^2$  and so  $N_{\mathbb{K}/\mathbb{Q}}(\alpha) = \frac{N_{\mathbb{K}/\mathbb{Q}}(\beta)}{7^3} = \frac{1}{\sqrt{d_{\mathbb{K}}}}$ . Let  $\mathcal{M}_1$  be the  $3 \times 3$  matrix whose  $(i, j)$ -th element is given by  $\sigma^{i-1}(\alpha\theta^{j-1})$ , the Gramm matrix is defined as  $\mathcal{G} = \mathcal{M}_1\mathcal{M}_1^T$ :

$$\mathcal{G} = \begin{bmatrix} 2 & -3 & 6 \\ -3 & 6 & -10 \\ 6 & -10 & 19 \end{bmatrix} \quad (3.20)$$

The basis  $\{\alpha, \alpha\theta, \alpha\theta^2\}$  is not unitary. Applying the change of basis:

$$T = \begin{bmatrix} -1 & 1 & 1 \\ 3 & 0 & -1 \\ 2 & -1 & -1 \end{bmatrix} \quad (3.21)$$

we obtain the new unitary basis  $7\{v_1, v_2, v_3\} = \{u, \sigma(u), \sigma^2(u)\}$  with  $u = -2 + 2\theta + 3\theta^2$  and  $\text{Tr}_{\mathbb{K}/\mathbb{Q}}(v_i v_j) = \delta_{i,j}$  for  $i, j = 1, 2, 3$ . The  $3 \times 3$  code can be constructed from eq. (3.13) where the  $(i, j)$ -th element of  $\mathcal{M}$  is given by  $\sigma^{i-1}(v_j) = \sigma^{i-1}(\sigma^{j-1}(u)) = (-2 + 2\theta_k + 3\theta_k^2)/7$  with  $k = (i + j - 2) \bmod 3$ ,  $\theta_0 = \theta$  and  $\theta_i = 2\cos(\frac{2\pi(i+1)}{7})$  for  $i = 1, 2$ .

### 3.2.3 4 × 4 code

Let  $\mathbb{K} = \mathbb{Q}(2\cos(\frac{2\pi}{15}))$  which has a discriminant of  $d_{\mathbb{K}} = 3^2 5^3$ .  $\gamma = 2$  verifies Proposition 1.2 since the ideal  $2\mathcal{O}_{\mathbb{K}}$  is prime. Since  $d_{\mathbb{K}}$  is not a perfect square, the code is constructed from eq. (3.9). Using KANT

software [101], we find that the prime factorizations of the ideals  $3O_{\mathbb{K}}$  and  $5O_{\mathbb{K}}$  are given by:

$$\begin{aligned} 3O_{\mathbb{K}} &= (\beta_3 O_{\mathbb{K}})^2 ; \quad \beta_3 = -2 + 3\theta + \theta^2 - \theta^3 \\ 5O_{\mathbb{K}} &= (\beta_5 O_{\mathbb{K}})^4 ; \quad \beta_5 = 1 + \theta \end{aligned}$$

Choosing  $\beta = \beta_3\beta_5/15$  verifies eq. (3.10) since  $N_{\mathbb{K}/\mathbb{Q}}(\beta) = \frac{1}{d_{\mathbb{K}}}$ , but a problem arises since the first and second conjugates of  $\beta$  are negative. Using KANT, we find the unit  $e = -1 + 4\theta - \theta^3$  whose conjugates have the same sign as those of  $\beta$  and whose norm is equal to 1. Therefore, choosing  $\alpha = \beta e = (5 + 6\theta - \theta^2 + 2\theta^3)/15$  results in a totally positive element verifying eq. (3.10). Once again, the rotation matrix  $\mathcal{M}$  whose  $(i, j)$ -th element is given by  $\sqrt{\sigma^{i-1}(\alpha)}\sigma^{i-1}(\theta^{j-1})$  is not unitary and a change of basis must be performed. Denote by  $\mathcal{G} = \mathcal{M} \mathcal{M}^T$  the Gramm matrix of  $\mathcal{M}$ , it is easy to find that the  $(i, j)$ -th element of  $\mathcal{G}$  is given by  $\text{Tr}_{\mathbb{K}/\mathbb{Q}}(\alpha\theta^{i-1}\theta^{j-1})$ .

$$\mathcal{G} = 5 \begin{bmatrix} 3 & 0 & 3 & 0 \\ 0 & 3 & 0 & 9 \\ 3 & 0 & 9 & -3 \\ 0 & 9 & -3 & 30 \end{bmatrix} \quad (3.22)$$

Now, an orthogonal basis can be obtained by applying the Lenstra-Lenstra-Lovász (LLL) reduction algorithm [37] on  $\mathcal{G}$ . This basis is given by  $15\{v_i\}_{i=1}^4 = \{1, -1 - 3\theta + \theta^2 + \theta^3, -1 - 2\theta + \theta^2 + \theta^3, -1 + 3\theta - \theta^3\}$ . It is easy to verify that the  $(i, j)$ -th element of the new Gramm matrix is equal to  $\text{Tr}_{\mathbb{K}/\mathbb{Q}}(\alpha v_i v_j) = \delta_{i,j}$  for  $i, j = 1, \dots, 4$ . Finally, the codewords are constructed from eq. (3.13) where the  $(i, j)$ -th element of  $\mathcal{M}$  is given by  $\sqrt{\sigma^{i-1}(\alpha)}\sigma^{i-1}(v_j)$  with  $\sigma^i(\theta) = 2\cos(\frac{2\pi(i+1)}{15})$  for  $i = 1, 2, 3$ .

### 3.2.4 $5 \times 5$ code

This code is built from  $\mathbb{K} = \mathbb{Q}(2\cos(\frac{2\pi}{11}))$  whose integral basis and discriminant are given by  $\{\theta_i = 2\cos(\frac{2\pi(i+1)}{11})\}_{i=0}^4$  and  $d_{\mathbb{K}} = 11^4$  respectively. Once again we can choose  $\gamma = 2$  since the ideal  $2O_{\mathbb{K}}$  is prime. So there are no elements in  $\mathbb{K}$  having norms equal to  $\gamma^t$  for  $t = 1, \dots, 4$ . The code is constructed according to eq. (3.13) where the  $(i, j)$ -th element of the  $(5 \times 5)$  matrix  $\mathcal{M}$  is given by  $\sigma^{i-1}(v_j)$  with  $11\{v_i\}_{i=1}^5 = \{u, \sigma(u), \sigma^4(u), -\sigma^2(u), -\sigma^3(u)\}$  where  $u = 4 + 2\theta + 2\theta^2 - \theta^4$  whose norm is equal to  $11^3$  which verifies eq. (3.10) since  $\text{vol}(\Lambda(uO_{\mathbb{K}})) = 11^5$ .

### 3.2.5 $6 \times 6$ code

Let  $\mathbb{K} = \mathbb{Q}(2\cos(\frac{2\pi}{13}))$  which has a discriminant of  $d_{\mathbb{K}} = 13^5$ . Once again, we can choose  $\gamma = 2$  since the ideal  $2O_{\mathbb{K}}$  is prime. Using KANT, we find that:  $13O_{\mathbb{K}} = (\beta O_{\mathbb{K}})^6$  where  $\beta = 2 + \theta - \theta^2$ . The conjugates of the unit  $e = [0, 2, 2, -3, -1, 1]$  have the same sign as those of  $\beta$ ; therefore  $\alpha = \beta e/13$  is a totally positive element verifying eq. (3.10) since  $N_{\mathbb{K}/\mathbb{Q}}(\alpha) = \frac{N_{\mathbb{K}/\mathbb{Q}}(\beta)N_{\mathbb{K}/\mathbb{Q}}(e)}{13^6} = \frac{13 \times 1}{13^6} = \frac{1}{13^5}$ . An orthogonal basis is obtained from  $\{\theta_i\}_{i=0}^5$  by using the matrix:

$$T = \begin{bmatrix} -2 & 1 & 1 & 0 & 0 & 0 \\ -1 & 6 & 1 & -5 & 0 & 1 \\ 3 & -5 & -1 & 5 & 0 & -1 \\ 1 & -8 & 0 & 6 & 0 & -1 \\ 0 & 6 & -3 & -5 & 1 & 1 \\ -1 & -3 & 3 & 4 & -1 & -1 \end{bmatrix} \quad (3.23)$$

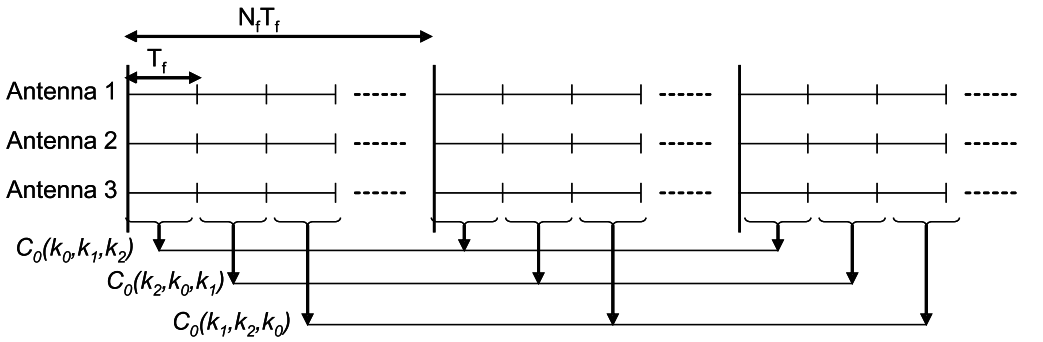


Figure 3.2: A schematic representation of error-balancing with 3 transmit antennas.

The new basis is given by  $[v_1, v_2, \dots, v_6]^T = T[1, \theta, \dots, \theta^5]^T$ . The code is constructed from eq. (3.13) where the  $(i, j)$ -th element of  $\mathcal{M}$  is given by  $\sqrt{\sigma^{i-1}(\alpha)}\sigma^{i-1}(v_j)$  with  $\sigma^i(\theta) = 2\cos(\frac{2\pi(i+1)}{13})$ .

### 3.2.6 Balanced codes

The transmitted energy of eq. (3.6) (and consequently that of eq. (3.13)) can be distributed in a more balanced way among the different transmit antennas and symbol durations resulting in a balanced version  $C'_0$  [60].  $C'_0$  is constructed in the same way as in eq. (3.6) by removing  $\gamma$  from the lower triangular part of  $C_0$  and by replacing the constituent elements  $k_i$  by  $\gamma^i k_i$  for  $i = 0, \dots, n - 1$ . This will be referred to as “energy” balancing and the properties of eq. (3.6) and eq. (3.13) are conserved since  $C_0$  and  $C'_0$  have the same determinant. Even when “energy” balancing is performed and since  $|\gamma| > 1$ , the amplitudes attributed to each value of  $k_i$  (and its conjugates) are not the same and, consequently, the  $n$  symbols contained in the conjugates of  $k_i$  are not equally protected against error events. For example, when  $|\gamma| > 1$ , the symbols  $a_1, \dots, a_n$  are the most vulnerable while the biggest portion of the energy is used to transmit symbols  $a_{n(n-1)}, \dots, a_{n^2}$ . An additional kind of balancing (referred to as “error” balancing hereafter) can be performed when  $N_f$  is a multiple of  $n$  according to:

$$C^{(j)} = \sum_{i=0}^{n-1} \text{diag}(\mathcal{M} [a_{[(i+(j-1))n+1]_{n^2}}, \dots, a_{[(i+j)n]_{n^2}}]^T) \Omega^i \quad (3.24)$$

$$C_{bal} = [C^{(1)} \quad \dots \quad C^{(n)}] \quad (3.25)$$

where  $[x]_n = (x - 1) \bmod n + 1$ . In other words, when including the pulse repetitions, instead of transmitting  $C \otimes \mathbf{1}_{1 \times N_f}$ , error-balancing corresponds to transmitting  $C_{bal} \otimes \mathbf{1}_{1 \times N_f/n}$ . In what follows, energy balancing will be applied systematically to all constructed codes, while the subscript “bal” will be reserved to “error” balancing. For example, the error-balanced version of eq. (3.19) is given by:

$$\begin{bmatrix} \sqrt{\alpha}(a_1 + a_2\theta) & \sqrt{2\alpha}(a_3 + a_4\theta) & \sqrt{\alpha}(a_3 + a_4\theta) & \sqrt{2\alpha}(a_1 + a_2\theta) \\ \sqrt{2\alpha_1}(a_3 + a_4\theta_1) & \sqrt{\alpha_1}(a_1 + a_2\theta_1) & \sqrt{2\alpha_1}(a_1 + a_2\theta_1) & \sqrt{\alpha_1}(a_3 + a_4\theta_1) \end{bmatrix} \quad (3.26)$$

Writing  $C_0$  in eq. (3.6) as  $C_0(k_0, k_1, k_2)$ , a schematic representation of error-balancing with the  $3 \times 3$  code is given in Fig. 3.2.

### 3.2.7 Relation with the TAST codes

For  $n \neq 4$ , the procedure used to choose an element  $\alpha$  verifying eq. (3.10) coincides with that used to construct the fully-diverse rotation matrices in [58]. These matrices were used to construct the Threaded Algebraic Space-Time (TAST) codes in [57]. Taking this fact, as well as the structure of  $C'_0$  into account, we conclude that the constructed codes have the same structure as the TAST codes but now real Diophantine numbers (in contrast to complex ones in [57]) are used to render the different layers transparent to each other. The utility of following the design procedure presented in this section resides in the fact that we showed that  $\{1, \gamma^{\frac{1}{n}}, \dots, \gamma^{\frac{n-1}{n}}; \gamma = 2\}$  is in fact the best possible choice of the Diophantine numbers for all  $M'$ -ary PAM constellations since the minimum of the coding gain of eq. (3.6) is equal to 1. For  $n = 4$ , the matrix  $\mathcal{M}$  used for constructing the ST code from eq. (3.13) is different from the rotation matrix given in [58]. While using  $\mathcal{M}$  with  $\gamma = 2$  results in a ST code with non-vanishing determinant, full diversity is lost when using the rotation matrix given in [58] with  $\gamma = 2$ .

### 3.2.8 Coding Gain

Since  $|\gamma| \neq 1$ , eq. (3.13) must be multiplied by a normalization factor  $\sqrt{c_n(\gamma)}$  in order to insure the same transmitted energy as in uncoded systems where  $c_n(\gamma) = n / \sum_{i=0}^{n-1} \gamma^{\frac{2i}{n}}$ . The coding gain of eq. (3.13) is given by [50]:

$$\min_{C \in \mathbb{Z}^{n \times n}, C \neq \mathbf{0}_{n \times n}} (\det(CC^T))^{\frac{1}{n}} = c_n(\gamma)(d_\infty(C))^{\frac{2}{n}} = c_n(\gamma)d_{\mathbb{K}}^{-\frac{1}{n}} \triangleq d_\infty(\gamma) \quad (3.27)$$

where  $d_\infty(\gamma)$  is defined over  $\mathbb{Z}$ . The coding gain of finite code-books constructed over  $M$ -PAM constellations is denoted by  $d_M(\gamma)$  for a given value of  $\gamma$ . Since the constructed codes have a non-vanishing determinant, then for finite values of  $M$ :

$$d_M(\gamma) = 4d_\infty(\gamma) = 4c_n(\gamma)d_{\mathbb{K}}^{-\frac{1}{n}} \quad (3.28)$$

The multiplying factor 4 follows from the fact that  $\{a - b ; a, b \in \mathcal{C}_{M-\text{PAM}}\} = 2\{-M, \dots, M\} \subset 2\mathbb{Z}$  where  $\mathcal{C}_{M-\text{PAM}}$  is the  $M$ -PAM signal set given in eq. (1.4).

A good question arises: what if there exists a TAST code associated with a certain  $\gamma \notin \mathbb{Z}$  and which, for a particular value of  $M$ , results in a coding gain that is greater than  $d_M$ . For  $n = 2$  and  $n = 3$  transmit antennas, we can show that this can never happen since:

$$d_M(\gamma) \leq d_2(\gamma) \leq d_2(2) = d_M(2) \quad (3.29)$$

The first inequality follows from the inclusion of 2-PAM in  $M$ -PAM for  $M \geq 2$  and the last equality follows from the NVD property that is satisfied by  $\gamma = 2$ . In order to prove the second inequality, we first consider the case of  $n = 2$ . For  $C_{2,\text{rot}}$  given in eq. (3.19), the coding gain verifies:

$$d_M(\gamma) = 4d_K^{-\frac{1}{2}} \frac{2}{1 + \gamma} \min_{X, Y \in \mathcal{A}^2 \setminus \{(0,0)\}} |X - \gamma Y| \quad (3.30)$$

where  $4X = b_1^2 - b_2^2 + b_1 b_2$  and  $4Y = b_3^2 - b_4^2 + b_3 b_4$  where  $b_i = a_i - a'_i$  with  $a_i, a'_i \in \mathcal{C}_{M-\text{PAM}}$  for  $i = 1, \dots, 4$ . It is evident from eq. (3.30) that  $\gamma$  and  $1/\gamma$  give the same coding gain. So, without loss of generality, we will limit ourselves to the case  $\gamma \geq 1$ . For 2-PAM constellations,  $\mathcal{A} = \{0, \pm 1\}$ . For  $1 \leq \gamma \leq 2$ , the minimum of the right hand side of eq. (3.30) is obtained for  $X = Y = \pm 1$  and so  $d_2(\gamma)$  varies as  $f_1(\gamma) = \frac{\gamma-1}{\gamma+1}$ . For  $\gamma > 2$ , the minimum is obtained for  $X = \pm 1$  and  $Y = 0$  and  $d_2(\gamma)$  varies as

$f_2(\gamma) = \frac{1}{\gamma+1}$  in this interval. Following the variations of  $f_1(\gamma)$  and  $f_2(\gamma)$ , we find that the maximum value of eq. (3.30) is obtained for  $\gamma = 2$  resulting in  $d_2(2) = \frac{8}{3\sqrt{5}}$ . This proves the second inequality in eq. (3.29) showing that  $\gamma = 2$  is the optimal choice. Choosing  $1 < \gamma < 2$ , can be a good compromise for a given tolerated value of the peak to average power ratio (PAPR) because the code can still achieve full diversity with a NVD (for example with  $\gamma = 3/2$  since 2 and 3 are non-norm elements in  $\mathbb{Q}(\theta)$ ). However, choosing  $\gamma > 2$  is a bad choice because this increases the PAPR and reduces the coding gain.

For 4-PAM,  $5\mathcal{A} = \{0, \pm 1, \pm 4, \pm 5, \pm 9, \pm 11\}$  where the factor 5 corresponds to the average energy of the constellation. Following a similar approach as for 2-PAM, it can be shown that starting from 1 and increasing the value  $\gamma$ , the coding gain will vary following the set of curves:  $(1/(\gamma+1))\{\gamma-1, |9\gamma-11|, |4\gamma-5|, \gamma-1, |5\gamma-9|, |5\gamma-11|, |4\gamma-9|, |4\gamma-11|, |\gamma-4|, |\gamma-5|, \gamma-1, |\gamma-9|, |\gamma-11|, \gamma-1\}$ . Once again, the coding gain attains its maximum value for  $\gamma = 2$ . Equation (3.30) is plotted in Fig. 3.3 for  $M$ -PAM with  $M = 2, 4, 8, 16$ .

For  $n = 3$  antennas, the second inequality in eq. (3.29) can be checked out through computer simulations. Fig. 3.4 shows the coding gain of the  $3 \times 3$  code constructed in Section 3.2.2 with 2-PAM constellations. The maximal coding gain is obtained for  $\gamma = 2$  and is equal to  $4c_3(2)7^{-\frac{2}{3}} = 0.65$ . For  $n > 3$ , the second inequality in eq. (3.29) can not be verified by a computer search given the very large number of codewords. In this case,  $\gamma = 2$  is the best possible choice since the validity of another choice can not be verified.

Note that a relation similar to eq. (3.29) can be also applied on  $C_{2,eq}$  given in eq. (3.17) since this code was constructed to maximize the coding gain with 2-PAM constellations.

### 3.2.9 ISC with hybrid PPM-PAM constellations

Consider a hybrid  $M$ -PPM- $M'$ -PAM constellation with  $M > 1$ . In this case, the scalars  $k_0, \dots, k_{n-1}$  in eq. (3.6) are replaced by  $M$ -dimensional vectors given by  $k_i = \sum_{j=0}^{n-1} a_{ni+j+1}\theta^j$  where  $a_1, \dots, a_{n^2}$  are the vector representations of the information symbols. Extending eq. (3.13) to  $M$ -dimensional constellations, the  $nM \times n$  codewords can be expressed as:

$$C = \sum_{i=0}^{n-1} \sum_{m=1}^M \left( \text{diag} \left( \mathcal{M} [a_{in+1,m}, \dots, a_{(i+1)n,m}]^T \right) \Omega^i \right) \otimes e_m \quad (3.31)$$

where  $e_m$  is the  $m$ -th column of the  $M \times M$  identity matrix  $I_M$  and  $a_{i,m}$  is the  $m$ -th component of the vector  $a_i$  for  $i = 1, \dots, n^2$  and  $m = 1, \dots, M$ .

Designate by  $C^{(m)}$  the  $n \times n$  matrix composed of the rows  $iM + m$  of  $C$  for  $i = 0, \dots, n-1$  and  $m = 1, \dots, M$ . Denote by  $C'$  the matrix obtained from the vertical concatenation of  $C^{(1)}, \dots, C^{(M)}$ .  $C'$  is obtained from  $C$  by performing row permutations and therefore  $C'$  and  $C$  have the same rank. Now, each matrix  $C^{(m)}$  has the same structure as the  $n \times n$  codes in eq. (3.13). As this code was constructed to be fully-diverse,  $C^{(m)}$  is rank deficient only if the  $m$ -th components of  $a_1, \dots, a_{n^2}$  are all equal to zero. In other words, for non-zero information vectors, there is at least one value of  $m \in \{1, \dots, M\}$  such that  $C^{(m)}$  has full rank. Therefore,  $C'$  (and consequently  $C$ ) have full rank and the code given in eq. (3.31) is fully diverse with all  $M$ -PPM- $M'$ -PAM constellations.

Designate by  $r$  the number of values of  $m \in \{1, \dots, M\}$  for which the matrix  $C^{(m)}$  is different from the all-zero matrix. We then rearrange the superscripts of the constituent matrices so that  $C^{(m)} \neq O_{n \times n}$  for  $m = 1, \dots, r$  and  $C^{(m)} = O_{n \times n}$  for  $m = r+1, \dots, M$ . The following relation holds:

$$\det(C^T C) \geq r^n \min_{m=1, \dots, r} \left\{ \det(C^{(m)T} C^{(m)}) \right\} \quad (3.32)$$

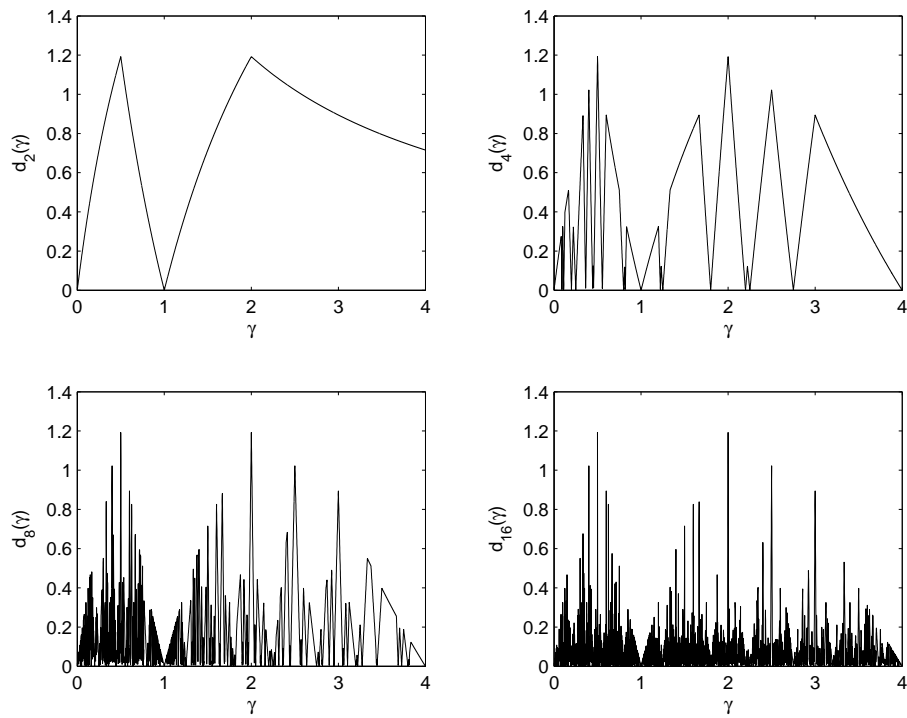


Figure 3.3: The coding gain  $d_M(\gamma)$  of  $C_{2,rot}(\gamma)$  in eq. (3.19) for  $M = 2, 4, 8, 16$ .

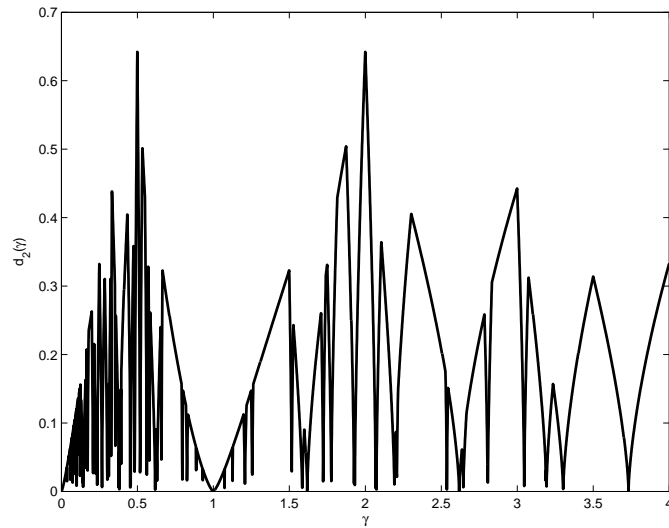


Figure 3.4: The coding gain of ISC with 3 transmit antennas and 2-PAM.

For  $r = 1$ , eq. (3.13) and eq. (3.31) have the same determinant and for non-zero symbols:  $\det(C^T C) \geq 2^{2n}(d_\infty(\gamma))^n$  where  $d_\infty(\gamma)$  is given in eq. (3.27). For  $r > 1$  and for non-zero symbols,  $\det(C^T C) \geq r^n(d_\infty(\gamma))^n$  since the difference between two components of the matrices  $C^{(m)}$  now belongs to  $\mathbb{Z}$  rather than  $2\mathbb{Z}$  as for PAM constellations (or when  $r = 1$ ). Therefore, the minimum determinant is obtained for symbols that occupy exactly 2 positions among the  $M$  modulation positions ( $r = 2$ ). Designate by  $\delta_{M,M'}(\gamma)$  the coding gain of ISC with  $M$ -PPM- $M'$ -PAM constellations for a given non-norm element  $\gamma$ , then the value of  $\gamma$  that maximizes the coding gain is the same for all values of  $M$ . From eq. (3.28) and eq. (3.32), we obtain:

$$\delta_{M,M'}(\gamma) = \begin{cases} 4c_n(\gamma)d_{\mathbb{K}}^{-\frac{1}{n}} & ; M = 1, \forall M' \\ 2c_n(\gamma)d_{\mathbb{K}}^{-\frac{1}{n}} & ; M > 1, \forall M' \end{cases} \quad (3.33)$$

### 3.3 Inter-Pulse Coding (IPC)

#### 3.3.1 Code Construction

When IPC is performed, orthogonal sequences are associated with the pulses transmitted from each antenna. In other words, the spreading matrix  $B$  in Section 2.1.3 is chosen to verify  $BB^T = N_f I_n$  ( $n = P$  is the number of transmit antennas). In this case, the despread matrix in eq. (2.33) is given by  $D = I_{Q_0} \otimes (B \otimes I_M)$  where  $Q_0 = \{QLP, QL, QP\}$  for SRakes, PRakes and correlation receivers respectively. In this case, eq. (2.33) can be expressed as:

$$Y_{Q'P \times T} = H_{Q'P \times PM} C_{PM \times T} + N_{Q'P \times T} \quad (3.34)$$

where  $Q' = \{QLM, QM\}$  for Rake and correlation receivers respectively. For Rake receivers,  $H$  is the vertical concatenation of  $H_{q,l}$  for  $q = 1, \dots, Q$  and  $l = 0, \dots, L - 1$  where  $H_{q,l}$  is a  $PM \times PM$  matrix given by:

$$H_{q,l} = \text{diag}(R_{q,l,1,1} \cdots R_{q,l,P,P}) \quad (3.35)$$

where the entries of the  $M \times M$  matrix  $R_{q,l,p,p}$  are given in eq. (2.19) for  $p = 1, \dots, P$ . In the same way, for correlation receivers,  $H$  is the vertical concatenation of  $H_q$  for  $q = 1, \dots, Q$  with:

$$H_q = \text{diag}(R_{q,1,1} \cdots R_{q,P,P}) \quad (3.36)$$

where the entries of the  $M \times M$  matrix  $R_{q,p,p}$  are given in eq. (2.32).

By rearranging the entries of eq. (3.34), it can be expressed as:

$$Y'_{Q' \times PT} = H'_{Q' \times PM} A_{PM \times PT} + N'_{Q' \times PT} \quad (3.37)$$

In this case the constituent matrices in eq. (3.35) and eq. (3.36) are transformed to  $H'_{q,l} = [R_{q,l,1,1} \cdots R_{q,l,P,P}]$  and  $H'_q = [R_{q,1,1} \cdots R_{q,P,P}]$  respectively. We limit ourselves to PAM for the moment. If  $C$  corresponds to the energy-balanced ISC, then for a given value of  $\gamma$ ,  $A$  can be written as:

$$A(\gamma) = \sqrt{c_n(\gamma)} \text{diag}(\alpha_0, \dots, \alpha_{n-1}) F(\gamma) \quad (3.38)$$

where  $\alpha_i = \sigma^i(\alpha)$  for  $n$  odd and  $\alpha_i = \sqrt{\sigma^i(\alpha)}$  for  $n$  even where  $\alpha$  is chosen to verify eq. (3.10).  $F(\gamma)$  is an  $n \times n^2$  matrix given by:

$$F(\gamma) = \begin{bmatrix} f_0^0 & 0 & \cdots & 0 & f_1^0 & 0 & \cdots & 0 & \cdots & f_{n-1}^0 & 0 & \cdots & 0 \\ 0 & f_{n-1}^1 & \vdots & \vdots & 0 & f_0^1 & \ddots & \vdots & \cdots & 0 & f_{n-2}^1 & \ddots & \vdots \\ \vdots & \ddots & \ddots & 0 & \vdots & \ddots & \ddots & 0 & \cdots & \vdots & \ddots & \ddots & 0 \\ 0 & \cdots & 0 & f_1^{n-1} & 0 & \cdots & 0 & f_2^{n-1} & \cdots & 0 & \cdots & 0 & f_0^{n-1} \end{bmatrix} \quad (3.39)$$

where  $f_i^j = \gamma^{\frac{j}{n}} \sigma^j(k_i)$  for  $i, j = 0, \dots, n-1$ .

The matrix  $F(\gamma)F(\gamma)^T$  admits  $n$  eigenvalues. These eigenvalues are given by  $\lambda_j = \sigma^j(\lambda)$  for  $j = 0, \dots, n-1$  and  $\lambda = \sum_{i=0}^{n-1} \gamma^{\frac{2i}{n}} k_i^2$ . Therefore, when  $\alpha$  verifies eq. (3.10), the coding gain of  $A(\gamma)$  verifies:

$$\begin{aligned} \delta_{\min}(\gamma) &= d_{\mathbb{K}}^{-\frac{1}{n}} c_n(\gamma) \min \left( N_{\mathbb{K}/\mathbb{Q}} \left( \sum_{i=0}^{n-1} \gamma^{\frac{2i}{n}} k_i^2 \right) \right)^{\frac{1}{n}} \\ &\geq d_{\mathbb{K}}^{-\frac{1}{n}} c_n(\gamma) \min \left( \sum_{i=0}^{n-1} \gamma^{2i} N_{\mathbb{K}/\mathbb{Q}}(k_i)^2 \right)^{\frac{1}{n}} \end{aligned} \quad (3.40)$$

Consider the case  $\gamma \geq 1$ . The minimum of the right hand side of eq. (3.40) is obtained when  $k_i = 0$  for  $i = 1, \dots, n-1$  and  $N_{\mathbb{K}/\mathbb{Q}}(k_0) = \pm 1$ . The value of  $\gamma$  that maximizes the coding gain is  $\gamma = 1$  since  $c_n(\gamma)$  is a decreasing function of  $\gamma$  for  $\gamma \geq 1$ .

For  $\gamma < 1$ , the minimum of the right hand side of eq. (3.40) is obtained for  $k_0 = \dots = k_{n-2} = 0$  and  $N_{\mathbb{K}/\mathbb{Q}}(k_{n-1}) = \pm 1$ . Maximizing over  $\gamma$  results in  $\gamma = 1$  since now  $c_n(\gamma) \gamma^{\frac{2(n-1)}{n}}$  is an increasing function of  $\gamma$ . The optimal choice  $\gamma = 1$  shows that since the transmitted streams are separated at the receiver side (by the use of orthogonal spreading sequences), the best strategy consists of evenly distributing the available energy among the different data streams. For IPC, the achieved coding gain over  $\mathbb{Z}$  is equal to  $d_{\mathbb{K}}^{-\frac{1}{n}}$ . For finite PAM constellation, the coding gain is equal to  $4d_{\mathbb{K}}^{-\frac{1}{n}}$ .

Arranging the columns of eq. (3.38), we obtain:

$$A = \text{diag}(\alpha_0, \dots, \alpha_{n-1}) \begin{bmatrix} \text{diag}(k_0, \dots, \sigma^{n-1}(k_0)) & \cdots & \text{diag}(k_{n-1}, \dots, \sigma^{n-1}(k_{n-1})) \end{bmatrix} \quad (3.41)$$

Equation (3.41) shows that encoding adjacent symbols is not needed since each information symbol is contained in the conjugates of only one value  $k_i$  for  $i = 0, \dots, n-1$ . Therefore, the temporal length ( $T$ ) of the codewords can be chosen to be equal to 1. In this case, the amplitudes of the pulses transmitted from the  $n$  antennas during each symbol duration are given by the  $n \times N_f$  matrix:

$$C = \text{diag} \left( \mathcal{M} [a_1, \dots, a_n]^T \right) B \quad (3.42)$$

where  $B / \sqrt{N_f}$  is any unitary  $n \times N_f$  matrix and  $\mathcal{M}$  is calculated in the same way as in Section 3.2. Since the transmitted date streams are decoupled,  $\mathcal{M}$  can be any one of the rotation matrix constructed in [36] or [58].

IPC presents the following advantages over ISC:

- ISC achieves a coding gain  $c_n(2)$  times smaller than that of IPC systems ( $c_n(2) < 1$  for all values of  $n$ ).

- IPC has a lower decoding complexity since each codeword contains  $n$  rather than  $n^2$  symbols.
- IPC has a lower peak-to-average-power-ratios (PAPR). Moreover, IPC transmits a uniform average energy per antenna.
- IPC has a lower decoding delay which is equal to 1 symbol duration rather than  $n$  symbol durations for ISC.

However, unlike ISC that can be applied with any IR-UWB system, IPC can be applied only when  $N_f \geq n$ .

### 3.3.2 IPC with hybrid PPM-PAM constellations

For hybrid  $M$ -PPM- $M'$ -PAM constellations, eq. (3.42) can be expressed in a more explicit form as:

$$C(a) = \begin{bmatrix} s_{1,1} & 0 & \cdots & 0 \\ \vdots & \vdots & \ddots & \vdots \\ s_{1,M} & 0 & \cdots & 0 \\ \vdots & \ddots & \ddots & \vdots \\ 0 & \cdots & 0 & s_{n,1} \\ \vdots & \ddots & \vdots & \vdots \\ 0 & \cdots & 0 & s_{n,M} \end{bmatrix} B = S(a)B \quad (3.43)$$

where  $s_{n',m}$  stands for the  $((n'-1)M+m)$ -th component of the  $nM$ -dimensional vector  $s$  for  $n' = 1, \dots, n$  and  $m = 1, \dots, M$ .  $s$  is related to the information vector  $a$  by:

$$s = (\mathcal{M} \otimes I_M) a \quad (3.44)$$

Let  $x = a - a'$  be the difference between two information vectors. From eq. (3.43), we have  $C(x)C^T(x) = S(x)BB^TS^T(x) = N_f S(x)S^T(x)$  since  $B/\sqrt{N_f}$  is unitary. Therefore, the matrix  $C(x)C^T(x)$  has  $n$  eigenvalues  $\lambda_{n'}$  that are given by ( $n' = 1, \dots, n$ ):

$$\lambda_{n'} = \sum_{m=1}^M y_{n',m}^2 \quad (3.45)$$

where  $y = (\mathcal{M} \otimes I_M)x$ .

$\lambda_{n'}$  is equal to zero if and only if  $y_{n',m} = 0$  for  $m = 1, \dots, M$ . For a given value of  $m$ , we have  $y_{n',m} = \mathcal{M}_{n'}[x_{1,m}, \dots, x_{n,m}]^T$  where  $\mathcal{M}_{n'}$  stands for the  $n'$ -th row of  $\mathcal{M}$ . Since  $\mathcal{M}$  is chosen to achieve full modulation diversity [36],  $y_{n',m} = 0$  implies that  $x_{n',m} = 0$  for  $n' = 1, \dots, n$ . Therefore,  $\lambda_{n'}$  can not be equal to zero unless when  $x_{n',m} = 0$  for  $n' = 1, \dots, n$  and  $m = 1, \dots, M$ , in other words when  $a = a'$ . Therefore,  $C(x)$  has  $n$  non-zero eigenvalues and thus it achieves the maximum transmit diversity order of  $n$ .

The coding gain of eq. (3.43) can be expressed as:

$$\delta_{\min} = \min_{x \neq \mathbf{0}_{nM \times 1}} \left( \prod_{n'=1}^n \lambda_{n'} \right)^{\frac{1}{n}} = \min_{x \neq \mathbf{0}_{nM \times 1}} \left( \prod_{n'=1}^n \left( \sum_{m=1}^M y_{n',m}^2 \right) \right)^{\frac{1}{n}} \quad (3.46)$$

For one dimensional constellations ( $M = 1$ ), the sum in eq. (3.45) contains only one summand and eq. (3.46) reduces to  $\delta_{min} = 4d_{min}^{2/n}$ . The factor 4 comes from the fact that the coding gain is defined over the PAM constellation.  $d_{min}$  is the minimum product distance achieved by  $\mathcal{M}$  that is defined as [36]:

$$d_{min} = \min_{\substack{a \neq a' \\ a, a' \in \mathbb{Z}^n}} \prod_{i=1}^n |s_i - s'_i| \quad (3.47)$$

where  $s = \mathcal{M}a$  and  $s' = \mathcal{M}a'$ . From [36, 58],  $d_{min} = d_{\mathbb{K}}^{-1/2}$  where  $d_{\mathbb{K}}$  is the discriminant of the field over which the rotation matrix is constructed.

For multi-dimensional constellations, suppose that the sum in eq. (3.45) contains  $r$  non zero summands. For  $r = 1$  we obtain  $\delta_{min} = 4d_{min}^{2/n}$ . If  $r > 1$ ,  $\delta_{min}^n$  is increased  $r$  times but it will be further reduced 4 times since the difference between 2 data symbols now belongs to  $\{m'\}^M$  rather than  $\{2m'\}$  as in the case of PAM symbols for  $m' \in \{-M', \dots, M'\}$ . So, the minimum value of the coding gain will be obtained for  $r = 2$  and it is equal to  $\delta_{min} = 2d_{min}^{2/n} = 2d_{\mathbb{K}}^{-1/n}$ .

## 3.4 Modulation-specific ST codes

In Section 3.2, we showed the non-existence of totally-real and energy-efficient (the magnitude of the non-norm element is equal to 1) ST codes based on cyclic division algebras for  $n \geq 3$  transmit antennas. In the same way, for  $n = 2$  antennas, energy efficiency comes at the expense of shaping losses (refer to Section 3.2.1).

In this section, instead of adopting the classical approach of constructing ST codes over infinite fields ( $\mathbb{Z}$  in the totally-real case), we profit from the particular structure of the PPM-PAM constellations in order to construct new coding schemes suitable for these modulations. The proposed schemes are energy-efficient, information-lossless and they introduce no shaping losses. Unlike balanced-ISC (Section 3.2.6) and IPC (Section 3.3) that profit from the pulse repetitions to achieve energy-efficiency and shaping-efficiency, the codes that we propose in this section can be applied even in the absence of pulse repetitions. However, unlike ISC and IPC that can be associated with any PPM, PAM or hybrid PPM-PAM constellation, the new codes are exclusive to  $M$ -PPM- $M'$ -PAM constellations for specific values of  $M$ . Finally, we show that for certain values of  $M$ , it is possible to construct ST codes that satisfy all the construction constraints of the perfect codes in the addition to the constraint of being totally-real.

### 3.4.1 Construction 1: Achieving full transmit diversity via position permutation

#### Code Construction

For  $M$ -PPM- $M'$ -PAM with  $n$  transmit antennas, the minimal-delay codewords are given by:

$$C = \begin{bmatrix} k_0 & k_1 & k_2 & \cdots & k_{n-1} \\ \Omega\sigma(k_{n-1}) & \sigma(k_0) & \sigma(k_1) & \cdots & \sigma(k_{n-2}) \\ \Omega\sigma^2(k_{n-2}) & \Omega\sigma^2(k_{n-1}) & \sigma^2(k_0) & \cdots & \sigma^2(k_{n-3}) \\ \vdots & \vdots & \vdots & \ddots & \vdots \\ \Omega\sigma^{n-1}(k_1) & \Omega\sigma^{n-1}(k_2) & \cdots & \Omega\sigma^{n-1}(k_{n-1}) & \sigma^{n-1}(k_0) \end{bmatrix} \quad (3.48)$$

where:

$$k_i = \sum_{j=0}^{n-1} a_{ni+j+1} \theta^j \in O_{\mathbb{K}}^M \quad (3.49)$$

$\mathcal{O}_{\mathbb{K}}$  is the ring of integers of a  $n$ -dimensional totally-real field extension  $\mathbb{K}$ .  $a_1, \dots, a_{n^2}$  are  $M$ -dimensional vectors that belong to the  $M$ -PPM- $M'$ -PAM constellation given in eq. (1.8).  $C$  is a  $nM \times n$  matrix whose  $((p-1)M+m, t)$ -th element corresponds to the amplitude of the pulse transmitted from the  $p$ -th transmit antenna during the  $m$ -th modulation position of the  $t$ -th symbol duration for  $p, t \in \{1, \dots, n\}$  and  $m \in \{1, \dots, M\}$ .

In comparison with eq. (3.6), the non-norm scalar  $\gamma$  is replaced by the  $M \times M$  permutation matrix  $\Omega$  given by:

$$\Omega = \begin{bmatrix} 0 & \cdots & \cdots & 0 & 1 \\ 1 & 0 & \cdots & 0 & 0 \\ 0 & 1 & \ddots & \vdots & \vdots \\ \vdots & \ddots & \ddots & 0 & \vdots \\ 0 & \cdots & 0 & 1 & 0 \end{bmatrix} \quad (3.50)$$

It can be directly seen that the code in eq. (3.48) is not fully-diverse with PAM constellations ( $M = 1$ ) since in this case eq. (3.48) corresponds to the code constructed from cyclic algebras with  $\Omega = \gamma = 1$  which is not a non-norm element.

### Diversity Order

**Proposition 3.1** *For  $n$  transmit antennas, the association of the codewords given in eq. (3.48) with the permutation matrix given in eq. (3.50) permits to achieve full transmit diversity with  $M$ -PPM- $M'$ -PAM constellations for all values of  $M'$  and for  $M \geq 2n - 1$  or for the values of  $M$  verifying  $\mathcal{E}(M) \geq n$  where  $\mathcal{E}(.)$  stands for Euler's function.*

For example, the proposed scheme achieves full diversity with  $M$ -PPM- $M'$ -PAM constellations for all values of  $M'$  and for  $M \geq 3$ ,  $M \geq 5$ ,  $\{M = 5, M \geq 7\}$ ,  $\{M = 7, M \geq 9\}$  and  $\{M = 7, 9, M \geq 11\}$  with  $n = 2, 3, 4, 5$  and 6 transmit antennas respectively.

In order to get more insights on the properties of the proposed code, we next present the proof of Proposition 3.1 with  $n = 2$ . The proof for  $n > 2$  is given in Appendix D.1.

Designate by  $\Delta C(X_1, X_2)$  the difference between any two codewords given in eq. (3.48):

$$\Delta C(X_1, X_2) = C - C' = \begin{bmatrix} X_1 & X_2 \\ \Omega \sigma(X_2) & \sigma(X_1) \end{bmatrix} \quad (3.51)$$

where  $C$  and  $C'$  are the codewords associated with the vector pairs  $(k_0, k_1)$  and  $(k'_0, k'_1)$  respectively where  $k_0, k'_0, k_1, k'_1$  are  $M$ -dimensional vectors whose structure verifies eq. (3.49).  $X_1 = k_0 - k'_0$  and  $X_2 = k_1 - k'_1$  belong to the set  $\mathcal{A}$  given by:

$$\mathcal{A} = \{(a - a') + (b - b')\theta \mid a, a', b, b' \in \mathcal{C}\} \subset \mathcal{O}_{\mathbb{K}}^M \quad (3.52)$$

where  $\mathcal{C}$  stands for the  $M$ -PPM- $M'$ -PAM constellation given in eq. (1.8).

We will now show that all non-zero vector couples  $(X_1, X_2)$  that result in a rank deficient matrix  $\Delta C(X_1, X_2)$  do not belong to the set  $\mathcal{A}$  given in eq. (3.52) for all values of  $M'$ . In other words, full transmit diversity is achieved with  $M$ -PPM- $M'$ -PAM constellations if:

$$\text{rank}(\Delta C(X_1, X_2)) = 2 ; \forall (X_1, X_2) \in \mathcal{A}^2 \setminus \{(\mathbf{0}_M, \mathbf{0}_M)\} \quad (3.53)$$

where  $\mathbf{0}_M$  is the  $M$ -dimensional all-zero vector. In what follows,  $\Delta C(X_1, X_2)$  will be referred to as  $\Delta C$  when there is no ambiguity. Denote by  $X_{i,m}$  the  $m$ -th component of the vector  $X_i$  for  $i = 1, 2$  and  $m = 1, \dots, M$ .

*Proposition:* if  $\exists i, m | X_{i,m} = 0$  then  $\text{rank}(\Delta C(X_1, X_2)) = 2$  unless  $X_1 = X_2 = \mathbf{0}_M$ .

*Proof:* Designate by  $\pi$  the cyclic permutation given by:

$$\pi(i) = i \pmod{M} + 1 ; i = 1, \dots, M \quad (3.54)$$

$\pi$  defines a bijection over  $\{1, \dots, M\}$  where  $\pi^{-1}(i) = i - 2 \pmod{M} + 1$  for  $i = 1, \dots, M$ . The  $2M \times 2$  matrix  $\Delta C(X_1, X_2)$  can be written as:

$$\begin{bmatrix} X_{1,1} & \dots & X_{1,M} & \sigma(X_{2,\pi^{-1}(1)}) & \dots & \sigma(X_{2,\pi^{-1}(M)}) \\ X_{2,1} & \dots & X_{2,M} & \sigma(X_{1,1}) & \dots & \sigma(X_{1,M}) \end{bmatrix}^T \quad (3.55)$$

Suppose that  $X_{1,m} = 0$  for a given value of  $m$ . When  $\text{rank}(\Delta C) < 2$ , the two columns of  $\Delta C$  have the same direction. Therefore, considering the first  $M$  rows of  $\Delta C$ ,  $X_{1,m} = 0 \Rightarrow X_{2,m} = 0$ . Now we have  $\sigma(X_{2,m}) = 0$  (since  $X_{2,m} = 0$  and  $\{1, \theta\}$  is an integral basis of  $\mathcal{O}_{\mathbb{K}}$ ). Considering the last  $M$  rows of  $\Delta C$ ,  $\sigma(X_{2,m}) = 0 \Rightarrow \sigma(X_{1,\pi(m)}) = 0 \Rightarrow X_{1,\pi(m)} = 0$ . Starting the same procedure again with  $\pi(m)$  rather than  $m$ , we conclude by iteration that  $X_{1,m} = X_{1,\pi(m)} = \dots = X_{1,\pi^{M-1}(m)} = 0$  and  $X_{2,m} = X_{2,\pi(m)} = \dots = X_{2,\pi^{M-1}(m)} = 0 \Leftrightarrow X_1 = X_2 = \mathbf{0}_M$  since  $\pi$  defines a bijection over  $\{1, \dots, M\}$ . The same proof holds if  $\exists m | X_{2,m} = 0$ .

*Lemma:* For  $n = 2$  transmit antennas, the code in eq. (3.48) achieves full diversity with  $M$ -PPM- $M'$ -PAM constellations for  $M > 4$  and for all values of  $M'$ .

*Proof:* From the definition of  $\mathcal{A}$  in eq. (3.52),  $X_1$  and  $X_2$  are linear combinations of any four columns of the  $M \times M$  identity matrix  $I_M$ . Therefore for  $M > 4$ ,  $X_1$  and  $X_2$  each have at least one zero component resulting in full rank as shown in the last proposition.

We must now verify that  $\Delta C$  has a full rank when all of its components are different from zero. In this case,  $X_{1,m}, X_{2,m} \in \mathcal{O}_{\mathbb{K}}^* = \mathbb{Z}^* \oplus \theta\mathbb{Z}^* \oplus \mathcal{O}'_{\mathbb{K}}$  for all values of  $m$  where  $\mathcal{O}'_{\mathbb{K}} = \{a + b\theta \mid a, b \in \mathbb{Z}^*\}$ . When all the components of  $\Delta C$  are different from zero,  $\text{rank}(\Delta C) < 2$  implies that:

$$\frac{X_{2,1}}{X_{1,1}} = \dots = \frac{X_{2,M}}{X_{1,M}} = \frac{\sigma(X_{1,1})}{\sigma(X_{2,\pi^{-1}(1)})} = \dots = \frac{\sigma(X_{1,M})}{\sigma(X_{2,\pi^{-1}(M)})} = k \quad (3.56)$$

where  $k$  is any element of  $\mathbb{K}$ . After some manipulations, eq. (3.56) becomes:

$$X_{1,1} = (\mathbf{N}_{\mathbb{K}/\mathbb{Q}}(k))^{M+1-m} X_{1,m} ; m = M, M-1, \dots, 2 \quad (3.57)$$

Since  $\mathbf{N}_{\mathbb{K}/\mathbb{Q}}(k) \in \mathbb{Q}$ , eq. (3.57) implies that  $X_{1,1}, \dots, X_{1,M}$  (and in an equivalent manner  $X_{2,1}, \dots, X_{2,M}$ ) must belong simultaneously to one of the following sets  $\mathbb{Z}^*$ ,  $\theta\mathbb{Z}^*$  or  $\mathcal{O}'_{\mathbb{K}}$ .

Following from the structure of  $\mathcal{A}$  in eq. (3.52), a maximum number of two components of  $X_1$  (or  $X_2$ ) can contain an integer or an integral multiple of  $\theta$ . For  $M = 2$ , eq. (3.57) does not contradict the structure of  $\mathcal{A}$  implying that the proposed code is not fully diverse with  $M = 2$ . Designate by  $x_1, \dots, x_4$  any four elements of the  $M'$ -PAM constellation and by  $i$  and  $j$  two integers verifying  $i, j \in \{1, 2\}$  and  $i \neq j$ . From eq. (3.52), both entries of  $X_1$  can belong to  $\mathbb{Z}^*$  when  $b = b'$  and  $(a, a') = (x_1 e_i, x_2 e_j)$  ( $e_m$  is the  $m$ -th column of  $I_M$ ). In the same way, both entries of  $X_1$  can belong to  $\theta\mathbb{Z}^*$  when  $a = a'$  and  $(b, b') = (x_1 e_i, x_2 e_j)$ . Finally,  $X_{1,1}$  and  $X_{1,2}$  can both be in  $\mathcal{O}'_{\mathbb{K}}$  when  $X_1$  takes the form:  $X_1 = (x_1 + \theta x_2)e_i + (x_3 + \theta x_4)e_j$ .

For  $M = 3$ , when  $X_{1,m} \neq 0$  for  $m = 1, \dots, M$ ,  $X_1 \in \mathcal{A}$  implies that  $X_1$  must belong to the set of all possible permutations of:

$$\mathcal{A}' = \left\{ [x_1, x_2, x_3 \theta]^T, [x_1, x_2 \theta, x_3 \theta]^T, [x_1, x_2 \theta, x_3 + x_4 \theta]^T \right\} \quad (3.58)$$

where  $x_1, \dots, x_4 \in \mathbb{Z}^*$ . Therefore, a maximum number of 2 components of  $X_1$  can be in  $\mathbb{Z}^*$  (or  $\theta \mathbb{Z}^*$ ) at the same time while only one component can belong to  $\mathcal{O}'_{\mathbb{K}}$ . This is in contradiction with eq. (3.57) which proves that the proposed code is fully diverse for  $M = 3$ .

For  $M = 4$ , a vector  $X_i \in \mathcal{A}$  occupies four positions without having any zero entry only if it is a permutation of the vector  $(x_1 e_1 + \theta x_2 e_2 + x_3 e_3 + \theta x_4 e_4)$ . This implies that there are two components of  $X_i$  that belong to  $\mathbb{Z}^*$  while the other 2 components belong to  $\theta \mathbb{Z}^*$ . Such vectors do not verify eq. (3.57) and, consequently, they do not result in rank deficient matrices  $\Delta C$ . Considering the last lemma and the cases  $M = 3$  and  $M = 4$ , we conclude that the proposed code achieves full diversity for  $n = 2$ ,  $M \geq 3$  and  $\forall M'$ .

For the general values of  $n$ , the reader is referred to Appendix D.1.

### Coding Gain

Designate by  $\delta_{M,M'}$  the coding gain of the code given in eq. (3.48) with  $M$ -PPM- $M'$ -PAM constellations. We have  $\delta_{N,M'} \geq \delta_{M,M'}$  for  $N \geq M$  since in this case  $N$ -PPM- $M'$ -PAM is obtained by adding new dimensions to the initial  $M$ -PPM- $M'$ -PAM signal set. On the other hand,  $\delta_{M,N'} \leq \delta_{M,M'}$  for  $N' \geq M'$  since  $M'$ -PAM is a subset of  $N'$ -PAM for  $N' \geq M'$ . Therefore, unlike the QAM constellations where an increase in the spectral efficiency results in a possible reduction in the coding gain, the coding gain and the spectral efficiency of the hybrid PPM-PAM constellations can be increased by increasing the dimensionality of the considered constellation. Therefore, we can argue that for  $M \gg 1$ ,  $\delta_{M,M'}$  keeps the same value for all values of  $M'$ . This follows from the fact that the multiplication by the matrix  $\Omega$  simply permutes the coordinates of the information vectors over the  $M$ -dimensional signal subspace without introducing any constellation expansion. Formally speaking, the proposed code verifies the following property:

**Proposition 3.2** *For a system equipped with  $n$  transmit antennas with  $M$ -PPM- $M'$ -PAM constellations, eq. (3.48) has a non-vanishing determinant for  $M > n^2$  and for all values of  $M'$ .*

The proof is provided in Appendix D.2.

### Shaping and Information Losses

In order to verify the shaping constraint, the basis  $\{1, \theta, \dots, \theta^{n-1}\}$  in eq. (3.48) can be replaced by a new orthonormal basis  $\{v_i\}_{i=1}^n$ . In this case, eq. (3.48) takes the general form:

$$C = \sum_{i=0}^{n-1} \text{Diag}((\mathcal{M} \otimes I_M)[a_{in+1}^T \cdots a_{(i+1)n}^T]^T)^T \Lambda^i \quad (3.59)$$

For a  $nM$ -dimensional vector  $X$ ,  $\text{Diag}(X) = \text{diag}([X_1 \cdots X_n])$  where  $X_i$  is the  $M$ -dimensional vector composed of the  $j$ -th components of  $X$  for  $j = (i-1)M+1, \dots, iM$  where  $i \in \{1, \dots, n\}$ . The  $(i, j)$ -th element

of  $\mathcal{M}$  is equal to  $\sigma^{i-1}(v_j)$  and  $\Lambda$  is the  $nM \times nM$  matrix given by:

$$\Lambda = \begin{bmatrix} \mathbf{0}_{M \times M} & I_M & \cdots & \mathbf{0}_{M \times M} \\ \vdots & \mathbf{0}_{M \times M} & \ddots & \vdots \\ \mathbf{0}_{M \times M} & \vdots & \ddots & I_M \\ \Omega & \mathbf{0}_{M \times M} & \cdots & \mathbf{0}_{M \times M} \end{bmatrix} \quad (3.60)$$

Concerning the choice of the basis  $\{v_i\}_{i=1}^n$ , the orthonormal basis constructed in Section 3.2 can be readily used for all values of  $n$ . In the same way,  $\mathcal{M}$  can be any fully diverse rotation matrix [100].

**Proposition 3.3** *The code given in eq. (3.59) is information lossless for all values of  $n$ .*

The proof follows from the fact that the basis  $\{v_i\}_{i=1}^n$  is constructed to be orthonormal and that the matrix  $\Omega$  is unitary. A detailed proof is provided in Appendix D.3.

### 3.4.2 Construction 2: Achieving full transmit diversity via position combining

In this section, we propose the construction of a new family of ST codes for  $M$ -PPM- $M'$ -PAM constellations with the values of  $M$  spanning intervals that are potentially different from the ones given in proposition 3.1. In particular, the proposed codes can be applied with any number of transmit antennas for all even values of  $M$ . In order to achieve full transmit diversity with these values of  $M$ , we propose to keep the same structure of the codewords (as in eq. (3.48)) and to find an appropriate structure of the  $M \times M$  matrix  $\Omega$  that permits to achieve this diversity order. For a given number of transmit antennas,  $\Omega$  is constructed as follows:

**Proposition 3.4** *For  $n$  transmit antennas, consider the code given in eq. (3.48) constructed over  $\mathbb{K}(\theta)$  with  $\theta = 2\cos(\frac{2\pi}{N})$  and  $\mathbb{E}(N) = 2n$ . This code is fully diverse with  $M$ -PPM- $M'$ -PAM constellations for all values of  $M'$  and for even values of  $M$  if:*

$$\Omega = I_{M/2} \otimes \begin{bmatrix} \cos(\theta') & \sin(\theta') \\ -\sin(\theta') & \cos(\theta') \end{bmatrix} \quad (3.61)$$

such that  $\theta = \frac{2\pi}{N'}$  and  $N'$  is an integer that is relatively prime with  $N$  verifying  $\mathbb{E}(N') \geq n$ .

*Proof:* The proof is provided in Appendix E.1.

In order to have more insights on the properties of the constructed code, we further investigate the case  $n = M = 2$ . In this case,  $N = 5$  and the choice  $N' = 4$  verifies the conditions in proposition 3.4 and the matrix  $\Omega$  takes the following form:

$$\Omega = \begin{bmatrix} 0 & 1 \\ -1 & 0 \end{bmatrix} \quad (3.62)$$

As in eq. (3.51), denote by  $\Delta C$  the difference between two codewords. For  $M = n = 2$  and for  $\Omega$  verifying eq. (3.62),  $\Delta C$  can be expressed as:

$$\Delta C = \begin{bmatrix} X_{1,1} & X_{1,2} & \sigma(X_{2,2}) & -\sigma(X_{2,1}) \\ X_{2,1} & X_{2,2} & \sigma(X_{1,1}) & \sigma(X_{1,2}) \end{bmatrix}^T \quad (3.63)$$

$\Delta C$  is rank deficient if  $\Delta C_2 = k\Delta C_1$  for a certain value  $k \in \mathbb{K}$  where  $\Delta C_i$  is the  $i$ -th column of  $\Delta C$ . This results in:

$$\begin{aligned} X_{2,1} &= kX_{1,1} = k\sigma(k)X_{2,2} = k^2\sigma(k)X_{1,2} = -k^2(\sigma(k))^2X_{2,1} \\ &= -(N_{\mathbb{K}/\mathbb{Q}}(k))^2X_{2,1} \end{aligned} \quad (3.64)$$

$(1 + (N_{\mathbb{K}/\mathbb{Q}}(k))^2)X_{2,1} = 0$  implies that  $X_{2,1} = 0$  since  $k$  is real. From the first row of  $\Delta C$ ,  $\text{rank}(\Delta C) < 2$  and  $X_{2,1} = 0 \Rightarrow X_{1,1} = 0$ . Considering the third row of  $\Delta C$ , this implies that  $X_{2,2} = 0$  which further results in  $X_{1,2} = 0$  from the linear dependence between the elements of the second row of  $\Delta C$ . Therefore, only the all-zero matrix is rank-deficient and the code is fully diverse for all values of  $M'$ .

For the special case of 2-PPM constellations ( $M = 2$  and  $M' = 1$ ), the following proposition holds:

**Proposition 3.5** *If  $\Omega$  has the structure given in eq. (3.62), then the code is fully diverse with 2-PPM constellations for all values of  $n$ .*

*Proof:* Designate by  $\mathcal{A}$  the set whose elements consist of the difference between two  $M$ -dimensional vectors having the structure given in eq. (3.49). In other words:

$$\mathcal{A} = \left\{ \sum_{i=0}^{n-1} (a_i - a'_i)\theta^i ; a_0, a'_0, \dots, a_{n-1}, a'_{n-1} \in \mathcal{C} \right\} \quad (3.65)$$

where  $\mathcal{C}$  stands for the PPM-PAM signal set. For binary PPM constellations,  $\mathcal{C} = \{[1 \ 0]^T, [0 \ 1]^T\}$ . Following from this structure of  $\mathcal{C}$ , an element  $A$  of  $\mathcal{A}$  can be written as  $A = [a - a']^T$  where  $a \in \mathbb{K}$ . For example, with  $n = 2$  transmit antennas, consider the following matrix:

$$A = \begin{bmatrix} 0 & 1 & \theta & 1+\theta & 1-\theta \\ 0 & -1 & -\theta & -1-\theta & -1+\theta \end{bmatrix} \quad (3.66)$$

then, the elements of  $\mathcal{A}$  are equal to the columns of the above matrix multiplied by  $\pm 1$ .

In Appendix E.2, we show that this particular structure of the elements of  $\mathcal{A}$  results in  $\text{rank}(\Delta C) = n$  for non-zero matrices  $\Delta C$  and for all values of  $n$ . Note that for binary PPM, full diversity can be achieved with the values of  $\Omega$  respecting proposition 3.4 or with  $\Omega$  as in eq. (3.62). It is better to choose the matrix form given in eq. (3.62) because in this case the multiplication by  $\Omega$  does not result in an additional constellation extension. Moreover, this choice of  $\Omega$  results in an additional advantage stated in the next proposition.

**Proposition 3.6** *If  $\Omega$  has the structure given in eq. (3.62), then the code proposed in eq. (3.48) and the perfect codes [64] have the same coding gain with 2-PPM constellations for all values of  $n$ .*

*Proof:* The proof is given in Appendix E.3.

As in section 3.4.1, the basis  $\{1, \dots, \theta^{n-1}\}$  can be replaced by an orthonormal basis resulting in information lossless and shaping efficient codes obtained from the association of eq. (3.59) with the values of  $\Omega$  given in eq. (3.61) or eq. (3.62). The proof is similar to the one given in Appendix D.3.

Finally, combining the constructions proposed in this section and in section 3.4.1 permits to achieve full transmit diversity with  $M$ -PPM- $M'$ -PAM constellations for all values of  $M'$  and for  $M \geq 2$ ,  $\{M \geq 2, M \neq 3\}$ ,  $\{M \geq 2, M \neq 3\}$ ,  $\{M \geq 2, M \neq 3, 5\}$  and  $\{M \geq 2, M \neq 3, 5\}$  with  $n = 2, 3, 4, 5$  and 6 transmit antennas respectively. If a certain values of  $M$  verifies proposition 3.1 and proposition 3.4 simultaneously, it is better to choose the matrix form given in eq. (3.50) that simply permutes the coordinates of the transmitted information vectors rather than combining them.

### 3.4.3 Comparison with codes from cyclic division algebras

In what follows, we compare the modulation-specific codes with the totally-real codes constructed from cyclic division algebras (ISC in section 3.2) for the values of  $M$  respecting proposition 3.1 or proposition 3.4.

For the values of  $M$  respecting proposition 3.2, construction 1 has a coding gain that does not decrease with the size of the embedded PAM constellation ( $M'$ ). However, this happen for  $M > n^2$  which corresponds to constellations having a large number of dimensions and consequently for systems having a high receiver complexity. For constellations with limited dimensions, the modulation specific codes do not have a non-vanishing determinant. The advantage of these codes is that they are energy-efficient and information lossless. On the other hand, ISC has a non-vanishing determinant. However, this comes at the expense of not having uniform average transmitted energy per antenna. Moreover, ISC are not information lossless codes. For UWB communications, we argue that energy efficiency can be more important than the NVD property for the following reasons:

- Over Rayleigh fading channels, codes with NVD achieve the diversity-multiplexing tradeoff of the underlying channel [49]. However, UWB signals are subject to lognormal fading (refer to section 2.3). For these channels, the asymptotic analysis applied in [49] gives no insights whether or not codes with NVD achieve the D-MG tradeoff over the UWB channels. First, because of the complex nature of the channel matrices (that are no more complex Gaussian). Second, because it was seen in section 2.3 that an infinite diversity order can be reached for asymptotic values of the SNR. Over the UWB channels, the absence of a direct connection between the NVD property and the achievable tradeoffs reduces the importance of the NVD property.
- In [49], the tradeoff is achieved with a family of codes whose spectral efficiency scales with the SNR. For QAM constellations, this reduces the coding gain unless when the code has a NVD. On the other hand, at high SNRs, the spectral efficiency of  $M$ -PPM- $M'$ -PAM can be increased by extending the constellation in the time domain (increasing  $M$ ) rather than the amplitude domain (increasing  $M'$ ). For construction 1, this extension does not introduce a decrease in the coding gain since the dimensionality of the signal subspace is increased with no additional constellation expansion.
- High order PAM constellations have a very poor performance [7]. This is why, the highest order PAM constellation used in the literature of the UWB was the 2-PAM constellation.

Finally, the modulation-specific codes verify a large number of constraints. 1) They are totally-real. 2) They achieve full rate and full diversity. 3) They introduce no shaping losses. 4) They are information lossless. 5) They are energy efficient. 6) They achieve the best known coding gains (those of the complex-valued perfect codes) in the following cases:

- $M$ -PPM- $M'$ -PAM constellations for all values of  $M'$  and for  $M > n^2$  with any number of transmit antennas  $n$  (from proposition 3.2).
- 2-PPM constellations with any number of transmit antennas (from proposition 3.6).
- 2-PPM-2-PAM, 2-PPM-4-PAM and 2-PPM-8-PAM constellations with  $n = 2$  transmit antennas (with the value of  $\Omega$  given in eq. (3.62)).

- $M$ -PPM constellations for all values of  $M \geq 3$  and for  $n = 2$  transmit antennas (construction 1).
- $M$ -PPM-2-PAM (bi-orthogonal) constellations and  $M$ -PPM-4-PAM for  $M \geq 4$  and for  $n = 2$  transmit antennas (construction 1).

The third case is verified by computer simulations. The last two cases follow from the numerical evaluation of the coding gain of the code in eq. (3.59) associated with the value of  $\Omega$  in eq. (3.50) with  $M$ -PPM and  $M$ -PPM- $M'$ -PAM ( $M' \in \{2, 4\}$ ) for  $M = 3$  and  $M = 4$  respectively. Since the coding gain of construction 1 increases with  $M$ , this proves the last two conditions.

## 3.5 Numerical Results

In order to compare different modulation schemes, the energy of the PPM-PAM constellation is normalized to one. For systems that do not use modified Hermite pulses, the pulse waveform  $w(t)$  is chosen to be the second derivative of the Gaussian pulse with a duration of  $T_w = 0.5$  ns normalized to have unit energy. When modified Hermite pulses are used, the first-order pulse (the one with the shortest duration) has a duration of 0.5 ns. Orthogonal PPM modulations are used with  $\delta = T_w = 0.5$  ns. In order to eliminate ISI, the frame time is fixed to  $T_f = 100$  ns. In single user situations, the performance is independent from the number of time frames  $N_f$ . In this case, we fix  $N_f = P$  in order to render IPC and the balancing of ISC possible. In multi-user scenarios, all users are assumed to have the same transmission levels and random TH sequences are used. Simple PRake receivers are deployed and the sphere decoder [102] is used for detection.

The transmit and the receive arrays are supposed to be sufficiently spaced so the each one of the  $PQ$  sub-channels is generated independently from the other sub-channels using the standard IEEE 802.15.3a channel model [17]. For simplicity, we assume that the relative time delays between the signals received at the different antennas ( $\epsilon_{q,p}^{(k)}$  in eq. (2.4)) are negligible. In this way, simulations highlight the diversity and multiplexing advantage of the proposed schemes independently from the relative orientations and positions of the transmit and receive arrays.

The number of matched filters at the receiver increases with the dimensionality of the transmitted constellations. Therefore, when evaluating the performance of the different diversity schemes, we compare systems that use  $M$ -PPM- $M'$ -PAM constellations having the same value of  $M$ . In what follows, the term uncoded systems corresponds to spatial multiplexing.

### 3.5.1 Performance with PAM

First, we compare systems using modified Hermite pulses with ST coded systems. For MIMO systems using PRakes, the diversity scheme based on Hermite pulses deploys  $QLP$  matched filters (from eq. (3.2)) while only  $QL$  matched filters are necessary when only one pulse waveform is used (from eq. (2.33)). Moreover, the estimation of the channel matrix necessitates the estimation of  $QLP^2$  rather than  $QLP$  parameters as in uncoded and ST-coded systems. Therefore, it is interesting to compare Hermite systems having  $L$  fingers with uncoded systems having  $PL$  fingers since in this case the number of matched filters, decoding complexity and the data rate are the same.

Fig. 3.5 shows the performance at a rate of 4 bits PCU. In particular, we compare Hermite systems (section 3.1), orthogonal codes (section 2.2) and ISC (section 3.2). The legend “Hermite” stands for the system using Hermite pulses with no modulation diversity. To achieve the given rate, all schemes

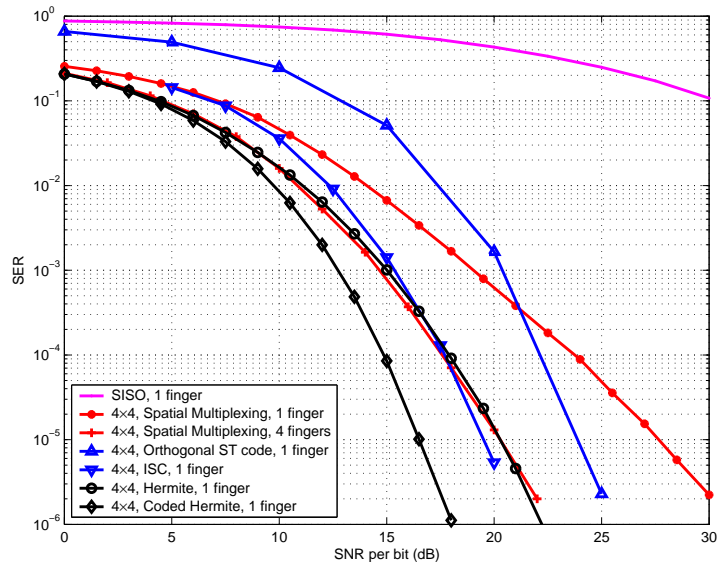


Figure 3.5: Performance on CM2 with PAM constellations at a rate of 4 bits PCU.

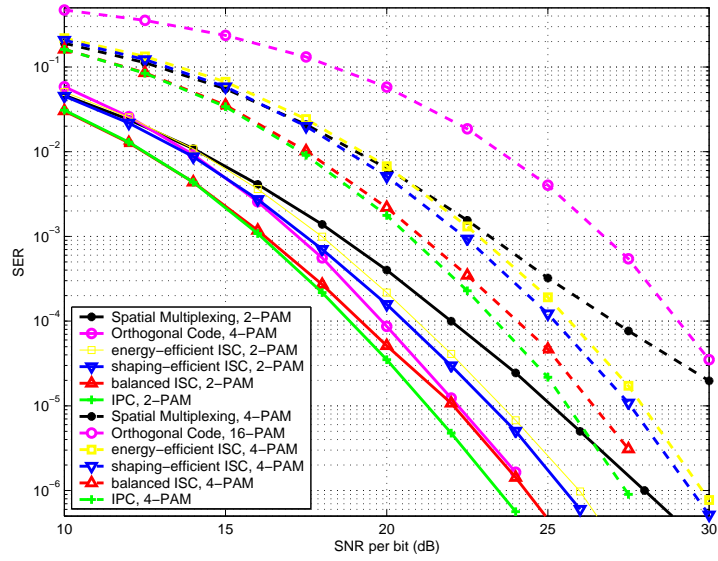


Figure 3.6: Performance on CM2 with 2 transmit antennas, 2 receive antennas and a PRake with 6 fingers.

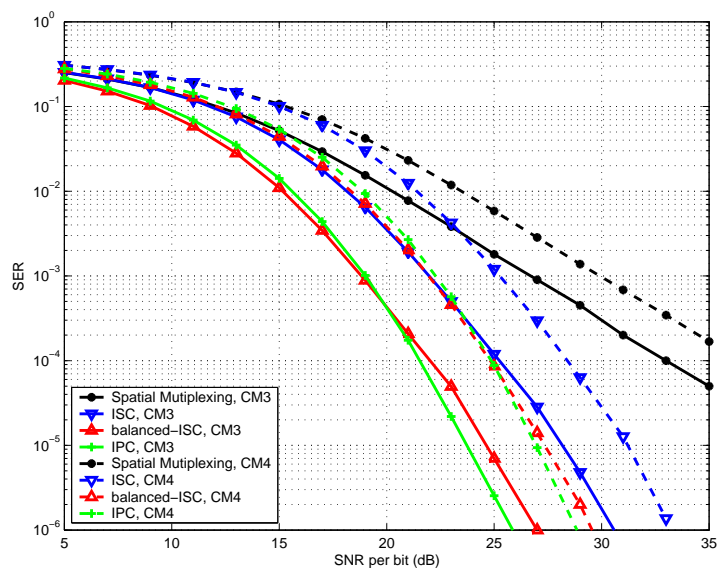


Figure 3.7: Performance of  $3 \times 3$  systems over CM3 and CM4 with 2-PAM and a 1-finger PRake.

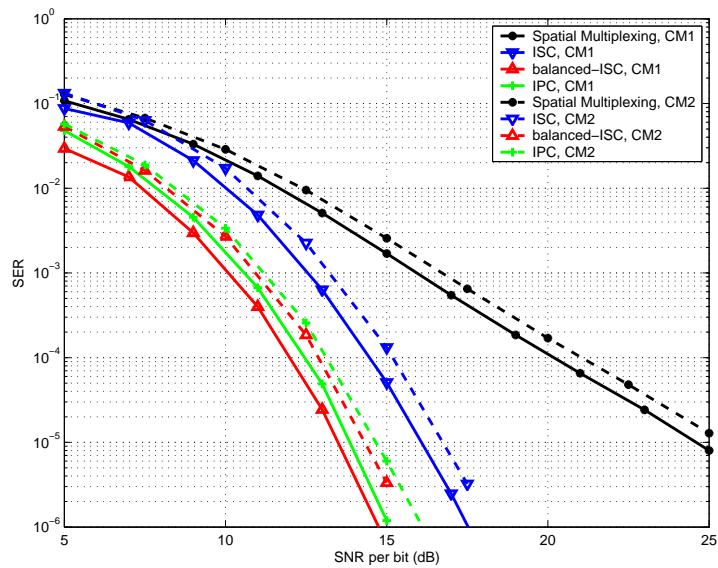


Figure 3.8: Performance of  $5 \times 5$  systems over CM1 and CM2 with 2-PAM and a 1-finger PRake.

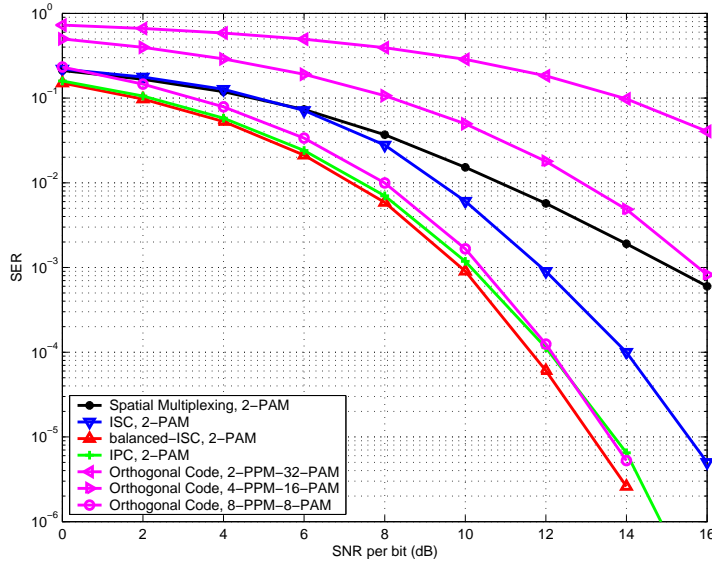


Figure 3.9: Performance on CM2 with 6 transmit antennas, 6 receive antennas and a 1-finger PRake at 6 bits PCU.

use 2-PAM except for SISO systems and the orthogonal codes that must use 16-PAM. Results show the importance of merging the use of Hermite pulses with modulation diversity. For example, at an error rate of  $10^{-4}$ , the coded Hermite system with 1-finger outperforms the uncoded 4-fingers system by 2 dB while having the same number of matched filters and decoding complexity. With respect to ISC, coded Hermite systems show better performance at the expense of using  $P = 4$  times more correlators with the advantage of a lower decoding complexity.

In Fig. 3.6, we show the performance of energy-efficient, shaping-efficient and balanced ISC taken from eq. (3.17), eq. (3.19) and eq. (3.26) respectively. We compare the above codes with the orthogonal codes and IPC from section 2.2 and section 3.3 respectively. With PAM, the coding gains of  $C_{2,eq}$  and  $C_{2,rot}$  given in eq. (3.17) and eq. (3.19) are equal to  $\frac{4}{\sqrt{13}}$  and  $\frac{8}{3\sqrt{5}}$  respectively. This justifies the difference in the performance between these two codes at high SNRs. We can also notice the performance improvement introduced by balancing ISC. Note that at 2 bits PCU, the orthogonal code approaches the performance of balanced-ISC at high SNR. At 4 bits PCU (and for the same number of correlators fixed by the dimensionality of the constellation), it must use 16-PAM which results in important performance losses with respect to ISC and IPC.

In Fig. 3.7, we show the performance on CM3 and CM4 with  $P = Q = 3$  and  $L = 1$  finger PRake using 2-PAM constellations. Once again IPC outperforms all the other codes and balanced-ISC outperforms ISC. At low SNRs, the pulse permutations render balanced-ISC more resistant against noise resulting in limited performance ameliorations with respect to IPC.

In Fig. 3.8, the performance at 5 bits PCU is shown for  $P = Q = 5$  and  $L = 1$  on CM1 and CM2. In this case, balanced-ISC slightly outperforms IPC for all values of the SNR. This can be explained by the fact that in this case balanced-ISC performs a large number of permutations (5 permutations) of the codewords in eq. (3.13). This results in a better immunity against noise explaining the slight performance gain at all SNRs. Similar results are obtained in Fig. 3.9 for  $P = Q = 6$ ,  $L = 1$  and at a rate of 6 bits PCU. Notice that even with 8-dimensional constellations, the orthogonal code performs worse than balanced-

ISC. As a conclusion, when the pulse repetitions are present, balanced-ISC shows the best performance for sufficiently large number of antennas. On the other hand, IPC shows comparable performance with lower complexity.

### 3.5.2 Performance with hybrid PPM-PAM

First, we compare MIMO-UWB systems using modified Hermite pulses with uncoded systems using ML and MMSE receivers. Fig. 3.10 shows the performance with 8-PPM-8-PAM,  $P = 3$ ,  $Q = 1$  and  $L = 8$ . MIMO and single-antenna systems transmit at 180 Mbits/s and 60 Mbits/s respectively. Results show that the better conditioned channel matrix that follows from the use of Hermite pulses permits linear receivers to close the gap with respect to the optimal detectors. Therefore, even though the use of the Hermite pulses achieves partial transmit diversity with an increased number of matched filters, high performance levels can be obtained even with non-optimal linear receives.

In Fig. 3.11, we compare PRake and SRake receivers on CM1 with 2-PPM-2-PAM constellations and  $L = 1$ . Results show that the uncoded  $2 \times 2$  systems using SRakes outperform coded systems using PRakes at low SNRs. At high SNR, the diversity order of the latter turns out to be better. Note that SRake receivers suffer from low fading margins since the strongest multi-path component is chosen. Therefore, the performance gap between coded and uncoded systems is smaller for systems equipped with SRakes. However, despite the low fading margins of SRake systems, IPC results in a performance gain of about 1 dB at a SER of  $10^{-3}$  with respect to uncoded MIMO systems.

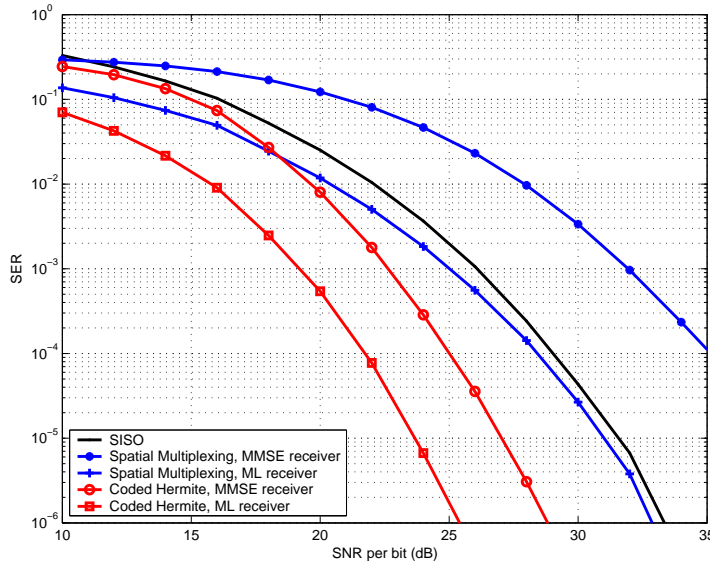


Figure 3.10: Performance on CM2 with 8-PPM-8-PAM,  $P = 3$ ,  $Q = 1$  and  $L = 8$  using ML and MMSE receivers.

Fig. 3.12 compares ISC with the modulation-specific codes using  $M$ -PPM- $M'$ -PAM constellations. The values of  $M$  are chosen to verify proposition 3.1 and therefore  $\Omega$  can take the value given in eq. (3.50). Results show that the modulation-specific codes outperform codes from totally-real cyclic division algebras without the need of any pulse repetitions or additional number of matched filters. This shows the importance of having energy-efficient codes. A gain of about 1 dB is observed at an error rate

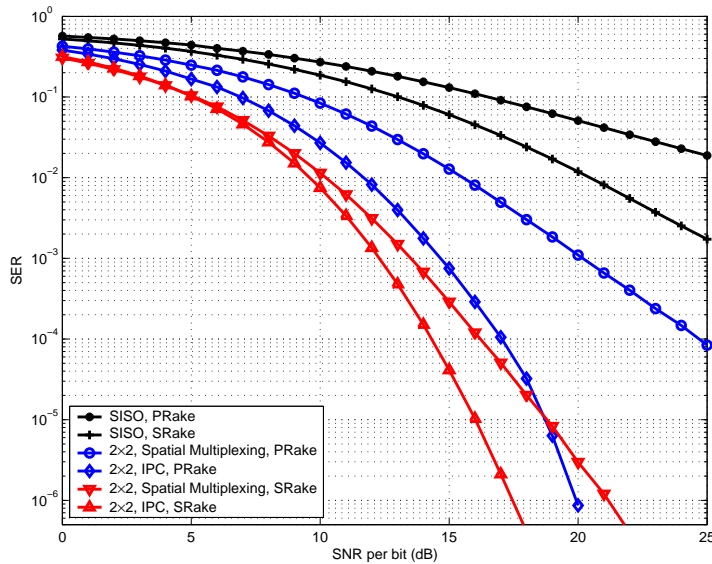


Figure 3.11: Performance on CM1 with 2-PPM-2-PAM and a 1-finger Rake.

of  $10^{-3}$  using three transmit antennas and 5-PPM-2-PAM constellations. This gain increases to 1.5 dB with four transmit antennas and 5-PPM.

In Fig. 3.13, we consider 2-PPM constellations on CM2. The receiver is equipped with a 1-finger PRake and we fix  $P = Q = n$  where  $n = 2, \dots, 5$ . Following from proposition 3.5,  $\Omega$  can take the form given in eq. (3.62). In this case, the association of construction 2 with 2-PPM achieves the best known coding gain (proposition 3.6). As a result, performance gains in the order of 2 dB can be obtained with respect to ISC with 3 transmit antennas at a BER of  $10^{-3}$ .

In Fig. 3.14, we show the performance of the proposed ST codes over the space-variant UWB channel model proposed in [22, 23]. In this case, the relative delays between the elements of the antenna arrays are provided by this model ( $\epsilon_{q,p}^{(k)}$  in eq. (2.4)). We fix,  $P = 3$ ,  $Q = 1$  and  $L = 5$  with 4-PPM constellations. For the modulation-specific codes,  $\Omega$  has the structure given in eq. (3.61) with  $N' = 5$  (since  $N = 7$ ). We consider profile 3 that corresponds to an “office-to-office” scenario. We compare the cases where the distance  $d$  between the elements of the transmit antenna array is equal to 5 cm and 15 cm respectively. Results show that even though construction 2 introduces an additional constellation extension, its good energetic distribution results in a performance gain of about 1.2 dB with respect to ISC at a SER of  $10^{-3}$ . The slopes of the error curves of the ST coded systems highlight the enhanced diversity order with respect to the uncoded MIMO systems. Closely separated antenna arrays ( $d = 5$  cm) result in a performance loss of about 0.6 dB with respect to arrays whose inter-antenna separation is equal to 15 cm. However, this performance loss is not associated with any degradation in the diversity order and the same diversity advantage can be obtained for both inter-antenna separations.

In Fig. 3.15, the modulation-specific codes are compared with the perfect codes for the values of  $M$  and  $M'$  that result in the best known coding gain (refer to section 3.4.3). For comparison reasons, and even though it may seem practically infeasible, the UWB receivers are supposed to be equipped with IQ front ends. The results show the high performance levels of the proposed modulation-specific schemes. Even though they are real-valued, they show exactly the same performance as the best known codes.

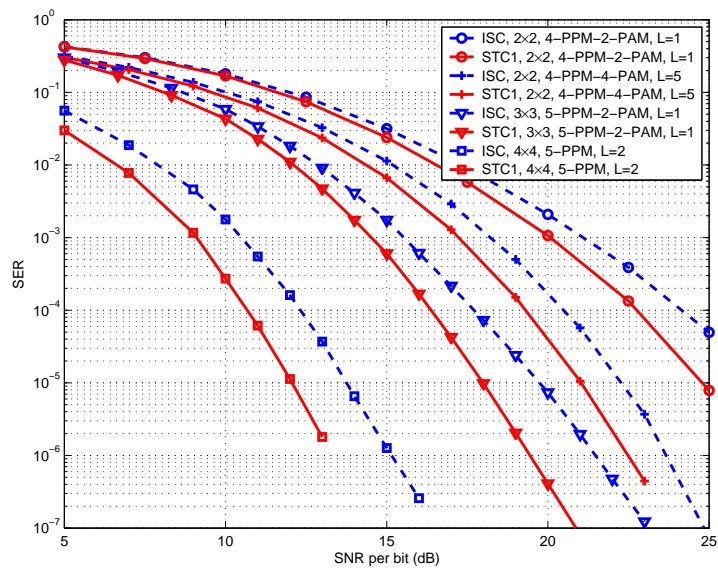


Figure 3.12: ISC versus construction 1 (STC1) on CM2.

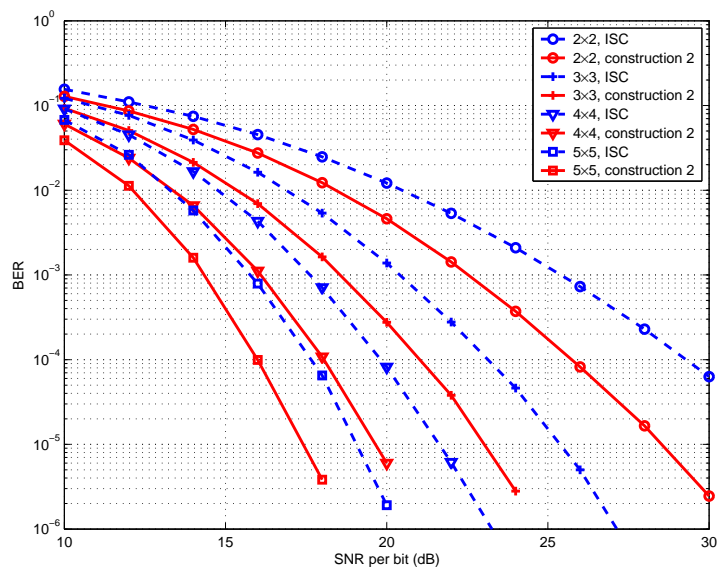


Figure 3.13: ISC versus construction 2 on CM2 with 2-PPM and  $L = 1$ .

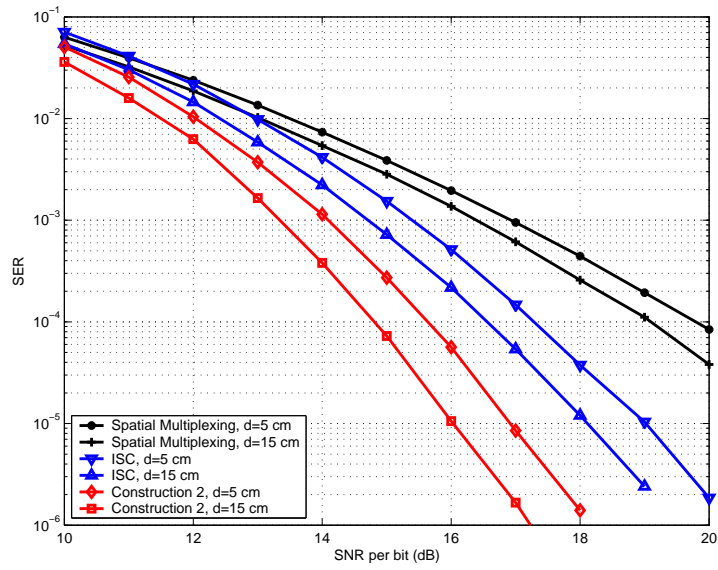


Figure 3.14: ISC versus construction 2 on the Kunisch-Pamp channel model (profile 3) using 4-PPM,  $P = 3$ ,  $Q = 1$  and  $L = 5$ .  $d$  corresponds to the inter-antenna separation.

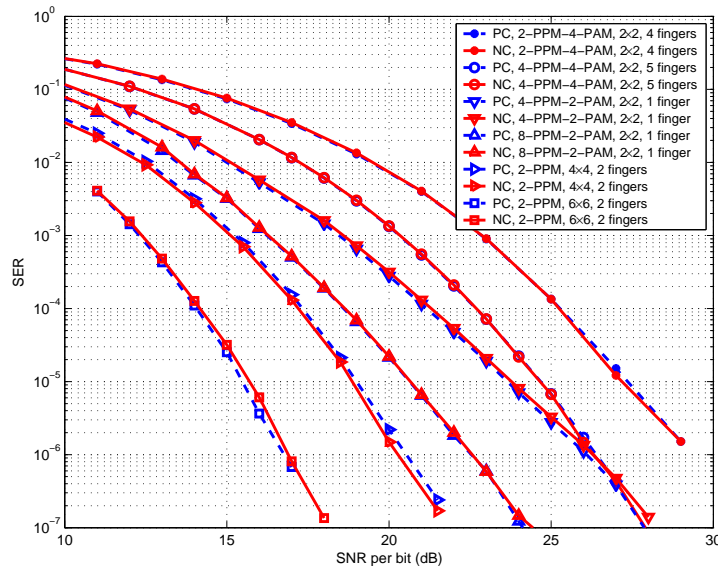


Figure 3.15: The new modulation-specific codes (NC) versus the perfect codes (PC) on CM2.

### 3.5.3 Construction 1 versus Construction 2

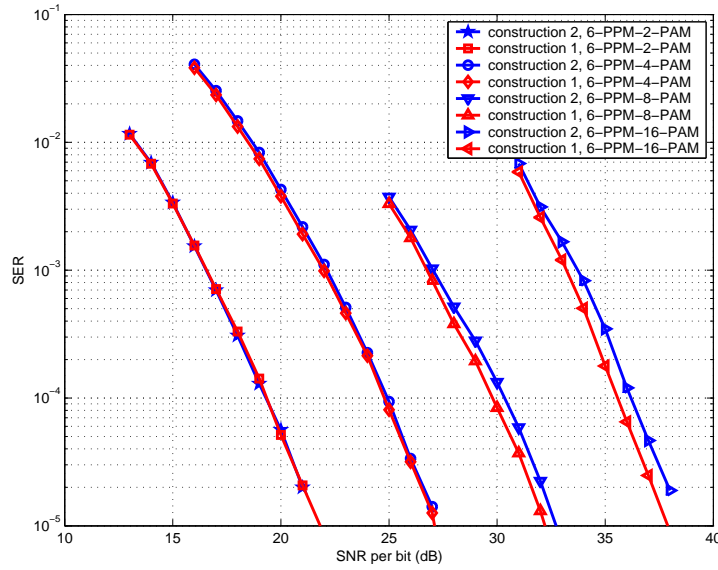


Figure 3.16: Construction 1 versus construction 2 with 3 transmit antennas, 3 receive antenna and 6-PPM- $M'$ -PAM constellations over CM2. A 1-finger PRake is used.

In Fig. 3.16, we compare construction 1 and construction 2 with  $M$ -PPM- $M'$ -PAM constellations for the values of  $M$  that verify proposition 3.1 and proposition 3.4 simultaneously. In particular, we perform simulations over CM2 with  $P = 3$  transmit antennas, 3 receive antennas and a 1-finger Rake for  $M = 6$  and  $M' \in \{2, 4, 8, 16\}$ . Given the high dimensionality of the transmitted constellation ( $P^2M = 54$ ), we apply the algorithm proposed in [103] for detection. This decoding algorithm is based on the Schnorr-Euchner enumeration strategy and a Fano-like metric bias is introduced in order to enhance the convergence time. Moreover, the MMSE-DFE preprocessing is performed [104] (refer to chapter 5 for more details). As expected, construction 1 outperforms construction 2 and the simulation results show that the performance difference between these two constructions becomes significant for large values of  $M'$ . While construction 2 shows practically the same performance as construction 1 for  $M' = 2, 4$ , the former construction results in a performance loss in the order of 0.5 dB for  $M' = 8, 16$ .

### 3.5.4 Performance in the presence of MUI

In this section, we determine the impact of MUI on the performance of the proposed ST codes. In particular, we determine the performance gains that result from the association of IPC with the user-specific unitary amplitude spreading matrices given in section 2.4.4.

Fig. 3.17 shows the performance with  $P = Q = 2$ ,  $N_f = 2P = 4$ ,  $N_c = 200$ , 2-PAM and  $L = 5$  for  $K = 10$  and  $K = 15$  interfering users in a synchronous environment. MMSE filters are used at the receiver side in order to reduce the level of MUI. For ISC and balanced-ISC, the same amplitude spreading sequence is associated with the  $P$  transmit antennas and MUI can be controlled uniquely by the choice of the time-hopping sequence. For IPC, the amplitude spreading matrix can be taken to be user dependent. In this case, it chosen to verify eq. (2.107).

Balanced-ISC is compared with IPC in the two following cases. In the first case, each one of the  $K + 1$  users is attributed with a random unitary matrix whose elements are taken from  $\{\pm 1\}$ . In the second case, to each user is given a matrix form the family of  $4^4 = 256$  matrices constructed from eq. (2.107) using 4-PAM elements. Results show that appropriately choosing the spreading matrices results in a gain of about 1 dB at  $10^{-4}$  for  $K = 10$ . The dotted lines associated with each curve correspond to the Gaussian approximation given in eq. (2.96). This approximation turns out to be accurate with any number of users.

Fig. 3.18 shows the degradation introduced by MUI when using IPC with  $P = Q = 2$ ,  $L = 7$ ,  $N_c = 200$  and  $N_f = 4$  in an asynchronous environment at a signal to noise ratio of 25 dB. The random matrices whose elements are taken from  $\{\pm 1\}$  and the designed matrices from eq. (2.107) are attributed to the different users in the same way as in Fig. 3.17. Results show that the performance gain becomes more significant with large number of users since in this case interference becomes more critical on the system performance. For example with 4-PPM-2-PAM constellations and at an error rate of  $10^{-4}$ , about 5 additional users can share the same physical channel without any bandwidth loss, increased receiver complexity or additional medium access control procedures. However, the application of eq. (2.107) may result in increased PAPR and higher dynamic ranges.

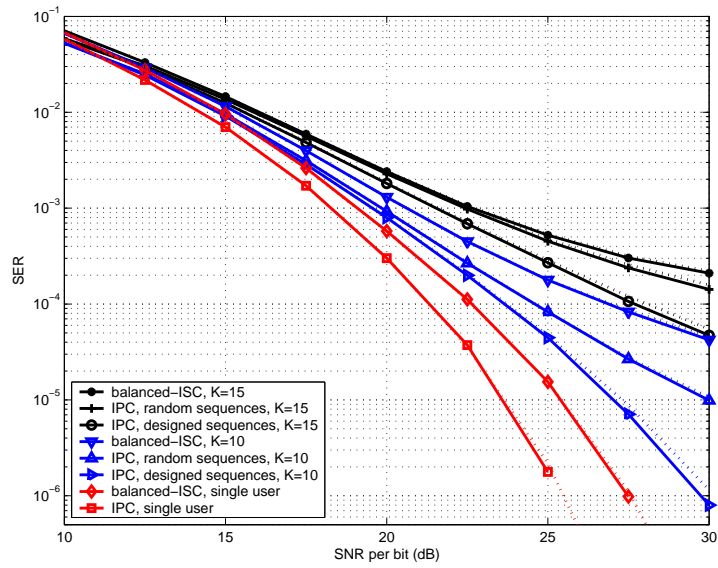


Figure 3.17: Performance with  $P = Q = 2$ , 2-PAM and 5 fingers PRake with  $K$  interfering users in a synchronous environment. The dotted lines associated with each curve correspond to the Gaussian approximation.

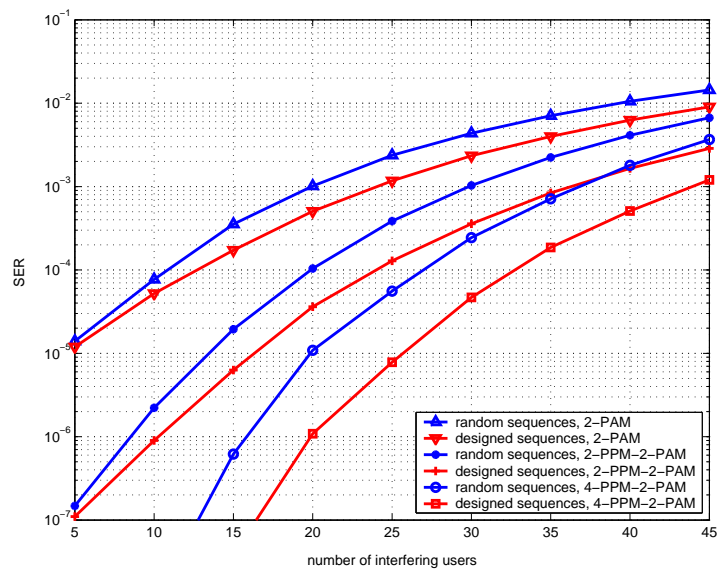


Figure 3.18: Performance of IPC in the presence of MUI with  $P = Q = 2$  and 7 fingers PRake in an asynchronous environment at 25 dB.

# Chapter 4

## Cooperative Diversity

In this chapter, we extend the cooperative diversity schemes to the context of IR-UWB systems. While cooperative systems were extensively studied with narrow band communications (refer to section 1.3.5 and the references therein), the benefits of associating these techniques with UWB communications were never investigated before. The nature of the IR-UWB transmissions and the high frequency selectivity of the UWB channels result in additional challenges on the design of the transmitter, receiver and the cooperating relays. Moreover, the analysis must take into account the synchronization problems, such as the timing jitter effects, which are prominent problems in UWB communications and which might not advantage a cooperative scenario if mistiming delays are propagated through several nodes.

In what follows, we develop appropriate schemes that exploit the spatial diversity in a distributed manner among the different terminals of a wireless network. We first consider the amplify-and-forward (AF) strategy and we apply the techniques presented in [74] for the construction of new totally-real distributed ST codes that are suitable for carrier-less UWB transmissions. At a second time, we apply the same approach that was adopted in section 3.2 and section 3.3 for profiting from the pulse repetitions to ameliorate the performance of the above codes and to introduce inter-pulse coding schemes. Then we propose new modulation-specific coding schemes that can be associated with  $M$ -PPM- $M'$ -PAM constellations for  $M \geq 2$  and for any number of relays.

We also consider the decode-and-forward (DF) strategy and we propose new coherent and differential DF schemes that take advantage of the pulse repetitions used to convey each information symbol.

Note that in what follows, we discuss uniquely issues related to the physical layer and code design. In comparison with other existing cooperative protocols, the proposed schemes do not impose any additional constraints on the medium access control layer and the routing protocols (refer to [105] and the references therein).

### 4.1 System design with the AF scheme

Consider the case of a wireless network composed of a certain number of synchronous and half-duplex radio terminals each equipped with a single antenna. The high frequency selectivity of the underlying channel results in two major differences in the system model with respect to the AF narrow band systems. Because of this frequency selectivity, diversity combining must be performed at the relays prior to amplification and retransmission. Moreover, the high temporal resolution might necessitate a feedback from the destination to the relays in order to overcome the different propagation delays.

### 4.1.1 Diversity combining at the relays

Designate by  $\Gamma$  the channel delay spread. In non-cooperative systems, ISI can be eliminated by choosing  $T_f \geq \Gamma$  where  $T_f$  is the frame duration. Applying a simple AF strategy at each relay will result in a received signal that is spread over a duration of  $2\Gamma$  at the destination. Consequently, ISI can only be eliminated by choosing  $T_f \geq 2\Gamma$  resulting in larger symbol durations and lower data rates. Moreover, higher order Rake receivers must be implemented at the destination since the energy collected by each finger is now very small.

A possible solution for this problem is by amplifying and retransmitting a limited part of the received signal. Designate by  $w(t)$  the pulse waveform. During the cooperation phase, the signal transmitted by each relay can be seen as a train of distorted versions of  $w(t)$ . This signal will have a duration  $\Gamma_1 < \Gamma$ . Moreover, the signals transmitted by the relays will have different shapes. Therefore, using a filter matched to  $w(t)$  at the destination is highly suboptimal given that these new transmitted pulse waveforms will be further distorted by the channels between the relays and the destination. Therefore, these systems will suffer from an increased intra-pulse interference. On the other hand, a Rake receive (at the destination) that combines the multi-path components during  $\Gamma_1$  will integrate a very limited part of the signal energy resulting in important performance degradations.

In order to overcome the above mentioned limitations,  $L$  multi-paths are combined at each relay prior to amplifying and retransmission. On the other hand, the channel parameters between the source and the relays must be known at the destination in order to achieve optimal detection with all AF schemes [70, 73]. For example, each relay can estimate its underlying channel and then it forwards the estimated parameters to the destination during the control phase. Therefore, using the available channel parameters to perform maximum ratio combining (MRC) does not result in a significant increase in the complexity of the relays. In what follows, we consider PRake receivers having  $L$  fingers.

### 4.1.2 Systems with feedback

Consider the case where  $K$  neighboring terminals (relays) can help the source in delivering its message to a given destination. Denote by  $h'_k(t)$  the impulse response of the channel from the source to the  $k$ -th relay for  $k = 1, \dots, K$ . In the same way, denote by  $g'_k(t)$  and  $h'_0(t)$  the channel impulse responses from the  $k$ -th node to the destination and from the source to the destination respectively. Let  $h_k(t) = h'_k(t) * w(t)$  for  $k = 0, \dots, K$  and  $g_k(t) = g'_k(t) * w(t)$  for  $k = 1, \dots, K$ . The channel seen by the destination and corresponding to the  $k$ -th relay can be expressed as:

$$g''_k(t) = g_k(t - \varepsilon_k) \quad (4.1)$$

where  $\varepsilon_k$  corresponds to the propagation delay between the  $k$ -th relay and the destination for  $k = 1, \dots, K$ . It is determined with respect to the arrival time of the first multi-path component between the source and the destination ( $\varepsilon_0 = 0$ ). In general, the relay selection protocol chooses relays that are closer to the destination than the source and  $\varepsilon_k$  is a negative quantity.

Based on this formulation, we can differentiate between two cases. In the first case, a feedback between the destination and the relays indicates the quantity by which each relay must advance or delay its transmission. In this case, the different delays are compensated and we can set  $\varepsilon_k = 0$  for  $k = 1, \dots, K$ . In other words, the first arriving rays of the different relays are aligned at the destination before performing matched filtering. In the second case, the first finger delay of the Rake corresponds to the first arriving

ray between the source and the destination. As will be seen later, this feedback can have a non negligible impact on the system performance.

### 4.1.3 System model

Consider the non-orthogonal AF (NAF) scheme proposed in [73] and described in Fig. 1.3. For this protocol, each relay enters in cooperation with the source during a period of  $2N_s$  symbol durations. The  $N_s$  symbols received during the first half of this cooperation period are amplified and retransmitted by the cooperating relay during the second half. In what follows, we denote by  $\mathcal{A}_{k,1}$  and  $\mathcal{A}_{k,2}$  the  $M \times N_s$  matrices given by:  $\mathcal{A}_{k,1} = [A_{2(k-1)N_s+1} \cdots A_{(2k-1)N_s}]$  and  $\mathcal{A}_{k,2} = [A_{(2k-1)N_s+1} \cdots A_{2kN_s}]$ .  $\mathcal{A}_{k,i}$  is transmitted during the  $i$ -th half of the  $k$ -th cooperation interval for  $i = 1, 2$  and  $k = 1, \dots, K$ .  $A_j$  is the  $M$ -dimensional vector that corresponds to the  $j$ -th information symbol and it belongs to the  $M$ -PPM- $M'$ -PAM constellation given in eq. (1.8). In the same way, the  $1 \times N_f$  amplitude spreading vectors corresponding to  $A_j$  will be denoted by  $B_1$  and  $B_2$  for  $j = 2(k-1)N_s + 1, \dots, (2k-1)N_s$  and  $j = (2k-1)N_s + 1, \dots, 2kN_s$  respectively and for  $k = 1, \dots, K$ . Moreover, the source and its relays will share the same time hopping sequence.

Taking these notations into consideration, the decision variables collected at the  $k$ -th relay during the first half of the  $k$ -th cooperation period can be expressed as:

$$X_k = \sqrt{\frac{\beta_1 \rho_k}{N_f}} H_k (\mathcal{A}_{k,1} \otimes B_1) + N'_k \quad (4.2)$$

where  $\rho_k$  is a gain factor corresponding to the relative quality of the channel between the source and the  $k$ -th relay with respect to the channel between the source and the destination ( $\rho_0 = 1$ ). When transmitting during the first half of each one of the  $K$  cooperation periods, the energy transmitted by the source is scaled by  $\beta_1$ .  $H_k$  is a  $LM \times M$  matrix corresponding to the channel between the source and the  $k$ -th relay. As in section 2.1.1, its  $(lM+m, m')$ -th element is equal to  $\int h_k(t)w(t - (m-m')\delta - lMT_w)dt$  for  $l = 0, \dots, L-1$  and  $m, m' = 1, \dots, M$ .

As in eq. (4.2), the decision variables collected at the destination during the first half of the  $k$ -th cooperation period can be expressed as:

$$Y_{k,1} = \sqrt{\frac{\beta_1}{N_f}} H_0 (\mathcal{A}_{k,1} \otimes B_1) + N_{k,1} \quad (4.3)$$

At each relay, MRC is performed before retransmitting. In other words, the signal transmitted from the  $k$ -th relay during the second half of the  $k$ -th cooperation period is given by:

$$X'_k = \sqrt{\beta_2} \Psi_k H_k^T X_k \quad (4.4)$$

where  $\Psi_k$  is the amplification matrix verifying:

$$\Psi_k = (H_k^T H_k)^{-\frac{1}{2}} \left( \beta_1 \rho_k H_k^T H_k + \frac{N_0}{2} I_M \right)^{-\frac{1}{2}} \quad (4.5)$$

When transmitting simultaneously during the second half of the  $k$ -th cooperation period, the  $k$ -th relay and the source are supposed to have the same transmission levels (determined by  $\beta_2$ ) for  $k = 1, \dots, K$ . Transmitting the same energy as in non-cooperative systems corresponds to fixing  $\beta_1 + 2\beta_2 = 2$ .

Finally, the decision matrix at the destination during the second half of the  $k$ -th cooperation period can be expressed as:

$$\begin{aligned} Y_{k,2} &= \sqrt{\frac{\beta_2}{N_f}} H_0 (\mathcal{A}_{k,2} \otimes B_2) + \sqrt{\lambda_k} G_k X'_k + N_{k,2} \\ &= \sqrt{\frac{\beta_2}{N_f}} H_0 (\mathcal{A}_{k,2} \otimes B_2) + \sqrt{\frac{\beta_1 \beta_2 \rho_k \lambda_k}{N_f}} G_k \Psi_k H_k^T H_k (\mathcal{A}_{k,1} \otimes B_1) + \sqrt{\beta_2 \lambda_k} G_k \Psi_k H_k^T N'_k + N_{k,2} \quad (4.6) \end{aligned}$$

where  $\lambda_k$  is determined in a similar way as  $\rho_k$  and it stands for the quality of the channel between the  $k$ -th relay and the destination.  $G_k$  is a  $LM \times M$  matrix that stands for the channel between the  $k$ -th relay and the destination. Its  $(lM+m, m')$ -th element is equal to  $\int g_k''(t) w(t - (m-m')\delta - lMT_w) dt$  for  $l = 0, \dots, L-1$  and  $m, m' = 1, \dots, M$  where  $g_k''(t)$  is given in eq. (4.1).

Combining eq. (4.3) and eq. (4.6), the decision variables collected at the destination during the  $k$ -th cooperation period can be expressed as:

$$\begin{bmatrix} Y_{k,1} \\ Y_{k,2} \end{bmatrix} = \begin{bmatrix} \sqrt{\beta_1} H_0 & \mathbf{0}_{LM \times M} \\ \sqrt{\beta_1 \beta_2 \rho_k \lambda_k} G_k \Psi_k H_k^T H_k & \sqrt{\beta_2} H_0 \end{bmatrix} \begin{bmatrix} \mathcal{A}_{k,1} \otimes B_1 \\ \mathcal{A}_{k,2} \otimes B_2 \end{bmatrix} + \mathcal{N}_k \quad (4.7)$$

where the factor  $N_f$  is included in the noise variance and  $\mathcal{N}_k$  is a zero-mean colored Gaussian noise whose covariance matrix is given by:

$$E[\mathcal{N}_k \mathcal{N}_k^T] = \frac{N_f N_0}{2} \begin{bmatrix} I_{LM} & \mathbf{0}_{LM \times LM} \\ \mathbf{0}_{LM \times LM} & I_{LM} + \Sigma_k \end{bmatrix} \quad (4.8)$$

where:

$$\Sigma_k = \beta_2 \lambda_k G_k \Psi_k H_k^T H_k \Psi_k^T G_k^T \quad (4.9)$$

After noise whitening, eq. (4.7) can be written as:

$$Y_k = \tilde{H}_k \begin{bmatrix} \mathcal{A}_{k,1} \otimes B_1 \\ \mathcal{A}_{k,2} \otimes B_2 \end{bmatrix} + N_k \quad (4.10)$$

where  $N_k$  is white and  $\tilde{H}_k$  is the  $2LM \times 2M$  matrix given by:

$$\tilde{H}_k = \begin{bmatrix} \sqrt{\beta_1} H_0 & \mathbf{0}_{LM \times M} \\ \sqrt{\beta_1 \beta_2 \rho_k \lambda_k} \Sigma_k^{-\frac{1}{2}} G_k \Psi_k H_k^T H_k & \sqrt{\beta_2} \Sigma_k^{-\frac{1}{2}} H_0 \end{bmatrix} \quad (4.11)$$

Stacking the decision matrices corresponding to the  $K$  different cooperation intervals horizontally, we obtain the following relation:

$$Y_{(2LM \times KN_s N_f)} = \tilde{H}_{(2LM \times 2KM)} \mathcal{A}_{(2KM \times KN_s N_f)} + N_{(2LM \times KN_s N_f)} \quad (4.12)$$

where the subscripts indicate the corresponding matrices' dimensions.  $Y$ ,  $\tilde{H}$  and  $N$  are obtained by stacking the matrices  $Y_k$ ,  $\tilde{H}_k$  and  $N_k$  horizontally for  $k = 1, \dots, K$ .  $\mathcal{A}$  is given by:

$$\mathcal{A} = \text{diag} \left( \begin{bmatrix} \mathcal{A}_{1,1} \otimes B_1 \\ \mathcal{A}_{1,2} \otimes B_2 \end{bmatrix} \dots \begin{bmatrix} \mathcal{A}_{K,1} \otimes B_1 \\ \mathcal{A}_{K,2} \otimes B_2 \end{bmatrix} \right) \quad (4.13)$$

The cooperative scheme is determined by the choice of the matrix  $\mathcal{A}$ .

## 4.2 Code construction for the NAF scheme

In this section, we present different techniques for constructing the codewords given in eq. (4.13).

### 4.2.1 Inter Symbol Coding (ISC)

The construction is first considered with PAM constellations and the extension to PPM-PAM constellations is discussed later. For ISC, we fix  $B_1 = B_2 = B = \mathbf{1}_{1 \times N_f}$ . Equation (4.13) can be expressed as:  $\mathcal{A} = C \otimes B$  where  $C$  is a  $2K \times KN_s$  matrix and it corresponds to the distributed space-time coding scheme. It is given by:

$$C = \text{diag}(C_1 \cdots C_K) \quad (4.14)$$

$$C_k = [A_{k,1}^T \ A_{k,2}^T]^T \quad (4.15)$$

where  $C_k$  is a  $2 \times N_s$  matrix for  $k = 1, \dots, K$ .

From eq. (4.12), combining the decision variables corresponding to the different pulses of the same symbol is equivalent to calculating:

$$Y(I_{KN_s} \otimes B^T) = \tilde{H}(C \otimes B)(I_{KN_s} \otimes B^T) + N \quad (4.16)$$

$$= N_f \tilde{H}C + N \quad (4.17)$$

where it is easy to verify that the noise term is still white (with variance  $\frac{N_f^2 N_0}{2}$ ).

Since  $C_k$  is a  $2 \times N_s$  matrix, it can be directly seen that there is no interest in choosing  $N_s > 2$ . Therefore, in what follows we fix  $N_s = 2$  resulting in minimal-delay codes. Moreover, in order to achieve full rate,  $2KN_s$  symbols must be included in each codeword  $C$ . Furthermore, in order to achieve full diversity, all of these  $4K$  symbols must be included in the sub-matrices  $C_k$  for all values of  $k$ .

For the construction of  $C$ , we extend the family of codes proposed in [74] to UWB communications by performing the construction in totally-real field extensions. The family of codes constructed in [74] is based on cyclic division algebras and permits to achieve the diversity-multiplexing tradeoff given in [73] with any number of relays (refer to section 1.3.5).

Let  $\mathbb{K} = \mathbb{Q}(\theta)$  and  $\mathbb{F} = \mathbb{Q}(\phi)$  be  $K$  and 2 dimensional real cyclic number field extensions of  $\mathbb{Q}$  respectively. Their Galois groups are given by  $\text{Gal}(\mathbb{K}/\mathbb{Q}) = \langle \sigma \rangle$  (with  $\sigma^K = 1$ ) and  $\text{Gal}(\mathbb{F}/\mathbb{Q}) = \langle \tau \rangle$  (with  $\tau^2 = 1$ ). Moreover, we fix  $\mathbb{L} = \mathbb{Q}(\theta, \phi)$  and  $\phi = \frac{1+\sqrt{5}}{2}$ . From [74], the sub-matrix  $C_k$  takes the following structure:

$$C_k = D\sigma^{k-1}(C_0) \quad (4.18)$$

$$= \text{diag}\left((1+\phi^2)^{-\frac{1}{2}} \ (1+\phi_1^2)^{-\frac{1}{2}}\right)\sigma^{k-1}(C_0) \quad (4.19)$$

where  $\phi_1 = \tau(\phi) = \frac{1-\sqrt{5}}{2}$  and the diagonal matrix  $D$  is introduced for normalization purposes. The matrix  $C_0$  is given by:

$$C_0 = \lambda \begin{bmatrix} k_1 + \phi k_2 & k_3 + \phi k_4 \\ \gamma(k_3 + \phi_1 k_4) & k_1 + \phi_1 k_2 \end{bmatrix} \quad (4.20)$$

where  $\gamma, k_1, \dots, k_4 \in \mathcal{O}_\mathbb{K}$  where  $\mathcal{O}_\mathbb{K}$  is the ring of integers of  $\mathbb{K}$  resulting in a non-vanishing coding gain when  $\gamma$  is a non-norm element (refer to section 3.2 for more details). The scalar  $\lambda$  is introduced for

normalization purposes and it must verify:

$$N_{\mathbb{K}/\mathbb{Q}}(\lambda) = \frac{1}{\sqrt{d_{\mathbb{K}/\mathbb{Q}}}} \quad (4.21)$$

When  $K$  is odd, we fix  $\lambda = \alpha \in \mathbb{K}$ . When  $K$  is even, we fix  $\lambda = \sqrt{\alpha}$  and, in this case,  $\alpha$  must be totally positive.

From eq. (4.14) and eq. (4.21), the determinant of  $C$  verifies:

$$\begin{aligned} \frac{\det(C)}{\det(D)^K} &= \prod_{k=1}^K \det(\sigma^{k-1}(C_0)) = \prod_{k=1}^K \sigma^{k-1}(\det(C_0)) \\ &= N_{\mathbb{K}/\mathbb{Q}}(\lambda^2) N_{\mathbb{L}/\mathbb{F}}(N_{\mathbb{L}/\mathbb{K}}(k_1 + \phi k_2) - \gamma N_{\mathbb{L}/\mathbb{K}}(k_3 + \phi k_4)) \\ &= d_{\mathbb{K}/\mathbb{Q}}^{-1} N_{\mathbb{L}/\mathbb{F}}(x - \gamma y) \end{aligned} \quad (4.22)$$

Since there is no element in  $\mathbb{L}$  whose norm is equal to  $\gamma$ , we obtain  $x - \gamma y \neq 0$ . Furthermore,  $x - \gamma y \in \mathcal{O}_{\mathbb{K}}$  since  $x, y, \gamma \in \mathcal{O}_{\mathbb{K}}$ . Therefore, the minimum of the absolute value of eq. (4.22) is equal to  $d_{\mathbb{K}/\mathbb{Q}}^{-1}$ . As a conclusion, the minimum determinant of  $C$  is given by:

$$\begin{aligned} \delta_{min} &= \min_{C \neq \mathbf{0}_{2K \times 2K}} |\det(C)| = \det(D)^K d_{\mathbb{K}/\mathbb{Q}}^{-1} \\ &= (d_{\mathbb{F}/\mathbb{Q}})^{-\frac{K}{2}} d_{\mathbb{K}/\mathbb{Q}}^{-1} \\ &= (d_{\mathbb{L}/\mathbb{Q}})^{-\frac{1}{2}} > 0 \end{aligned} \quad (4.23)$$

where  $d_{\mathbb{L}/\mathbb{Q}}$  is the absolute discriminant of  $\mathbb{L}$ .

Equation (4.20) can be expressed in an equivalent manner as:

$$C_0 = \sum_{i=0}^1 \text{diag} \left( R \left[ a_{2iK+1} \cdots a_{2(i+1)K} \right]^T \right) \Omega^i \quad (4.24)$$

$$R = \begin{bmatrix} 1 & \phi \\ 1 & \phi_1 \end{bmatrix} \otimes \mathcal{M} ; \quad \Omega = \begin{bmatrix} 0 & 1 \\ \gamma & 0 \end{bmatrix} \quad (4.25)$$

where  $a_1, \dots, a_{4K}$  are the PAM symbols and  $\mathcal{M} = \lambda [1 \ \theta \ \cdots \ \theta^{K-1}]$ . In the same way,  $\mathcal{M}$  can be determined from any orthonormal basis  $\{\sigma^k(v)\}_{k=0}^{K-1}$ :

$$\mathcal{M} = \begin{bmatrix} v & \sigma(v) & \cdots & \sigma^{K-1}(v) \end{bmatrix} \quad (4.26)$$

### Energy balancing and shaping

As in section 3.2, we can show the nonexistence of energy-efficient and information lossless codes based on CDAs. Therefore,  $|\gamma| \neq 1$  and the energy-balanced version of eq. (4.20) can be written as:

$$C_0 = c(\gamma) \lambda \begin{bmatrix} k_1 + \phi k_2 & \text{sgn}(\gamma) |\gamma|^{\frac{1}{2}} (k_3 + \phi k_4) \\ |\gamma|^{\frac{1}{2}} (k_3 + \phi_1 k_4) & k_1 + \phi_1 k_2 \end{bmatrix} \quad (4.27)$$

where  $c(\gamma)^2 = \frac{2}{1+|\gamma|}$  is a normalization factor insuring the same transmitted energy as in non-cooperative systems. In this case, and when  $\gamma$  is totally positive, eq. (4.23) becomes:

$$\delta_{min} = \frac{2^K}{N_{\mathbb{K}/\mathbb{Q}}(1+\gamma)} (d_{\mathbb{L}/\mathbb{Q}})^{-\frac{1}{2}} \quad (4.28)$$

When it is possible to choose  $\gamma \in \mathbb{Z}^+$ , multiplying by the conjugates of  $\lambda$  results in a transmitted constellation that is a rotation of the original PAM signal set on each layer of the codeword. Let  $k'_i = \gamma'_i k_i$  for  $i = 1, \dots, 4$  where  $\gamma'_i = 1$  for  $i = 1, 2$  and  $\gamma'_i = \gamma^{\frac{1}{2}}$  for  $i = 3, 4$ . Since  $\sigma^k(\gamma'_i) = \gamma'_i$  for  $k = 0, \dots, K-1$ , we have the following relation (for  $i = 1, \dots, 4$ ):

$$[k'_1 \ \dots \ \sigma^{K-1}(k'_4)]^T = \gamma'_i \Gamma [a_{(i-1)K+1} \ \dots \ a_{iK}]^T \quad (4.29)$$

where  $\Gamma$  is a  $K \times K$  matrix whose  $k$ -th row is given by  $\Gamma_k = \sigma^{k-1}(\mathcal{M})$  where  $\mathcal{M}$  is given in eq. (4.26). Moreover,  $\Gamma \Gamma^T = I_K$  which follows from eq. (4.21) and from the choice of an orthonormal basis resulting in a simple rotation of the PAM constellation. More precisely, the symbols contained in the conjugates of  $k_1$  and  $k_2$  are a simple rotation of the original information symbols while the symbols contained in the conjugates of  $k_3$  and  $k_4$  are an amplified version of this same rotation. When  $\gamma$  is not a positive integer, eq. (4.29) does not hold for  $i = 3, 4$  and shaping losses are introduced on the symbols contained in the conjugates of  $k_3$  and  $k_4$ .

As a conclusion, the construction procedure consists of the correct choice of  $\mathbb{K}$ , a “non-norm” element  $\gamma$  of  $O_{\mathbb{K}}$  and of an algebraic element  $\alpha$  such that  $\lambda = \alpha$  (resp.  $\lambda = \sqrt{\alpha}$ ) when  $K$  is odd (resp. even). Moreover, if the basis  $\{\lambda \theta^k\}_{k=0}^{K-1}$  is not orthogonal, then an appropriate basis transformation must be performed before applying eq. (4.24) and eq. (4.26). In what follows, we will outline the construction procedure for  $K = 1, \dots, 5$ .

### 1, 3 and 5 relays

For  $K = 1$  relay,  $C$  can be equal to any one of the  $2 \times 2$  totally-real ST codes  $C_{2,eq}$  and  $C_{2,rot}$  given in eq. (3.17) and eq. (3.19) respectively. For  $K = 3, 5$ , the construction is performed in the field  $\mathbb{Q}(2 \cos(\frac{2\pi}{N}), \phi)$  where  $N$  verifies  $\mathcal{E}(N) = 2K$  ( $N = 7, 11$  for  $K = 3, 5$  respectively). In both cases, we can choose  $\gamma = 2$  since the ideals  $2O_{\mathbb{L}}$  are prime. The rotation matrix in eq. (4.25) can be determined from the orthogonal basis determined in section 3.2.2 and section 3.2.4 for  $K = 3$  and  $K = 5$  respectively.

### 2 relays

In this case, we choose  $\mathbb{K} = \mathbb{Q}(\theta)$  with  $\theta = 1 + \sqrt{2}$  and  $d_{\mathbb{K}/\mathbb{Q}} = 2^3$ . The choice  $\lambda = \frac{\sqrt{3-\theta}}{2}$  verifies eq. (4.21) resulting in no shaping losses on the symbols contained in the conjugates of  $k_1$  and  $k_2$  as explained earlier. Moreover,  $\lambda$  and its conjugate are both real since  $3 - \theta > 0$  and  $3 - \theta_1 > 0$  where  $\theta_1 = \sigma(\theta) = 1 - \sqrt{2}$ . The rotation matrix in eq. (4.25) can be calculated from  $\mathcal{M} = \lambda [1 \ \theta]$  since the basis  $\{\lambda, \lambda\theta\}$  is orthonormal.

In order to have a division algebra, we choose  $\gamma = 1 + \theta$  since the ideal  $\gamma O_{\mathbb{L}}$  is prime implying that there is no element in  $\mathbb{L}$  whose norm is equal to  $\gamma$ . Moreover,  $\gamma$  and  $\sigma(\gamma)$  are both positive resulting in a minimum determinant that verifies eq. (4.28) (more precisely,  $\delta_{min} = \frac{1}{70}$ ).

### 4 relays

We fix  $\mathbb{L} = \mathbb{Q}(\theta, \phi)$  with  $\theta = 2 \cos(\frac{2\pi}{16})$  and  $d_{\mathbb{Q}(\theta)/\mathbb{Q}} = 2^{11}$ . Using KANT [101], we find that the prime factorization of the ideal  $2O_{\mathbb{K}}$  is given by:

$$2O_{\mathbb{K}} = (\theta O_{\mathbb{K}})^4 \quad (4.30)$$

Choosing  $\alpha = \theta/8$  verifies eq. (4.21) since  $N_{\mathbb{K}/\mathbb{Q}}(\alpha) = \frac{1}{d_{\mathbb{K}/\mathbb{Q}}}$ , but a problem arises since the second and third conjugates of  $\alpha$  are negative. Using KANT software, we find the unit  $e = 1 - \theta^2 + \theta^3$  whose conjugates have the same sign as those of  $\alpha$  and whose norm is equal to 1. Therefore, choosing  $\alpha = \theta e/8 = (-2 + \theta + 4\theta^2 - \theta^3)/8$  results in a totally-positive algebraic number such that  $\lambda = \sqrt{\alpha}$  verifies eq. (4.21).

The basis  $\{\sqrt{\alpha}\theta^k\}_{k=0}^{K-1}$  is not orthogonal. Applying the LLL reduction [37] on the Gramm matrix corresponding to the previous basis, we obtain the new basis given by:  $\{\sqrt{\sigma^k(2+3\theta-\theta^3)/8}\}_{k=0}^3$ . Equation (4.26) can be calculated from the preceding basis. The element  $\gamma = \theta$  results in a fully diverse code since its generated ideal is prime.

### Error balancing

As in section 3.2.6, we can profit from the presence of the pulse repetitions in order to evenly distribute the available energy among the different information symbols. Suppose that  $N_f$  is even, instead of transmitting  $C_k \otimes 1_{1 \times N_f}$  in the  $k$ -th cooperation period, we can transmit:

$$C_{k,bal} = \begin{bmatrix} C_k & C'_k \end{bmatrix} \otimes 1_{1 \times N_f/2} \quad (4.31)$$

where  $C'_k$  is obtained in the same way as  $C_k$  from eq. (4.18) by applying a cyclic permutation of order  $2K$  on the information symbols.

#### 4.2.2 Inter Pulse Coding (IPC)

In this case, the spreading vectors  $B_1$  and  $B_2$  in eq. (4.13) are chosen to be orthogonal to each other. It is worth noting that IPC is equivalent to the non-orthogonal AF scheme [73] even though the source and the relays are using low-dimensional orthogonal vectors during each cooperation interval. In fact, the multiple access is controlled by the TH sequence which is common to the source and to all its cooperating relays. If there is another source transmitting at the same moment, its corresponding relays can use the same vectors  $B_1$  and  $B_2$ .

From eq. (4.12), combining the decision variables corresponding to the different pulses of the same symbol duration is equivalent to calculating:

$$\begin{aligned} Y(I_{KN_s} \otimes B^T) &= \tilde{H}A(I_{KN_s} \otimes B^T) + N \\ &= N_f \tilde{H}F + N \end{aligned} \quad (4.32)$$

where  $B$  is a  $2 \times N_f$  matrix given by  $B = [B_1^T \ B_2^T]^T$  and the noise term is always white. The matrix  $F$  can be expressed as:

$$F = \text{diag} \left( \begin{bmatrix} A_{1,1} \otimes e_1 \\ A_{1,2} \otimes e_2 \end{bmatrix} \dots \begin{bmatrix} A_{K,1} \otimes e_1 \\ A_{K,2} \otimes e_2 \end{bmatrix} \right) \quad (4.33)$$

where  $e_i$  is the  $i$ -th row of the  $2 \times 2$  identity matrix. Since the dimensions of  $F$  are equal to  $(2K, 2KN_s)$ , there is no benefit in choosing  $N_s > 1$ , therefore we fix  $N_s = 1$ . In this case,  $F$  is diagonal and any fully diverse rotation [58] of the  $2K$  information symbols is sufficient for achieving full diversity.

ISC and IPC can be readily applied with  $M$ -PPM- $M'$ -PAM constellations. More precisely, during the cooperation with the  $k$ -th relay, the codewords can be expressed as:

$$C_k = \text{diag} \left( (1 + \phi^2)^{-\frac{1}{2}} 1_{1 \times M} \quad (1 + \phi_1^2)^{-\frac{1}{2}} 1_{1 \times M} \right) \sigma^{k-1}(C_0) \quad (4.34)$$

where  $C_0$  takes the same form as in eq. (4.27), but now the information symbols are replaced by  $M$ -dimensional vectors.

### 4.2.3 Modulation-specific codes

A new coding scheme that is specific to  $M$ -PPM- $M'$ -PAM constellations can be obtained if the scalar  $\gamma$  in eq. (4.20) is replaced by a  $M \times M$  matrix  $\Omega$ . The constituent matrix  $C_0$  in eq. (4.20) takes the following from:

$$C_0 = \lambda \begin{bmatrix} k_1 + \phi k_2 & k_3 + \phi k_4 \\ \Omega(k_3 + \phi_1 k_4) & k_1 + \phi_1 k_2 \end{bmatrix} \quad (4.35)$$

where:

$$k_i = \sum_{j=0}^{K-1} a_{ni+j+1} \theta^j \in O_{\mathbb{K}}^M \quad (4.36)$$

with  $a_1, \dots, a_{4K}$  being  $M$ -dimensional vectors that belong to the  $M$ -PPM- $M'$ -PAM constellation given in eq. (1.8).  $\Omega$  is chosen to verify the following proposition.

**Proposition 4.1** *For a cooperative system with  $K$  relays, combining eq. (4.18) and eq. (4.35) permits to achieve a spatial diversity order of  $K + 1$  with  $M$ -PPM- $M'$ -PAM constellations for  $M \geq 2$  and for all values of  $K$  and  $M'$  if  $\Omega$  verifies:*

$$\Omega = \begin{bmatrix} 0 & 1 \\ -1 & 0 \end{bmatrix} \quad \text{for } M = 2 \quad (4.37)$$

$$\Omega = \begin{bmatrix} \mathbf{0}_{1 \times (M-1)} & 1 \\ I_{M-1} & \mathbf{0}_{(M-1) \times 1} \end{bmatrix} \quad \text{for } M > 2 \quad (4.38)$$

*Proof:* Ignoring  $\lambda$  in eq. (4.35) that is common to all codewords, denote by  $\Delta C_0(X, Y)$  the difference between two codewords:

$$\Delta C_0(X, Y) = C_0 - C'_0 = \begin{bmatrix} X & Y \\ \Omega \tau(Y) & \tau(X) \end{bmatrix} \quad (4.39)$$

where  $X, Y \in \mathcal{A}$ :

$$\mathcal{A} = \left\{ \sum_{i=1}^{2K} (a_i - a'_i) t_i ; a_1, a'_1, \dots, a_{2K}, a'_{2K} \in \mathcal{C} \right\} \subset O_{\mathbb{L}}^M \quad (4.40)$$

where  $\{t_i\}_{i=1}^{2K} = \{1, \theta, \dots, \theta^{K-1}, \phi, \phi\theta, \dots, \phi^{K-1}\}$  and it forms a basis over  $\mathbb{Q}^{2K}$ . With respect to this basis, the  $m$ -th component of  $X$  (and  $Y$ ) is represented by  $2K$  coordinates for  $m = 1, \dots, M$ .

From eq. (4.39),  $\text{rank}(\Delta C_0(X, Y)) < 2$  implies that there exists a non-zero constant  $l \in \mathbb{L}$  such that:  $Y = lX$  and  $\tau(X) = l\Omega\tau(Y)$ . Solving these equations, we obtain that  $X$  and  $Y$  must verify the equation:

$$\Omega X = \frac{1}{N_{\mathbb{L}/\mathbb{K}}(l)} X \quad (4.41)$$

showing that  $X$  and  $Y$  are the eigenvectors of  $\Omega$ .

For  $M = 2$ , the eigenvalues of the matrix  $\Omega$  given in eq. (4.37) are equal to  $\pm\sqrt{-1}$ . Therefore, being real-valued, the non-zero vectors  $X$  and  $Y$  can not verify eq. (4.41). This shows that non-zero vectors  $X$  and  $Y$  that result in a rank deficient matrix  $\Delta C_0(X, Y)$  do not belong to  $\mathcal{A}$  for  $M = 2$ .

For  $M > 2$ , the eigenvalues of  $\Omega$  given in eq. (4.38) are equal to  $\omega_M^m$  for  $m = 0, \dots, M - 1$  where  $\omega_M = e^{\frac{2\pi i}{M}}$  is the  $M$ -th root of unity. We have  $N_{\mathbb{L}/\mathbb{K}}(l) \in \mathbb{K}^*$  since  $l \neq 0$ . Therefore, being real-valued,  $X$  and  $Y$  correspond to the real eigenvalues of  $\Omega$  that are equal to  $\pm 1$ . When  $M$  is odd, the real vectors verifying eq. (4.41) are the real-multiples of  $1_{M \times 1}$ . When  $M$  is even, the real solutions of eq. (4.41) are the real-multiples of  $1_{M \times 1}$  or of  $[1 \ -1 \ \dots \ 1 \ -1]^T$ . Therefore in both cases, when  $X \in \mathcal{O}_{\mathbb{L}}^M$ ,  $\exists k \in \{1, \dots, 2K\}$  such that the  $k$ -th coordinates of the  $M$  components of  $X$  (and  $Y$ ) are all different from zero. This shows that  $X$  and  $Y$  do not belong to the set  $\mathcal{A}$  for  $M > 2$ . In fact, from eq. (4.40), only two vectors  $a_k$  and  $a'_k$  can result in non-zero  $k$ -th coordinates. Therefore, the vectors that result in rank deficient codewords do not belong to  $\mathcal{A}$  for  $M > 2$ .

Combining the last two cases, and since the proof is independent from  $M'$ , we conclude that the code achieves full diversity with  $M \geq 2$  and for all values of  $M'$ .

**Proposition 4.2** *For binary PPM, combining eq. (4.18), eq. (4.35) and eq. (4.37) permits to achieve the same coding gain as the optimal complex-valued codes proposed in [74].*

*Proof:* From 2-PPM constellations,  $X$  and  $Y$  can be written as  $X = [x \ -x]^T$  and  $Y = [y \ -y]^T$  where  $x, y \in \mathbb{L}$ . In this case, for the value of  $\Omega$  given in eq. (4.37), eq. (4.39) takes the following form:

$$\Delta C_0(X, Y) = \begin{bmatrix} x & -x & -\tau(y) & -\tau(y) \\ y & -y & \tau(x) & -\tau(x) \end{bmatrix}^T \quad (4.42)$$

This results in the following relation:

$$\begin{aligned} \det((\Delta C_0)^T \Delta C_0) &= \sum_{i_1=1}^4 \sum_{i_2=i_1+1}^4 \left( \det \left( [(\Delta C_{0,i_1})^T \ (\Delta C_{0,i_2})^T]^T \right) \right)^2 \\ &\geq \sum_{i_1=1}^2 \sum_{i_2=3}^4 \left( \det \left( [(\Delta C_{0,i_1})^T \ (\Delta C_{0,i_2})^T]^T \right) \right)^2 \\ &= 4 \left( (N_{\mathbb{L}/\mathbb{K}}(x))^2 + (N_{\mathbb{L}/\mathbb{K}}(y))^2 \right) \end{aligned} \quad (4.43)$$

where  $\Delta C_{0,i}$  is the  $i$ -th row of  $\Delta C_0$ . Let  $\Delta C = \text{diag}(\Delta C_0 \ \dots \ \sigma^{K-1}(\Delta C_0))$ , then:

$$\det((\Delta C)^T \Delta C) \geq 4^K \left( (N_{\mathbb{L}/\mathbb{Q}}(x))^2 + (N_{\mathbb{L}/\mathbb{Q}}(y))^2 \right) \quad (4.44)$$

Therefore, the minimum non-zero value of eq. (4.44) is equal to  $4^K$  since  $N_{\mathbb{L}/\mathbb{Q}}(x) \in \mathbb{Z}$  and  $N_{\mathbb{L}/\mathbb{Q}}(y) \in \mathbb{Z}$ .

**Proposition 4.3** *For a cooperative system with  $K$  relays, combining eq. (4.18), eq. (4.35) and eq. (4.38) permits to achieve a non-vanishing coding gain with  $M$ -PPM- $M'$ -PAM constellations for  $M \geq 4K + 1$  and for all values of  $K$ .*

*Proof:* From eq. (4.40),  $X$  and  $Y$  are linear combinations of  $4K$  columns of  $I_M$ . Therefore, for  $M \geq 4K + 1$ ,  $X$  and  $Y$  each contain at least one zero component. Suppose that  $X_m = 0$  for a given value of  $m \in \{1, \dots, M\}$ . As in eq. (3.55), eq. (4.39) can be written in a more explicit form as:

$$\Delta C_0(X, Y) = \begin{bmatrix} X_1 & \dots & X_M & \tau(Y_{\pi^{-1}(1)}) & \dots & \tau(Y_{\pi^{-1}(M)}) \\ Y_1 & \dots & Y_M & \tau(X_1) & \dots & \tau(X_M) \end{bmatrix}^T \quad (4.45)$$

where the cyclic permutation  $\pi$  is defined in eq. (3.54). Considering the  $m$ -th and the  $(M + \pi(m))$ -th rows of  $\Delta C_0$ , we obtain:

$$\det((\Delta C_0)^T \Delta C_0) \geq \left( \det \left( [(\Delta C_{0,m})^T \ (\Delta C_{0,M+\pi(m)})^T]^T \right) \right)^2 = N_{\mathbb{L}/\mathbb{K}}(Y_m^2) \quad (4.46)$$

This implies that:

$$\det((\Delta C)^T \Delta C) \geq N_{\mathbb{L}/\mathbb{Q}}(Y_m^2) \quad (4.47)$$

proving that  $\det((\Delta C)^T \Delta C) \geq 1$  unless when  $Y_m = 0$ . Now, considering the  $\pi(m)$ -th and the  $(M + \pi(m))$ -th rows of  $\Delta C_0$ , we obtain:

$$\det((\Delta C_0)^T \Delta C_0) \geq \left( \det \left( [(\Delta C_{0,\pi(m)})^T \ (\Delta C_{0,M+\pi(m)})^T]^T \right) \right)^2 = N_{\mathbb{L}/\mathbb{K}}(X_{\pi(m)}^2) \quad (4.48)$$

implying that  $\det((\Delta C)^T \Delta C) \geq 1$  unless when  $X_{\pi(m)} = 0$ . Starting the same procedure again with  $\pi(m)$  rather than  $m$ , we can show by recurrence that  $\det((\Delta C)^T \Delta C) \geq 1$  unless when  $X_m = \dots = X_{\pi^{M-1}(m)} = 0$  and  $Y_m = \dots = Y_{\pi^{M-1}(m)} = 0$ . Since  $\{m, \dots, \pi^{M-1}(m)\}$  scans the entire set  $\{1, \dots, M\}$  for all values of  $m$ , this implies that  $\det((\Delta C)^T \Delta C) \geq 1$  unless when  $X = Y = \mathbf{0}_M$  completing the proof.

As with ISC and IPC, the basis  $\lambda\{\theta^k\}_{k=0}^{K-1}$  can be replaced by an orthonormal basis  $\{\sigma^k(v)\}_{k=0}^{K-1}$ . In a way similar to appendix D.3, we can prove that choosing  $\Omega$  to be unitary and the basis  $\{\sigma^k(v)\}$  to be orthonormal results in an information lossless code.

### 4.3 Code construction for the DF scheme

The decode-and-forward (DF) strategy was associated with coded cooperation [70, 72] and space-time (ST) cooperation [106, 107]. In the first case, a channel-coded frame is partitioned into several sub-frames retransmitted by the different cooperating nodes. In the second case, after a broadcast phase where the source transmits information to the relays, the relays transmit simultaneously in the relay phase. Their data streams are encoded by an appropriate ST code. If  $K$  is the number of nodes, the proposed schemes result in a diversity order of  $K$ .

As with the AF strategy, the superiority of the non-orthogonal schemes was reported in [73]. In this context, the extension of [72, 106, 107] to the non-orthogonal scheme will result in a data-rate reduction. In what follows, we present the construction of new non-orthogonal ST-coded DF schemes that achieve a diversity order of  $K + 1$  with no data rate losses and without transmitting on the relays' signal sub-spaces. This is rendered possible by taking advantage of the pulse repetitions that are inherent to TH-UWB systems. If  $N_f$  is the number of pulses per symbol, the coherent scheme is based on joint symbol and pulse coding and achieves full diversity with any number of relays for  $N_f > 1$ . The differential scheme is based on pulse coding and achieves full diversity with a maximum number of  $N_f - 1$  relays.

#### 4.3.1 Coherent systems

Designate by  $K$  the number of relays and let  $K' = K + 1$ . The proposed scheme is periodic with a period of  $K'N_f T_f$ . We suppose that this duration is smaller than the channel coherence time and we focus on the first period. The source and the cooperating relays will share the same TH sequence. For non-cooperative systems, the transmitted signal in eq. (1.9) can be written as:

$$s(t) = \sum_{k'=1}^{K'} \sum_{n=0}^{N_f-1} b_{k',n} \sum_{m=0}^{M-1} a_{k',m} w(t - (k' - 1)T_s - nT_f - m\delta) \quad (4.49)$$

Suppose that  $N_f$  is even and let  $\mathbf{N}_f = \frac{N_f}{2}$ . Let  $\mathbf{T}_s = \mathbf{N}_f T_f$  designate the new symbol duration. In the cooperative mode, we write eq. (4.49) as:

$$s(t) = \sum_{k'=1}^{2K'} \alpha_{k'} \sum_{n=0}^{\mathbf{N}_f-1} b_{k',n} \sum_{m=0}^{M-1} \mathbf{a}_{k',m} w(t - (k' - 1)\mathbf{T}_s - nT_f - m\delta) \quad (4.50)$$

Designate by  $A_{k'} = [a_{k',0}, \dots, a_{k',M-1}]^T$  and  $\mathbf{A}_{k'} = [\mathbf{a}_{k',0}, \dots, \mathbf{a}_{k',M-1}]^T$  the vector representations of the  $k'$ -th uncoded and coded symbol respectively. The encoding scheme is given by:

$$\mathbf{A}_{k'} = A_{k'} \quad ; \quad k' = 1, \dots, K' \quad (4.51)$$

$$\mathbf{A}_{k'} = A^{(0)} = (\mathcal{R}_0 \otimes I_M) [A_1^T \ \cdots \ A_{K'}^T]^T \quad ; \quad k' = K' + 1, \dots, 2K' \quad (4.52)$$

where  $\mathcal{R}$  is any  $K' \times K'$  fully diverse rotation matrix [100] and  $\mathcal{R}_k$  is the  $(k+1)$ -th row of  $\mathcal{R}$ . The choice of  $\alpha_{k'}$  and  $b_{k',n}$  is given later.

The DF cooperation strategy is as follows. Each one of the  $K$  relays will listen to  $s(t)$  given in eq. (4.50) during the first  $K'$  symbol durations  $\mathbf{T}_s$ . After that Rake reception is performed and decisions concerning the values of the first  $K'$  symbols are taken. The estimated value of  $A_{k'}$  at the  $k$ -th relay is designated by  $\hat{A}_{k'}^{(k)}$  for  $k' = 1, \dots, K'$  and  $k = 1, \dots, K$ . After that, the relays transmit simultaneously during the second half of the cooperation period. Designate by  $A_{k'}^{(k)}$  the vector representation of the  $k'$ -th symbol transmitted by the  $k$ -th relay for  $k' = K' + 1, \dots, 2K'$  and  $k = 1, \dots, K$ . We fix:

$$A_{k'}^{(k)} = A^{(k)} = (\mathcal{R}_k \otimes I_M) [\hat{A}_1^{(k)T} \ \cdots \ \hat{A}_{K'}^{(k)T}]^T \quad (4.53)$$

In eq. (4.50), we fix  $\alpha_{k'} = \beta_1$  for  $k' = 1, \dots, K'$  and  $\alpha_{k'} = \beta_2$  for  $k' = K' + 1, \dots, 2K'$ . Moreover, during the second half of the cooperation period, the energy transmitted by each relay is scaled by  $\beta_2$ . The energy transmitted by the source and its  $K$  relays during the entire cooperation period is taken to be the same as in non-cooperative systems. This normalization can be performed by fixing  $\beta_1 + K'\beta_2 = 1$ .

In eq. (4.50), we fix  $b_{k',n} = \frac{1}{\sqrt{N_f}}$  for  $k' = 1, \dots, K'$  and  $n = 0, \dots, \mathbf{N}_f - 1$ . Designate by  $B^{(0)}$  the  $1 \times K'N_f$  matrix given by  $B^{(0)} = [B_{K'+1}^{(0)} \ \cdots \ B_{2K'}^{(0)}]$  where  $B_{k'}^{(0)} = [b_{k',0} \ \cdots \ b_{k',N_f-1}]$ . We fix  $B^{(0)} = \mathcal{B}_0 \otimes 1_{1 \times N_f}$ . In the same way, when transmitting during the second half of the cooperation period, the  $1 \times K'N_f$  spreading sequence associated with the  $k$ -th relay is given by  $B^{(k)} = \mathcal{B}_k \otimes 1_{1 \times N_f}$ . We choose  $\mathcal{B}_k$  to be the  $(k+1)$ -th row of the matrix  $\mathcal{B} = \frac{1}{\sqrt{N_f}}U$  for  $k = 0, \dots, K$  where  $U$  is any unitary  $K' \times K'$  matrix. In this way, the spreading sequences transmitted by the source and the relays during the second half of the cooperation period are orthogonal to each other.

In the case where all the decisions taken at the relays during the first half of the cooperation period are correct, the cooperation during the second half of the cooperation period coincides with the IPC scheme given in section 3.3. This permits to achieve a spatial diversity order of  $K'$ . Since the construction of ST codes over cooperative channels is based on the rank criterion and determinant criterion [72, 74], we expect that the proposed scheme continues to show good performance even when erroneous decisions are taken at some relays.

As in eq. (4.2), the decision variables collected at the  $k$ -th relay during the  $k'$ -th symbol duration can be expressed as:

$$X_{k'}^{(k)} = \sqrt{\beta_1 \rho_k} H_k A_{k'} + N_{k'}^{(k)} \quad (4.54)$$

The last equation is valid for  $k' = 1, \dots, K'$  and  $k = 1, \dots, K$ . As in eq. (4.2),  $X_{k'}^{(k)}$  and  $H_k$  correspond to the  $LM$ -dimensional decision vector and to the  $LM \times M$  channel matrix respectively. The decision

variables at the destination during the first half of the cooperation period are obtained by setting  $k = 0$  in eq. (4.54) (with  $\rho_0 = 1$ ).

During the second half of the cooperation period,  $K'$  separate despreading branches are applied at the outputs of the matched filters (refer to section 3.3). The orthogonality of the amplitude spreading sequences during the second half of the cooperation period results in  $K'$  decision vectors that can be expressed as (for  $k = 0, \dots, K$ ):

$$Y^{(k)} = \sqrt{\beta_2 \lambda_k} G_k A^{(k)} + N'^{(k)} \quad (4.55)$$

$Y^{(k)}$  stands for the decision vector corresponding to the data stream that is transmitted from the  $k$ -th relay.  $\lambda_k$  stands for the gain between the  $k$ -th relay and the destination while  $G_k$  has the same structure as in section 4.1.  $A^{(k)}$  is given in eq. (4.52) and eq. (4.53) for  $k = 0$  and  $k = 1, \dots, K$  respectively. The decision vector corresponding to the signal transmitted from the source during the second half of the cooperation period can be obtained by setting  $k = 0$  in eq. (4.55) (with  $\lambda_0 = 1$  and  $G_0 = H_0$ ).

Finally, the decision at the destination is based on the  $2K'LM$ -dimensional vector  $Z$  that is the vertical concatenation of vectors  $X_1^{(0)}, \dots, X_{K'}^{(0)}$  given in eq. (4.54) and vectors  $Y^{(0)}, \dots, Y^{(K')}$  given in eq. (4.55):

$$Z = \text{diag}(\tilde{H}_1 \ \tilde{H}_2) [\mathcal{A}_1^T \ \mathcal{A}_2^T]^T + N \quad (4.56)$$

where  $\mathcal{A}_1 = [A_1^T \ \dots \ A_{K'}^T]^T$  and  $\mathcal{A}_2 = [A^{(0)T} \ \dots \ A^{(K)T}]^T$ .  $A_1, \dots, A_{K'}$  correspond to the information symbols.  $A^{(k)}$  is given in eq. (4.52) and eq. (4.53) for  $k = 0$  and  $k = 1, \dots, K$  respectively. The  $K'LM \times K'M$  matrices  $\tilde{H}_1$  and  $\tilde{H}_2$  are given by:

$$\tilde{H}_1 = \sqrt{\beta_1} (I_{K'} \otimes H_0) \quad (4.57)$$

$$\tilde{H}_2 = \sqrt{\beta_2} \text{diag} \left( H_0 \ \sqrt{\lambda_1} G_1 \cdots \sqrt{\lambda_K} G_K \right) \quad (4.58)$$

As in all decode-and-forward schemes, the decoding at the destination is based on the assumption of correct decisions at the relays. The ML decoding at the destination is based on:

$$\underset{\mathcal{A} \in \mathcal{C}^{K'}}{\text{argmin}} \|Z - \begin{bmatrix} \tilde{H}_1 \\ \tilde{H}_2 (\mathcal{R} \otimes I_M) \end{bmatrix} \mathcal{A}\|^2 \quad (4.59)$$

where  $\mathcal{C}$  is the PPM-PAM signal set given in eq. (1.8). When  $N_f > 1$  is odd, the above cooperation scheme can be applied with  $N_f = \frac{N_f-1}{2}$ . In this case,  $N_f+1$  (resp.  $N_f$ ) pulses can be used to convey each information symbol in the first (resp. second) half of the cooperation period. Therefore, the only case in which the proposed scheme can not be applied is when  $N_f = 1$ ; in other words, for systems that do not use any pulse repetitions.

### 4.3.2 Differential systems

Recently differential and non-coherent IR-UWB systems have drawn considerable attention as a means of obtaining a good compromise between performance and complexity [33, 108–110]. Differential transmitted reference (DTR) systems proposed in [108, 109] are extensions of differential binary phase shift keying (DBPSK) to UWB systems where the data is conveyed through the phase difference between two consecutive symbols. On the other hand, PPM was associated uniquely with non-coherent energy detectors [110] and with simple transmitted reference systems (STR) [33] where each data pulse is preceded by a reference pulse which carries no information. The association of energy detectors and PPM was extended to multi-antenna systems in [81] (refer to section 1.4.3).

In this section, we propose a new differential DF strategy based on inter-pulse-coding. This strategy is associated with a new modulation scheme where the information is conveyed through the phase difference and/or the time shift between two consecutive symbols. Unlike the non-coherent UWB diversity schemes that are associated with energy detectors and PPM [81], the proposed scheme can be associated with all constant-modulus real constellations such as  $M$ -PPM, 2-PAM and  $M$ -PPM-2-PAM. For energy detectors, the modulation delay  $\delta$  must be larger than the channel delay spread ( $\Gamma$ ) and thus the symbol duration increases significantly with  $M$  (refer to section 1.4.3). In this case, the association of the proposed scheme with  $M$ -PPM-2-PAM results in an enhanced data rate. An additional advantage with respect to energy detectors is that we can profit from the long coherence time of indoor channels to develop decision-feedback receivers that can ameliorate the performance by reducing the noise level in the reference signal. Finally, the proposed scheme can be used when  $\delta < \Gamma$  resulting in high data rate differential DF systems.

### Encoder/Decoder structure

In what follows, we fix  $K = N_f - 1$ . The period of the proposed cooperation scheme is equal to  $K'N_fT_f$  where  $K'$  is determined from the channel coherence time. In the cooperative mode, the signal transmitted from the source node during the first cooperation period is written as:

$$s(t) = \beta_1 \sum_{n=0}^{N_f-1} \sum_{k'=1}^{K'} b_{k',n} a_{k',m} w(t - nK'T_f - (k' - 1)T_f - m\delta) \quad (4.60)$$

where  $b_{k',n} = \frac{1}{\sqrt{N_f}}\delta(n)$  where  $\delta(\cdot)$  is the Dirac delta function. In other words, instead of transmitting continuously during  $K'N_f$  time frames, the source transmits uniquely during the first  $K'$  time frames in the cooperative mode. Denote by  $s_k$  and  $\Delta_k$  the amplitude and the position of the  $k$ -th information symbol respectively, the multi-dimensional differential encoding scheme corresponds to transmitting the vector  $A_k = [a_{k,0}, \dots, a_{k,M-1}]^T$  such that:

$$A_k = s_k \Omega^{\Delta_k} A_{k-1} \quad (4.61)$$

where  $A_0$  is equal to the first column of the  $M \times M$  identity matrix  $I_M$  and  $\Omega$  is the permutation matrix given by:

$$\Omega = \begin{bmatrix} \mathbf{0}_{1 \times (M-1)} & 1 \\ I_{M-1} & \mathbf{0}_{(M-1) \times 1} \end{bmatrix} \quad (4.62)$$

The decision variables collected at the  $k$ -th relay during the  $k'$ -th symbol duration can be expressed as:

$$X_{k'}^{(k)} = \sqrt{\beta_1 \rho_k} H_k (I_L \otimes A_{k'}) + N_{k'}^{(k)} \quad (4.63)$$

where  $H_k$  in this case is the  $M \times LM$  matrix whose  $(m, lM + m')$ -th element is equal to  $\int h_k(t)w(t - (m - m')\delta - lMT_w)dt$  for  $l = 0, \dots, L - 1$  and  $m, m' = 1, \dots, M$ . The decision variables at the destination are obtained by setting  $k = 0$  in eq. (4.63). The decoding strategy at the  $k$ -th relay is defined as:

$$(\hat{s}_{k'}^{(k)}, \hat{\Delta}_{k'}^{(k)}) = \arg \max_{\substack{s=\pm 1 \\ m \in \{0, \dots, M-1\}}} \left( \text{maxdiag} \left( s X_{k'}^{(k)} (X_{k'-1}^{(k)})^T \Omega^{M-m} \right) \right) \quad (4.64)$$

where the function  $\text{maxdiag}(X)$  returns the maximum value of the diagonal of matrix  $X$ . This decoding strategy shows to be superior to the one employing the trace of the decision matrix in eq. (4.64) since the

$(M - 1)$  noisy diagonal elements are excluded from the sum. For PPM constellations, we set  $s = 1$  in eq. (4.64) while for BPSK signals the restored polarity corresponds to the sign of the scalar  $X_{k'}^{(k)}(X_{k'-1}^{(k)})^T$ .

At a second time, the detected symbols at the  $k$ -th relay are encoded differentially according to eq. (4.61) and transmitted during the frame durations  $kK' + 1, \dots, (k+1)K'$ . The energy transmitted by the relays is scaled by  $\beta_2$  with  $\beta_1 + K\beta_2 = 1$ .

The decision variables at the destination corresponding to the signal transmitted by the  $k$ -th relay during the  $(kK' + k')$ -th time frame can be expressed as:

$$Y_{k'}^{(k)} = \sqrt{\beta_2 \lambda_k} G_k \left( I_L \otimes \hat{s}_{k'}^{(k)} e_{\hat{\Delta}_{k'}^{(k)} + 1} \right) + N_{k'}^{(k)} \quad (4.65)$$

$\hat{s}_{k'}^{(k)}$  and  $\hat{\Delta}_{k'}^{(k)}$  are given in eq. (4.64) and  $e_m$  is the  $m$ -th column of  $I_M$ .

Finally, the destination node decides in the favor of:

$$(\hat{s}_{k'}, \hat{\Delta}_{k'}) = \arg \max_{\substack{s=\pm 1 \\ m \in \{0, \dots, M-1\}}} (\text{maxdiag}(s Z_{k'} Z_{k'-1}^T \Omega^{M-m})) \quad (4.66)$$

where:

$$Z_{k'} = X_{k'}^{(0)} + \sum_{k=1}^K Y_{k'}^{(k)} \quad (4.67)$$

Suppose that  $\beta_1 = \beta_2$ . In the absence of noise and under the assumption of correct decisions at the relays, the maximum value of the right hand side of eq. (4.66) for orthogonal PPM or PPM-PAM constellations ( $\delta \geq \Gamma$ ) is equal to:

$$\frac{1}{N_f(K+1)} \sum_{l=0}^{L-1} \left( h_{0,l}^2 + \sum_{k=1}^K \lambda_k g_{k,l}^2 \right) \quad (4.68)$$

where  $h_{0,l} = \int h_0(t) w(t - lMT_w) dt$  and  $g_{k,l} = \int g_k(t) w(t - lMT_w) dt$  for  $k = 1, \dots, K$ .

Suppose that the relay-selection protocol does not select relays that are very far from the destination [105]. In other words, the values of  $\lambda_k$  are not very small. In this case, eq. (4.68) implies that the captured energy is small only if the magnitudes of  $(K+1)L$  quantities are small. In other words, the signal is lost only if  $K+1$  channels suffer from fading during a duration of  $LMT_w$ . Therefore, the proposed system exploits the spatial and multi-path diversity and it has the same diversity advantage as the non-coherent multi-antenna system in [81] with  $K+1$  transmit antennas and  $L$  fingers.

### Decision feedback

The differential receiver in eq. (4.64) and eq. (4.66) is based on comparing two consecutive symbols where the  $(k'-1)$ -th symbol acts as a reference for the detection of the  $k'$ -th symbol. Performance can be ameliorated if this noisy reference is replaced by another one based on more than one symbol. This is referred to as decision feedback or decision directed receivers [109, 111]. This principle can be readily adapted to multi-dimensional constellations. In this case, eq. (4.64) and eq. (4.66) can be written as:

$$(\hat{s}_{k'}, \hat{\Delta}_{k'}) = \arg \max_{\substack{s=\pm 1 \\ m \in \{0, \dots, M-1\}}} (\text{maxdiag}(s X_{k'} R_{k'-1}^T \Omega^{M-m})) \quad (4.69)$$

where  $X_{k'} = X_{k'}^{(k)}$  in eq. (4.64) and  $X_{k'} = Z_{k'}$  in eq. (4.66).

The reference signal  $R_{k'}$  is updated during the channel coherence time based on previously detected symbols as:

$$R_{k'} = \chi_{k'} + \hat{s}_{k'} \Omega^{\hat{\Delta}_{k'}} R_{k'-1} \quad (4.70)$$

with  $R_0 = \chi_0$ . It was shown in the literature that decision-feedback receivers do not suffer from error propagation and that the performance converges to that of a coherent receiver especially at high signal to noise ratios [111].

An equivalent encoding scheme to the one proposed in eq. (4.61) can be obtained by performing separate differential codec on the amplitude and non-coherent codec on the position. The encoding scheme in eq. (4.61) is modified to  $A_k = a_k e_{\Delta_k+1}$  such that  $a_k = s_k a_{k-1}$ . The decoder will now perform separate decisions on the amplitudes and the positions of the transmitted symbols:

$$\hat{\Delta}_{k'} = \arg \max_{m \in \{0, \dots, M-1\}} (\chi_{k',m} \chi_{k',m}^T) \quad (4.71)$$

$$\hat{s}_{k'} = \text{sgn}(\chi_{k',\hat{\Delta}_{k'}} \chi_{k'-1,\hat{\Delta}_{k'-1}}^T) \quad (4.72)$$

where  $\chi_{k',m}$  is the  $(m+1)$ -th row of  $\chi_{k'}$ .

In the absence of feedback, this system shows negligible performance losses with respect to the differential systems. However, feedback can not be performed for the position detection, and thus performance will be limited by the energy detector irrespective from the possible amplitude feedback. In other words, feedback can not ameliorate the performance of such systems.

For non-coherent systems based on energy integration, we can fix  $K' = 1$  in eq. (4.60). In this way, the cooperative diversity can be obtained by simply interleaving the  $N_f$  pulses among the source node and the  $K$  relays. In this case, the decision at the destination node is based on the association of eq. (4.67) with eq. (4.71).

### 4.3.3 Selective Relaying and Fixed Relaying

For coherent, non-coherent and differential systems, the coding scheme depends on the number of relays. These  $K$  cooperating relays are chosen among  $K_{\max}$  nodes that are in the neighborhood of the source and the destination. Moreover, a maximum number of  $K_{tol}$  relays can be tolerated by each cooperation scheme. For example, with coherent systems, the decoding complexity grows with the number of relays while for non-coherent and differential systems the maximum number of relays is determined from the number of pulse repetitions and the channel coherence time. For the selection of the relays, we differentiate between Fixed-Relaying (FR) and Selective-Relaying (SR).

For FR, any node can become a cooperating relay. If  $K_{\max} \leq K_{tol}$ , then we set  $K = K_{\max}$ . If  $K_{\max} > K_{tol}$ , then  $K = K_{tol}$  relays are chosen randomly. For SR, a node cooperates with the source only if the channel between the source and this node is “good”. We assume that a certain number of control symbols, that are known by all nodes, are transmitted before each data burst. A node can help the source only if it correctly decodes these symbols. Once again, if the number of these nodes exceeds  $K_{tol}$ , we fix  $K = K_{tol}$ . This protocol is similar to the one proposed in [70] where each coded frame is preceded by a CRC. A node is allowed to cooperate with the source only if the CRC check is correct. Note that the proposed strategy is less stringent since the length of the control frame is very short compared to the data bursts. Moreover, decision errors on the information symbols can occur even if the control symbols are correctly decoded.

## 4.4 Numerical Results

### 4.4.1 The NAF strategy

#### Performance with PAM

The objective of the first simulation setup is to compare the distributed ST codes with PAM. Namely, we perform comparisons between ISC, balanced-ISC and IPC. In order to highlight the effect of the achieved diversity order, we consider systems that do not have any energetic gain. In other words, we fix  $\rho_k = \lambda_k = 1$  in eq. (4.11). In this case, the distances source-relay, relay-destination and source-destination are supposed to be the same. The transmitted energy is chosen to be equally distributed among the two halves of the cooperation period (we fix  $\beta_1 = \beta_2$  in eq. (4.11)). At the destination, the sphere decoder [112] is used for detection. At a first time, we fix  $\varepsilon_k = 0$  for  $k = 1, \dots, K$  in eq. (4.1). The choice of  $N_f$  has no effect on the performance in single user scenarios. It is chosen to be a multiple of two to render error balancing and inter pulse coding possible. We fix  $\delta = 0.5$  ns for coherent systems while  $\delta = 100$  ns for differential and non-coherent systems.

Fig. 4.1 shows the performance on CM2 with one relay and 2-PAM. The relay and the destination are equipped with 5-fingers PRakes. The performance gains resulting from the proposed distributed ST codes are evident. Fig. 4.1 shows the importance of error balancing. ISC shows poor performance especially at low signal to noise ratios since the performance is limited by the error events occurring on the less protected symbols  $a_1$  and  $a_2$ . Using balanced-ISC from eq. (4.31) results in a gain of about 2.5 dB at a BER of  $10^{-3}$ . IPC shows comparable performance with respect to balanced-ISC. The gap between the two codes results from the interleaving imposed by eq. (4.31) resulting in a better immunity against noise.

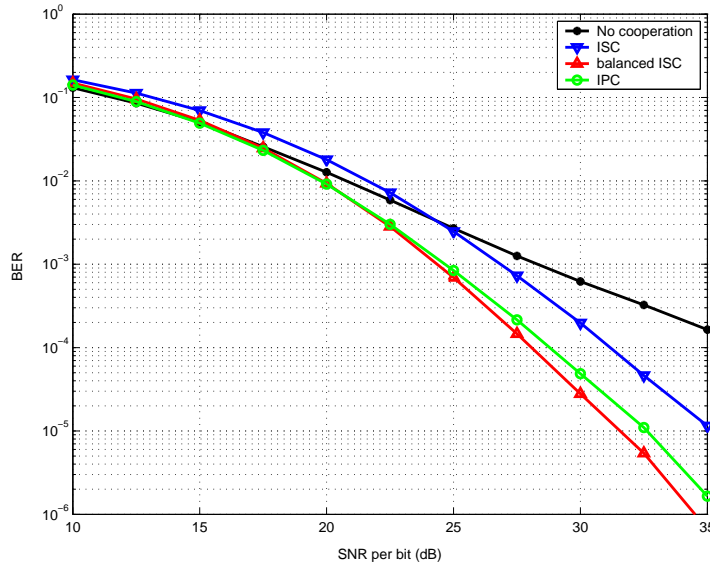


Figure 4.1: Performance on CM2 with one relay, 2-PAM and a 5-finger PRake.

Fig. 4.2 shows the performance on CM2 with 2-PAM and a 5-finger PRake. Simulation results with  $K = 2$  and  $K = 4$  relays are presented. The reduced decoding complexity of IPC incurs a loss that is less than 1 dB with respect to balanced-ISC that shows the best performance. Similar results are

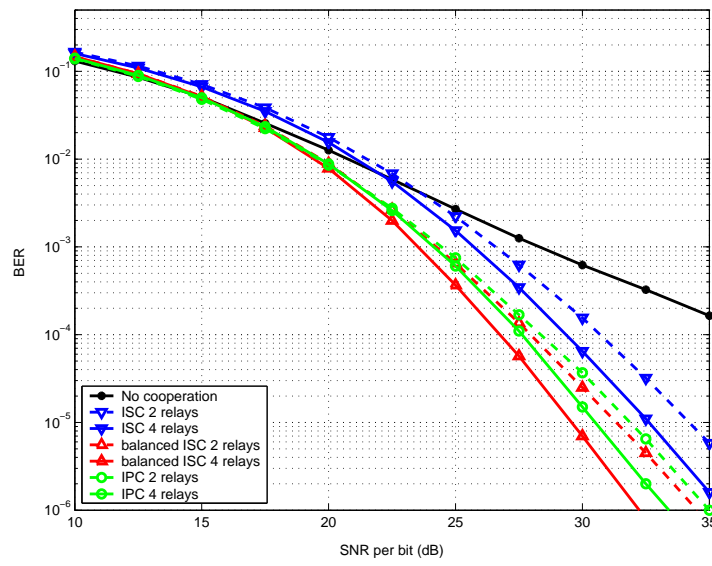


Figure 4.2: Performance on CM2 with 2-PAM and a 5-finger PRake using 2 and 4 relays.

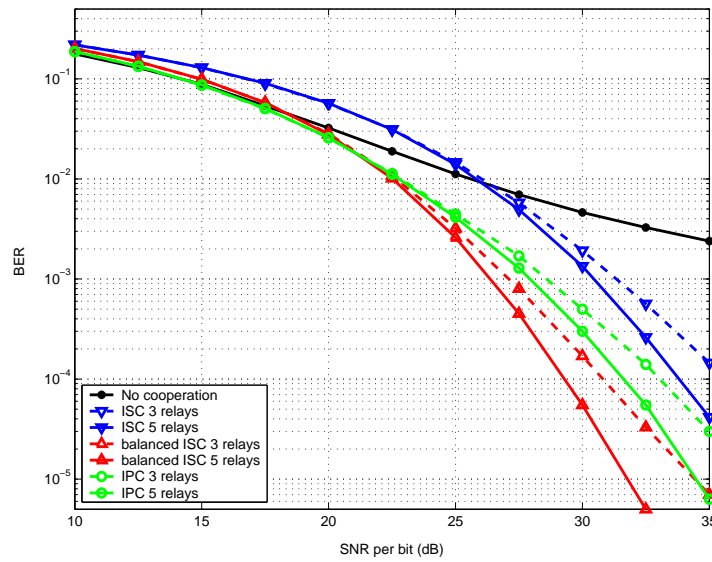


Figure 4.3: Performance on CM2 with 2-PAM and a 1-finger PRake using 3 and 5 relays.

obtained in Fig. 4.3 with 3 and 5 relays using a 1-finger PRake. Since the amplitude of the first arriving multi-path component can be very small in NLOS configurations [17], the noise events have a critical role in determining the system performance. This explains the relatively large gap between IPC and balanced-ISC.

### Performance with PPM-PAM and PPM

We keep the same simulation setup as in the preceding subsection and we consider the performance of multi-dimensional constellations. In Fig. 4.4 we compare ISC, balanced-ISC and the modulation-specific codes over CM2. Results show the interest of using the modulation-specific codes rather than the extension of codes constructed over infinite fields. The PPM-PAM-specific code outperforms ISC and approaches the performance of balanced-ISC without performing any kind of intra-symbol coding. This shows the importance of using energy-efficient and information-lossless codes.

In Fig. 4.5, we compare ISC and the modulation-specific code with one relay and 2-PPM- $M'$ -PAM constellations for  $M' \in \{2, 4, 16, 32, 64\}$  over CM1 using a 5-finger PRake. It was previously shown that ISC has a non-vanishing determinant while the modulation-specific codes are information lossless. For the latter codes, there is no explicit expression of the coding gain given that the determinants of the codewords are not rational integers. We might imagine that ISC will outperform the modulation-specific codes for large values of  $M'$  since the coding gain of the former remains constant. However, the results in Fig. 4.5 show the superiority of the modulation-specific codes even at very high spectral efficiencies. Note also that for large values of  $M'$ , the performance losses of both ISC and the modulation-specific codes are very important even at very large values of the SNR. Therefore, practical non-cooperative and cooperative UWB systems might not use these high order embedded PAM constellations.

### Impact of timing errors

In Fig. 4.6, we determine the impact of the synchronization errors on the performance of cooperative UWB systems. Simulations are performed on CM2 with 4-PAM constellations and a 8-finger PRake. For the cooperative systems, the case of one cooperating relay is considered. The relative synchronization between the source-relay, source-destination and relay-destination is determined by a zero-mean Gaussian random variable having a variance of 1 ns (twice the pulse-width  $T_w$ ). Results show the superiority of the cooperative schemes even in the presence of synchronization errors.

In the second simulation setup,  $\rho_k$  and  $\lambda_k$  in eq. (4.11) are determined from the relative positions of the terminals assuming free space propagation. The source and destination are separated by a distance of  $d = 10$  m. The positions of the  $K$  relays are uniformly distributed in the surface determined from the intersection of the two circles whose radii are equal to  $d$  and centered at the source and the destination respectively. We compare the two following cases. Case 1: perfect feedback from the destination to the relays ( $\varepsilon_k = 0$  in eq. (4.1)). Case 2: systems with no feedback. In this case,  $\varepsilon_k$  is determined from the positions of the destination and the  $k$ -th relay. IPC is used with 2-PAM, one relay and a 5-finger PRake. Results presented in Fig. 4.7 show the performance losses that result in the case where the propagation delays between the relays and the destination are not compensated. CM1 is more vulnerable to this ‘misalignment’. In fact, it is possible not to combine the strongest path between the relay and the destination when  $|\varepsilon_1|$  has a large value.

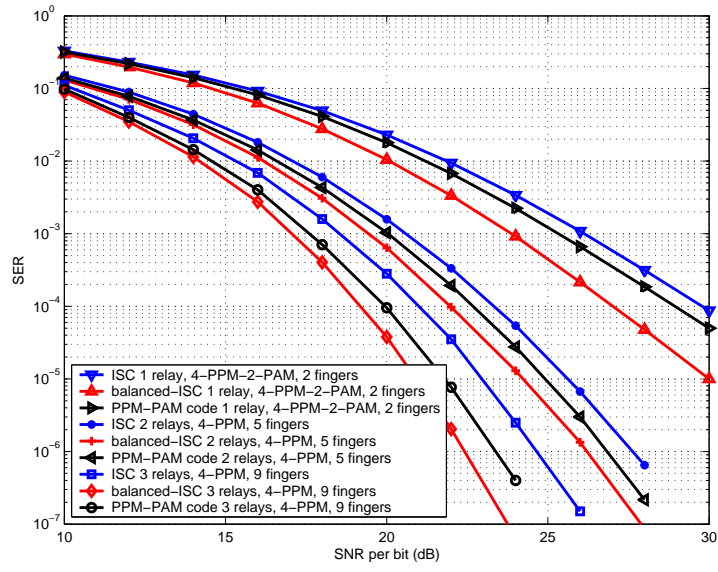


Figure 4.4: The modulation-specific PPM-PAM code versus ISC and balanced-ISC over CM2.

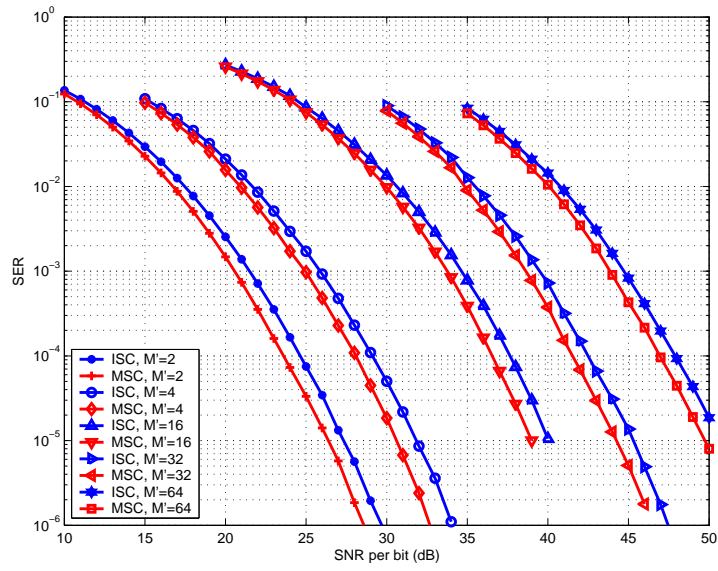


Figure 4.5: The modulation-specific code (MSC) versus ISC with one relay and 2-PPM- $M'$ -PAM constellations over CM1. A 5-finger PRake is used.

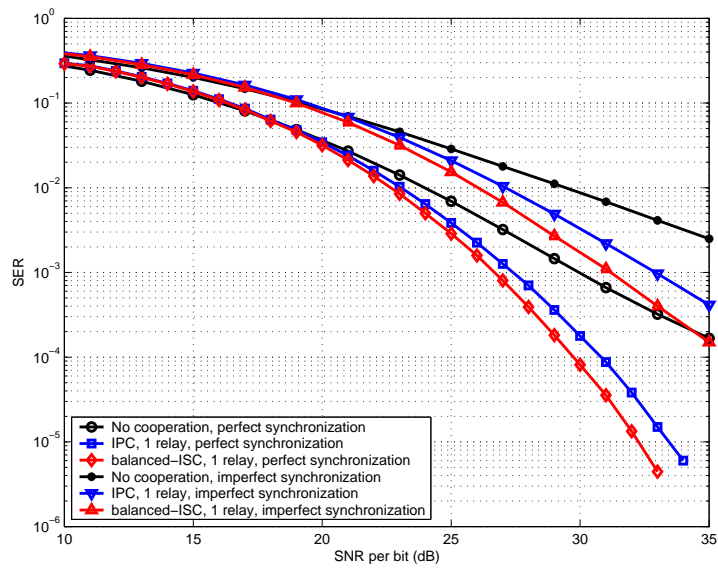


Figure 4.6: Impact of the synchronization errors over CM2. 4-PAM constellations are used and the receiver is equipped with a 8-finger PRake.

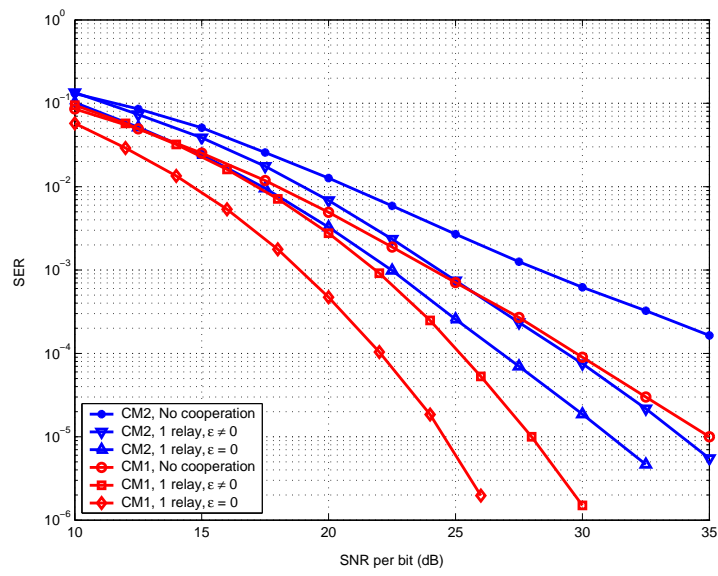


Figure 4.7: Performance with 2-PAM and a 5-finger PRake.  $\varepsilon = 0$  corresponds to perfect feedback while  $\varepsilon \neq 0$  corresponds to no feedback.

## Performance over realistic indoor channels

In the third setup, simulations are performed over a realistic indoor channel. In this context, the site-specific channel modeling tools [19, 20] can be beneficial in simulating wireless networks in realistic indoor environments. These tools are based on “Ray-Tracing” and they take the geometry of the explored environment into consideration. The explored environment corresponds to a typical office building whose map is given in Fig. 4.8. The transmitted signal corresponds to a Gaussian pulse occupying the band [3 5] GHz. The gain parameters  $\rho_k$  and  $\lambda_k$  in eq. (4.11) are determined explicitly from this model that determines the path loss associated with each multi-path component from a given transmitter to one of the four reference nodes. We consider systems with feedback ( $\varepsilon_k = 0$  for  $k = 1, \dots, K$  in eq. (4.1)).

We consider the communication between the reference nodes “2” and “4” with two cooperating relays that can occupy any position in the rooms (A), (B) and (C). Simulations of balanced-ISC with 4-PAM and a 4-finger Rake are shown in Fig. 4.9. Results show that in realistic indoor channels, important performance gains can be achieved depending on the relative positions of the source, destination and the relays. Moreover, a “bad” channel between the source and a relay can be more penalizing than a channel having the same quality between this relay and the destination. Performance gains as high as 11 dB can be obtained if the relays are in room (B). Therefore, in addition to the enhanced diversity order, space-time cooperation can result in important energetic gains that can be very beneficial for UWB systems that suffer from low admissible transmission levels.

### 4.4.2 The DF strategy

#### Coherent systems

Once again, we fix  $\varepsilon_k = 0$  and  $\rho_k = \lambda_k = 1$  in eq. (4.1) and eq. (4.11) respectively for  $k = 1, \dots, K$ . Fig. 4.10 shows the performance of coherent systems on CM2 with 2-PAM and a 5-finger PRake. In this case, we fix  $\beta_1 = \beta_2$ . In particular, we compare Fixed-Relaying (FR) and Selective-Relaying (SR) with  $K = 1, 2, 3$  relays. For SR, a relay participates in the transmission if it correctly decodes the control sequence (composed of 16 symbols). FR shows poor performance with any number of relays. In fact, it is better not to cooperate rather than transmitting completely erroneous decisions from the cooperating relays. On the other hand, cooperation with SR shows high performance gains for any number of relays. Note that even in SR errors can occur at the relays but the encoding scheme turns out to be robust against these errors.

The impact of the energy distribution among the two halves of the cooperation period on the system performance is shown in Fig. 4.11. We consider coherent systems with 1 relay, 2-PAM and a 4-finger PRake. A large value of  $r = \beta_1/\beta_2$  implies that, at the relays, lower energy is dedicated for the transmission of more accurate decisions on the received signals. On the other hand, for small values of  $r$ , a bigger proportion of the energy is transmitted by the relays. However, the “forwarded” symbols have a higher probability of being coded versions of erroneous decisions. For high SNR, the optimum is obtained around  $r=4$  dB over CM1 and CM2. This shows the importance of allocating more energy for enhancing the decisions at the relays.

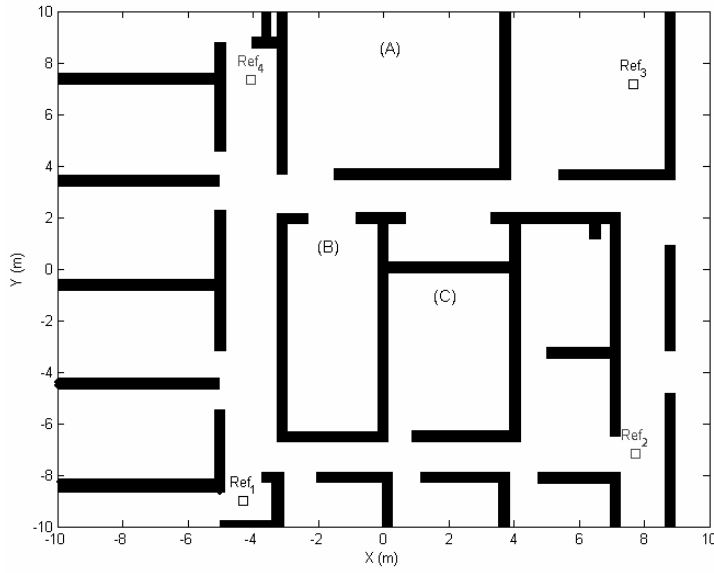


Figure 4.8: Map of the studied environment.

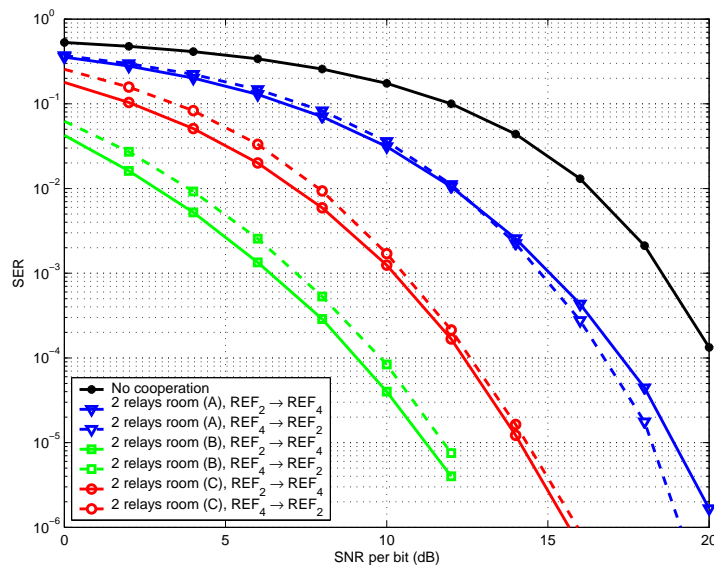


Figure 4.9: Performance in the studied environment with 4-PAM, 4-fingers PRake and 2 relays. The relays can occupy any position in rooms (A), (B) and (C) and they participate in the communication between REF<sub>2</sub> and REF<sub>4</sub>.

### Non-coherent and differential systems

For  $M$ -dimensional constellations, the frame duration is chosen to verify  $T_f = (M - 1)\delta + 100$  ns resulting in no ISI. For non-coherent systems based on energy integration, orthogonal PPM constellations are used with  $\delta = 100$  ns in order to eliminate the interference between the modulation positions.

Fig. 4.12 shows the performance of non-coherent systems on CM2 with 4-PPM and a 5-finger PRake. SR is used with 1 and 2 relays for different values of the ratio  $r = \beta_1/\beta_2$ . For non-coherent systems,  $r = 1$  means that the transmitted energy is evenly distributed among the source and the relays. In this case, the cooperative scheme shows the best performance. For  $r = 4$ , the energy transmitted by the relays is small resulting in some performance losses. Note that, in both cases, the proposed scheme outperforms the non-cooperative systems. Results in Fig. 4.12 also show that for  $r = 4$  it is interesting to have limited number of relays at low signal-to-noise ratios (SNR). In this region, the performance is dominated by the noise events (rather than fading). The amplitudes of the pulses transmitted during the time frames  $2, \dots, K+1$  are smaller for  $K = 2$  with respect to the case  $K = 1$  and therefore these pulses can be masked by the noise.

Fig. 4.13 shows the performance of differential systems over CM2 with 4-PPM-2-PAM, one cooperating relay and a 10-finger PRake. For the decision feedback receivers, the reference signal is averaged over 100 symbol durations which is supposed to be smaller than the channel coherence time. We compare high data rate (HDR) and low data rate (LDR) differential systems that correspond to  $\delta = 2.5$  ns and  $\delta = 100$  ns respectively. Note that for the HDR systems, the increase in the symbol duration is not very high when increasing the value of  $M$  (and hence the spectral efficiency) showing the interest of associating the proposed differential systems with high dimensional modulations. While the HDR differential systems suffer from high error floors, the DF cooperative diversity permits to decrease these error floors. An additional reduction in the error floors can be obtained by the association of the DF scheme with decision feedback receivers. In the same way, the differential DF scheme shows important performance gains with LDR systems. Note that for  $\delta = 2.5$  ns, the decision feedback receivers can not ameliorate the performance at high SNRs. In fact, for high SNRs, the performance is dominated by the interference between the modulation positions and the decision feedback receivers, whose role is to reduce the noise level in the reference signal, can not eliminate this kind of interference.

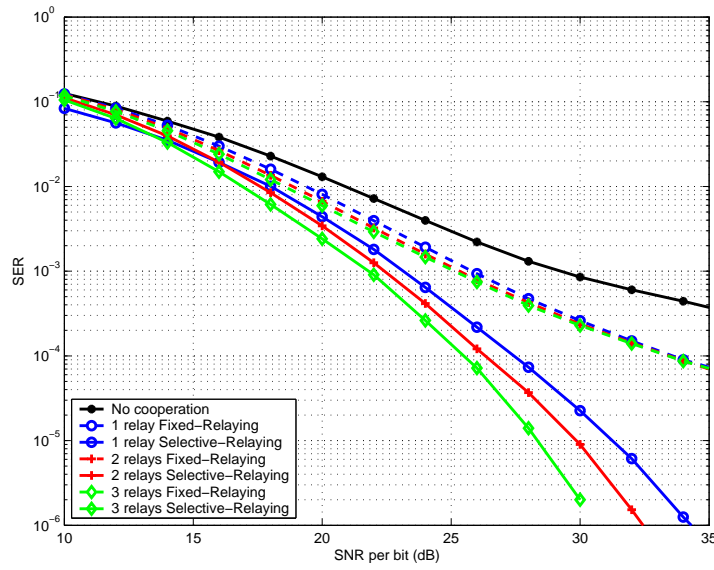


Figure 4.10: Fixed-Relaying versus Selective-Relaying on CM2 with coherent systems, 2-PAM and a 5-finger PRake using 1, 2 and 3 relays.

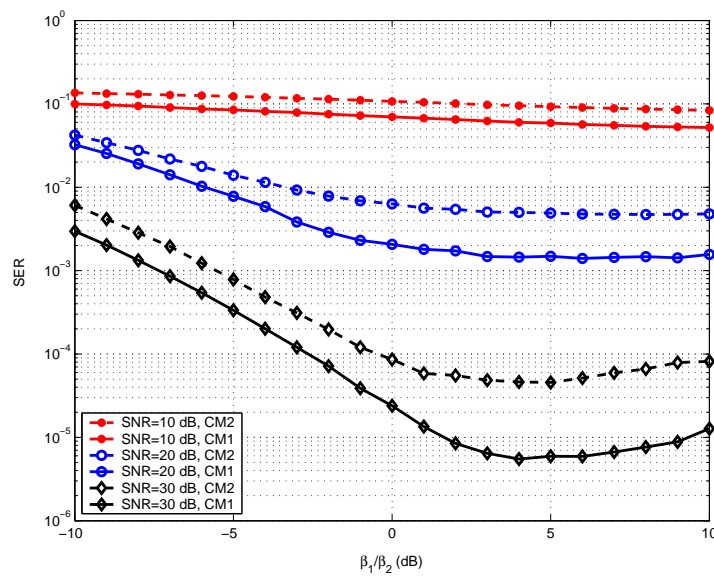


Figure 4.11: The impact of the energy distribution among the two halves of the cooperation period. Coherent systems are used with 1 relay, 2-PAM and a 4-finger PRake.

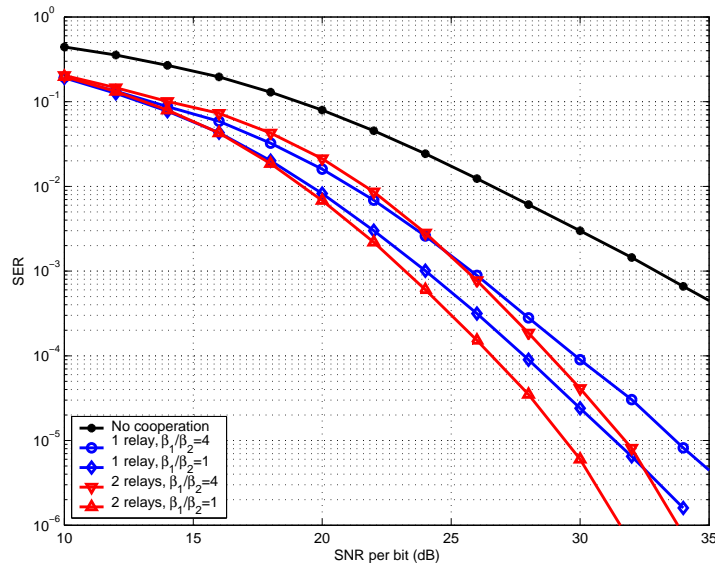


Figure 4.12: Performance of non-coherent systems on CM2 with 4-PPM and a 5-finger PRake using 1 and 2 relays.

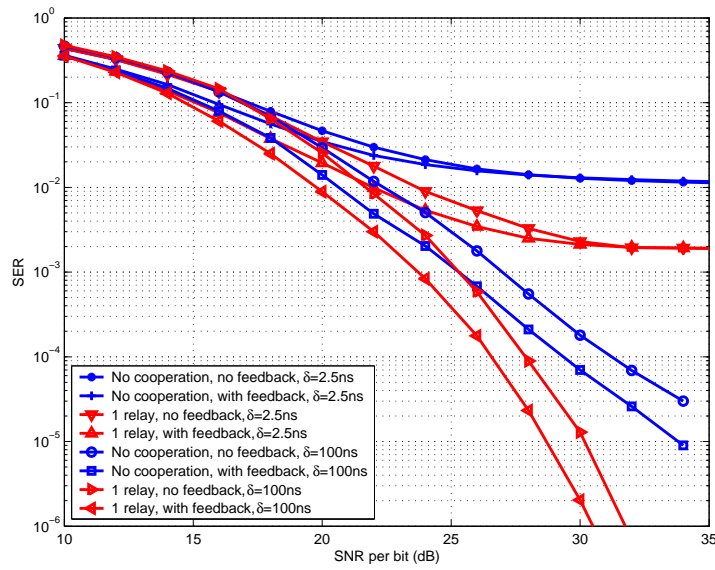


Figure 4.13: Performance of decision-feedback differential systems on CM2 with 4-PPM-2-PAM and a 10-finger PRake using 1 relay.

# Chapter 5

## Decoding the multi-dimensional constellations

In the literature, space-time block codes were principally associated with PAM and QAM constellations. For PAM constellations, decoding a  $P \times T$  ST block code transmitting at a rate of  $n$  symbols PCU is equivalent to the detection in a signal-space of dimension  $nT$ . For QAM, the real and imaginary parts of each information symbol can be decoded separately and the decoding problem corresponds to the detection in a  $2nT$ -dimensional space where all the components of the information vectors are independent from each other. For these linear modulations, the linearity of a ST code facilitates the design of maximum-likelihood (ML) decoders. The sphere decoder algorithms [102, 113] constitute a possible practical implementation of these ML decoders.

$M$ -PPM and hybrid  $M$ -PPM- $M'$ -PAM are non-linear modulations where only one component, among the  $M$ -dimensional vector representations of the information symbols, can have a non-zero value. Therefore, even when linear ST codes are used (for example the codes proposed in chapter 3 and chapter 4), the sphere decoders can not be applied when these codes are associated with PPM and PPM-PAM.

In this chapter, we consider, for the first time, the problem of ML detection with multi-dimensional and non-linear PPM and PPM-PAM constellations. We propose non-trivial modifications of the sphere decoder that allow to enhance the convergence time and that avoid the convergence towards non-valid points. We also consider the adaptation of non-optimal decoders, such as the V-BLAST decoding algorithm [42, 43] and the Fano algorithm [103], to the considered modulations.

### 5.1 Problem formulation

The baseband linear dependence between the output and the input of uncoded and linearly ST-coded  $P \times Q$  MIMO-UWB systems can be expressed as:

$$X_{Q'MT \times 1} = \mathcal{H}_{Q'MT \times P'M} A_{P'M \times 1} + N_{Q'MT \times 1} \quad (5.1)$$

where the noise term  $N$  is white.  $M$  is the number of modulation positions and  $T$  is the number of symbol durations occupied by each codeword.  $Q' = QLP$ ,  $Q' = QL$  and  $Q' = Q$  for SRakes, PRakes and correlation receivers respectively (refer to chapter 2).  $P' = P$  and  $P' = Pn$  for uncoded and ST-coded systems respectively ( $n$  is the number of symbols PCU).  $\mathcal{H}$  stands for the channel matrix of uncoded systems while the linear dependence of the transmitted symbols on the information symbols can be

included in  $\mathcal{H}$  for ST-coded systems (refer to appendix D.3). We suppose than  $Q' \geq P$ . In this case, the matrix  $\mathcal{H}$  has full-rank and eq. (5.1) can be written in an equivalent way as:

$$X_{P'M \times 1} = H_{P'M \times P'M} A_{P'M \times 1} + N_{P'M \times 1} \quad (5.2)$$

where  $H = (\mathcal{H}^T \mathcal{H})^{\frac{1}{2}}$ . The ML detection corresponds to deciding in the favor of the vector  $\hat{a}$  verifying:

$$\hat{a} = \arg \min_{a \in \mathcal{C}^{P'}} \|X - Ha\|^2 \quad (5.3)$$

where  $\mathcal{C}$  stands for the PAM, PPM or the PPM-PAM signal sets given in eq. (1.4), eq. (1.6) and eq. (1.8) respectively.

For  $M$ -PPM- $M'$ -PAM, the coordinates of the  $MP'$  dimensional information vector  $A$  in eq. (5.2) are not independent.  $A$  is composed of  $P'$  sub-vectors that are multiples of the columns of the  $M \times M$  identity matrix. Taking this fact into consideration, the transmit antenna array can be seen as composed of  $P'$  sub-arrays each having  $M$  “virtual” antennas from which only one antenna is active at a time. But because of the co-channel interference and the frequency selectivity of the UWB channels, each one of the  $P'M$  data streams will interfere with all the other streams.

Moreover, the generated lattice has a cardinality of  $(M'+1)^{MP'}$  since the amplitude in each position can be equal to zero in addition to the  $M'$  nonzero values. However, among these points only  $(MM')^{P'}$  points are valid. Therefore, applying the sphere decoder without any modifications can result in non-valid points. This can be simply remedied by applying a validity test at the end of the algorithm. In this case, if the resulting vector does not belong to the constellation it is not kept and the search is restarted. However, this results in an additional complexity since the modified algorithm will “zigzag” between a large number of non-valid points before reaching the closest valid point. Moreover, this complexity increases with  $M$  and  $M'$  since the resulting constellations become sparser.

In Fig. 5.1, we plot a 3-PPM-4-PAM constellation and a 3-dimensional extension of the 4-PAM (that, for example, corresponds to the constellation transmitted in the case of spatial multiplexing with 3 transmit antennas). This figure shows the degree of sparsity of the PPM-PAM constellations. While each component of the vector representation of a 3-PPM-4-PAM constellation can take 4 possible non-zero values, only 12 points are valid among the  $4^3$  points that are obtained if the 3 components are allowed to vary independently. An efficient decoding algorithm must iterate only between the intersection of the x-axis, y-axis and z-axis with the spheres of radii 1 and 3 that are centered at the origin.

2-PPM-2-PAM constellations constitute an exception. In fact, the components of the transmitted information symbols can be rendered independent by applying a simple 2-dimensional rotation. In other words, the vector  $A$  in eq. (5.2) can be written as:

$$A = \mathcal{R}A_0 = (I_{P'} \otimes R)A_0 \quad ; \quad R = \frac{1}{2} \begin{bmatrix} 1 & -1 \\ 1 & 1 \end{bmatrix} \quad (5.4)$$

where  $A_0 \in \{\pm 1\}^{2P'}$ . In this case, the components of  $A_0$  can be decoded separately by applying the sphere decoder and the restored vectors are then demapped back to construct the ML decision on  $A$ .

## 5.2 Layered space-time detection

The layered space-time detection technique (V-BLAST) is able to achieve good compromise between ML and linear receivers [42, 43]. It was extended to tapped-delay UWB channels with 2-PPM constellations in [114]. However, unlike QAM, PAM or 2-PPM constellations,  $M$ -PPM- $M'$ -PAM signals

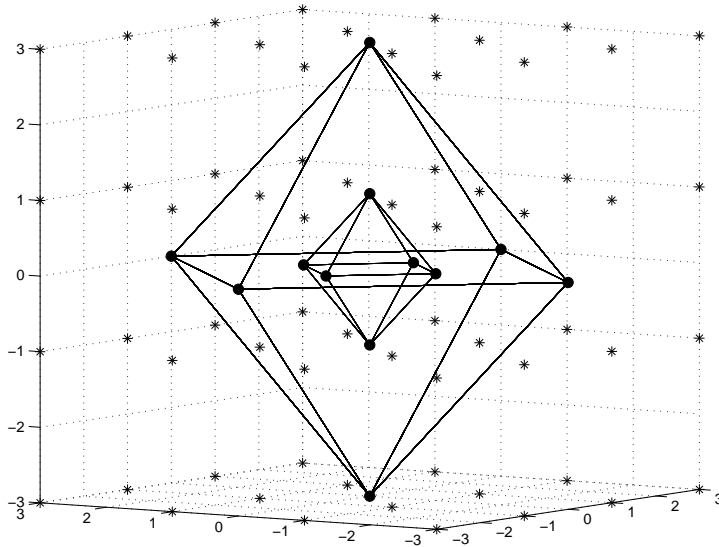


Figure 5.1: The 3-PPM-4-PAM constellation (in filled circles). The stars corresponds to a  $\{4\text{-PAM}\}^3$  constellation.

necessitate decision vectors of length  $M$ . Therefore, the nulling, interference cancelation and decision operations will now concern groups of  $M$  columns of the matrix  $H$  in eq. (5.2) rather than one column. The modified version of [42] decides in the favor of  $\hat{a}$  where  $\hat{a}$  is given by the following algorithm:

**Layered Space-Time Detection** (Input:  $H, X, M, P'$ . Output:  $\hat{a}$ )

*Initialization:*

$$i = 1, H_1 = H, X_1 = X$$

*P' Iterations:*

- 1:  $G_i = H_i^+$
- 2:  $k_i = \operatorname{argmin}_{j \notin \{k_1, \dots, k_{i-1}\}} \sum_{m=1}^M \| (G_i)_{(j-1)M+m} \|^2$
- 3:  $y_{k_i} = [(G_i)_{(k_i-1)M+1}^T \dots (G_i)_{k_iM}^T]^T X_i$
- 4:  $\hat{p}_{k_i} = \operatorname{argmax}_{m=1, \dots, M} |y_{k_i, m}|$
- 5:  $\hat{a}_{k_i} = \lceil y_{k_i, \hat{p}_{k_i}} \rceil e_{\hat{p}_{k_i}}$
- 6:  $X_{i+1} = X_i - [(H_i)_{(k_i-1)M+1} \dots (H_i)_{k_iM}] \hat{a}_{k_i}$
- 7:  $H_{i+1} = H_i^{-k_i}$
- 8:  $i = i + 1$

where:  $(G_i)_k$  corresponds to the  $k$ -th row of  $G_i$ ,  $(H_i)_k$  is the  $k$ -th column of  $H_i$  and  $X^+$  is the pseudo inverse of  $X$  based on the MMSE criterion.  $X^{-k}$  corresponds to zeroing the columns  $(k-1)M+1, \dots, kM$  of the matrix  $X$ . The function  $\lceil x \rceil$  rounds  $x$  to the closest  $M'$ -PAM point.

Step 2 corresponds to the ordering of the sub-arrays based on the norm of  $M$  consecutive columns of  $H$ . These columns will multiply the components of one  $M$ -dimensional vector that corresponds to ones of the  $P'$  transmitted symbols. In the  $i$ -th iteration, step 3 corresponds to the construction of the decision vector of length  $M$  after nulling the interference caused by  $P' - i$  sub-streams that correspond to  $(P' - i)M$  components of  $\hat{a}$ . The scalar  $\hat{p}_{k_i}$  in step 4 corresponds to the position of the  $k_i$ -th restored sub-stream while  $\hat{a}_{k_i}$  in step 5 stands for the  $M$ -dimensional vector corresponding to the  $k_i$ -th symbol. Steps 6 and

7 correspond to canceling the interference of the  $k_i$ -th detected sub-stream from the remaining  $P' - i$  streams.

### 5.3 Sphere detection based on Pohst enumeration (SD)

The sphere decoding algorithms are based either on the Pohst enumeration strategy [102, 112] or on the Schnorr-Euchner enumeration strategy [103, 113]. The enumeration strategies correspond to two different techniques adopted for spanning the set of admissible values at each layer of the decoded information vector. In what follows, these techniques are adopted for decoding finite and non-linear PPM and PPM-PAM constellations. In what follows, and for notational simplicity, we consider the detection in a  $PM$ -dimensional signal-space (we set  $P' = P$ ).

Denote by  $Q$  and  $R$  the unitary matrix and the upper triangular matrix (with positive diagonal elements) obtained by performing the QR decomposition on the matrix  $H$  in eq. (5.2). Denoting by  $z = Q^T X$  a rotated version of the initial decision vector  $X$ , eq. (5.3) is equivalent to finding the point  $a \in \mathcal{C}^P$  that minimizes  $\|z - Ra\|^2$ .

#### 5.3.1 SD with PPM-PAM constellations (algorithm 0)

In order to have reproducible results that are independent from the speed of the simulating machines, the convergence times of all the proposed algorithms are determined with respect to the following algorithm referred to as algorithm 0. Besides constituting a relative time reference, it is also presented to show how far the trivial solution is from the proposed algorithms. Algorithm 0 is based on a straight-forward modification of the SD that is based on the Pohst strategy. It consists of a continuous checking of the validity of each part of the sub-vectors. If the validity test fails, an adjacent node at the same level is checked. If the failure corresponds to the last node at a given level, algorithm 0 passes to a lower dimension (one with a higher index). In what follows, we give the pseudo code of algorithm 0.  $P$  is the number of transmit antennas for uncoded systems while  $P$  is replaced by  $P^2$  for decoding the full rate and minimal-delay codes proposed in chapter 3.

In what follows,  $r_{i,j}$  corresponds to the  $(i, j)$ -th element of the upper triangular matrix  $R$ . The function  $\text{enum}(a, b)$  enumerates all elements of the set  $S = \{0, \pm 1, \dots, \pm(M' - 1)\}$  that belong to the interval  $[a \ b]$ . The function  $\text{length}(a, b)$  returns the number of elements in  $\text{enum}(a, b)$ .

**Algorithm 0** (Input:  $z, R, P, M, M', C$ . Output:  $\hat{a}$ )

**Step 1:** Set  $P' = PM$ ,  $i = P'$ ,  $T_{P'} = 0$ ,  $\xi_{P'} = 0$ ,  $d = C$  (sphere squared radius)

**Step 2:** If  $d < T_i$  go to Step 4 else

$$\begin{aligned} A_i &= \max \left( 1 - M', \left\lceil \frac{z_i - \xi_i - \sqrt{d - T_i}}{r_{i,i}} \right\rceil \right) \\ B_i &= \min \left( M' - 1, \left\lfloor \frac{z_i - \xi_i + \sqrt{d - T_i}}{r_{i,i}} \right\rfloor \right) \end{aligned}$$

$y_i = \text{enum}(A_i, B_i)$ ,  $N_i = \text{length}(A_i, B_i)$ ,  $x_i = 0$  endif.

**Step 3:**  $x_i = x_i + 1$ ,

if  $x_i \leq N_i$  {for  $j = i, \dots, \lceil \frac{i}{M} \rceil M$  do  $u_j = y_j(x_j)$  endfor,  
if validity\\_test( $u$ ) = 1 go to Step 5 else go to Step 3 endif} endif.

**Step 4:** If  $i = P'$  terminate else  $i = i + 1$ , go to Step 3 endif.

**Step 5:** If  $i > 1$ ,  $\xi_{i-1} = \sum_{j=i}^{P'} r_{i-1,j} y_j(x_j)$ ,

$T_{i-1} = T_i + |z_i - \xi_i - r_{i,i} y_i(x_i)|^2$ , let  $i = i - 1$  and go to Step 2 endif.

**Step 6:**  $\hat{d} = T_1 + |z_1 - \xi_1 - r_{1,1} y_1(x_1)|^2$ .

If  $\hat{d} < d$  let  $d = \hat{d}$ , for  $i = 1, \dots, P'$ ,  $\hat{a}_i = y_i(x_i)$  endfor endif go to Step 3.

The function “validity\\_test” in Step 3 assures that a part consisting of  $m$  coordinates of a sub-vector contains no more than one nonzero entry and that this part contains exactly one nonzero entry for  $m = M$ . The disadvantage of algorithms 0 is that the function “validity\\_test” is performed each time we pass from one dimension to another. The complexity is higher than that of the classical SD with  $PM$  dimensions. Note that algorithm 0 is based on a straightforward modification of the SD. In fact, for PAM constellations, algorithm 0 can be readily applied by setting  $M = 1$  and by removing the part between parenthesis in Step 3. In this case, the function “enum” is applied on the set  $S = \{\pm 1, \dots, \pm (M' - 1)\}$ .

We now propose two versions of the modified multi-dimensional sphere decoder (SD) that are based on the Pohst enumeration strategy. Even though the first version is not the best solution, it is presented for comprehensive reasons and it constitutes an intermediary step for deriving the second algorithm.

### 5.3.2 SD with PPM-PAM constellations (algorithm 1)

The first algorithm is a direct modification of the SD obtained by a continuous adaptation of the boundaries at each level based on the tested points at previous levels. The parts of the algorithm that are specific to this extension are written between parenthesis while the remaining parts correspond to the Pohst strategy as can be found in [112] for example.

**Algorithm 1** (Input:  $z, R, P, M, M', C$ . Output:  $\hat{a}$ )

**Step 1:** Set  $P' = PM$ ,  $i = P'$ ,  $T_{P'} = 0$ ,  $\xi_{P'} = 0$ ,  $\{flag = \mathbf{0}_{P'}\}$ ,  $d = C$  (sphere squared radius)

**Step 2:** If  $d < T_i$  go to Step 4 else {If  $flag(i) = 1$   $A_i = B_i = 0$  else

$$A_i = \max \left( 1 - M', \left\lceil \frac{z_i - \xi_i - \sqrt{d - T_i}}{r_{i,i}} \right\rceil \right)$$

$$B_i = \min \left( M' - 1, \left\lfloor \frac{z_i - \xi_i + \sqrt{d - T_i}}{r_{i,i}} \right\rfloor \right)$$

endif},  $y_i = \text{enum}(A_i, B_i)$ ,  $N_i = \text{length}(A_i, B_i)$ ,  $x_i = 0$  endif.

**Step 3:**  $x_i = x_i + 1$ , if  $x_i > N_i$  go to Step 4 else {if  $y_i(x_i) \neq 0$ ,  $j = i - 1 \bmod (M)$ ,

for  $k = 1, \dots, j$   $flag(i-k) = 1$  endfor elseif  $i = 1 \bmod (M)$

for  $k = i, \dots, i+M-1$   $u_k = y_k(x_k)$  endfor, if  $u = \mathbf{0}_M$  go to Step 3 endif endif}, go to Step 5 endif.

**Step 4:** If  $i = P'$  terminate else  $i = i + 1$ ,  $\{flag = \mathbf{0}_{P'}\}$  go to Step 3 endif.

**Step 5:** If  $i > 1$ ,  $\xi_{i-1} = \sum_{j=i}^{P'} r_{i-1,j} y_j(x_j)$ ,  
 $T_{i-1} = T_i + |z_i - \xi_i - r_{i,i} y_i(x_i)|^2$ , let  $i = i - 1$  and go to Step 2 endif.

**Step 6:**  $\hat{d} = T_1 + |z_1 - \xi_1 - r_{1,1} y_1(x_1)|^2$ .  
If  $\hat{d} < d$  let  $d = \hat{d}$ , for  $i = 1, \dots, P'$ ,  $\hat{a}_i = y_i(x_i)$  endfor endif go to Step 3.

Algorithm 1 is based on the idea that whenever a nonzero coordinate is found (Step 3), the remaining coordinates having smaller indices and corresponding to the nominal positions of the same transmit antenna are set to zero without checking the boundaries of the sphere along these dimensions (Step 2). This follows from the structure of the transmitted information vector  $A$  that can be divided into  $P$  sub-vectors each consisting of  $M - 1$  zeros and one non-zero component that belongs to the  $M'$ -PAM constellation. In a similar way, all-zero sub-vectors are avoided (Step 3). This can be seen as “forcing” the algorithm to zigzag only between valid nodes. This algorithm avoids calculating and spanning many intervals corresponding to the set of valid coordinates. In other words, if a non-zero coordinate is found at the  $m$ -th component of a given sub-vector, algorithm 1 “short circuits” the remaining  $m - 1$  dimensions at higher levels (levels with smaller indices).

### 5.3.3 SD with PPM-PAM constellations (algorithm 2)

At the  $i$ -th level, and for some given values of  $a_l \in \text{enum}(A_l, B_l)$  for  $l = i+1, \dots, PM$ , algorithm 1 tries to find the set of valid values of  $a_i$  verifying:

$$\left| z_i - \sum_{j=i}^{PM} r_{i,j} a_j \right|^2 = \left| z_i - r_{i,i} a_i - \sum_{j=i+1}^{PM} r_{i,j} a_j \right|^2 \triangleq |z_i - r_{i,i} a_i - \xi_i|^2 \leq d - T_i \quad (5.5)$$

where  $T_i$  and  $\xi_i$  are updated recursively in the order from  $PM$  to 1 and  $d$  is changed adaptively along the search (at level 1). We argue that the complexity of algorithm 1 follows from solving eq. (5.5) over  $PM$  dimensions. We propose to group  $M$  equations in the form of eq. (5.5) together and to solve them simultaneously. This is rendered possible because of the structure of the PPM-PAM constellations. These  $M$  equations are solved at levels  $(p-1)M+1$  for  $p = P, \dots, 1$ . Grouping the  $M$  equations at levels  $(p-1)M+1, \dots, pM$ , we obtain:

$$\sum_{m=1}^M \left| z_m^{(p)} - \sum_{j=f(p,m)}^{PM} r_{f(p,m),j} a_j \right|^2 \leq d - T_p \quad (5.6)$$

where  $f(p,m) = (p-1)M+m$  and  $T$  is changed recursively after each  $M$  levels.  $z^{(p)}$  corresponds to the  $M$ -dimensional vector composed of the elements  $z_{(p-1)M+1}, \dots, z_{pM}$  of the  $PM$ -dimensional vector  $z$ . The  $m$ -th component of  $z^{(p)}$  is denoted by  $z_m^{(p)}$ . We construct the vectors  $a^{(1)}, \dots, a^{(P)}$  in the same way. As in the preceding algorithm,  $r_{i,j}$  is the  $(i, j)$ -th element of  $R$ .

Given that only one value among  $a_{f(p,1)}, \dots, a_{f(p,M)}$  can be different from zero, determining the boundaries at the level  $f(p,m')$  is equivalent to solving (for  $m' = 1, \dots, M$ ):

$$\sum_{m=1}^M \left| z_m^{(p)} - r_{f(p,m),f(p,m')} a_{f(p,m')} - \xi'_{p,m} \right|^2 \leq d - T_p \quad (5.7)$$

where:

$$\xi'_{p,m} = \sum_{j=f(p+1,1)}^{PM} r_{f(p,m),j} a_j \quad (5.8)$$

We introduce the following notations:  $a_{m'}^{(p)} = a_{f(p,m')}$  and  $R^{(i,j)}$  is the  $M \times M$  matrix composed of the elements  $r_{m,m'}$  for  $m = (i-1)M + 1, \dots, iM$  and  $m' = (j-1)M + 1, \dots, jM$ . Finally,  $R^{(i)} = R^{(i,i)}$ . The  $k$ -th column of a matrix  $X$  is denoted by  $X_{:,k}$ . For a given value of  $m' \in \{1, \dots, M\}$ , eq. (5.6) can be expressed as:

$$\left\| z^{(p)} - a_{m'}^{(p)} R_{:,m'}^{(p)} - \xi_{:,p} \right\|^2 \leq d - T_p \quad (5.9)$$

where  $\xi$  is a  $M \times P$  matrix whose  $p$ -th column is given by:

$$\xi_{:,p} = \sum_{p'=p+1}^P a_{c_{p'}}^{(p')} R_{:,c_{p'}}^{(p,p')} \quad (5.10)$$

where  $c_{p'} \in \{1, \dots, M\}$  is the position of the pulse transmitted by the  $p'$ -th antenna. These values are obtained by back-substitution. The boundaries at the level  $(p'-1)M + c_{p'}$  are determined taking into consideration that the amplitudes at levels  $(p'-1)M + 1, \dots, (p'-1)M + c_{p'} - 1, (p'-1)M + c_{p'} + 1, \dots, p'M$  are all equal to zero.  $a_{c_{p'}}^{(p')}$  is allowed to vary between the boundaries at this level. For the detection of the symbol transmitted from the  $p$ -th antenna, the different notations that we introduced in eq. (5.9) and eq. (5.10) can be visualized as in what follows (with  $M = 4$ ,  $c_p = 3$ ,  $c_{p+1} = 2$  and  $c_P = 1$ ):

$$\begin{bmatrix} - \\ - \\ - \\ - \\ - \end{bmatrix} \begin{bmatrix} - & - & - & - \\ - & - & - & - \\ - & - & - & - \\ - & - & - & - \end{bmatrix} \begin{bmatrix} - & - & - & - \\ - & - & - & - \\ - & - & - & - \\ - & - & - & - \end{bmatrix} \begin{bmatrix} - & - & - & - \\ - & - & - & - \\ - & - & - & - \\ - & - & - & - \end{bmatrix} \begin{bmatrix} - \\ - \\ - \\ - \end{bmatrix} \begin{bmatrix} - & - & - & - \\ - & - & - & - \\ - & - & - & - \\ - & - & - & - \end{bmatrix}$$

$$\underbrace{\begin{bmatrix} * \\ * \\ * \\ * \\ \hline z^{(p)} \end{bmatrix}}_{R^{(p)}} \underbrace{\begin{bmatrix} - & * & - & - \\ - & * & - & - \\ * & - & - & - \\ - & - & * & - \end{bmatrix}}_{R_{:,c_{p+1}}^{(p,p+1)}} \quad (c_{p+1} = 2) \quad \begin{bmatrix} * & - & - & - \\ * & - & - & - \\ * & - & - & - \\ * & - & - & - \end{bmatrix}$$

We now give the pseudo code of algorithm 2. In what follows,  $I$  stands for the  $M \times M$  identity matrix.

#### Algorithm 2 (Input: $z$ , $R$ , $P$ , $M$ , $M'$ , $C$ . Output: $\hat{a}$ )

**Step 1:** Set  $i = P$ ,  $T_i = 0$ ,  $\xi_{:,i} = \mathbf{0}_M$ ,  $d = C$  (sphere squared radius).

**Step 2:** If  $d < T_i$  go to Step 4 else  $f = (z^{(i)} - \xi_{:,i})^T (z^{(i)} - \xi_{:,i}) - d + T_i$ , for  $m = 1, \dots, M$ ,  
 $a = R_{:,m}^{(i)T} R_{:,m}^{(i)}$ ,  $b = -R_{:,m}^{(i)T} (z^{(i)} - \xi_{:,i})$ ,  $\delta = b^2 - af$ . If  $\delta < 0$   $A_m^{(i)} = B_m^{(i)} = 0$  else

$$A_m^{(i)} = \max \left( 1 - M', \left\lceil \frac{-b - \sqrt{\delta}}{a} \right\rceil \right)$$

$$B_m^{(i)} = \min \left( M' - 1, \left\lfloor \frac{-b + \sqrt{\delta}}{a} \right\rfloor \right)$$

endif,  $x_m^{(i)} = A_m^{(i)} - 2$  endfor  $c_i = 1$  endif.

**Step 3:**  $x_m^{(i)} = x_m^{(i)} + 2$ , if  $x_m^{(i)} > B_m^{(i)}$  go to Step 4 else go to Step 5 endif.

**Step 4:**  $c_i = c_i + 1$ , if  $c_i = M + 1$  if  $i = P$  terminate else  $i = i + 1$  endif endif go to Step 3.

**Step 5:** If  $i > 1$   $\xi_{:,i-1} = \sum_{j=i}^P x_{c_j}^{(j)} R_{:,c_j}^{(i-1,j)}$ ,  $T_{i-1} = T_i + \|z^{(i)} - \xi_{:,i} - x_{c_i}^{(i)} R_{:,c_i}^{(i)}\|^2$ ,  
 $i = i - 1$  go to Step 2 endif.

**Step 6:**  $\hat{d} = T_1 + \|z^{(1)} - \xi_{:,1} - x_{c_1}^{(1)} R_{:,c_1}^{(1)}\|^2$ . If  $\hat{d} < d$  let  $d = \hat{d}$ , for  $p = 1, \dots, P$   $\hat{a}_p = x_{c_p}^{(p)} I_{:,c_p}$  endfor endif  
go to Step 3.

Algorithm 2 is the recursive solution of eq. (5.9). It is equivalent to considering  $P$  levels where each level has  $M$  sub-levels whose boundaries are determined jointly. Note that there is no need to the function “enum” as in algorithm 1 because the checked amplitude levels now belong to the set  $\{\pm 1, \dots, \pm(M' - 1)\}$  rather than  $\{0, \pm 1, \dots, \pm(M' - 1)\}$ .

Fig. 5.2 compares the complexity of algorithms 1 and 2 for different hybrid constellation sizes for systems with 2 transmit antennas, 2 receive antennas and 1 finger PRake on CM2. The ordinate corresponds to the value:  $t_0/t_i$  for  $i = 1, 2$  where  $t_j$  is the average time needed by algorithm  $j$  ( $j = 0, 1, 2$ ) to detect one symbol vector. The signal to noise ratio is fixed at 20 dB and the initial sphere radius is set to infinity. For example, the combined 32-PPM-16-PAM constellation corresponds to a generated lattice with  $2^{18}$  valid points in a 64 dimensional space. In this case, algorithm 1 can “shortcut” up to 31 dimensions and converges 6 times faster than algorithm 0. Results show that algorithm 2 has the best convergence time.

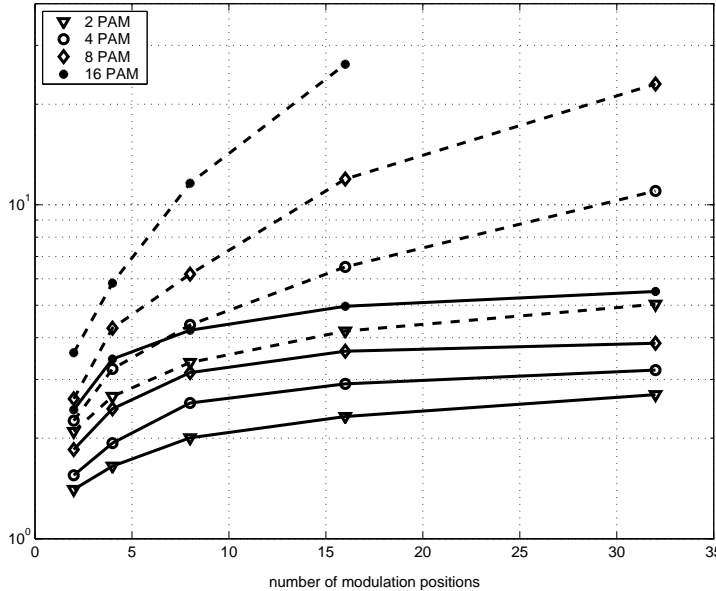


Figure 5.2: Solid and dashed lines correspond to algorithm 1 and algorithm 2 respectively. 2 transmit antennas, 2 receive antennas and a 1-finger PRake are used.

## 5.4 Sphere detection based on Schnorr-Euchner enumeration (SE)

### 5.4.1 SE with PAM constellations

The Schnorr-Euchner enumeration strategy was first applied in [113] for searching for the closest lattice point. This enumeration enhances the spanning of the admissible interval at each level of the received symbol vector. Consider for example the  $k$ -th level for a certain value of  $k \in \{1, \dots, P\}$ . Designate by  $e_{k,k}$  the value of the received signal after applying a zero-forcing decision feedback equalization (ZF-DFE) (in other words,  $e_{k,k}$  is considered in the subspace of the transmitted constellation). Designate by  $R$  the upper triangular matrix obtained by applying a QR decomposition on the channel matrix and denote by  $r_{i,j}$  its  $(i, j)$ -th component. When determining the squared Euclidean distance between the received vector and the current node (the point we are checking in a search algorithm), the influence of the  $k$ -th level is determined by the quantity:

$$d_k^2 = (r_{k,k}(e_{k,k} - x_k))^2 \triangleq \left( \frac{e_{k,k} - x_k}{V_{k,k}} \right)^2 \quad (5.11)$$

where  $V = R^{-1}$  (implying that  $V_{k,k} = r_{k,k}^{-1}$  since  $R$  is upper triangular),  $x_k$  is the  $k$ -th component of the checked lattice point and the squared Euclidean distance is given by:

$$d^2 = \sum_{k=1}^P d_k^2 \quad (5.12)$$

where the interference of the levels  $k+1, \dots, P$  on the  $k$ -th level is eliminated recursively by applying a ZF-DFE. Suppose that  $R$  has positive diagonal elements,  $d_k^2$  is a second degree function of  $x_k$ . The integer that minimizes  $d_k^2$  is given by  $x_k = \text{round}(e_{k,k})$  where the function  $\text{round}(x)$  rounds  $x$  to the closest integer. The second closest lattice point is given by  $x_k + 1$  (resp.  $x_k - 1$ ) when  $e_{k,k} > x_k$  (resp.  $e_{k,k} < x_k$ ). In other words, spanning the interval corresponding to the values of the  $k$ -th coordinate of the lattice point in the order of increasing distance is equivalent to the following enumeration:

$$\text{round}(e_{k,k}), \text{round}(e_{k,k}) + \rho, \text{round}(e_{k,k}) - \rho, \text{round}(e_{k,k}) + 2\rho, \text{round}(e_{k,k}) - 2\rho, \dots \quad (5.13)$$

where  $\rho = \text{sign}(e_{k,k} - x_k)$  (since  $V_{k,k} > 0$  for  $k = 1, \dots, P$ ).

For finite constellations, this spanning can be readily modified in order not to check lattice points that are outside the boundaries of the transmitted constellation. The Schnorr-Euchner enumeration with a 4-PAM constellation is represented schematically in Fig. 5.3. The enumeration is the same as in eq. (5.13) but now  $\rho$  is replaced by  $2\rho$ . Moreover,  $i\rho$ , for a certain integer  $i$ , is replaced by  $-(i+1)\rho$  each time one of the upper or lower boundaries is exceeded. The first time when both  $i\rho$  and  $-(i+1)\rho$  exceed the constellation's boundaries, the search process is terminated and the resulting point ( $\pm(M' - 1)$  for  $M'$ -PAM) corresponds to the point that has the largest distance from the received point.

A possible implementation of the sphere decoder based on the Schnorr-Euchner enumeration and taking the boundaries of a  $M'$ -PAM constellation into consideration is given below:

**SE with PAM** (Input:  $z, V = R^{-1}, P, M', C$ . Output:  $\hat{a}$ )

**Step 1:** Set  $k = P + 1$ ,  $dist(k) = 0$ ,  $\rho = 0$ ,  $bestdist = C$  (sphere squared radius)

**Step 2:**  $newdist = dist(k) + \rho^2$ ,

if ( $newdist < bestdist$ )&( $k \neq 1$ ) go to Step 3 else go to Step 4 endif.

**Step 3:** if  $k=P+1$ ,  $e_{:,k-1} = Vz$  else

for  $i = 1, \dots, k-1$ ,  $e_{i,k-1} = e_{i,k} - \rho V_{i,k}$  endfor endif.

$k = k-1$ ,  $dist(k) = newdist$ ,  $x_k = \lceil e_{k,k} \rceil$ ,  $x_k = \max(1 - M', x_k)$ ,  $x_k = \min(M' - 1, x_k)$ ,

$\rho = (e_{k,k} - x_k)/V_{k,k}$ ,  $step(k) = 2\text{sign}(\rho)$ , go to Step 2.

**Step 4:** if  $newdist < bestdist$ ,  $\hat{a} = x$ ,  $bestdist = newdist$  elseif  $k = P$ , terminate else  $k = k + 1$  endif.

$x(k) = x(k) + step(k)$ ,

if  $x(k) < 1 - M'$  or  $x(k) > M' - 1$ ,  $step(k) = -step(k) - 2\text{sign}(step(k))$ ,  $x(k) = x(k) + step(k)$  endif.

if  $x(k) < 1 - M'$  or  $x(k) > M' - 1$ , go to Step 4 endif.

$\rho = (e_{k,k} - x_k)/V_{k,k}$ ,  $step(k) = -step(k) - 2\text{sign}(step(k))$  go to Step 2.

where:

$$\lceil x \rceil = 2\text{round}\left(\frac{x+M'-1}{2}\right) - M' + 1 \quad (5.14)$$

corresponds to choosing the closest element of the  $M'$ -PAM signal set  $\{\pm 1, \dots, \pm(M' - 1)\}$  to  $x$ .

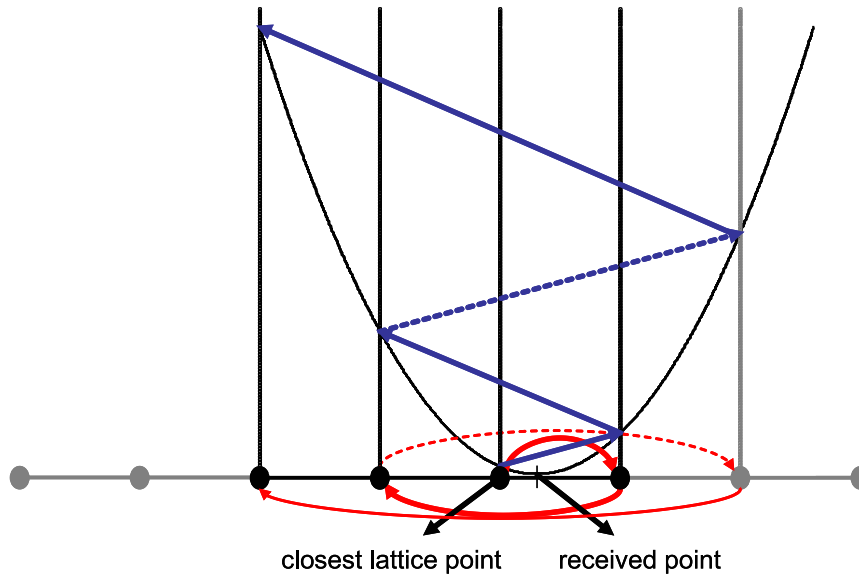


Figure 5.3: The Schnorr-Euchner enumeration with a 1-dimensional 4-PAM constellation. The black points correspond to the 4-PAM amplitude levels ( $\{\pm 1, \pm 3\}$ ) while the gray points correspond to the infinite extension of the 4-PAM (the set of odd integers). Dashed lines are used each time the enumeration results in a point that falls outside the boundaries of the 4-PAM constellation. The plotted parabola corresponds to the squared Euclidean distance between the received point and the visited lattice point.

#### 5.4.2 SE with PPM constellations

Consider the case of multi-dimensional PPM or PPM-PAM constellations. The received vector of length  $PM$  is now seen as composed of  $P$  layers. However, in this case, each layer is composed of a hypercube

of dimension  $M$  rather than a finite interval of points (of dimension 1) as with PAM constellations. The  $M$  components of each hypercube can not span different intervals independently because only one component can have a nonzero value. Suppose that, for a given layer (composed of  $M$  dimensions), we can efficiently order all the valid  $M$ -dimensional sub-vectors of the PPM or PPM-PAM constellation as a function of their increasing distances from a certain received point. In this case, the sphere decoder based on the Schnorr-Euchner enumeration can be readily modified by replacing the natural span given in eq. (5.13) by the new ordering function.

Consider the  $k$ -th level and denote by  $R^{(k)}$  the  $M \times M$  matrix composed of the elements  $r_{i,j}$  of the  $PM \times PM$  matrix  $R$  for  $i, j = (k-1)M+1, \dots, kM$ . Designate by  $R_{:,m}^{(k)}$  the  $(m, m')$ -th element of  $R^{(k)}$  for  $m, m' = 1, \dots, M$ . The enumeration given in eq. (5.13) can not be applied on each one of the  $M$  components of the  $k$ -th level independently while setting the other  $M - 1$  components to zero. In fact, for the  $m$ -th component of the  $k$ -th layer, no ZF-DFE is applied on the components  $1, \dots, m-1$  of this layer.

Consider first the case of  $M$ -PPM and denote by  $e^{(k)}$  the  $M$ -dimensional vector obtained by applying ZF-DFE on the levels  $k+1, \dots, P$ . The influence of the  $k$ -th layer on the squared Euclidean distance when a pulse is transmitted at the  $m$ -th position is given by:

$$d_k^2 = \left\| R^{(k)} \left( e^{(k)} - I_{:,m} \right) \right\|^2 = \left\| E^{(k)} - R_{:,m}^{(k)} \right\|^2 \quad (5.15)$$

where  $E^{(k)} \triangleq R^{(k)}e^{(k)}$ .  $R_{:,m}^{(k)}$  and  $I_{:,m}$  correspond to the  $m$ -th column of  $R^{(k)}$  and the  $M \times M$  identity matrix  $I$  respectively. Therefore, it is easy to sort the  $M$  valid sub-vectors of the  $k$ -th layer by ordering the  $M$  elements of the following set in increasing order:

$$\left\{ -2(R_{:,m}^{(k)})^T E^{(k)} + (R_{:,m}^{(k)})^T R_{:,m}^{(k)} ; m = 1, \dots, M \right\} \quad (5.16)$$

Therefore, a principle similar to the Schnorr-Euchner enumeration can be applied with PPM constellations. For PPM constellations that are orthogonal at the receiver (the modulation duration is larger than the channel delay spread),  $R$  is diagonal and the sorting function in eq. (5.16) is equivalent to sorting the  $M$  components of  $E^{(k)}$  in a decreasing order (given that the applied QR decomposition results in a matrix  $R$  with positive diagonal elements).

The decoding algorithm is given after fixing the following notations.  $\rho$  is a  $M$ -dimensional vectors.  $e$  and  $E$  are  $MP \times P$  matrices.  $x$  and  $Order$  are  $M \times P$  matrices. The entries of  $Order$  belong to the set  $\{1, \dots, M\}$ .  $X_{:,k}$  corresponds to the  $k$ -th column of matrix  $X$ .  $X^{(p)}$  corresponds to the elements  $(p-1)M+1, \dots, pM$  of the  $MP$ -dimensional vector  $X$  for  $p = 1, \dots, P$ . In the same way,  $X^{(p,p')}$  corresponds to the  $M \times M$  matrix composed of the elements  $X_{i,j}$  of the  $PM \times PM$  matrix  $X$  for  $i = (p-1)M+1, \dots, pM$  and  $j = (p'-1)M+1, \dots, p'M$  for  $p, p' = 1, \dots, P$ . The function  $\text{Diag}(X)$  returns a vector composed of the diagonal elements of the matrix  $X$ . The function  $\text{sort}(x)$  returns the indices of the components of vector  $x$  when these latter are arranged in an increasing order.

### **SE with PPM** (Input: $z, R, P, M, C$ . Output: $\hat{a}$ )

**Step 1:** Set  $k = P + 1$ ,  $dist(k) = 0$ ,  $V = R^{-1}$ ,  $\rho = \mathbf{0}_M$ ,  $bestdist = C$  (sphere squared radius)

**Step 2:**  $newdist = dist(k) + \rho^T \rho$ ,

if ( $newdist < bestdist$ )&( $k \neq 1$ ) go to Step 3 else go to Step 4 endif.

**Step 3:** if  $k=P+1$ ,  $e_{:,k-1} = Vz$  else

for  $i = 1, \dots, k-1$ ,  $e_{:,k-1}^{(i)} = e_{:,k}^{(i)} - V^{(i,k)}\rho$  endfor endif.  
 $k = k-1$ ,  $dist(k) = newdist$ ,  $E_{:,k}^{(k)} = R^{(k,k)}e_{:,k}^{(k)}$ ,

$$Order_{:,k} = \text{sort} \left( -2(R^{(k,k)})^T E_{:,k}^{(k)} + \text{Diag} \left( (R^{(k,k)})^T R^{(k,k)} \right) \right)$$

$step(k) = 1$ ,  $pos(k) = Order_{step(k),k}$ ,  $x_{:,k} = I_{:,pos(k)}$ ,  $\rho = E_{:,k}^{(k)} - R_{:,pos(k)}^{(k,k)}$  go to Step 2.

**Step 4:** if  $newdist < bestdist$ , for  $i = 1, \dots, P$ ,  $\hat{a}^{(i)} = x_{:,i}$  endfor

$bestdist = newdist$  elseif  $k = P$ , terminate else  $k = k + 1$  endif.

$step(k) = step(k) + 1$ ,

if  $step(k) > M$ , go to Step 4 endif,

$pos(k) = Order_{step(k),k}$ ,  $x_{:,k} = I_{:,pos(k)}$ ,  $\rho = E_{:,k}^{(k)} - R_{:,pos(k)}^{(k,k)}$  go to Step 2.

### 5.4.3 SE with PPM-PAM constellations

We would have obtained the same algorithm if the function “sort” can be replaced by an efficient sorting function for the PPM-PAM constellations. Unfortunately, ordering the  $MM'$  elements of a  $M$ -PPM- $M'$ -PAM constellation is not a simple task and the complexity of this ordering might increase with the value of  $M'$ . In what follows, we present a modified algorithm that performs a “joint”  $M$ -dimensional span. It is not necessary to sort all the valid  $MM'$  elements, it is sufficient to develop an efficient way that permits to generate the  $M$ -dimensional vectors, at each layer, in a recursive manner (just like the Schnorr-Euchner enumeration). In this case, the recursion is stopped if the point falls outside the current sphere. The complexity of the proposed solution does not increase with  $M'$ . As all the other decoders, the complexity increases with  $M$  because this results in increasing the dimensionality of the signal subspace.

The main difference between the Schnorr-Euchner enumeration for PAM constellations and the proposed enumeration strategy for PPM-PAM constellations is as follows. For the enumeration with finite PAM constellations, falling outside the boundaries of the constellation can be simply remedied by performing a jump in the opposite sense (third line of Step 4 in the SE algorithm with PAM). This is possible because we are sure that this double jump results in an increase in the Euclidean distance as shown in Fig. 5.3. For PPM-PAM, we must be sure that the next candidate node is a valid node before passing to this node. In fact, the relative increase in the minimum distance resulting from this jump (at a certain component of a given layer) must be compared with the increase induced by passing to a next candidate node at the other components of the same layer.

To be more explicit, we further highlight this point by an example. Consider a 2-PPM-4-PAM constellation given by:

$$\{(-3,0), (-1,0), (1,0), (3,0), (0,-3), (0,-1), (0,1), (0,3)\} \quad (5.17)$$

and represented in Fig. 5.4. In this example, the closest lattice point to the received point is given by  $(3,0)$ . Applying the SE enumeration on the x-axis, the next lattice node in the sense of increasing the minimum distance is the point  $(1,0)$ . Continuing the SE enumeration on this axis, the next candidate node is  $(5,0)$ . This is not a valid 4-PAM point and the SE enumeration will pass to the point  $(-1,0)$ . Denote by  $d_{A \rightarrow B}$  the relative increase in the minimum distance when passing from point  $A$  to point  $B$ .

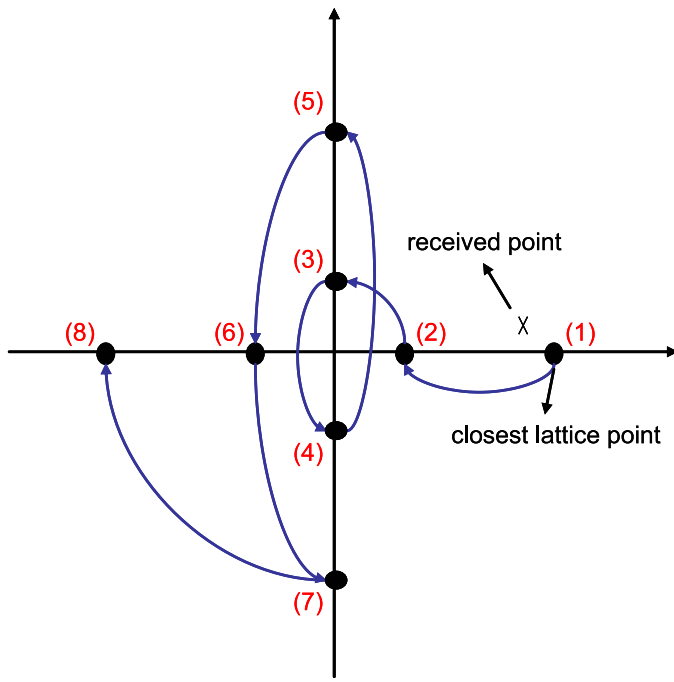


Figure 5.4: The enumeration with a 2-dimensional 2-PPM-4-PAM constellation. This enumeration must be performed jointly between the points of the x-axis and the y-axis that correspond to the two modulation positions.

While  $d_{(1,0) \rightarrow (5,0)} < d_{(1,0) \rightarrow (0,1)}$ , we have  $d_{(1,0) \rightarrow (-1,0)} > d_{(1,0) \rightarrow (0,1)}$  and therefore, unlike the SE, the next node is  $(0, 1)$  rather than the node obtained by performing a double SE jump from  $(1, 0)$  (the point  $(-1, 0)$ ). Therefore, a joint 2-dimensional enumeration is needed and the values of  $d_{A \rightarrow B}$  at the two different levels of the same layer must be only evaluated (and compared) for valid points  $A$  and  $B$ . An example of a 2-dimensional span is shown in Fig. 5.4. In general, a  $M$ -dimensional span must be applied and a new decoding algorithm for PPM-PAM is needed.

We first give the pseudo code of the function “decide” that will be used in the decoding algorithm. Consider the  $m$ -th component of the  $k$ -th layer with  $m \in \{1, \dots, M\}$  and  $k \in \{1, \dots, P\}$ . If the  $m$ -th coordinate of the  $M$ -dimensional sub-vector at the  $k$ -th layer is given by  $x\_pam_m^{(k)}$ , then the influence of the  $k$ -th layer on  $d_{min}^2$  is given by:

$$d_k^2 = \|R^{(k)} \left( e^{(k)} - x\_pam_m^{(k)} I_{:,m} \right) \|^2 \triangleq \|E^{(k)} - x\_pam_m^{(k)} R_{:,m}^{(k)}\|^2 \quad (5.18)$$

$$= (E^{(k)})^T E^{(k)} - 2x\_pam_m^{(k)} (R_{:,m}^{(k)})^T E^{(k)} + (x\_pam_m^{(k)})^2 (R_{:,m}^{(k)})^T R_{:,m}^{(k)} \quad (5.19)$$

$$\triangleq (E^{(k)})^T E^{(k)} + nextpos\_metric_m^{(k)} \quad (5.20)$$

Therefore, when the  $m$ -th level of the  $k$ -th layer is considered alone (the levels  $1, \dots, m-1, m+1, \dots, M$  have zero values and the  $m$ -th level is considered as a PAM constellation), then this level can be spanned in the following way:

$$x\_pam_m^{(k)}, x\_pam_m^{(k)} + 2p_m^{(k)}, x\_pam_m^{(k)} - 2p_m^{(k)}, x\_pam_m^{(k)} + 4p_m^{(k)}, x\_pam_m^{(k)} - 4p_m^{(k)}, \dots \quad (5.21)$$

where:

$$X_m^{(k)} = \frac{(R_{:,m}^{(k)})^T E^{(k)}}{(R_{:,m}^{(k)})^T R_{:,m}^{(k)}} \quad (5.22)$$

$$x\_pam_m^{(k)} = \lceil X_m^{(k)} \rceil ; \quad \rho_m^{(k)} = \text{sign}(X_m^{(k)} - x\_pam_m^{(k)}) \quad (5.23)$$

At the  $k$ -th layer, the input of the function “decide” consists of  $R^{(k)}$  and  $E^{(k)}$ . The outputs consists of the  $M$ -dimensional vectors  $\text{nextpos\_pam}^{(k)}$ ,  $X^{(k)}$  and  $x\_pam^{(k)}$  whose  $m$ -th components are given in eq. (5.20), eq. (5.22) and eq. (5.23) respectively.  $x\_pam^{(k)}$  contains the coordinates of the first node to be visited at the  $M$  levels of the  $k$ -th layer (if these layers are consider separately).  $\text{nextpos\_pam}^{(k)}$  stores the distance corresponding to these nodes while  $X^{(k)}$  is used to determine the SE span at the  $M$  levels. At this stage, we know simply the starting point of each one of the  $M$  levels as well their corresponding SE enumerations without taking into account the possibility of passing from one level to another during the joint  $M$ -dimensional span (for example, in Fig. 5.4, when passing from (2) → (3), (5) → (6), (6) → (7) and (7) → (8)).

In addition to  $\text{nextpos\_pam}^{(k)}$ ,  $X^{(k)}$  and  $x\_pam^{(k)}$ , the function “decide” returns the scalars  $pos$  and  $amp$  that correspond to the position and the amplitude of the closest lattice point respectively. The pseudo code of the function “decide” is given by:

**decide** (Input:  $Y, R, M'$ . Output:  $pos, amp, x\_pam, X, \text{nextpos\_metric}$ )

$$\begin{aligned} Y_1 &= R^T Y ; \quad \tilde{Y}_1 = \text{diag}(Y_1) \\ Y_2 &= \text{Diag}(R^T R) ; \quad \tilde{Y}_2 = \text{diag}(Y_2) \\ X &= \text{Diag}(\tilde{Y}_1 (\tilde{Y}_2)^{-1}) \\ x\_pam &= 2\text{round}\left(\frac{X + M' - 1}{2}\right) - M' + 1 \\ x\_pam &= \max(1 - M', x\_pam) ; \quad x\_pam = \min(M' - 1, x\_pam) \\ \text{nextpos\_metric} &= -2\text{Diag}(\tilde{Y}_1 \text{diag}(x\_pam)) + \text{Diag}(\tilde{Y}_2 (\text{diag}(x\_pam))^2) \\ pos &= \arg \min(\text{nextpos\_metric}) ; \quad amp = x\_pam(pos) \end{aligned}$$

In what follows, the variables  $step$ ,  $flag1$  and  $flag$  are  $M \times P$  matrices. At the  $k$ -th layer  $step_{:,k}$  is a  $M$ -dimensional vector that permits to determine, at each one of the  $M$  levels, the difference between the next generated node and the current node. Throughout the algorithm,  $step$  is permanently modified to assure that  $x\_pam_{m,k} + step_{m,k}$  (the next node) is always a valid PAM symbol when  $x\_pam_{m,k}$  (the current node) is valid. This constraint is added since, as explained earlier, only valid points must be considered. Note that  $step_{m,k}$  can be equal to zero. In this case, performing  $x\_pam_{m,k} + step_{m,k}$  permits to pass to the  $m$ -th level (from anyone of the other  $M - 1$  levels). Once the  $m$ -th component is allowed to have a nonzero value,  $step_{m,k}$  is updated according to:

$$\left\{ 2\rho_m^{(k)}, -4\rho_m^{(k)}, 6\rho_m^{(k)}, \dots, i\rho_m^{(k)}, -2\text{sign}(i\rho_m^{(k)}), \dots, -2\text{sign}(i\rho_m^{(k)}) \right\} \quad (5.24)$$

where  $\rho_m^{(k)}$  is defined in eq. (5.23).  $i$  is the integer for which  $x\_pam_{m,k} + i\rho_m^{(k)}$  falls outside the boundaries of the PAM constellation for the first time. When this happens,  $flag1_{m,k}$  is set to zero. In this case, for

testing the remaining nodes, we fix  $step_{m,k} = -2\text{sign}(i\rho_m^{(k)})$ . When  $x\_pam_{m,k} + step_{m,k}$  falls outside the boundaries for the second times, the spanning is stopped at the  $m$ -th level and we set  $flag_{m,k}$  to one. All the levels of the  $k$ -th layer are spanned when  $flag_{:,k} = \mathbf{1}_M$ . The pseudo code of the sphere decoder with  $M$ -PPM- $M'$ -PAM constellations is given by:

**SE with PPM-PAM** (Input:  $z, R, P, M, M', C$ . Output:  $\hat{a}$ )

**Step 1:** Set  $k = P + 1$ ,  $dist(k) = 0$ ,  $V = R^{-1}$ ,  $\rho = \mathbf{0}_M$ ,  $bestdist = C$  (sphere squared radius). Let  $C_0$  be a very large positive number.

**Step 2:**  $newdist = dist(k) + \rho^T \rho$ ,  
if ( $newdist < bestdist$ )&( $k \neq 1$ ) go to Step 3 else go to Step 4 endif.

**Step 3:** if  $k = P + 1$ ,  $e_{:,k-1} = Vz$  else  
for  $i = 1, \dots, k - 1$ ,  $e_{:,k-1}^{(i)} = e_{:,k}^{(i)} - V^{(i,k)}\rho$  endfor endif.  
 $k = k - 1$ ,  $dist(k) = newdist$ ,  $E_{:,k}^{(k)} = R^{(k,k)}e_{:,k}^{(k)}$   
 $[pos(k), amp(k), x\_pam_{:,k}, X_{:,k}, nextpos\_metric_{:,k}] = \text{decide}(E_{:,k}^{(k)}, R^{(k,k)}, M')$   
 $x_{:,k} = amp(k)I_{:,pos(k)}$   
 $step_{:,k} = \mathbf{0}_M$ ,  $step_{pos(k),k} = 2\text{sign}(X_{step(k),k} - x_{step(k),k})$   
 $flag_{:,k} = \mathbf{0}_M$ ,  $flag1_{:,k} = \mathbf{1}_M$   
if ( $x\_pam_{pos(k),k} + step_{pos(k),k} < 1 - M'$ ) or ( $x\_pam_{pos(k),k} + step_{pos(k),k} > M' - 1$ ),  
 $step_{pos(k),k} = -2\text{sign}(step_{pos(k),k})$ ,  $flag1_{pos(k),k} = 0$  endif  
 $\rho = E_{:,k}^{(k)} - amp(k)R_{:,pos(k)}^{(k,k)}$  go to Step 2.

**Step 4:** if  $newdist < bestdist$ , for  $i = 1, \dots, P$ ,  $\hat{a}^{(i)} = x_{:,i}$  endfor  
 $bestdist = newdist$  elseif  $k = P$ , terminate else  $k = k + 1$  endif.  
if  $\prod_{m=1}^M flag_{m,k} = 1$  go to Step 4 endif

**generate the next node:**

$$\begin{aligned} nextpos\_metric_{step(k),k} = & -2 \left( R_{:,pos(k)}^{(k,k)} \right)^T E_{:,k}^{(k)} (x\_pam_{pos(k),k} + step_{pos(k),k}) \\ & + \left( \left( R_{:,pos(k)}^{(k,k)} \right)^T R_{:,pos(k)}^{(k,k)} \right) (x\_pam_{pos(k),k} + step_{pos(k),k})^2 + C_0 flag_{pos(k),k} \end{aligned}$$

$$\begin{aligned} pos(k) &= \arg \min_{m=1, \dots, M} (nextpos\_metric_{m,k}) \\ x\_pam_{pos(k),k} &= x\_pam_{pos(k),k} + step_{pos(k),k} \\ \text{if } step_{pos(k),k} &= 0, step_{pos(k),k} = 2\text{sign}(X_{pos(k),k} - x\_pam_{pos(k),k}) \text{ else} \end{aligned}$$

$$step_{pos(k),k} = (-1)^{flag1_{pos(k),k}} step_{pos(k),k} - 2flag1_{pos(k),k} \text{sign}(step_{pos(k),k})$$

endif.  
if ( $x\_pam_{pos(k),k} + step_{pos(k),k} < 1 - M'$ ) or ( $x\_pam_{pos(k),k} + step_{pos(k),k} > M' - 1$ )  
if  $flag1_{pos(k),k} \neq 0$ ,  $flag1_{pos(k),k} = 0$ ,  $step_{pos(k),k} = -2\text{sign}(step_{pos(k),k})$  else  $flag_{pos(k),k} = 1$  endif.  
if ( $x\_pam_{pos(k),k} + step_{pos(k),k} < 1 - M'$ ) or ( $x\_pam_{pos(k),k} + step_{pos(k),k} > M' - 1$ ),  $flag_{pos(k),k} = 1$  endif endif.

$$amp(k) = x\_pam_{pos(k),k}, x_{:,k} = amp(k)I_{:,pos(k)}, \rho = E_{:,k}^{(k)} - amp(k)R_{:,pos(k)}^{(k,k)}$$

go to Step 2.

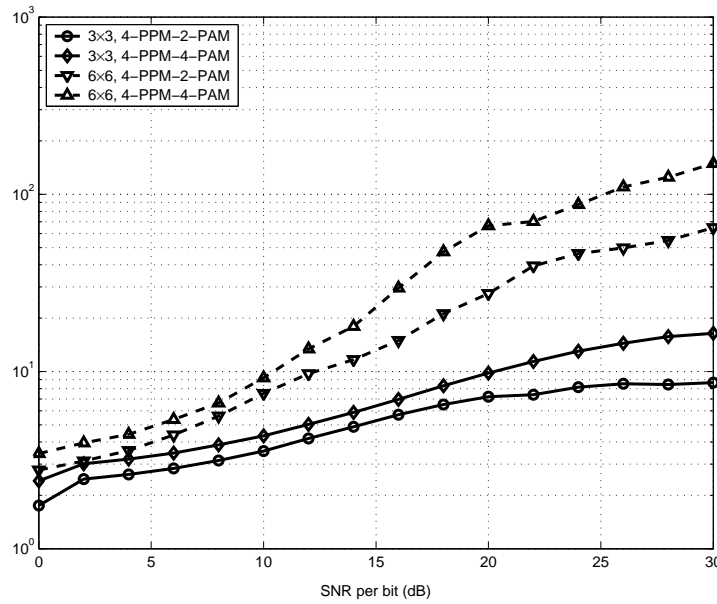


Figure 5.5: Convergence of SE with respect to algorithm 2 with a 1-finger PRake on CM2.

Lines 8 and 9 of Step 3 as well as lines 11 – 14 of Step 4 assure that the next node does not fall outside the boundaries of the PAM constellation. This is why  $\text{nextpos\_metric}_{\text{pos}(k),k}$  can be evaluated at the fourth and fifth lines of Step 4. At these lines, having  $\text{flag}_{\text{pos}(k),k}$  equal to one avoids spanning the level  $\text{pos}(k)$  of the  $k$ -th layer. Updating  $\text{step}_{\text{pos}(k),k}$  as in the ninth line of Step 4 permits to generate the enumeration given in eq. (5.24).

In Fig. 5.5, we compare the convergence times of the SE and algorithm 2 with 4-dimensional constellations. Simulations are performed over CM2 with  $P \times P$  uncoded MIMO UWB systems and a 1-finger PRake. The initial sphere radius is set to infinity in both cases. The ordinate corresponds to  $t_2/t_{\text{SE}}$  where  $t_2$  and  $t_{\text{SE}}$  are the convergence times of algorithm 2 and the SE respectively. The superiority of the SE is evident especially for large dimensions (the dimensionality is equal to  $4P$ ).

#### 5.4.4 SE with a Fano-like metric bias

The complexity of the sphere decoders can become excessively high especially at low signal to noise ratios. For these SNRs, the first node, corresponding to the babai point (or the output of a ZF-DFE receiver), can be very far from the closest node. Therefore, the algorithm will zigzag between a large number of nodes before reaching the ML solution. The convergence of the sphere decoders can be enhanced by enhancing the quality of the first checked node. For example, the first checked point can correspond to a MMSE-DFE receiver rather than a ZF-DFE receiver. This approach can result in some performance losses (especially at low SNRs) since the resulting noise term has a non-Gaussian component. However, MMSE-DFE preprocessing can be beneficial since very important enhancements in the convergence time can be obtained at the expense of limited performance losses [104]. In the same way, a V-BLAST-like ordering can be applied on the columns of the channel matrix in order to have the best possible decisions at the lower layers [112]. For PPM and PPM-PAM constellations, this ordering must be applied on groups of  $M$  columns (refer to section 5.2).

Another possible simplification is by spanning limited parts of the set of admissible values at the

different layers. The smaller the number of spanned points is (especially at lower levels), the lower the complexity of the resulting decoder. The authors of [103] proposed relating the length of the spanned intervals to the noise variance and the channel matrix by using a Fano-like metric bias. For PAM constellations, define the sequence  $\{F_k\}_{k=1}^P$  by:

$$F_k = F_{k-1} + \alpha \sigma^2 V_{k-1,k-1} ; \quad k = 2, \dots, P \quad (5.25)$$

where  $F_1 = 0$ ,  $\sigma^2$  is the noise variance and  $V = R^{-1}$ . The scalar  $\alpha \in [0, 1]$  controls the achieved compromise between complexity and performance. The modifications of the algorithm given in section 5.4.1 are straightforward. Step 2 of the considered algorithm is now replaced by:

**Step 2:**  $newdist = dist(k) + \rho^2$ ,  $fanodist = newdist + F_k$   
 if ( $fanodist < bestdist$ )&( $k \neq 1$ ) go to Step 3 else go to Step 4 endif.

In the same way the first line of Step 4 is replaced by:

if  $fanodist < bestdist$  ...

The same modifications can be applied on the algorithms given in section 5.4.2 and section 5.4.3 and used for the detection of PPM and PPM-PAM constellations respectively. In this case, the sequence  $\{F_k\}$  is determined from:

$$F_k = F_{k-1} + \alpha \sigma^2 \sum_{m=1}^M V_{(k-2)M+m, (k-2)M+m} ; \quad k = 2, \dots, P \quad (5.26)$$

with  $F_1 = 0$ .

## 5.5 Numerical Results

In this section, we perform computer simulations in order to compare the complexity and performance of SE and the associated decoder with the Fano metric. We also compare the MMSE-DFE and ZF-DFE preprocessing. In what follows, we fix  $\alpha = 0.5$  in eq. (5.26) and no column ordering is performed.

We first consider spatial multiplexing with 4-PPM-4-PAM constellations over CM2. 5 transmit antennas, 5 receive antennas and a 1-finger PRake are used. Note that in this case, the decoding process consists of searching for the closest point among  $2^{20}$  valid points in a signal space of dimension 20. The resulting SER curves are shown in Fig. 5.6. The complexity is measured by the average number of evaluations of Step 2 (of the algorithm given in section 5.4.3) per transmitted symbol vector. This complexity is plotted in Fig. 5.7 as a function of the SNR. Results show that the performance losses resulting from using the Fano metric are small especially at high SNRs. For example, with ZF-DFE at an error rate of 0.3, the SE decoder with the Fano metric results in a loss of about 0.5 dB while converging three times faster than the SE decoder. For the SE, applying MMSE-DFE results in a performance loss of about 0.7 dB at high SNRs. However, MMSE-DFE significantly decreases the number of visited lattice points.

The same simulation setup is repeated in Fig. 5.8 and Fig. 5.9 but with the diversity scheme using the modified Hermite pulses (refer to section 3.1). In this case, the better conditioned channel matrix at the receiver side reduces the complexity of the decoders. The SE has practically the same performance as the SE with the Fano metric with both ZF-DFE and MMSE-DFE. For the SNRs higher than 15 dB, the babai point corresponds to the closest lattice point and the different algorithms have the same complexity.

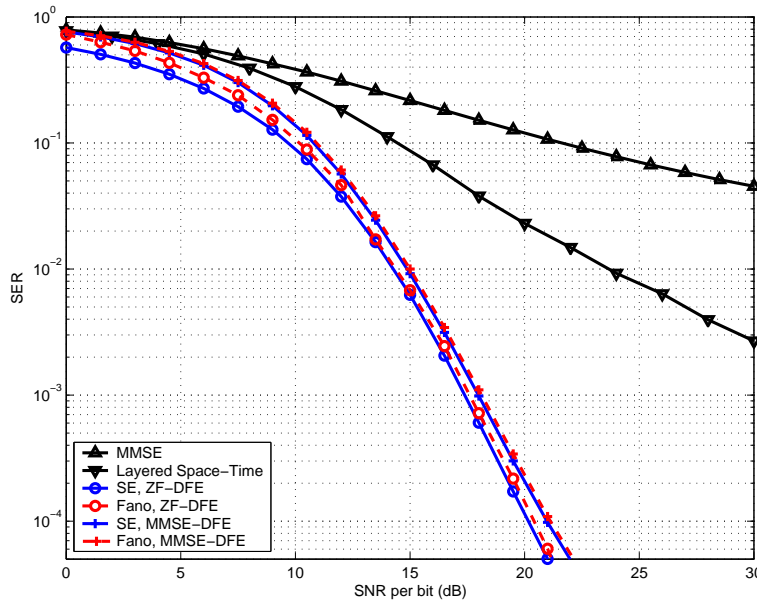


Figure 5.6: Performance of spatial multiplexing with 5 transmit antennas, 5 receive antennas and a 1-finger PRake on CM2. A 4-PPM-4-PAM constellation is used.

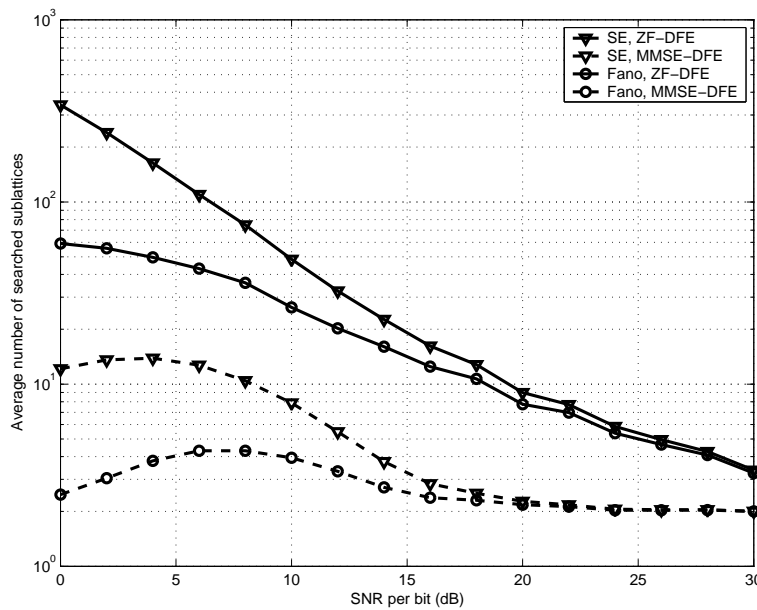


Figure 5.7: Complexity of the decoding algorithms with 4-PPM-4-PAM, 5 transmit antennas, 5 receive antennas and a 1-finger PRake on CM2. Spatial multiplexing is used.

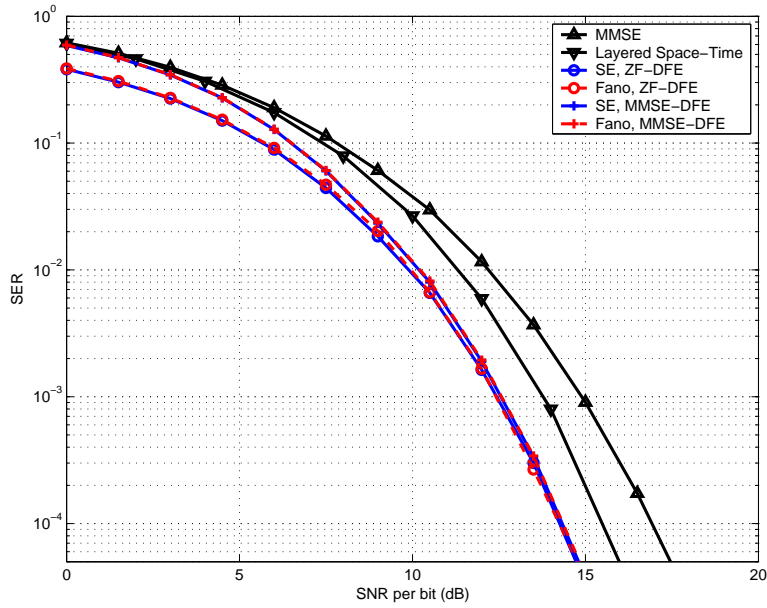


Figure 5.8: Performance of the diversity scheme using modified Hermite pulses on CM2. A 4-PPM-4-PAM constellation is used with 5 transmit antennas, 5 receive antennas and a 1-finger PRake.

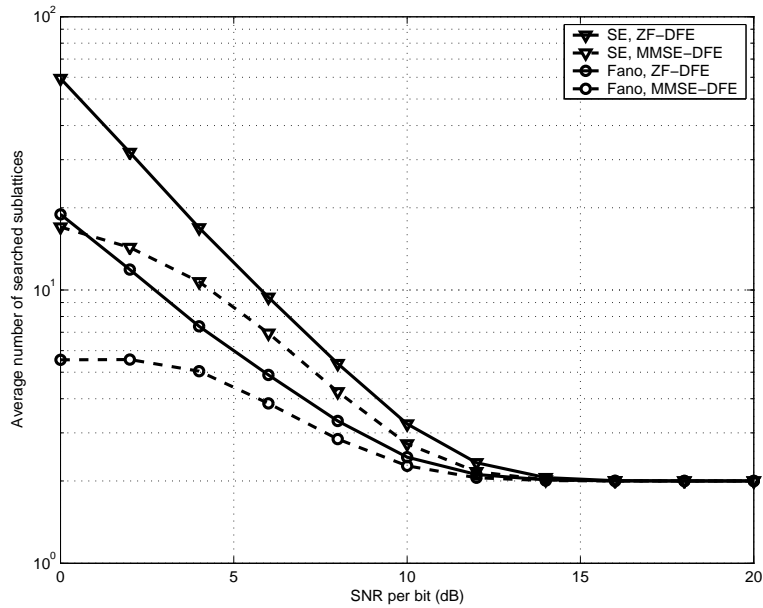


Figure 5.9: Complexity of the decoding algorithms with 4-PPM-4-PAM, 5 transmit antennas, 5 receive antennas and a 1-finger PRake on CM2. The diversity scheme using modified Hermite pulses is applied.



# Conclusion and Perspectives

In this work, we studied space-time coded impulse radio systems over highly frequency selective multi-antenna channels as a possible candidate solution for future broadband wireless personal area networks. Nonconventional modulation schemes that were exclusive to optical communication systems are now used over radio frequencies necessitating the design of new coding schemes that can combine the advantages of impulse radio and multi-antenna communications.

In particular, we presented the design of appropriate full rate and fully diverse ST codes with any number of transmit antennas. The advantage of such an approach is that a user located very close to an access point can exploit the multiplexing benefits, while a user at farther locations may benefit from an enhanced diversity order as well. For very high data rate systems that do not employ any pulse repetitions, these benefits are obtained at the expense of a more powerful software processing (ISC in section 3.2) or a more sophisticated RF circuitry (the use of Hermite pulses in section 3.1). For more conventional high data rate systems that perform coherent integrations, the decoding complexity is the same as that of spatial multiplexing thanks to the proposed inter-pulse coded schemes. For these schemes, an additional robustness against multiple access interference was obtained via the design of simple and efficient low-dimensional amplitude-randomizing matrices that can be used in conjunction with the time hopping sequences.

For PPM and PPAM constellations, we proposed novel coding schemes that are based on “position permutation” (construction 1 in section 3.4.1) and “position combining” (construction 2 in section 3.4.2). These modulation-specific codes have the additional advantages of being energy-efficient and information lossless and they outperform the classical approach of constructing totally-real ST codes based on cyclic division algebras. Since practical UWB systems are expected to associate PPM with PAM constellations having limited number of amplitude levels (in other words PPM or biorthogonal PPAM), the modulation-specific codes that do not have a non-vanishing determinant become particularly appealing. The totally-real modulation-specific codes are capable in delivering the same performance levels as the complex-valued perfect codes for sufficiently high dimensional constellations.

The principles of inter-symbol coding, inter-pulse coding and modulation-specific coding were further extended to the construction of distributed ST schemes for the nonorthogonal amplify-and-forward cooperation strategy with any number of relays. Furthermore, “position permutation” was shown to be sufficient for achieving full diversity with all PPM and PPAM constellations. Moreover, the modulation-specific ST codes and distributed AF ST codes turned out to be optimal with binary PPM (in the sense of maximizing the coding gain). New decode-and-forward strategies were also proposed for coherent, non-coherent and differential UWB systems. Studying the achieved diversity-multiplexing tradeoffs and error rates over realistic indoor UWB channels showed that exploiting the spatial diversity in a co-located or distributed manner can be very beneficial to IR-UWB systems.

We also considered the problems related to the receiver design and decoding algorithms. The ISI and MUI were included in the presented system model which permitted to evaluate the performance of dense and high data rate UWB networks. As for the decision block, we proposed to modify the sphere decoding algorithm to efficiently decode the nonlinear sparse multi-dimensional PPM and PPAM constellations. We also presented the performance of sub-optimal linear decoders that are appealing with correlation receivers that suffer from limited co-channel interference. An analytical analysis over the IEEE 802.15.3a channel models permitted to have more insights on the implications of these channels on the performance of single-antenna as well as multi-antenna UWB systems. While the presented analysis and code construction was limited to TH-UWB, the extension to DS-UWB is straightforward.

The realized work has given rise to a certain number of open questions that are worth to be considered in future work. The future research perspectives include the following aspects:

- MIMO-UWB radio channels are much less understood than the traditional single-antenna UWB channels. While the proposed codes were considered assuming uncorrelated sub-channels, the impact of the spatial correlation on the code design and system performance can be evaluated when an appropriate and a widely approved MIMO-UWB channel model is adopted. In this case, the impact of the relative delays between the first arriving multi-path components on the system performance can be also determined. The statistics over the new channel models can be further exploited for an appropriate design of two dimensional selective Rake receivers that enhance the energy capture.
- While we presented aspects related to the physical layer of cooperative UWB systems, the cross layer design can give more insights on the studied problem. For example, the important localization capabilities of IR-UWB systems can be exploited to optimize the choice of the cooperating relays and to determine the number of relays that is sufficient to achieve a certain compromise between performance and complexity.
- Optimizing the mapping of the information bits on the PPM or PPAM symbols. In this case, serial concatenation schemes based on turbo codes or LDPC codes and using the proposed ST block codes as inner codes can be evaluated. In this case, an iterative decoder is used at the receiver side and an analysis of the Extrinsic Information Transfer (EXIT) chart determines what mapping strategy to be adopted in order to accelerate the convergence of the considered schemes. The non-linearity of the PPM and PPAM constellations and the non-orthogonality of the ST codes render this problem a non-trivial one. Moreover, efficient lattice reduction techniques and trellis coding schemes that were recently proposed for the Golden code may be extended to the new modulation-specific codes that have a layered structure.

## Appendix A

# SIMO-UWB channel measurements and characterization

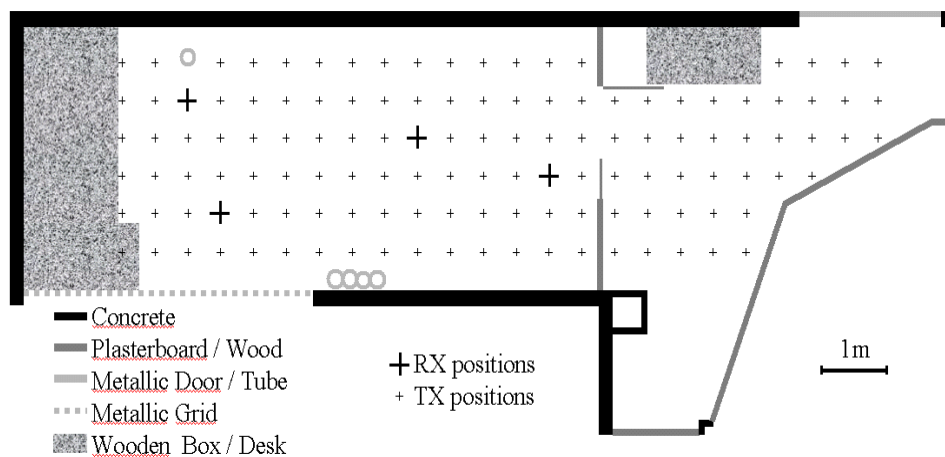


Figure A.1: Map of the explored environment.

A total number of about 100 SIMO channel measurements were performed in a line-of-sight (LOS) condition. The limited number of measured channels does not permit the construction of a statistical multi-antenna UWB channel model. However, these measurements are sufficient for highlighting some important aspects concerning the general behavior of multi-antenna UWB channels. In particular, we are interested in characterizing the fading margins and the spatial correlations of these channels.

The explored environment corresponds to a typical laboratory/industrial environment of approximately  $4 \times 14\text{m}^2$ . The ceiling (3 m) is composed of iron sheets and metallic beams. The floor and the walls are constructed from concrete materials. The room is quite empty except for the presence of some metallic elements. A map of this environment is presented in Fig. A.1. The receiver is fixed at one of the four positions represented by the bold points while the transmitter is moved on the remaining positions.

The transmitted pulse occupies the bandwidth [3.1 4.5] GHz. At the receiver side, an array of 4 antennas is used. The diameter of the ground plane is equal to 80 mm and the antennas are separated by a distance of 85 mm. Given that the four receiver branches are not perfectly identical, all the elements involved in the receiver link before the oscilloscope are deconvoluted out from the measurements (cables

and low noise amplifiers). Therefore, the measurements correspond to the convolution of the physical channel with a reference signal that corresponds to the convolution of the impulse responses of the transmit and receive antennas. This reference signal has a duration of 2 ns approximately.

We first determine the fading margin. Among the four measured sub-channels corresponding to a certain position of the transmitter and the receiver, we determine the ratio between the maximal value and minimal value of the energy integrated over a duration  $T_i$ . The variance of this ratio, calculated over all pairs of transmitter and receiver positions, corresponds to the fading margin. The fading margin versus  $T_i$  is plotted in Fig. A.2. Results show that the fading margin is not negligible for small integration times. In particular, a practical Rake receiver with 5 fingers ( $T_i = 10$  ns) suffers from a fading margin of about 3 dB even in LOS situations. On the other hand, spatial diversity is not very beneficial with very high order Rakes that profit from an important multi-path diversity.

The spatial correlation between the different antennas is plotted in Fig. A.3. In particular, we determine the cross-correlation coefficients among the side antennas (separated by 25.5 cm) and among adjacent antennas (separated by 8.5 cm). Results show that the entire channel responses present very low correlation levels. However, given that the channels are LOS, the first arriving parts of the received signals (corresponding to the strongest multi-path components) are more correlated than the other parts of the signals. The relatively low spatial correlation shows that spatial diversity can be beneficial for UWB systems.

The channel impulse response is divided into small time intervals called “bins” of 2 ns corresponding to the duration of the reference signal. We next analyze the spatial correlation between the different time bins. This is an important indicator on the performance of PRake receivers when extended to multi-antenna situations. To derive this kind of information, each bin is correlated with the reference signal.

For the  $l$ -th bin and the  $n$ -th SIMO channel realization, designate by  $g_{i,l}^{(n)}(\tau)$  the result of this correlation at the  $i$ -th receive antenna ( $i = 1, \dots, 4$ ) and let:

$$\Delta_{i,l}^{(n)} = \arg \max_{\tau \leq T_w} |g_{i,l}^{(n)}(\tau)| \quad (\text{A.1})$$

where  $T_w = 2$  ns is the duration of the reference signal.

The correlation between the signal at the output of the  $l$ -th Rake finger of the  $i$ -th receive antenna and the signal at the output of the  $l$ -th finger of the  $j$ -th receive antenna is given by:

$$r_{i,j,l} = \frac{E \left[ \Delta_{i,l}^{(n)} \Delta_{j,l}^{(n)} \right]}{\left( E \left[ \left( \Delta_{i,l}^{(n)} \right)^2 \right] E \left[ \left( \Delta_{j,l}^{(n)} \right)^2 \right] \right)^{\frac{1}{2}}} \quad (\text{A.2})$$

where the average is determined over the SIMO channel realizations (the superscript  $n$ ).

Fig. A.4 presents the average of  $r_{i,j,l}$  over the receive antennas  $i$  and  $j$  that are separated by 8.5 cm, 17 cm and 25.5 cm. Given that the channels are LOS and due to the presence of a dominant first path in the first bin of the different channel impulse responses, the first bins show relatively high correlation levels in the order of 0.6. Starting from the second bin, the correlation between the outputs of the Rake receivers falls below 0.4 for different antenna separations. The behavior is similar with different antenna separations showing the inutility of separating the receive antennas by more than 8.5 cm. Note that the results were presented in LOS conditions that correspond to the worst case situation (in what concerns spatial correlation). NLOS channels are expected to show lower correlations.

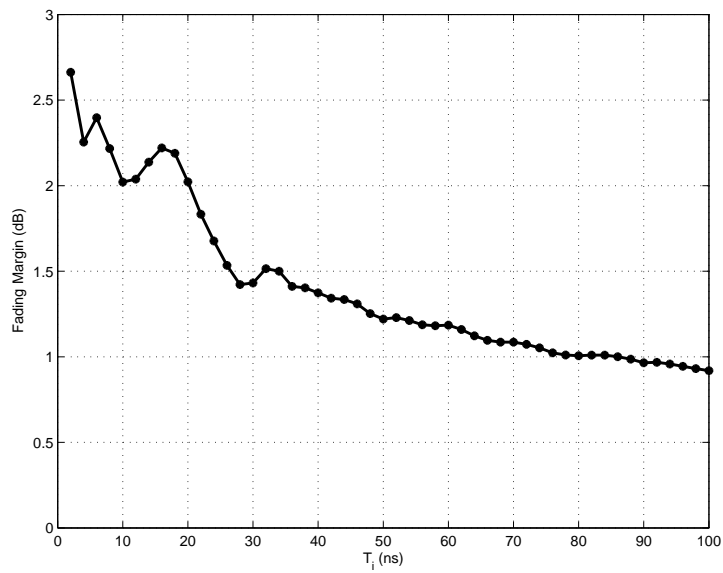


Figure A.2: Fading margin over a 4-element linear antenna array of length 25.5 cm.

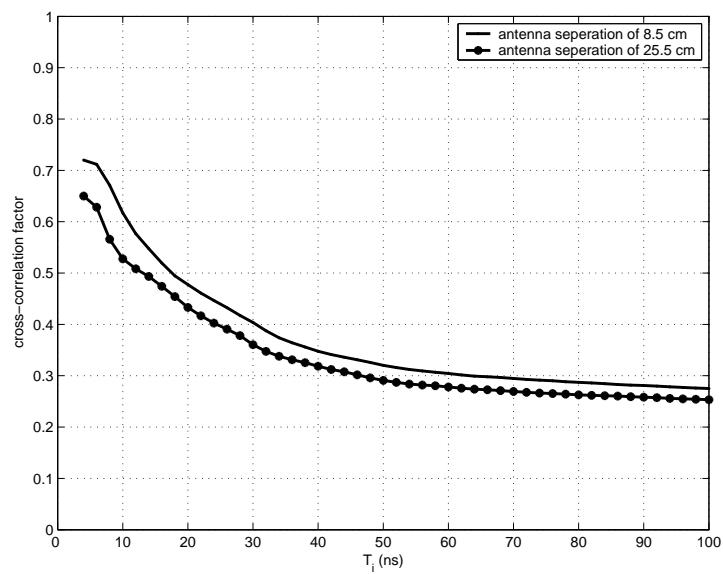


Figure A.3: Spatial correlation among the channels received by two antennas separated by 8.5 cm and 25.5 cm respectively.

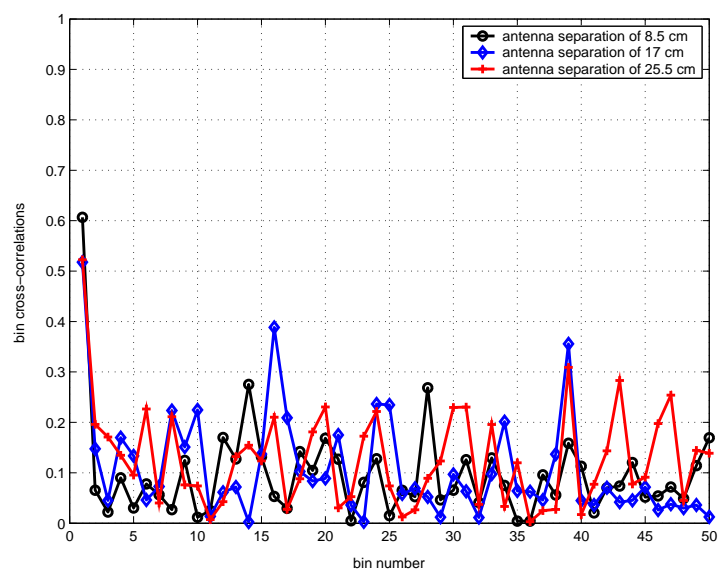


Figure A.4: Spatial correlation among the signals at the output of a Rake receiver.

## Appendix B

# Performance of bi-orthogonal Signalling

From eq. (2.39), the  $M$  decision variables are given by:

$$x_{m'} = X_{m'-m}s_m + n_{m'} \quad (\text{B.1})$$

where  $X_m = \sum_{q=1}^Q \sum_{p=1}^P \alpha_{q,p,m}$ . From eq. (2.38), the joint probability density function of the noise is given by:

$$p(n_m, n_{m'}) = \frac{1}{2\pi\sigma^2\gamma} \exp\left(\frac{-n_m^2 + 2\rho_{m,m'}n_m n_{m'} - n_{m'}^2}{2\sigma^2\gamma^2}\right)$$

where  $\rho_{m,m'} = \frac{\sum_{q,p} \alpha_{q,p,m-m'}}{\sum_{q,p} \alpha_{q,p,0}} = \frac{X_{m-m'}}{X_0}$ ,  $\gamma = \sqrt{1 - \rho_{m,m'}^2}$  and  $\sigma^2 = \frac{PN_0}{2E_s}X_0$ .

Apply the following transformation on the Gaussian random variables  $n_m$  and  $n_{m'}$ :

$$\begin{bmatrix} u \\ v \end{bmatrix} = \frac{1}{\sqrt{2}} \begin{bmatrix} 1 & 1 \\ 1 & -1 \end{bmatrix} \begin{bmatrix} n_{m'} \\ n_m \end{bmatrix} \quad (\text{B.2})$$

then  $u$  and  $v$  are zero-mean independent Gaussian random variables whose variances are given by:

$$\sigma_u^2 = \sigma^2(1 + \rho_{m,m'}) = \frac{PN_0}{2E_s}(X_0 + X_{m-m'}) \quad (\text{B.3})$$

$$\sigma_v^2 = \sigma^2(1 - \rho_{m,m'}) = \frac{PN_0}{2E_s}(X_0 - X_{m-m'}) \quad (\text{B.4})$$

The conditional error probability of  $M$ -PPM-2-PAM constellations can be determined from:

$$P_{e/H} = \frac{1}{2M} \sum_{b=\pm 1} \sum_{m=0}^{M-1} P_{e/(H, s_m=b)} \quad (\text{B.5})$$

where  $P_{e/(H, s_m=b)}$  corresponds to the probability of erroneous detection when a pulse with amplitude  $b = \pm 1$  was transmitted during the  $m$ -th modulation position. Following from the amplitude symmetry of the bi-orthogonal PPAM constellation, eq. (B.5) simplifies to:

$$P_{e/H} = \frac{1}{M} \sum_{m=0}^{M-1} P_{e/(H, s_m=1)} \leq \frac{1}{M} \sum_{m=0}^{M-1} P_{e/H}^{(m)} \quad (\text{B.6})$$

where  $P_{e/H}^{(m)}$  is given by:

$$\begin{aligned} P_{e/H}^{(m)} &= P_{e/H}(s_m = 1 \rightarrow s_m = -1) + \sum_{m'=0, m' \neq m}^{M-1} P_{e/H}(s_m = 1 \rightarrow s_{m'}) \\ &= p(x_m \leq 0, s_m = 1) + \sum_{m'=0, m' \neq m}^{M-1} p(|x_{m'}| \geq |x_m|, s_m = 1) \end{aligned} \quad (\text{B.7})$$

$$= Q\left(\sqrt{\frac{2E_s X_0}{PN_0}}\right) + I_1 + I_2 \quad (\text{B.8})$$

where:

$$\begin{aligned} I_1 &= p(x_{m'} \leq x_m \leq -x_{m'} ; x_{m'} \leq 0 ; s_m = 1) \\ &= \int_{-\infty}^{-X_{m'-m}} \int_{X_{m'-m}-X_0+n_{m'}}^{-X_{m'-m}-X_0-n_{m'}} p(n_m, n_{m'}) d_{n_m} d_{n_{m'}} \\ &= \int_{-\infty}^{-\frac{X_{m'-m}+X_0}{\sqrt{2}}} p(u) d(u) \int_{-\infty}^{\frac{X_0-X_{m'-m}}{\sqrt{2}}} p(v) d(v) \end{aligned} \quad (\text{B.9})$$

$$= Q_{m,m'}^{(1)} \left(1 - Q_{m,m'}^{(2)}\right) \quad (\text{B.10})$$

where eq. (B.9) follows from Fig. B.1 and:

$$Q_{m,m'}^{(1)} = Q\left(\frac{X_0 + X_{m'-m}}{\sqrt{2}\sigma_u^2}\right) = Q\left(\sqrt{\frac{E_s(X_0 + X_{m'-m})}{PN_0}}\right) \quad (\text{B.11})$$

$$Q_{m,m'}^{(2)} = Q\left(\frac{X_0 - X_{m'-m}}{\sqrt{2}\sigma_v^2}\right) = Q\left(\sqrt{\frac{E_s(X_0 - X_{m'-m})}{PN_0}}\right) \quad (\text{B.12})$$

In the same way:

$$\begin{aligned} I_2 &= p(-x_{m'} \leq x_m \leq x_{m'} ; x_{m'} \geq 0 ; s_m = 1) \\ &= \int_{-X_{m'-m}}^{+\infty} \int_{-X_{m'-m}-X_0-n_{m'}}^{X_{m'-m}-X_0+n_{m'}} p(n_m, n_{m'}) d_{n_m} d_{n_{m'}} \\ &= \int_{-\frac{X_{m'-m}+X_0}{\sqrt{2}}}^{+\infty} p(u) d(u) \int_{\frac{X_0-X_{m'-m}}{\sqrt{2}}}^{+\infty} p(v) d(v) \end{aligned} \quad (\text{B.13})$$

$$= \left(1 - Q_{m,m'}^{(1)}\right) Q_{m,m'}^{(2)} \quad (\text{B.14})$$

Replacing equations (B.10), (B.11), (B.12) and (B.14) in eq. (B.8), we obtain:

$$P_{e/H}^{(m)} = Q\left(\sqrt{\frac{2E_s \sum_{q,p} \alpha_{q,p,0}}{PN_0}}\right) + \sum_{m'=0, m' \neq m}^{M-1} Q_{m,m'}^{(1)} + Q_{m,m'}^{(2)} - 2Q_{m,m'}^{(1)} Q_{m,m'}^{(2)} \quad (\text{B.15})$$

where  $Q_{m,m'}^{(1)}$  and  $Q_{m,m'}^{(2)}$  can be expressed in a more explicit form as:

$$Q_{m,m'}^{(i)} = Q\left(\sqrt{\frac{E_s \sum_{q,p} (\alpha_{q,p,0} + (-1)^{i-1} \alpha_{q,p,m-m'})}{PN_0}}\right) \quad (\text{B.16})$$

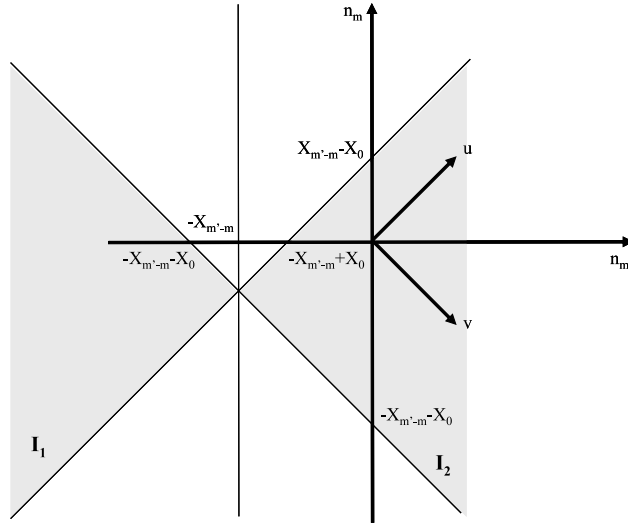


Figure B.1: The different integration areas.

$Q_{m,m'}^{(i)}$  depends uniquely on  $\alpha_{q,p,m-m'}$  and therefore on the difference between the pulse positions. Taking this into account, and summing up the terms corresponding to the same position difference, the conditional error probability in eq. (B.6) simplifies to:

$$P_{e/H} \leq Q \left( \sqrt{\frac{2E_s \sum_{q,p} \alpha_{q,p,0}}{PN_0}} \right) + \frac{2}{M} \sum_{m=1}^{M-1} (M-m) \left( p_m^{(1)} + p_m^{(2)} - 2p_m^{(1)} p_m^{(2)} \right) \quad (\text{B.17})$$

where:

$$p_m^{(i)} = Q \left( \sqrt{\frac{E_s \sum_{q,p} (\alpha_{q,p,0} + (-1)^{i-1} \alpha_{q,p,m})}{PN_0}} \right) \quad (\text{B.18})$$



## Appendix C

### -1 is not a norm in $\mathbb{Q}(\sqrt{3})$

For  $(\gamma, \theta, \theta_1) = (-1, 1 + \sqrt{3}, 1 - \sqrt{3})$ , the determinant of eq. (3.17) verifies:

$$\begin{aligned}\sqrt{13} \det(C_{2,eq}) &= a_1^2 + a_3^2 + 2(a_1 a_2 + a_3 a_4) - 2(a_2^2 + a_4^2) \\ &= (a^2 + c^2) - 3(b^2 + d^2)\end{aligned}\quad (\text{C.1})$$

where  $a = a_1 + a_2$ ,  $b = a_2$ ,  $c = a_3 + a_4$  and  $d = a_4$ .

In order to show that the minimum determinant of  $\frac{1}{\sqrt{13}}$  is achieved for all constellations, we need to prove that eq. (C.1) equals to zero for  $a, b, c, d \in \mathbb{Z}$  only when  $a = b = c = d = 0$ . Suppose that  $(a^2 + c^2) = 3(b^2 + d^2)$ , write  $a$  and  $c$  as:  $a = 3q_a + r_a$  and  $c = 3q_c + r_c$  with  $r_a, r_c \in \{0, 1, 2\}$ .  $3|a^2 + c^2 \Rightarrow 3|r_a^2 + r_c^2$ . It is straight forward to find that the only case where  $3|r_a^2 + r_c^2$  is  $r_a = r_c = 0 \Rightarrow 3|a, 3|c$  and  $9|a^2 + c^2$ . From eq. (C.1),  $9|a^2 + c^2 \Rightarrow 3|b^2 + d^2$  an in the same way  $3|b$  and  $3|d$ . Therefore,  $a, b, c, d$  are all divisible by 3. Writing  $a = 3a'$ ,  $b = 3b'$ ,  $c = 3c'$  and  $d = 3d'$ , we obtain an identical equation  $(a'^2 + c'^2) = 3(b'^2 + d'^2)$  where  $a', b', c', d' \in \mathbb{Z}$ . We can repeat the above operation and divide all parameters by 3 indefinitely. Therefore, the only possible solution is when  $a = b = c = d = 0 \Rightarrow a_1 = a_2 = a_3 = a_4 = 0$ . As a conclusion:

$$\delta_{min} = \min_{(0,0,0,0) \neq (a_1, a_2, a_3, a_4) \in \mathbb{Z}^4} |\det(C_{2,eq})| = \frac{1}{\sqrt{13}} \quad (\text{C.2})$$

since  $\sqrt{13} \det(C_{2,eq}) \in \mathbb{Z} \setminus \{0\}$  for  $(a_1, a_2, a_3, a_4) \neq (0, 0, 0, 0)$ .

Another more elegant solution consists of using the  $p$ -adic numbers [115] to show that there is no element  $x \in \mathbb{K}$  whose norm verifies  $N_{\mathbb{K}/\mathbb{Q}}(x) = -1$  where  $\mathbb{K} = \mathbb{Q}(\theta)$  with  $\theta = 1 + \sqrt{3}$ . Any element  $x \in \mathbb{K}$  can be written as  $x = a_1 + a_2\theta = a + b\sqrt{3}$  where  $a_1, a_2, a, b \in \mathbb{Q}$  with  $a = a_1 + a_2$  and  $b = a_2$ . We will show that the equation:

$$N_{\mathbb{K}/\mathbb{Q}}(x) = a^2 - 3b^2 = -1 \quad (\text{C.3})$$

has no solution in the field of 3-adic number  $\mathbf{Q}_3$  and consequently has no solution in  $\mathbb{K}$ . Let  $\mathbf{Z}_3 = \{x \in \mathbf{Q}_3, v_3(x) \geq 0\}$  be the valuation ring of  $\mathbf{Q}_3$  [115]. Using the embedding of  $\mathbb{Q}$  in  $\mathbf{Q}_3$ , eq. (C.3) can be written in  $\mathbf{Q}_3$  as:

$$a^2 - 3b^2 = 2 + 3x ; \quad a, b \in \mathbb{Q}, \quad x \in \mathbf{Z}_3 \quad (\text{C.4})$$

We take the valuations of both sides of eq. (C.4):

$$v_3(a^2 - 3b^2) = v_3(2 + 3x) \quad (\text{C.5})$$

to show that  $a$  and  $b$  must be in  $\mathbf{Z}_3$ . Since  $x \in \mathbf{Z}_3$ :

$$v_3(2+3x) \geq \min\{v_3(2), v_3(x)+1\} = 0 \quad (\text{C.6})$$

Since both valuations are distinct ( $v_3(2) = 0$  and  $v_3(x) \geq 0$ ), we have:

$$v_3(a^2 - 3b^2) \geq \min\{2v_3(a), 2v_3(b)+1\} = 0 \quad (\text{C.7})$$

Moreover we have equality since both valuations are distinct. Equation (C.7) holds if  $v_3(a) = 0$  which implies  $a \in \mathbf{Z}_3$  and consequently  $b \in \mathbf{Z}_3$ . Equation (C.4) can be now written as:

$$a^2 - 3b^2 = 2 + 3x ; \quad a, b, x \in \mathbf{Z}_3 \quad (\text{C.8})$$

Reducing eq. (C.8) modulo  $3\mathbf{Z}_3$ , we find that 2 should be a square in  $\text{GF}(3)$  which is a contradiction and therefore there are no elements  $a, b \in \mathbb{Q}$  that verify eq. (C.3).

## Appendix D

# Properties of construction 1

### D.1 Diversity Order

In this section, we determine the dimensions of the hybrid PPM-PAM constellation for which the code in eq. (3.48) is fully diverse for a given value of  $n$ .

Designate by  $\Delta C(X_1, \dots, X_n)$  the difference between two codewords having the structure given in eq. (3.48).  $X_i$  is a  $M$ -dimensional vector that can be written as:  $X_i = x_i^{(1)} - x_i^{(2)}$  where:

$$x_i^{(k)} = \sum_{j=0}^{n-1} x_{i,j}^{(k)} \theta^j ; k = 1, 2 \quad (\text{D.1})$$

where the vectors  $x_{i,j}^{(k)}$  belong to the  $M$ -PPM- $M'$ -PAM constellation  $C$  given in eq. (1.8) for  $k = 1, 2$ ,  $i = 1, \dots, n$  and  $j = 0, \dots, n-1$ . In other words, the vectors  $X_1, \dots, X_n$  belong to the set  $\mathcal{A}$  given by:

$$\mathcal{A} = \left\{ \sum_{j=0}^{n-1} (a_j - a'_j) \theta^j \mid a_0, a'_0, \dots, a_{n-1}, a'_{n-1} \in C \right\} \quad (\text{D.2})$$

The proof now consists of finding the set of values of  $M$  for which the following relation holds:  $\text{rank}(\Delta C(X_1, \dots, X_n)) = n$  for  $(X_1, \dots, X_n) \in \mathcal{A}^n \setminus \{(\mathbf{0}_M, \dots, \mathbf{0}_M)\}$ .

For an element  $k \in \mathbb{K} \mid k = \sum_{j=0}^{n-1} k_j \theta^j$ ,  $k_j \in \mathbb{Q}$  will be referred to as the  $j$ -th coordinate of  $k$ . In eq. (D.2),  $a_0, a'_0, \dots, a_{n-1}, a'_{n-1}$  are integer multiples of the columns of the  $M \times M$  identity matrix. Therefore, elements of  $\mathcal{A}$  have the property that at most two of their components can have their  $j$ -th coordinates different from zero for  $j = 0, \dots, n-1$ .

$\Delta C(X_1, \dots, X_n)$  will be referred to as  $\Delta C$  for simplicity.  $\text{rank}(\Delta C) < n$  if  $\exists k_1, \dots, k_{n-1}$  such that:

$$\Delta C_n = \sum_{i=1}^{n-1} k_i \Delta C_i \quad (\text{D.3})$$

where  $\Delta C_i$  is the  $i$ -th column of  $\Delta C$ . Moreover,  $k_1, \dots, k_{n-1} \in \mathbb{K}$  since all of the elements of  $\Delta C$  are in  $\mathbb{K}$ .

**Proposition D.1** *Equation (D.3) is verified if the vectors  $X_1, \dots, X_n$  verify the equation:*

$$\mathcal{M} X_i = \left( \sum_{j=0}^{n-1} \lambda_j \Omega^j \right) X_i = \mathbf{0}_M ; i = 1, \dots, n \quad (\text{D.4})$$

where  $\Omega$  is the permutation matrix given in eq. (3.50).  $\lambda_1, \dots, \lambda_{n-1} \in \mathbb{Q}$  and  $\lambda_0 = 1$  resulting in  $\mathcal{M} \in \mathbb{Q}^{M \times M}$ .

*Proof:* We first give an example with  $n = 3$ . Inserting eq. (3.48) in eq. (D.3), we obtain:

$$\begin{aligned} X_3 &= k_1 X_1 + k_2 X_2 \\ \sigma(X_2) &= \Omega k_1 \sigma(X_3) + k_2 \sigma(X_1) \\ \sigma^2(X_1) &= \Omega k_1 \sigma^2(X_2) + \Omega k_2 \sigma^2(X_3) \end{aligned}$$

Since the entries of  $\Omega$  are rational numbers, then  $\sigma(\Omega) = \Omega$  and the above equations can be written as:

$$\begin{aligned} X_3 &= k_1 X_1 + k_2 X_2 \\ X_2 &= \Omega \sigma^2(k_1) X_3 + \sigma^2(k_2) X_1 \\ X_1 &= \Omega \sigma(k_1) X_2 + \Omega \sigma(k_2) X_3 \end{aligned}$$

Solving these equations, we conclude that the vectors  $X_i$  for  $i = 1, \dots, 3$  must verify:

$$(I_M + \lambda_1 \Omega + \lambda_2 \Omega^2) X_i = \mathbf{0}_M \quad (\text{D.5})$$

$$\lambda_1 = -(\text{Tr}_{\mathbb{K}/\mathbb{Q}}(\sigma^2(k_1)k_2) + N_{\mathbb{K}/\mathbb{Q}}(k_2)) ; \lambda_2 = -N_{\mathbb{K}/\mathbb{Q}}(k_1) \quad (\text{D.6})$$

In the same way, with  $n = 4$  antennas, we have:

$$(I_M + \lambda_1 \Omega + \lambda_2 \Omega^2 + \lambda_3 \Omega^3) X_i = \mathbf{0}_M \quad (\text{D.7})$$

$$\begin{aligned} \lambda_1 &= -N_{\mathbb{K}/\mathbb{Q}}(k_3) - \text{Tr}_{\mathbb{K}/\mathbb{Q}}(k_1 \sigma(k_3)) - \text{Tr}_{\mathbb{K}/\mathbb{Q}}(k_2 \sigma(k_3) \sigma^2(k_3)) - \frac{1}{2} \text{Tr}_{\mathbb{K}/\mathbb{Q}}(k_2 \sigma^2(k_2)) \\ \lambda_2 &= N_{\mathbb{K}/\mathbb{Q}}(k_2) - \text{Tr}_{\mathbb{K}/\mathbb{Q}}(k_2 \sigma^2(k_1) \sigma^3(k_1)) - \text{Tr}_{\mathbb{K}/\mathbb{Q}}(k_2 \sigma(k_2) \sigma^3(k_1) \sigma^2(k_3)) \\ &\quad + \frac{1}{2} \text{Tr}_{\mathbb{K}/\mathbb{Q}}(\sigma(k_1) \sigma^3(k_1) k_3 \sigma^2(k_3)) \\ \lambda_3 &= -N_{\mathbb{K}/\mathbb{Q}}(k_1) \end{aligned}$$

We return now to the general case. The columns of  $\Delta C$  are considered as  $n$ -dimensional vectors composed of the parametric variables  $\Omega, X_1, \dots, X_n$  and their conjugates. Therefore, eq. (D.3) results in  $n$  linear equations. Taking the  $(n-i)$ -th conjugate of the  $i$ -th equation for  $i = 2, \dots, n$ , eq. (D.3) can be written as:

$$\underbrace{\begin{bmatrix} k_1 & k_2 & \cdots & k_{n-1} & -1 \\ \sigma^{n-1}(k_2) & \ddots & \sigma^{n-1}(k_{n-1}) & -1 & \Omega \sigma^{n-1}(k_1) \\ \vdots & \ddots & \ddots & \Omega \sigma^{n-2}(k_1) & \Omega \sigma^{n-2}(k_2) \\ \sigma^2(k_{n-1}) & -1 & \ddots & \ddots & \vdots \\ -1 & \Omega \sigma(k_1) & \Omega \sigma(k_2) & \cdots & \Omega \sigma(k_{n-1}) \end{bmatrix}}_R \begin{bmatrix} X_1 \\ X_2 \\ \vdots \\ X_{n-1} \\ X_n \end{bmatrix} = \mathbf{0}_{Mn} \quad (\text{D.8})$$

The last equation is verified if:

$$\det(R) X_i = \mathbf{0}_M ; i = 1, \dots, n \quad (\text{D.9})$$

when calculating the determinant,  $R$  is considered as a  $n \times n$  matrix and  $\Omega$  is taken as a parameter (rather than a  $M \times M$  matrix). By rearranging the rows of  $R$ , we obtain:

$$\det(R) = \det(\underbrace{[R_n^T, R_{n-1}^T, \dots, R_2^T, R_1^T]^T}_{R'}) = \det(R') \quad (\text{D.10})$$

where  $R_i$  is the  $i$ -th row of  $R$ .  $R'$  has the same structure as the matrix expression of the elements of a division algebra. In particular:

$$R' = C(-1, \sigma(k_1), \dots, \sigma(k_{n-1})) \quad (\text{D.11})$$

where the expression of  $C$  is given in eq. (1.20). From [39] and Proposition 1.1, the coefficients of the powers of  $\Omega$  in  $\det(C)$  are linear combinations of norms and traces that belong to  $\mathbb{Q}$ . Consequently, parameterized by  $\Omega$ ,  $\det(R)$  is a polynomial with rational coefficients having a degree of  $n - 1$ :

$$\det(R) = \sum_{i=0}^{n-1} \lambda_i \Omega^i ; \lambda_0, \dots, \lambda_{n-1} \in \mathbb{Q} \quad (\text{D.12})$$

Moreover, it can be easily shown that  $\lambda_0 = 1$  and  $\lambda_{n-1} = -N_{\mathbb{K}/\mathbb{Q}}(k_1)$ . Finally, replacing the parameter  $\Omega$  by its corresponding matrix form, we obtain eq. (D.4).

Consider the case  $M \geq n$ . The matrix  $\mathcal{M}$  in eq. (D.4) takes the form:

$$\mathcal{M} = \begin{bmatrix} 1 & 0 & \cdots & 0 & \lambda_{n-1} & \cdots & \lambda_1 \\ \lambda_1 & 1 & 0 & \cdots & 0 & \ddots & \vdots \\ \lambda_2 & \lambda_1 & 1 & 0 & \cdots & 0 & \lambda_{n-1} \\ \vdots & \ddots & \ddots & \ddots & \ddots & \ddots & \vdots \\ 0 & \lambda_{n-1} & \cdots & \lambda_1 & 1 & 0 & \vdots \\ \vdots & 0 & \lambda_{n-1} & \cdots & \lambda_1 & 1 & 0 \\ 0 & \cdots & 0 & \lambda_{n-1} & \cdots & \lambda_1 & 1 \end{bmatrix} \quad (\text{D.13})$$

where the number of zero entries in each row of  $\mathcal{M}$  is equal to  $M - n$ .

From eq. (D.13), it can be seen that the matrix composed of the first  $(M - n + 1)$  rows and the first  $(M - n + 1)$  columns of  $\mathcal{M}$  is a lower triangular matrix whose diagonal elements are all equal to 1. Therefore, its determinant is equal to 1 and consequently it has a rank of  $M - n + 1$ . Designate by  $r$  the rank of  $\mathcal{M}$ . Therefore,  $r \geq M - (n - 1)$ . In an equivalent manner:

$$r = M - k ; k \in \{0, 1, \dots, n - 1\} \quad (\text{D.14})$$

Since eq. (D.4) is valid for all values of  $i$ , we fix  $Y = X_i$ . Denote by  $Y_m$  the  $m$ -th component of  $Y$  for  $m = 1, \dots, M$ . The  $j$ -th coordinate of  $Y_m$  is denoted by  $Y_{m,j}$  for  $j = 0, \dots, n - 1$ .

For  $k = 0$ ,  $\mathcal{M} Y = \mathbf{0}_M \Rightarrow Y = \mathbf{0}_M$ . Therefore, the only matrix  $\Delta C$  that is rank deficient is the all-zero matrix.

For  $k = 1$ , the  $M$  components of  $Y$  can be determined from a single parameter  $t$ . Without loss of generality, we take  $t = Y_M$ . In this case,  $Y_m = \beta_m t$  with  $\beta_m \in \mathbb{Q}^*$  for  $m = 1, \dots, M - 1$  since  $\mathcal{M} \in \mathbb{Q}^{M \times M}$ .  $t = 0 \Rightarrow Y = \mathbf{0}_M$ . In other words, if one of the components of  $Y$  is equal to zero, then  $k = 1$  and  $\mathcal{M} Y = \mathbf{0}_M$  imply that  $Y = \mathbf{0}_M$ . For nonzero vectors, denote by  $Y_{M,j}$  the first non-zero coordinate of  $Y_M$  for a certain value of  $j \in \{0, \dots, n - 1\}$ . Since  $\beta_m \in \mathbb{Q}^*$ , all the components of  $Y$  will have their  $j$ -th coordinates different from zero. Therefore,  $Y$  will not belong to  $\mathcal{A}$  when  $M \geq 3$  since, from eq. (D.2), any element

of  $\mathcal{A}$  can have a maximum number of two components whose  $j$ -th coordinates are different from zero  $\forall j$ . Therefore, the only vector of  $\mathcal{A}$  that verifies  $\mathcal{M}Y = \mathbf{0}_M$  when  $r = M - 1$  is  $Y = \mathbf{0}_M$ . As a conclusion, when  $k = 1$ , the code is fully diverse for:

$$M \geq \max\{3, n\} \quad (\text{D.15})$$

as a special case, when  $n = 2$ , the code is fully diverse for  $M \geq 3$ .

For  $k > 1$ , the components of  $Y$  can be parameterized by  $k$  parameters. Without loss of generality, these parameters are taken to be equal to  $Y_{M-k+1}, \dots, Y_M$ . The other  $r$  parameters can be expressed as:

$$Y_m = \sum_{j=1}^k \beta_m^{(j)} Y_{M-k+j}; m = 1, \dots, r \quad (\text{D.16})$$

where  $\beta_m^{(1)}, \dots, \beta_m^{(k)}$  can not be equal to zero simultaneously for  $m = 1, \dots, r$ . We will consider the two following cases.

Case 1: Suppose that there is only one element among  $Y_{M-k+1}, \dots, Y_M$  that has its  $j$ -th coordinate different from zero for a given value of  $j$ . In other words, there are no two or more elements that have the same coordinate taking a nonzero value. Note that this can always happen since  $k \leq n - 1$ . Denote by  $j_l$  the first nonzero coordinate of  $Y_{M-k+l}$ . Among the first  $r$  components of  $Y$  there are  $r_l$  components whose  $j_l$ -th coordinates are not equal to zero with  $1 \leq r_l \leq r$  for  $l = 1, \dots, k$ . Along with  $Y_{M-k+l}$ , this results in a total of  $r_l + 1$  components of  $Y$  having their  $j_l$ -th components different from zero. The  $k$  coefficients  $\beta_m^{(1)}, \dots, \beta_m^{(k)}$  can not be all equal to zero simultaneously for a given value of  $m$  verifying  $1 \leq m \leq r$ . This implies that there are at least  $r$  nonzero coefficients among  $\beta_1^{(1)}, \dots, \beta_1^{(k)}, \dots, \beta_r^{(1)}, \dots, \beta_r^{(k)}$ . This results in:  $\sum_{l=1}^k r_l \geq r$ .

$Y$  will fall outside of  $\mathcal{A}$  (and consequently the code will be fully diverse) whenever  $\exists l \in \{1, \dots, k\} \mid r_l + 1 > 2$ . In this case, the maximum size of the constellation for which  $Y$  remains in  $\mathcal{A}$  corresponds to the case when  $r_l = 1$  for  $l = 1, \dots, k$ . Now,  $\sum_{l=1}^k r_l \geq r$  implies that  $k \geq r$ . Given that the maximal value of  $k$  is equal to  $n - 1$ ,  $Y$  falls outside of  $\mathcal{A}$  when  $r > k$  implying that:

$$M \geq 2n - 1 \quad (\text{D.17})$$

When considering the second case, we limit ourselves to the constellation sizes that respect eq. (D.17) (or equivalently  $r > k$ ).

Case 2: Following from the structure of  $\mathcal{A}$ , the complementary of case 1 takes place when there exist two distinct values  $k', k'' \in \{1, \dots, k\}$  such that  $Y_{M-k+k'}$  and  $Y_{M-k+k''}$  have their  $j$ -th coordinates different from zero for a certain value of  $j \in \{0, \dots, n - 1\}$ . Designate by  $\Upsilon$  the  $k \times k$  matrix whose  $(i, j)$ -th element is equal to  $\beta_i^{(j)}$  for  $i, j = 1, \dots, k$ .  $\Upsilon$  describes the linear dependence of the first  $k$  components of  $Y$  on  $Y_{M-k+1}, \dots, Y_M$ . Given the lower triangular structure of the matrix composed of the first  $k$  rows and  $k$  columns of  $\mathcal{M}$  and since  $r > k$ , this implies that  $\Upsilon$  has a rank  $k$ .

Among the first  $k$  components of  $Y$ , designate by  $r_1 \leq k$  the maximum number of components having their  $j$ -th components equal to zero simultaneously. Since the nonzero  $j$ -th coordinates are contained uniquely in  $Y_{M-k+k'}$  and  $Y_{M-k+k''}$ , this implies that there exists  $r_1$  indexes  $I(1), \dots, I(r_1)$  such that:

$$\beta_{I(i)}^{(k')} Y_{M-k+k',j} + \beta_{I(i)}^{(k'')} Y_{M-k+k'',j} = 0 ; i = 1, \dots, r_1 \quad (\text{D.18})$$

From eq. (D.18),  $r_1 = k$  implies that the  $k'$ -th and the  $k''$ -th columns of  $\Upsilon$  are linearly dependent which is in contradiction with the fact that  $\Upsilon$  has a full rank. Consequently  $r_1 < k$  and among the first  $r$

components of  $Y$  there is a minimum of  $r - (k - 1)$  components whose  $j$ -th coordinates are different from zero. Along with  $Y_{M-k+k'}$  and  $Y_{M-k+k''}$ , this will result in a total of  $r - (k - 3)$  components of  $Y$  having nonzero  $j$ -th coordinates.  $Y$  will fall outside of  $\mathcal{A}$  whenever  $r - (k - 3) > 2$  implying that  $M > 2k - 1$  or equivalently  $M \geq 2(n - 1)$ . Therefore, the values of  $M$  respecting eq. (D.17) will result in fully diverse codes in this second case.

From eq. (D.15) and eq. (D.17), we conclude that the proposed code is fully diverse with  $n$  transmit antennas if  $M \geq 2n - 1$ .

From eq. (D.13),  $\mathcal{M}$  is a circulant matrix that can be expressed as:

$$\mathcal{M} = \sum_{i=1}^M \alpha_i \Omega^i \quad (\text{D.19})$$

where  $\alpha_M = \lambda_0 = 1$  (since  $\Omega^M = I_M$ ),  $\alpha_i = \lambda_i$  for  $i = 1, \dots, n - 1$  and  $\alpha_i = 0$  for  $i = n, \dots, M - 1$ . From [116], the eigenvalues of  $\mathcal{M}$  can be expressed as:

$$\mu_k = \sum_{i=0}^{M-1} \omega_M^{ki} \lambda_{M-i} ; \quad k = 0, \dots, M - 1 \quad (\text{D.20})$$

where  $\omega_M = \exp\left(\frac{2\pi i}{M}\right)$  is the  $M$ -th root of unity.

Any subset composed of  $n'$  distinct elements of  $\{1, \omega_M, \dots, \omega_M^{M-1}\}$  forms a free set over  $\mathbb{Q}$  if  $2 \leq n' \leq \mathcal{E}(M)$  where  $\mathcal{E}(\cdot)$  is the Euler's function. Consider the case where  $\mathcal{E}(M) \geq n$ . In this case,  $\mu_k \neq 0$  for  $k = 1, \dots, M - 1$  since  $\lambda_0, \dots, \lambda_{n-1}$  multiply different elements of the set  $\{1, \dots, \omega_M^{M-1}\}$  and since  $\lambda_0 = 1$ . Only  $\mu_0 = \sum_{i=0}^{n-1} \lambda_i$  can be equal to zero. Therefore,  $r = \text{rank}(\mathcal{M}) \geq M - 1$ . From what preceded,  $\mathcal{M}Y = \mathbf{0}_M$ ;  $Y \in \mathcal{A}$ ;  $r \in \{M, M - 1\} \Rightarrow Y = \mathbf{0}_M$  for  $M \geq \max\{3, n\}$ . The condition  $M \geq \max\{3, n\}$  is verified by the values of  $M$  that respect  $\mathcal{E}(M) \geq n$  (since  $M > \mathcal{E}(M) \forall M$ ). This implies that the code is fully diverse with all values of  $M$  respecting  $\mathcal{E}(M) \geq n$ .

Finally, the proposed scheme achieves full transmit diversity with  $n$  transmit antennas and  $M$ -PPM- $M'$ -PAM constellations if:

$$M \in \{m \mid m \geq 2n - 1\} \cup \{m \mid \mathcal{E}(m) \geq n\} \quad (\text{D.21})$$

Note that the above proof does not depend on  $M'$ . Therefore, full diversity is achieved for the values of  $M$  respecting eq. (D.21) and for all values of  $M'$ .

## D.2 Coding Gain

Consider the codeword  $C$  given in eq. (3.48). Denote by  $C^{(i)}$  the  $M \times n$  matrix composed of the rows  $iM + 1, \dots, (i+1)M$  of  $C$  for  $i = 0, \dots, n - 1$ . The  $j$ -th row of  $C^{(i)}$  is denoted by  $C_j^{(i)}$ . In the same way,  $X_{i,m}$  denotes the  $m$ -th component of the  $M$ -dimensional vector  $X_i$  for  $m = 1, \dots, M$  and  $i = 1, \dots, n$ . For notational simplicity, we set  $\sigma^n(x) = x^{(n)}$ . From eq. (3.48),  $C^{(i)}$  takes the following form:

$$C^{(i)} = \begin{bmatrix} X_{n-i+1, \pi(1)}^{(i)} & \dots & X_{n, \pi(1)}^{(i)} & X_{1,1}^{(i)} & \dots & X_{n-i,1}^{(i)} \\ \vdots & \dots & \vdots & \vdots & \dots & \vdots \\ X_{n-i+1, \pi(M)}^{(i)} & \dots & X_{n, \pi(M)}^{(i)} & X_{1,M}^{(i)} & \dots & X_{n-i,M}^{(i)} \end{bmatrix} \quad (\text{D.22})$$

where  $\pi^k(\cdot)$  stands for the cyclic permutation of order  $k$  given by:

$$\pi^k(i) = (i + k - 1) \bmod M + 1 \quad (\text{D.23})$$

Let  $S = \{X_1, \dots, X_n\}$  be the set composed of  $n$  vectors drawn randomly from the set  $\mathcal{A}$  given in eq. (D.2). For  $M > n^2$ , among the  $n$  vectors of  $S$ , there exists  $n - 1$  vectors whose  $m$ -th coordinates are all equal to zero for a certain value of  $m \in \{1, \dots, M\}$ . This follows from the structure of  $\mathcal{A}$  whose elements can contain a maximum number of  $2n$  nonzero components. In what follows, we show that the code has a non-vanishing determinant for  $M > n^2$ .

Without loss of generality, suppose that  $X_{1,m} = \dots = X_{n-1,m} = 0$  for a given value of  $m \in \{1, \dots, M\}$ .

**Proposition D.2**  $X_{1,m} = \dots = X_{n-1,m} = 0$  implies that  $\det(C^T C) \geq 1$  unless  $X_{n,m} = 0$ .

*Proof:*

$$\begin{aligned} \det(C^T C) &= \sum_{i_1=1}^{nM} \sum_{i_2=i_1+1}^{nM} \dots \sum_{i_n=i_{n-1}+1}^{nM} \left( \det \left( [C_{i_1}^T \dots C_{i_n}^T]^T \right) \right)^2 \\ &\geq \sum_{i_1=1}^M \sum_{i_2=M+1}^{2M} \dots \sum_{i_n=(n-1)M+1}^{nM} \left( \det \left( [C_{i_1}^T \dots C_{i_n}^T]^T \right) \right)^2 \\ &= \sum_{i_1=1}^M \sum_{i_2=1}^M \dots \sum_{i_n=1}^M \left( \det \left( [(C_{i_1}^{(0)})^T \dots (C_{i_n}^{(n-1)})^T]^T \right) \right)^2 \end{aligned} \quad (\text{D.24})$$

Construct the  $n \times n$  matrix  $C'$  as:

$$C' = \begin{bmatrix} C_{\pi^{-1}(m)}^{(1)} \\ \vdots \\ C_{\pi^{-1}(m)}^{(n-1)} \\ C_m^{(0)} \end{bmatrix} = \begin{bmatrix} X_{n,m}^{(1)} & X_{1,\pi^{(-1)}(m)}^{(1)} & \dots & \dots & X_{n-1,\pi^{(-1)}(m)}^{(1)} \\ \vdots & \ddots & \ddots & \ddots & \vdots \\ X_{2,m}^{(n-1)} & \dots & \dots & X_{n,m}^{(n-1)} & X_{1,\pi^{-1}(m)}^{(n-1)} \\ X_{1,m} & \dots & \dots & X_{n-1,m} & X_{n,m} \end{bmatrix} \quad (\text{D.25})$$

Since  $X_{1,m} = \dots = X_{n-1,m} = 0$ ,  $C'$  is upper triangular. From eq. (D.24):

$$\det(C^T C) \geq (\det(C'))^2 = (\mathbf{N}_{\mathbb{K}/\mathbb{Q}}(X_{n,m}))^2 \quad (\text{D.26})$$

Since,  $\mathbf{N}_{\mathbb{K}/\mathbb{Q}}(X_{n,m}) \in \mathbb{Z}^*$  for  $X_{n,m} \neq 0$ , this completes the proof of proposition D.2.

**Proposition D.3**  $X_{1,m} = \dots = X_{n-1,m} = 0$  implies that  $\det(C^T C) \geq 1$  unless  $X_{n,\pi(m)} = 0$ .

*Proof:* Construct the matrix  $C'$  as:

$$C' = \begin{bmatrix} C_m^{(1)} \\ \vdots \\ C_m^{(n-1)} \\ C_{\pi(m)}^{(0)} \end{bmatrix} = \begin{bmatrix} X_{n,\pi(m)}^{(1)} & X_{1,m}^{(1)} & \dots & \dots & X_{n-1,m}^{(1)} \\ \vdots & \ddots & \ddots & \ddots & \vdots \\ X_{2,\pi(m)}^{(n-1)} & \dots & X_{n-1,\pi(m)}^{(n-1)} & X_{n,\pi(m)}^{(n-1)} & X_{1,m}^{(n-1)} \\ X_{1,\pi(m)} & \dots & \dots & X_{n-1,\pi(m)} & X_{n,\pi(m)} \end{bmatrix} \quad (\text{D.27})$$

Since  $X_{1,m} = \dots = X_{n-1,m} = 0$ ,  $C'$  is lower triangular. From eq. (D.24):

$$\det(C^T C) \geq (\det(C'))^2 = (\mathbf{N}_{\mathbb{K}/\mathbb{Q}}(X_{n,\pi(m)}))^2 \quad (\text{D.28})$$

completing the proof of proposition D.3.

**Proposition D.4**  $X_{1,m} = \dots = X_{n'-1,m} = X_{n'+1,\pi(m)} = \dots = X_{n,\pi(m)} = 0$  implies that  $\det(C^T C) \geq 1$  unless  $X_{n',\pi(m)} = 0$ .

*Proof:* For a given value of  $n'$ , define the function  $f(\cdot)$  as:

$$f(k) = (1 - n' - k) \mod n + 1 \quad (\text{D.29})$$

Construct the  $n \times n$  matrix  $C'$  such that:

$$C' = \begin{bmatrix} C_m^{(f(0))} \\ \vdots \\ C_m^{(n-1)} \\ C_{\pi(m)}^{(0)} \\ \vdots \\ C_{\pi(m)}^{(f(n-1))} \end{bmatrix} = \begin{bmatrix} X_{n',\pi(m)}^{(f(0))} & \cdots & \cdots & X_{n,\pi(m)}^{(f(0))} & X_{1,m}^{(f(0))} & \cdots & X_{n'-1,m}^{(f(0))} \\ \vdots & \ddots & \ddots & \ddots & \ddots & \ddots & \vdots \\ X_{2,\pi(m)}^{(n-1)} & \cdots & X_{n',\pi(m)}^{(n-1)} & X_{n'+1,\pi(m)}^{(n-1)} & \cdots & X_{n,\pi(m)}^{(n-1)} & X_{1,m}^{(n-1)} \\ X_{1,\pi(m)} & \cdots & \cdots & X_{n',\pi(m)} & X_{n'+1,\pi(m)} & \cdots & X_{n,\pi(m)} \\ \vdots & \ddots & \ddots & \ddots & \ddots & \ddots & \vdots \\ X_{n'+1,\pi^2(m)}^{(f(n-1))} & \cdots & X_{n,\pi^2(m)}^{(f(n-1))} & X_{1,\pi(m)}^{(f(n-1))} & \cdots & \cdots & X_{n',\pi(m)}^{(f(n-1))} \end{bmatrix} \quad (\text{D.30})$$

For  $X_{1,m} = \cdots = X_{n'-1,m} = X_{n'+1,\pi(m)} = \cdots = X_{n,\pi(m)} = 0$ ,  $C'$  is a lower triangular matrix. From eq. (D.24):

$$\det(C^T C) \geq (\det(C'))^2 = (\mathbb{N}_{\mathbb{K}/\mathbb{Q}}(X_{n',\pi(m)}))^2 \quad (\text{D.31})$$

completing the proof of proposition D.4.

**Proposition D.5**  $\det(C^T C) \geq 1$  unless  $C = \mathbf{0}_{nM \times n}$ .

*Proof:* Suppose that  $X_{1,m} = \cdots = X_{n-1,m}$  and  $\det(C^T C) < 1$ . This implies that  $X_{n,m} = X_{n,\pi(m)} = 0$  from proposition D.2 and proposition D.3 respectively. Now,  $X_{1,m} = \cdots = X_{n-2,m} = 0$  and  $X_{n,\pi(m)} = 0$  imply that  $X_{2,\pi(m)} = \cdots = X_{n-1,\pi(m)} = 0$  from the recursive application of proposition D.4 for  $n' = n-1, \dots, 2$ . Finally, from proposition D.2,  $X_{2,\pi(m)} = \cdots = X_{n-1,\pi(m)} = 0$  implies that  $X_{1,\pi(m)} = 0$ .

Therefore,  $X_{1,m} = \cdots = X_{n-1,m} = 0$  and  $\det(C^T C) < 1$  imply that the  $m$ -th and  $\pi(m)$ -th components of  $X_1, \dots, X_n$  are all equal to zero. Now,  $X_{1,\pi(m)} = \cdots = X_{n-1,\pi(m)} = 0$  and  $\det(C^T C) < 1$  imply that  $\pi(m)$ -th and  $\pi^2(m)$ -th components of  $X_1, \dots, X_n$  are all equal to zero. Starting the same operation again we conclude that  $\det(C^T C) < 1$  only when  $X_1 = \cdots = X_n = \mathbf{0}_M$  since  $\pi$  defines a bijection over the set  $S = \{1, \dots, M\}$  and consequently  $\{\pi^1(m), \dots, \pi^{M-1}(m)\}$  spans the entire set  $S$  for any value of  $m \in S$ . This proves that when  $M > n^2$ ,  $\det(C^T C) \geq 1$  for all values of  $M'$ .

### D.3 Information Losses

Consider the codeword  $C$  given in eq. (3.59). Concatenating the columns of  $C$  vertically one after the other, we obtain:

$$\text{vec}(C) = \Phi [a_1^T \cdots a_{n^2}^T]^T \quad (\text{D.32})$$

where  $\Phi$  is a  $n^2M \times n^2M$  matrix. In what follows, we will show that the matrix  $\Phi$  is unitary.  $\Phi$  can be written as:

$$\Phi = [\Phi_1^T \cdots \Phi_n^T]^T \quad (\text{D.33})$$

Following from the layered structure of the codewords, the constituent matrices of dimensions  $nM \times n^2M$  take the following form ( $k = 1, \dots, n$ ):

$$\Phi_k = \Psi_k \mathbf{M} \mathbf{P} \Upsilon_n^{k-1} \quad (\text{D.34})$$

where  $\Upsilon_n = \Omega_n^T \otimes I_{nM}$  and  $\Omega_n$  is the  $n \times n$  permutation matrix given by:

$$\Omega_n = \begin{bmatrix} \mathbf{0}_{1 \times n} & 1 \\ I_{n-1} & \mathbf{0}_{n \times 1} \end{bmatrix} \quad (\text{D.35})$$

In this case, the permutation matrix in eq. (3.50) can be written as  $\Omega_M$ . The  $nM \times nM$  matrix  $\Psi_k$  is given by:

$$\Psi_k = \text{diag}(\underbrace{I_M \cdots I_M}_k \text{ times}, \underbrace{\Omega_M \cdots \Omega_M}_{n-k \text{ times}}) \quad (\text{D.36})$$

$\mathbf{M}$  is a  $nM \times n^2M$  matrix related to the rotation matrix  $\mathcal{M}$  given in eq. (3.59) by:

$$\mathbf{M} = \mathfrak{M} \otimes I_M = \text{diag}(\mathcal{M}_1 \cdots \mathcal{M}_n) \otimes I_M \quad (\text{D.37})$$

where  $\mathcal{M}_i$  is the  $i$ -th row of  $\mathcal{M}$ . Finally, the matrix  $\mathbf{P}$  is given by:

$$\mathbf{P} = P \otimes I_{nM} = \begin{bmatrix} 1 & 0 & \cdots & 0 \\ 0 & 0 & \cdots & 1 \\ \vdots & \vdots & \ddots & \vdots \\ 0 & 1 & \cdots & 0 \end{bmatrix} \otimes I_{nM} \quad (\text{D.38})$$

For example, with  $n = 3$  transmit antennas:

$$\Phi_1 = \begin{bmatrix} \mathcal{M}_1 \otimes I_M & \mathbf{0}_{M \times Mn} & \mathbf{0}_{M \times Mn} \\ \mathbf{0}_{M \times Mn} & \mathbf{0}_{M \times Mn} & \mathcal{M}_2 \otimes \Omega_M \\ \mathbf{0}_{M \times Mn} & \mathcal{M}_3 \otimes \Omega_M & \mathbf{0}_{M \times Mn} \end{bmatrix}; \quad \Phi_2 = \begin{bmatrix} \mathbf{0}_{M \times Mn} & \mathcal{M}_1 \otimes I_M & \mathbf{0}_{M \times Mn} \\ \mathcal{M}_2 \otimes I_M & \mathbf{0}_{M \times Mn} & \mathbf{0}_{M \times Mn} \\ \mathbf{0}_{M \times Mn} & \mathbf{0}_{M \times Mn} & \mathcal{M}_3 \otimes \Omega_M \end{bmatrix}$$

$$\Phi_3 = \begin{bmatrix} \mathbf{0}_{1 \times n} & \mathbf{0}_{1 \times n} & \mathcal{M}_1 \\ \mathbf{0}_{1 \times n} & \mathcal{M}_2 & \mathbf{0}_{1 \times n} \\ \mathcal{M}_3 & \mathbf{0}_{1 \times n} & \mathbf{0}_{1 \times n} \end{bmatrix} \otimes I_M$$

From eq. (D.34), we have  $\Phi_k \Phi_{k'}^T = I_{nM}$  since the matrices  $\Psi_k$ ,  $\mathbf{M}$ ,  $\mathbf{P}$  and  $\Upsilon_n$  are all unitary (the matrix  $\mathbf{M}$  is unitary since the rotation matrix  $\mathcal{M}$  is unitary by construction). Now, for any integers  $k$  and  $k'$ , we have:

$$\begin{aligned} \Phi_k \Phi_{k'}^T &= \Psi_k \mathbf{M} \mathbf{P} \Upsilon_n^{k-1} (\Upsilon_n^{k'-1})^T \mathbf{P}^T \mathbf{M}^T \Psi_{k'}^T \\ &= \Psi_k \mathbf{M} (P \otimes I_{nM}) (\Omega_n^{1-k} \otimes I_{nM}) (\Omega_n^{k'-1} \otimes I_{nM}) (P^T \otimes I_{nM}) \mathbf{M}^T \Psi_{k'}^T \\ &= \Psi_k \mathbf{M} (P \Omega_n^{k'-k} P^T \otimes I_{nM}) \mathbf{M}^T \Psi_{k'}^T \\ &= \Psi_k (\mathfrak{M} (P \Omega_n^{k'-k} P^T \otimes I_n) \mathfrak{M}^T \otimes I_M) \Psi_{k'}^T \end{aligned} \quad (\text{D.39})$$

If a vector is multiplied by  $\Omega_n^k$ , then its  $i$ -th component is permuted to the  $\pi_n^k(i)$ -th position where:

$$\pi_n^k(i) = (i + k - 1) \bmod n + 1 \quad (\text{D.40})$$

In the same way, multiplying by  $P$  (or  $P^{-1}$ ) is equivalent to the following permutation:

$$p_n(i) = (1 - i) \bmod n + 1 \quad (\text{D.41})$$

Therefore, multiplying by the matrix  $P\Omega_n^{k'-k}P^T$  is equivalent to applying the permutation:

$$f_n(i) = p_n(\pi_n^{k'-k}(p_n(i))) = \pi_n^{k'-k}(i) \quad (\text{D.42})$$

Given that the matrix  $\mathcal{M}$  is block-diagonal, then the matrix  $\mathcal{M} \left( P\Omega_n^{k'-k}P^T \otimes I_n \right) \mathcal{M}^T$  in eq. (D.39) is a  $n \times n$  matrix having the property that each one of its rows can have at most one nonzero value. From eq. (D.42), the indices of the elements of this matrix that can possibly have nonzero values are equal to  $(i, f_n^{-1}(i))$  for  $i = 1, \dots, n$ . Their values are given by:

$$\mathcal{M}_i \mathcal{M}_{f_n^{-1}(i)}^T = \mathcal{M}_i \mathcal{M}_{\pi_n^{k'-k}(i)}^T = \delta(k' - k) ; i = 1, \dots, n \quad (\text{D.43})$$

where  $\delta(\cdot)$  is the Dirac delta function. The last equality follows from the fact that the fully diverse rotation matrix  $\mathcal{M}$  is constructed to be unitary [100].

Finally, from eq. (D.39) it follows that:

$$\Phi_k \Phi_{k'}^T = I_{nM} \delta(k - k') \quad (\text{D.44})$$

showing that the matrix  $\Phi$  given in eq. (D.33) is unitary.

As in [47], we write the input-output baseband relation of the MIMO system ( $Y = \sqrt{\frac{\rho}{n}} HC + N$ ) as:

$$\text{vec}(Y) = \sqrt{\frac{\rho}{n}} (I_T \otimes H) \text{vec}(C) + \text{vec}(N) \quad (\text{D.45})$$

$$= \sqrt{\frac{\rho}{n}} \underbrace{(I_T \otimes H)}_{H'} \Phi [a_1^T \ \dots \ a_{n^2}^T]^T + \text{vec}(N) \quad (\text{D.46})$$

where  $\rho$  is the SNR and  $T = n$  is the temporal extension of the ST code.

From eq. (D.46), the capacity of equivalent (coded) channel is given by:

$$C^{(c)}(\rho, n, r) = \frac{1}{n} E_H \log_2 \left( \det \left( I_{nr} + \frac{\rho}{n} (H' \Phi)(H' \Phi)^T \right) \right) \quad (\text{D.47})$$

where  $r$  is the number of rows of  $H$  and the factor  $\frac{1}{n}$  follows from the number of channel uses.

Since  $\Phi$  is unitary and  $H'$  is block diagonal, then eq. (D.47) can be written as:

$$C^{(c)}(\rho, n, r) = \frac{1}{n} E_H \log_2 \left( \left( \det \left( I_r + \frac{\rho}{n} H H^T \right) \right)^n \right) \quad (\text{D.48})$$

$$= E_H \log_2 \left( \det \left( I_r + \frac{\rho}{n} H H^T \right) \right) \quad (\text{D.49})$$

$$= C(\rho, n, r) \quad (\text{D.50})$$

where  $C(\rho, n, r)$  is the capacity of the uncoded MIMO channel ( $H$ ). This proves that the code given in eq. (3.59) is information lossless for all number of transmit antennas.



## Appendix E

# Properties of construction 2

### E.1 Choice of $\Omega$

We write the  $M \times M$  matrix  $\Omega$  given in eq. (3.61) as:

$$\Omega(\theta') = I_{M/2} \otimes \Omega'(\theta') ; \quad \Omega'(\theta') = \begin{bmatrix} \cos(\theta') & \sin(\theta') \\ -\sin(\theta') & \cos(\theta') \end{bmatrix} \quad (\text{E.1})$$

Suppose that  $\theta'$  is chosen such that  $\sigma(\Omega'(\theta')) = \Omega'(\theta')$ . This choice will be discussed at the end of this section. As in Appendix D.1, designate by  $\Delta C(X_1, \dots, X_n)$  the difference between two codewords that is associated with the vectors  $X_1, \dots, X_n$  belonging to the set  $\mathcal{A}$  given in eq. (D.2). The linear dependence between the columns of  $\Delta C$  when this latter is rank-deficient results in eq. (D.4) since  $\Omega(\theta')$  remains invariant when applying the embeddings of  $\mathbb{K}$ . Equation (D.4) can be written in a more convenient way as:

$$\mathcal{M}(\theta')X_i = \left( \sum_{j=1}^{n-1} \lambda_j \Omega^j(\theta') \right) X_i = X_i ; \quad i = 1, \dots, n \quad (\text{E.2})$$

where  $\lambda_1, \dots, \lambda_{n-1}$  are rational numbers.

$\Omega'(\theta')$  is a rotation matrix verifying  $(\Omega'(\theta'))^j = \Omega'(j\theta')$ . This implies that  $\Omega^j(\theta') = \Omega(j\theta')$  since  $\Omega(\theta')$  is a block-diagonal matrix. Therefore, the matrix  $\mathcal{M}(\theta')$  in eq. (E.2) takes the following form:

$$\mathcal{M}(\theta') = \begin{bmatrix} x(\theta') & y(\theta') & 0 & \cdots & 0 \\ -y(\theta') & x(\theta') & 0 & \cdots & 0 \\ \vdots & \ddots & \ddots & \ddots & \vdots \\ 0 & \cdots & 0 & x(\theta') & y(\theta') \\ 0 & \cdots & 0 & -y(\theta') & x(\theta') \end{bmatrix} \quad (\text{E.3})$$

where:

$$x(\theta') = \sum_{j=1}^{n-1} \lambda_j \cos(j\theta') \quad (\text{E.4})$$

$$y(\theta') = \sum_{j=1}^{n-1} \lambda_j \sin(j\theta') \quad (\text{E.5})$$

From eq. (E.2),  $X_i$  is an eigenvector of  $\mathcal{M}(\theta')$  for  $i = 1, \dots, n$ . Moreover, since we are limited to real-valued constellations, then  $X_i$  can only be associated with the real eigenvalues of  $\mathcal{M}(\theta')$ .

Solving the characteristic equation of  $\mathcal{M}(\theta')$  results in:

$$\left( (x(\theta') - \mu)^2 + (y(\theta'))^2 \right)^{\frac{M}{2}} = 0 \quad (\text{E.6})$$

where  $\mu$  stands for the eigenvalue of  $\mathcal{M}(\theta')$ .  $\mu$  is real only when  $y(\theta') = 0$ . In this case,  $X_i$  is the eigenvector associated with the eigenvalue  $\mu = x(\theta')$ . The idea is to choose  $\theta'$  such that  $x(\theta') = 0$  whenever  $y(\theta') = 0$ . In this case, if  $y(\theta') \neq 0$ ,  $X_i$  is complex-valued and hence it does not belong to  $\mathcal{A}$ . When  $y(\theta') = 0$ , then  $\mu = x(\theta') = 0$  and  $X_i$  is the all-zero vector for  $i = 1, \dots, n$ .

From eq. (E.5), this can happen when  $\{\sin(\theta'), \dots, \sin((n-1)\theta')\}$  forms a  $\mathbb{Z}$ -basis of degree  $n-1$ . In this case,  $y(\theta') = 0$  implies that  $\lambda_1 = \dots = \lambda_{n-1} = 0$  which implies that  $x(\theta') = 0$  from eq. (E.4). As a special case, we choose  $\theta'$  such that  $\{1, \sin(\theta'), \dots, \sin((n-1)\theta')\}$  forms an  $n$ -dimensional  $\mathbb{Z}$ -basis. Let  $\theta' = \frac{2\pi}{N'}$ . The set  $\{1, \exp(i\theta'), \dots, \exp((N'-1)i\theta')\}$  forms a basis of degree  $\mathcal{E}(N')$  over  $\mathbb{Z}[i]$  and consequently the sets  $\{1, \cos(\theta'), \dots, \cos((N'-1)\theta')\}$  and  $\{1, \sin(\theta'), \dots, \sin((N'-1)\theta')\}$  form two basis of degree  $\mathcal{E}(N')$  over  $\mathbb{Z}$ . Therefore, the desired property is obtained when  $\mathcal{E}(N') \geq n$ .

Finally,  $\mathbb{K}$  is chosen to be the real subfield of the cyclotomic field associated with the  $N$ -th root of unity ( $\mathbb{K} = \mathbb{Q}(2\cos(\frac{2\pi}{N}))$  and  $\mathcal{E}(N) = 2n$ ). Therefore,  $\sigma(\Omega(\theta')) = \Omega(\theta')$  when  $N$  and  $N'$  are relatively prime.

## E.2 Diversity Order with 2-PPM

For 2-PPM constellations, the elements of the set  $\mathcal{A}$  given in eq. (3.65) can be expressed as  $[a \ -a]^T$  where  $a \in \mathbb{K}$ . In other words, for any element  $A \in \mathcal{A}$ , we have  $\Omega A = -A$  where  $\Omega$  has the structure given in eq. (3.62). Therefore, the difference between two codewords takes the following form:

$$\Delta C(X_1, \dots, X_n) = \begin{bmatrix} x_1 & x_2 & \cdots & x_n \\ -x_1 & -x_2 & \cdots & -x_n \\ -\sigma(x_n) & \sigma(x_1) & \ddots & \vdots \\ -\sigma(x_n) & -\sigma(x_1) & \ddots & \vdots \\ \vdots & \ddots & \ddots & \sigma^{n-2}(x_2) \\ \vdots & \ddots & \ddots & -\sigma^{n-2}(x_2) \\ -\sigma^{n-1}(x_2) & \cdots & -\sigma^{n-1}(x_n) & \sigma^{n-1}(x_1) \\ -\sigma^{n-1}(x_2) & \cdots & -\sigma^{n-1}(x_n) & -\sigma^{n-1}(x_1) \end{bmatrix} \quad (\text{E.7})$$

where  $X_i \in \mathcal{A}$  is written as  $X_i = [x_i \ -x_i]^T$  for  $i = 1, \dots, n$ . When  $\Delta C$  is rank deficient, consider the relation given in eq. (D.3) that follows from the  $\mathbb{K}$ -linear dependence between the columns of  $\Delta C$ . The dependence between the columns of the last two rows of eq. (E.7) implies that:

$$\begin{cases} x_1 = -\sum_{j=1}^{n-1} \sigma(k_j) x_{\pi_n^k(j)} \\ x_1 = \sum_{j=1}^{n-1} \sigma(k_j) x_{\pi_n^k(j)} \end{cases} \quad (\text{E.8})$$

where  $\pi_n^k$  is the permutation given in eq. (D.40). Equation (E.8) implies that the linear dependence between the columns of  $\Delta C$  is possible only when  $x_1 = 0$ . In a more general way, the linear dependence

between the columns of the  $(2(n-i)+1)$ -th row of eq. (E.7) can be written as:

$$x_i = - \sum_{j=1}^{n-i} \sigma^i(k_j) x_{\pi_n^i(j)} + \sum_{j=n-i+1}^{n-1} \sigma^i(k_j) x_{\pi_n^i(j)} \quad (\text{E.9})$$

$$= - \sum_{j=1}^{n-i} \sigma^i(k_j) x_{\pi_n^i(j)} + \sum_{j=1}^{i-1} \sigma^i(k_{\pi_n^{-i}(j)}) x_j \quad (\text{E.10})$$

When  $x_1 = \dots = x_{i-1} = 0$ , this implies that:

$$x_i = - \sum_{j=1}^{n-i} \sigma^i(k_j) x_{\pi_n^i(j)} \quad (\text{E.11})$$

In the same way, the linear dependence between the columns of the  $(2(n-i)+2)$ -th row of eq. (E.7) when  $x_1 = \dots = x_{i-1} = 0$  can be written as:

$$x_i = \sum_{j=1}^{n-i} \sigma^i(k_j) x_{\pi_n^i(j)} \quad (\text{E.12})$$

Equations (E.11) and (E.12) imply that  $x_i = 0$ . Applying eq. (E.11) and eq. (E.12) recursively for  $i = 2, \dots, n$  along with eq. (E.8) (for  $x_1$ ) imply that  $x_1 = \dots = x_n = 0$ . From eq. (E.7), this implies that the only rank-deficient matrix  $\Delta C$  is the all-zero matrix. This shows that the choice of  $\Omega$  given in eq. (3.62) results in fully diverse ST codes with 2-PPM constellations for any number of transmit antennas.

### E.3 Coding Gain with 2-PPM

In a way similar to eq. (D.24),  $\det(\Delta C^T \Delta C)$  verifies the following relation:

$$\det(\Delta C^T \Delta C) \geq \sum_{i_1=1}^2 \dots \sum_{i_n=1}^2 \left( \det \left( \left[ (\Delta C_{i_1}^{(0)})^T \dots (\Delta C_{i_n}^{(n-1)})^T \right]^T \right) \right)^2 \quad (\text{E.13})$$

where  $\Delta C_j^{(i)}$  is the  $j$ -th row of the  $2 \times n$  matrix  $\Delta C^{(i)}$  composed of the  $(2i+1)$ -th and the  $2(i+1)$ -th rows of  $\Delta C$ . Following from eq. (E.7),  $\Delta C^{(i)}$  has the following form (for  $i = 0, \dots, n-1$ ):

$$\Delta C^{(i)} = \sigma^i \begin{bmatrix} -x_{n-i+1} & \dots & -x_n & x_1 & x_2 & \dots & x_{n-i} \\ -x_{n-i+1} & \dots & -x_n & -x_1 & -x_2 & \dots & -x_{n-i} \end{bmatrix} \quad (\text{E.14})$$

Note that  $\Delta C_1^{(0)} = -\Delta C_2^{(0)} = [x_1 \dots x_n]$ . Given that the absolute value of the determinant of a matrix remains invariant if one of its rows is multiplied by  $-1$ , then  $\Delta C_2^{(i)}$  can be replaced by  $-\Delta C_2^{(i)}$  in eq. (E.13). Therefore, eq. (E.13) can be written as:

$$\begin{aligned} \det(\Delta C^T \Delta C) &\geq 2 \sum_{i_2=1}^2 \dots \sum_{i_n=1}^2 \left( \det \left( \left[ (\Delta C_1^{(0)})^T (\Delta C_{i_2}^{(1)})^T \dots (\Delta C_{i_n}^{(n-1)})^T \right]^T \right) \right)^2 \\ &\triangleq 2 \sum_{i_2=1}^2 \dots \sum_{i_n=1}^2 (\det(C'(i_2, \dots, i_n)))^2 \end{aligned} \quad (\text{E.15})$$

where:

$$\begin{aligned} \mathcal{C}'(i_2, \dots, i_n) &= \left[ (\Delta C_1^{(0)})^T \quad (-1)^{i_2}(\Delta C_{i_2}^{(1)})^T \quad \dots \quad (-1)^{i_n}(\Delta C_{i_n}^{(n-1)})^T \right]^T \\ &= \underbrace{\begin{bmatrix} x_1 & x_2 & x_3 & \dots & x_n \\ j_1\sigma(x_n) & \sigma(x_1) & \sigma(x_2) & \dots & \sigma(x_{n-1}) \\ j_2\sigma^2(x_{n-1}) & j_2\sigma^2(x_n) & \sigma^2(x_1) & \dots & \sigma^2(x_{n-2}) \\ \vdots & \ddots & \ddots & \ddots & \vdots \\ j_{n-1}\sigma^{n-1}(x_2) & j_{n-1}\sigma^{n-1}(x_3) & \dots & j_{n-1}\sigma^{n-1}(x_n) & \sigma^{n-1}(x_1) \end{bmatrix}}_{\mathcal{C}(j_1, \dots, j_{n-1})} \quad (E.16) \end{aligned}$$

where  $j_k = (-1)^{i_{k+1}}$  for  $k = 1, \dots, n-1$ . Therefore, eq. (E.15) can be written as:

$$\det(\Delta C^T \Delta C) \geq 2 \sum_{j_1=\pm 1} \dots \sum_{j_{n-1}=\pm 1} \underbrace{(\det(\mathcal{C}(j_1, \dots, j_{n-1})))^2}_{\delta(j_1, \dots, j_{n-1})} \quad (E.17)$$

Since  $j_k$  appears in only one row of  $\mathcal{C}(j_1, \dots, j_{n-1})$  for  $k = 0, \dots, n-1$ , then the highest power of  $j_k$  that appears in the determinant of  $\mathcal{C}(j_1, \dots, j_{n-1})$  is equal to one for the different values of  $k$ . Consequently,  $\delta(j_1, \dots, j_{n-1})$  can be expressed as:

$$\delta(j_1, \dots, j_{n-1}) = \left( \sum_{(p_1, \dots, p_{n-1}) \in \{0,1\}^{n-1}} c_{p_1, \dots, p_{n-1}}(j_1, \dots, j_{n-1}) f_{p_1, \dots, p_{n-1}} \right)^2 \quad (E.18)$$

$$= \sum_{\substack{(p_1, \dots, p_{n-1}) \in \{0,1\}^{n-1} \\ (p'_1, \dots, p'_{n-1}) \in \{0,1\}^{n-1}}} c_{p_1, \dots, p_{n-1}}(j_1, \dots, j_{n-1}) c_{p'_1, \dots, p'_{n-1}}(j_1, \dots, j_{n-1}) f_{p_1, \dots, p_{n-1}} f_{p'_1, \dots, p'_{n-1}} \quad (E.19)$$

where the coefficients  $c_{p_1, \dots, p_{n-1}}(j_1, \dots, j_{n-1})$  are given by:

$$c_{p_1, \dots, p_{n-1}}(j_1, \dots, j_{n-1}) = \prod_{l=1}^{n-1} j_l^{p_l} \quad (E.20)$$

$f_{p_1, \dots, p_{n-1}}$  is a certain function of  $x_1, \dots, x_n$  and their conjugates (it can be equal to zero). For example, when  $n = 3$ :

$$\begin{cases} f_{0,0} = N_{\mathbb{K}/\mathbb{Q}}(x_1) \\ f_{1,0} = -x_2\sigma(x_3)\sigma^2(x_1) \\ f_{0,1} = N_{\mathbb{K}/\mathbb{Q}}(x_2) - x_1\sigma(x_2)\sigma^2(x_3) - x_3\sigma(x_1)\sigma^2(x_2) \\ f_{1,1} = N_{\mathbb{K}/\mathbb{Q}}(x_3) \end{cases}$$

From the structure of the matrix given in eq. (E.16), the following relations hold for any value of  $n$ :

$$f_{0,\dots,0} = N_{\mathbb{K}/\mathbb{Q}}(x_1) ; \quad f_{1,\dots,1} = (-1)^{n+1} N_{\mathbb{K}/\mathbb{Q}}(x_n) \quad (E.21)$$

Given that  $p_l \in \{0, 1\}$  for  $l = 1, \dots, n-1$ , from eq. (E.20), it follows that:

$$\begin{aligned} \sum_{j_1=\pm 1} \dots \sum_{j_{n-1}=\pm 1} c_{p_1, \dots, p_{n-1}}(j_1, \dots, j_{n-1}) c_{p'_1, \dots, p'_{n-1}}(j_1, \dots, j_{n-1}) &= \sum_{j_1=\pm 1} (j_1^{p_1+p'_1}) \dots \sum_{j_{n-1}=\pm 1} (j_{n-1}^{p_{n-1}+p'_{n-1}}) \\ &= \begin{cases} 0 ; & (p_1, \dots, p_{n-1}) \neq (p'_1, \dots, p'_{n-1}) \\ 2^{n-1} ; & (p_1, \dots, p_{n-1}) = (p'_1, \dots, p'_{n-1}) \end{cases} \quad (E.22) \end{aligned}$$

Therefore, from eq. (E.17):

$$\det(\Delta C^T \Delta C) \geq 2^n \sum_{(p_1, \dots, p_{n-1}) \in \{0,1\}^{n-1}} f_{p_1, \dots, p_{n-1}}^2 \quad (\text{E.23})$$

$$\geq 2^n (f_{0, \dots, 0}^2 + f_{1, \dots, 1}^2) \quad (\text{E.24})$$

$$= 2^n \left( (\mathbf{N}_{\mathbb{K}/\mathbb{Q}}(x_1))^2 + (\mathbf{N}_{\mathbb{K}/\mathbb{Q}}(x_n))^2 \right) \quad (\text{E.25})$$

Since  $\mathbf{N}_{\mathbb{K}/\mathbb{Q}}(x_i) \in \mathbb{Z}$  for all values of  $i$ , this implies that  $\det(\Delta C^T \Delta C) \geq 2^n$  unless when  $\mathbf{N}_{\mathbb{K}/\mathbb{Q}}(x_1) = \mathbf{N}_{\mathbb{K}/\mathbb{Q}}(x_n) = 0$ .

Suppose that  $\mathbf{N}_{\mathbb{K}/\mathbb{Q}}(x_1) = \mathbf{N}_{\mathbb{K}/\mathbb{Q}}(x_n) = 0$  implying that  $x_n = 0$ . The only time when  $j_1$  appears in eq. (E.16), it is multiplied by  $\sigma(x_n)$  which is equal to zero. Therefore,  $j_1$  will not appear neither in the expression of  $c_{p_1, \dots, p_{n-1}(j_1, \dots, j_{n-1})}$  nor in that of  $\delta(j_1, \dots, j_{n-1})$ . This implies that eq. (E.19) and eq. (E.20) can now be written as:

$$\delta(j_2, \dots, j_{n-1}) = \left( \sum_{(p_2, \dots, p_{n-1}) \in \{0,1\}^{n-2}} c_{p_2, \dots, p_{n-1}}(j_2, \dots, j_{n-1}) f_{p_2, \dots, p_{n-1}} \right)^2 \quad (\text{E.26})$$

where:

$$c_{p_2, \dots, p_{n-1}}(j_2, \dots, j_{n-1}) = \prod_{l=2}^{n-1} j_l^{p_l} \quad (\text{E.27})$$

with  $f_{1, \dots, 1} = \pm \mathbf{N}_{\mathbb{K}/\mathbb{Q}}(x_{n-1})$ . As in eq. (E.22), this implies that:

$$\det(\Delta C^T \Delta C) \geq 2^n \sum_{(p_2, \dots, p_{n-1}) \in \{0,1\}^{n-2}} f_{p_2, \dots, p_{n-1}}^2 \quad (\text{E.28})$$

$$\geq 2^n (\mathbf{N}_{\mathbb{K}/\mathbb{Q}}(x_{n-1}))^2 \quad (\text{E.29})$$

implying that  $\det(\Delta C^T \Delta C) \geq 2^n$  unless  $x_{n-1} = 0$ . Proceeding recursively in the same way, and noticing that at step  $k$ ,  $j_k$  is multiplied by the conjugates of  $x_n, \dots, x_{n-k+1}$  in eq. (E.16), we deduce that  $\det(\Delta C^T \Delta C) \geq 2^n$  unless  $x_1 = \dots = x_n = 0$ .

As in Section 3.2, limiting the construction in an ideal whose fundamental parallelotope has a volume of 1 is equivalent to multiplying the codewords by a diagonal matrix whose determinant is equal to  $\frac{1}{\sqrt{d_{\mathbb{K}}}}$ . Therefore, the coding gain of the proposed code with 2-PPM and  $n$  transmit antennas is equal to:

$$\delta_{min} = \min_{\substack{\Delta C(X_1, \dots, X_n) \\ (X_1, \dots, X_n) \in \mathcal{A}^n \setminus \{(0_{2 \times 1}, \dots, 0_{2 \times 1})\}}} (\det(\Delta C^T \Delta C))^{\frac{1}{n}} = 2d_{\mathbb{K}}^{-\frac{1}{n}} \quad (\text{E.30})$$

On the other hand, the perfect codes achieve a coding gain of  $d_{\mathbb{K}}^{-\frac{1}{n}}$  over  $\mathbb{Z}$  [64]. From eq. (3.33), this implies that the coding gain is equal to  $4d_{\mathbb{K}}^{-\frac{1}{n}}$  and  $2d_{\mathbb{K}}^{-\frac{1}{n}}$  with PAM and PPM constellations respectively. This shows that the proposed scheme achieves the same coding gain as the perfect codes.



# Publications

## Journal Papers

- Chadi Abou-Rjeily, Norbert Daniele and Jean-Claude Belfiore, “Space Time coding for multiuser ultra-wideband communications”, accepted for publication in the IEEE transactions on communications.
- Chadi Abou-Rjeily, Norbert Daniele and Jean-Claude Belfiore, “A  $2 \times 2$  antennas ultra-wideband system using biorthogonal pulse position modulation”, IEEE communications letters, vol. 10, pp. 366-368, May 2006.
- Chadi Abou-Rjeily, Norbert Daniele and Jean-Claude Belfiore, “Distributed algebraic space-time codes for ultra-wideband communications”, accepted for publication in the Kluwer journal (Springer - special issue on cooperation in wireless networks).
- Julien Keignart, Chadi Abou-Rjeily, Christophe Delaveaud and Norbert Daniele, “UWB SIMO channel measurements and simulations”, IEEE Transactions on Microwave Theory and Techniques, vol. 54, pp. 1812-1819, April 2006.
- Benoit Denis, Jean-Benoit Pierrot and Chadi Abou-Rjeily, “Joint distributed synchronization and positioning in UWB Ad Hoc networks using TOA”, IEEE Transactions on Microwave Theory and Techniques, vol. 54, pp. 1896-1911, April 2006.
- Chadi Abou-Rjeily, Norbert Daniele and Jean-Claude Belfiore, “Distributed algebraic space-time codes for ultra-wideband communications”, submitted for publication in the IEEE transactions on communications, February 2006.
- Chadi Abou-Rjeily, Norbert Daniele and Jean-Claude Belfiore, “On space-time coding with pulse position and amplitude modulations for time-hopping ultra-wideband systems”, submitted for publication in the IEEE transactions on information theory, June 2006.
- Chadi Abou-Rjeily, Norbert Daniele and Jean-Claude Belfiore, “A new family of optimal and totally-real distributed space-time codes for TH-UWB systems with PPM”, submitted for publication in the IEEE communications letters, June 2006.

## IEEE International Conferences

- Chadi Abou-Rjeily and Norbert Daniele, “Performance analysis of space time coding over ultra-wideband channels”, in proceedings IEEE international conference on signal processing and com-

munications (SPCOM), pp. 315-319, December 2004.

- Chadi Abou-Rjeily, Norbert Daniele and Jean-Claude Belfiore, “On high data rate space time codes for ultra-wideband systems”, in proceedings IEEE International Conference on Ultra wide-band (ICU), Zurich, September 2005.
- Chadi Abou-Rjeily, Norbert Daniele and Jean-Claude Belfiore, “Differential space time ultra wide-band communications”, in proceedings IEEE International Conference on Ultra wide-band (ICU), Zurich, September 2005.
- Chadi Abou-Rjeily, Norbert Daniele and Jean-Claude Belfiore, “Performance of MIMO UWB systems with biorthogonal pulse position modulation”, in proceedings IEEE International Zurich Seminar on Communications (IZS), Zurich, February 2006.
- Chadi Abou-Rjeily, Norbert Daniele and Jean-Claude Belfiore, “Full Rate fully diverse ST codes with nonvanishing determinants for TH-UWB communications”, in proceedings IEEE International Zurich Seminar on Communications (IZS), Zurich, February 2006.
- Chadi Abou-Rjeily, Norbert Daniele and Jean-Claude Belfiore, “A new family of space time codes for pulse amplitude and position modulated UWB systems”, in proceedings IEEE International Symposium on Information Theory (ISIT), Washington, July 2006.
- Chadi Abou-Rjeily, Norbert Daniele and Jean-Claude Belfiore, “Distributed space-time coding with ultra-wideband systems”, in the proceedings of the 17 IEEE Annual International Symposium on Personal, Indoor and Radio Communications (PIMRC), Helsinki, September 2006.
- Chadi Abou-Rjeily, Norbert Daniele and Jean-Claude Belfiore, “MIMO UWB communication systems using modified Hermite pulses”, in the proceedings of the 17 IEEE Annual International Symposium on Personal, Indoor and Radio Communications (PIMRC), Helsinki, September 2006.
- Chadi Abou-Rjeily, Norbert Daniele and Jean-Claude Belfiore, “An optimal  $2 \times 2$  space-time code for time hopping ultra wideband with binary PPM”, in the proceedings of the 2006 IEEE International Symposium on Wireless Communication Systems (ISWCS), Valencia, September 2006.
- Chadi Abou-Rjeily, Norbert Daniele and Jean-Claude Belfiore, “Amplify-and-forward cooperative diversity with space-time coded UWB systems”, in the proceedings of the 2006 IEEE International Conference on Ultra-wideband (ICUWB), Boston, September 2006.
- Chadi Abou-Rjeily, Norbert Daniele and Jean-Claude Belfiore, “On the decode-and-forward co-operative diversity with coherent and non-coherent UWB systems”, in the proceedings of the 2006 IEEE International Conference on Ultra-wideband (ICUWB), Boston, September 2006.
- Chadi Abou-Rjeily, Norbert Daniele and Jean-Claude Belfiore, “Diversity-Multiplexing tradeoff of single-antenna and multi-antenna indoor ultra-wideband channels”, in the proceedings of the 2006 IEEE International Conference on Ultra-wideband (ICUWB), Boston, September 2006.

## European Patents

- Chadi Abou-Rjeily, Norbert Daniele and Sébastien de Rivaz, “Multi-antenna ultra-wideband communication systems based on direct sampling”.
- Chadi Abou-Rjeily and Norbert Daniele, “MIMO UWB communications systems using modified Hermite pulses”.
- Chadi Abou-Rjeily, “A space-time code with 2 transmit antennas for pulse position modulations and hybrid pulse position and amplitude modulations”.
- Chadi Abou-Rjeily, “Space-time codes for 3 and 4 transmit antennas with pulse position modulations and hybrid pulse position and amplitude modulations”.
- Chadi Abou-Rjeily, “Cooperative diversity for non-coherent ultra-wideband communications”.
- Chadi Abou-Rjeily, “Cooperative diversity for coherent ultra-wideband communications”.
- Chadi Abou-Rjeily, “ $n \times n$  space-time codes for binary PPM and hybrid 2-PPM-PAM constellations”.
- Chadi Abou-Rjeily, “ $n \times n$  space-time codes based on pulse combining for PPM and PPAM constellations”.



# Bibliography

- [1] R. A. Scholtz, “Multiple access with time-hopping impulse radio,” in *Proceedings of the Milcom conference (Boston, USA)*, October 1993, pp. 447–450.
- [2] F. C. Commission, “First report and order, technical report FCC 02-48,” [www.fcc.gov](http://www.fcc.gov)., April 2002.
- [3] S. de Rivaz, B. Denis, J. Keignart, M. Pezzin, N. Daniele, and D. Morche, “Performances analysis of a UWB receiver using complex processing,” in *Proceedings IEEE Conference on UWB Systems and Technologies*, November 2003, pp. 229 – 233.
- [4] H. Harada, K. Ikemoto, and R. Kohno, “Modulation and hopping using modified Hermite pulses for UWB communications,” in *joint UWBST and IWUWBS*, May 2004, pp. 336–340.
- [5] W. Hu and G. Zheng, “Orthogonal Hermite pulses used for UWB M-ary communication,” in *IEEE International Conference on Information Technology Coding and Computing*, April 2005, pp. 97–101.
- [6] C. J. L. Martret and G. B. Giannakis, “All digital PAM impulse radio for multiple-access through frequency-selective multipath,” in *Proceedings IEEE Global Telecommunications Conference*, December 2000, pp. 77 – 81.
- [7] J. G. Proakis, *Digital Communication*. New York: McGrawHill, 4th edition 2000.
- [8] C. J. L. Martret and G. B. Giannakis, “All digital PPM impulse radio for multiple-access through frequency-selective multipath,” in *Proceedings IEEE Sensor Array and Multichannel Sig. Proc.*, March 2000, pp. 22–26.
- [9] S. Chaillou, D. Helal, and C. Cattaneo, “Timed simulator for UWB communication systems,” in *IEEE Conference on Ultra Wideband Systems and Technologies*, May 2002, pp. 7–11.
- [10] H. Zhang and T. A. Gulliver, “Biorthogonal pulse position modulation for time-hopping multiple access UWB communications,” *IEEE Trans. Wireless Commun.*, vol. 4, pp. 1154–1162, May 2005.
- [11] H. Zhang, W. Li, and T. A. Gulliver, “Pulse position amplitude modulation for time-hopping multiple-access UWB communications,” *IEEE Trans. Commun.*, vol. 53, pp. 1269–1273, August 2005.
- [12] J. R. Foerster, “The performance of a direct-sequence spread spectrum ultra-wideband system in the presence of multipath, narrowband interference and multiuser interference,” in *Proceedings IEEE Conference on UWB Systems and Technologies*, May 2002, p. 87–91.

- [13] V. Venkatesan, L. Huaping, C. Nilsen, R. Kyker, and M. Magana, “Performance of an optimally spaced PPM ultra-wideband system with direct sequence spreading for multiple access,” in *Proceedings IEEE Vehicular Technology Conference*, vol. 1, October 2003, pp. 602 – 606.
- [14] M. Z. Win and R. A. Scholtz, “Ultra-wide Bandwidth Time-hopping spread-spectrum impulse radio for wireless multiple-access communications,” *IEEE Trans. Commun.*, vol. 17, pp. 824–836, April 2000.
- [15] Y.-P. Nakache and A. F. Molisch, “Spectral shape of UWB signals - influence of modulation format, multiple access scheme and pulse shape,” in *Proceedings IEEE Vehicular Technology Conference*, vol. 4, April 2003, pp. 2510 – 2514.
- [16] Y. Kai, M. Bengtsson, B. Ottersten, D. McNamara, P. Karlsson, and M. Beach, “Modeling of wide-band MIMO radio channels based on NLoS indoor measurements,” *IEEE Trans. Veh. Technol.*, vol. 53, pp. 655 – 665, May 2004.
- [17] J. Foerster, “Channel modeling sub-committee Report Final,” Technical report IEEE 802.15-02/490, IEEE 802.15.3a Wireless Personal Area Networks, 2002.
- [18] A. F. Molisch, “Channel modeling subgroup final report,” Technical report IEEE 802.15-04/662r0, IEEE 802.15.4a Wireless Personal Area Networks, 2004.
- [19] B. Uguen, E. Plouhinec, Y. Lostanlen, and G. Chassay, “A deterministic ultra wideband channel modeling,” in *IEEE Conference on Ultra Wideband Systems and Technologies*, May 2002, pp. 1–5.
- [20] F. Tchoffo-Talom, B. Uguen, E. Plouhinec, and G. Chassay, “A site-specific tool for UWB channel modeling,” in *IEEE Conference on Ultra Wideband Systems and Technologies*, May 2004, pp. 18–21.
- [21] A. A. M. Saleh and R. A. Valenzuela, “A statistical model for indoor multipath propagation,” *IEEE J. Select. Areas Commun.*, vol. 5, pp. 128–137, February 1987.
- [22] J. Kunisch and J. Pamp, “Measurement results and modeling aspects for the UWB radio channel,” in *Proceedings IEEE Conference on UWB Systems and Technologies*, May, pp. 19 – 23.
- [23] ——, “An ultra-wideband space-variant multipath indoor radio channel model,” in *Proceedings IEEE Conference on UWB Systems and Technologies*, November, pp. 290 – 294.
- [24] R. M. Buehrer, A. Safaai-Jazi, W. Davis, and D. Sweeney, “Ultra-wideband propagation measurements and modeling,” DARPA NETEX program final report, January 2004, [http://www.mprg.org/people/buehrer/ultra/darpa\\_netex.shtml](http://www.mprg.org/people/buehrer/ultra/darpa_netex.shtml).
- [25] V. Bharadwaj and R. M. Buehrer, “Spatial fading characteristics of UWB signals in indoor environments,” September 2004, submitted for publication.
- [26] C. Prettie, D. Cheung, L. Rusch, and M. Ho, “Spatial correlation of UWB signals in a home environment,” in *Proceedings IEEE Conference on UWB Systems and Technologies*, May 2002, pp. 65–69.

- [27] J. Keignart, C. Abou-Rjeily, C. Delaveaud, and N. Daniele, "UWB SIMO channel measurements and simulations," 2005, accepted for publication.
- [28] S. Venkatesh, V. Bharadwaj, and R. Buehrer, "A new spatial model for impulse-based ultra-wideband channels," in *Proceedings IEEE Vehicular Technology Conference*, vol. 4, September 2005, pp. 2617 – 2621.
- [29] S. Venkatesh, J. Ibrahim, and R. Buehrer, "A new 2-cluster model for indoor UWB channel measurements," in *Proceedings IEEE Antennas and Propagation Society International Symposium*, vol. 1, June 2004, pp. 946 – 949.
- [30] M. Z. Win and R. Scholtz, "On the energy capture of ultrawide bandwidth signals in dense multipath environments," *IEEE Commun. Lett.*, vol. 2, pp. 245–247, September 1998.
- [31] D. Cassioli, M. Z. Win, F. Vatalaro, and A. F. Molisch, "Performance of low-complexity rake reception in a realistic UWB channel," in *Proceedings IEEE International Conference on Communications*, vol. 2, May 2002, pp. 763–767.
- [32] S. Hoyos, B. Sadler, and G. Arce, "Monobit digital receivers for ultrawideband communications," *IEEE Trans. Wireless Commun.*, vol. 4, pp. 1337 – 1344, July 2005.
- [33] J. Choi and W. Stark, "Performance of ultra-wideband communications with suboptimal receivers in multipath channels," *IEEE J. Select. Areas Commun.*, vol. 20, pp. 1754–1766, 2002.
- [34] E. Cohn, *Advanced Number Theory*. New York: Dover, 1980.
- [35] H. Hasse, *Number Theory*. Berlin Heidelberg New York: Springer-Verlag, 1980.
- [36] E. Viterbo and J. J. Boutros, "Signal space diversity: a power- and bandwidth-efficient diversity technique for the rayleigh fading channel," *IEEE Trans. Inform. Theory*, vol. 44, no. 4, pp. 1453–1467, July 1998.
- [37] A. Lenstra, H. Lenstra, and L. Lovász, "Factorizing polynomials with rational coefficients," *Math. Ann.*, vol. 261, pp. 515–534, 1982.
- [38] I. Berenguer and W. Xiaodong, "MIMO antenna selection with lattice-reduction-aided linear receivers," *IEEE Trans. Veh. Technol.*, vol. 53, no. 5, pp. 1289 – 1302, September 2004.
- [39] B. A. Sethuraman, B. S. Rajan, and V. Shashidhar, "Full-diversity, high rate space-time block codes from division algebras," *IEEE Trans. Inform. Theory*, vol. 49, pp. 2596–2616, October 2003.
- [40] E. Telatar, "Capacity of multi-antenna gaussian channels," European Trans. on Telecomm. ETT, pp. 585–596, November 1999.
- [41] G. J. Foschini and M. J. Gans, "On limits of wireless communication in a fading environment when using multiple antennas," *Wireless Personal Communications*, pp. 311–335, March 1998.
- [42] P. W. Wolniansky, G. J. Foschini, G. D. Golden, and R. A. Valenzuela, "V-blast: an architecture for realizing very high data rates over the rich-scattering wireless channel," in *Int. Symp. on Signal, Systems and Electronics*, September 1998, pp. 295–300.

- [43] G. J. Foschini, "Layered space-time architecture for wireless communication in a fading environment when using multi-element antennas," *Bell Labs Tech. J.*, p. 41–59, 1996.
- [44] S. M. Alamouti, "A simple transmit diversity technique for wireless communications," *IEEE J. Select. Areas Commun.*, vol. 16, pp. 1451–1458, October 1998.
- [45] V. Tarokh, H. Jafarkhani, and A. R. Calderbank, "Space-time block codes from orthogonal design," *IEEE Trans. Inform. Theory*, vol. 45, pp. 1456–1466, July 1999.
- [46] M. O. Damen, K. Abed-Meraim, and J.-C. Belfiore, "Diagonal algebraic space-time block codes," *IEEE Trans. Inform. Theory*, vol. 48, pp. 628–636, March 2002.
- [47] M. O. Damen, A. Tewfik, and J.-C. Belfiore, "A construction of a space-time code based on number theory," *IEEE Trans. Inform. Theory*, vol. 48, no. 3, pp. 753–760, March 2002.
- [48] L. Zheng and D. N. C. Tse, "Diversity and multiplexing: A fundamental tradeoff in multiple-antenna channels," *IEEE Trans. Inform. Theory*, vol. 49, no. 5, pp. 1073–1096, May 2003.
- [49] P. Elia, K. R. Kumar, S. A. Pawar, P. V. Kumar, and H. Lu, "Explicit, minimum-delay space-time codes achieving the diversity-multiplexing gain tradeoff," *IEEE Trans. Inform. Theory*, submitted for publication.
- [50] V. Tarokh, N. Seshadri, and A. Calderbank, "Space-time codes for high data rate wireless communication : Performance criterion and code construction," *IEEE Trans. Inform. Theory*, vol. 44, pp. 744–765, 1998.
- [51] J. Yuan, Z. Chen, B. Vucetic, and W. Firmanto, "Performance and design of space-time coding in fading channels," *IEEE Trans. Commun.*, vol. 51, no. 12, pp. 507–517, December 2003.
- [52] M. Dohler, B. Rassool, and H. Aghvami, "Performance evaluation of STTCs for virtual antenna arrays," in *Proceedings IEEE Vehicular Technology Conference*, April 2003, pp. 57–60.
- [53] M. Uysal and C. N. Georghiades, "Effect of shadowing on the performance of space-time trellis-coded systems," *IEEE Trans. Wireless Commun.*, vol. 3, pp. 1037–1042, July 2004.
- [54] M. Uysal, "Pairwise error probability of space-time codes in rician-nakagami channel," *IEEE Commun. Lett.*, vol. 8, pp. 132–134, March 2004.
- [55] A. J. Hammons and H. El Gamal, "On the theory of space-time codes for PSK modulation," *IEEE Trans. Inform. Theory*, vol. 46, no. 2, pp. 524 – 542, March 2000.
- [56] H. Yao and G. Wornell, "Structured space-time block codes with optimal diversity-multiplexing tradeoff and minimum delay," in *Proceedings IEEE Global Telecommunications Conference*, vol. 4, December 2003, pp. 1941 – 1945.
- [57] H. El Gamal and M. O. Damen, "Universal space-time coding," *IEEE Trans. Inform. Theory*, vol. 49, pp. 1097–1119, May 2003.
- [58] E. Bayer, F. Oggier, and E. Viterbo, "New algebraic constructions of rotated  $\mathbb{Z}^n$  lattice constellations for the Rayleigh fading channel," *IEEE Trans. Inform. Theory*, vol. 50, pp. 702–714, April 2004.

- [59] B. A. Sethuraman, B. S. Rajan, and V. Shashidhar, "STBCs using capacity achieving designs from cyclic division algebras," in *Proceedings IEEE Global Communications Conference*, vol. 4, December 2003, pp. 1957–1962.
- [60] J.-C. Belfiore and G. Rekaya, "Quaternionic lattices for space-time coding," in *Proceedings IEEE Information Theory Workshop*, vol. 2, April 2003, pp. 267–270.
- [61] T. Kiran and B. S. Rajan, "STBC-schemes with nonvanishing determinant for certain number of transmit antennas," *IEEE Trans. Inform. Theory*, vol. 51, no. 8, pp. 2984–2992, August 2005.
- [62] G. Rekaya, J. C. Belfiore, and E. Viterbo, "Algebraic  $3 \times 3$ ,  $4 \times 4$  and  $6 \times 6$  space-time codes with non-vanishing determinants," to appear in IEEE Int. Conference on Information Theory and its Applications.
- [63] J.-C. Belfiore, G. Rekaya, and E. Viterbo, "The Golden code: a  $2 \times 2$  full-rate space-time code with nonvanishing determinant," *IEEE Trans. Inform. Theory*, vol. 51, no. 4, pp. 1432–1436, April 2005.
- [64] F. Oggier, G. Rekaya, J.-C. Belfiore, and E. Viterbo, "Perfect space time block codes," *IEEE Trans. Inform. Theory*, submitted for publication.
- [65] P. Elia, B. Sethuraman, and P. Kumar, "Perfect space-time codes with minimum and non-minimum delay for any number of antennas," in *IEEE Int. Conf. on Wireless Networks, Communications and Mobile Computing*, vol. 1, June 2005, pp. 722 – 727.
- [66] P. Dayal and M. Varanasi, "An optimal two transmit antenna space-time code and its stacked extensions," *IEEE Trans. Inform. Theory*, vol. 51, no. 12, pp. 4348 – 4355, December 2005.
- [67] H. El Gamal, G. Caire, and M. O. Damen, "Lattice coding and decoding achieve the optimal diversity-multiplexing tradeoff of MIMO channels," *IEEE Trans. Inform. Theory*, vol. 50, pp. 968 – 985, June 2004.
- [68] A. Sendonaris, E. Erkip, and B. Aazhang, "User cooperation diversity. Part I. System description," *IEEE Trans. Commun.*, vol. 51, no. 11, pp. 1927 – 1938, November, 2003.
- [69] ———, "User cooperation diversity. Part II. Implementation aspects and performance analysis," *IEEE Trans. Commun.*, vol. 51, no. 11, pp. 1939 – 1948, November, 2003.
- [70] J. Laneman, D. Tse, and G. Wornell, "Cooperative diversity in wireless networks: Efficient protocols and outage behavior," *IEEE Trans. Inform. Theory*, vol. 50, pp. 3062–3080, December 2004.
- [71] J. Laneman and G. Wornell, "Distributed space time coded protocols for exploiting cooperative diversity in wireless networks," *IEEE Trans. Inform. Theory*, vol. 49, no. 10, pp. 2415–2425, October 2003.
- [72] R. U. Nabar and H. Bolcskei, "Space-time signal design for fading relay channels," in *IEEE Global Telecommunications Conference*, December 2003, pp. 1952 – 1956.

- [73] K. Azarian, H. El Gamal, and P. Schinter, “On the achievable diversity-multiplexing tradeoffs in half-duplex cooperative channels,” *IEEE Trans. Inform. Theory*, vol. 51, no. 12, pp. 4152–4172, December 2005.
- [74] S. Yang and J.-C. Belfiore, “Optimal space-time codes for the MIMO amplify-and-forward cooperative channel,” *IEEE Trans. Inform. Theory*, accepted for publication.
- [75] M. Hussain, “Principles of space-time array processing for ultrawide-band impulse radar and radio communications,” *IEEE Trans. Veh. Technol.*, vol. 51, no. 3, pp. 393 – 403, May 2002.
- [76] L. Xu, S. Davis, S. Hagness, D. van der Weide, and B. V. Veen, “Microwave imaging via space-time beamforming: experimental investigation of tumor detection in multilayer breast phantoms,” *IEEE Trans. Microwave Theory Tech.*, vol. 52, no. 8, pp. 1856 – 1865, August 2004.
- [77] H. Zhang and T. Gulliver, “Performance and capacity of PAM and PPM UWB systems with multiple receive antennas,” in *Proceedings IEEE Pacific Rim Conference on Communications, Computers and signal Processing*, vol. 2, August 2003, pp. 740 – 743.
- [78] C. Tsung-Hui, C. Yu-Jung, P. Chun-Hsien, L. Yu-Hang, and C. Chong-Yung, “Space time MSINR-SRAKE receiver with finger assignment strategies in UWB multipath channels,” in *Proceedings IEEE International Conference on Ultra-Wideband*, September 2005, pp. 242 – 247.
- [79] T. Ezaki and T. Ohtsuki, “Performance evaluation of space hopping ultra wideband impulse radio (SH-UWB-IR) system,” in *Proceedings IEEE International Conference on Communications*, vol. 6, June 2004, pp. 3591–3595.
- [80] L. Yang and G. B. Giannakis, “Space-time coding for impulse radio,” in *Proceedings IEEE Conference on UWB Systems and Technologies*, 2002, pp. 235–239.
- [81] ———, “Analog space-time coding for multi-antenna ultra-wideband transmissions,” *IEEE Trans. Commun.*, vol. 52, pp. 507–517, March 2004.
- [82] W. Siriwongpairat, M. Olfat, and K. J. R. Liu, “On the performance evaluation of TH and DS UWB MIMO systems,” in *Proceedings IEEE Wireless Communications and Networking Conference*, vol. 3, March 2004, pp. 1800–1805.
- [83] ———, “Performance analysis of time hopping and direct sequence UWB space-time systems,” in *Proceedings IEEE Global Telecommunications Conference*, vol. 6, December 2004, pp. 3526–3530.
- [84] M. Weisenhorn and W. Hirt, “Performance of binary antipodal signaling over the indoor UWB MIMO channel,” in *Proceedings IEEE International Conference on Communications*, vol. 4, May 2003, pp. 2872–2878.
- [85] L. Zhiwei, B. Premkumar, and A. S. Madhukumar, “MMSE detection for high data rate UWB MIMO systems,” in *Proceedings IEEE Vehicular Technology Conference*, vol. 2, September 2004, pp. 1463–1467.
- [86] Y. Kim, B. Jang, C. Shin, and B. Womack, “Orthonormal pulses for high data rate communications in indoor UWB systems,” *IEEE Commun. Lett.*, vol. 9, no. 5, pp. 405–407, May 2005.

- [87] E. Baccarelli, M. Biagi, C. Pelizzoni, and P. Bellotti, "A novel multi-antenna impulse radio UWB transceiver for broadband high-throughput 4G WLANs," *IEEE Commun. Lett.*, vol. 8, pp. 419 – 421, July 2004.
- [88] E. Baccarelli, M. Biagi, and C. Pelizzoni, "A simple multiantenna transceiver for ultra wide band based 4GWLANs," in *IEEE Wireless Communications and Networking Conference*, March 2004, pp. 1782 – 1787.
- [89] L. Huaping, R. C. Qiu, and T. Zhi, "Error performance of pulse-based ultra-wideband MIMO systems over indoor wireless channels," *IEEE Trans. Wireless Commun.*, vol. 4, pp. 2939–2944, November 2005.
- [90] W. Li-Chun, L. Wei-Cheng, and S. Kuan-Jiin, "On the performance of using multiple transmit and receive antennas in pulse-based ultrawideband systems," *IEEE Trans. Wireless Commun.*, vol. 4, pp. 2738–2750, November 2005.
- [91] N. C. Beaulieu and Q. Xie, "An optimal lognormal approximation to lognormal sum distributions," *IEEE Trans. Commun. Technol.*, vol. 53, pp. 479–489, March 2004.
- [92] A. Abu-Daya and N. Norman, "Comparison of methods of computing correlated lognormal sum distributions and outages for digital wireless applications," in *Proceedings IEEE Vehicular Technology Conference*, June 1994, pp. 175–179.
- [93] B. Mielczarek, M. Wessman, and A. Svensson, "Performance of coherent UWB Rake receivers with channel estimators," in *IEEE Vehicular Technology Conference*, vol. 3, October 2003, pp. 1880 – 1884.
- [94] R. Narasimhan, A. Ekbal, and J. Cioffi, "Finite-SNR diversity-multiplexing tradeoff of space-time codes," in *IEEE International Conference on Communications*, May 2005, pp. 458 – 462.
- [95] S. Verdu, *Multiuser Detection*. Cambridge U.K.: Cambridge University Press, 1998.
- [96] S. Gezici, H. Kobayashi, V. Poor, and A. F. Molisch, "Performance evaluation of impulse radio uwb systems with pulse-based polarity randomization," *IEEE Trans. Signal Processing*, vol. 53, pp. 2537–2549, July 2005.
- [97] M. Brehler and M. K. Varanasi, "Optimum receivers and low-dimensional spreaded modulation for multiuser space-time communications," *IEEE Trans. Inform. Theory*, vol. 49, pp. 901–918, April 2003.
- [98] ——, "Asymptotic error probability analysis of quadratic receivers over Rayleigh fading channels with applications to a unified analysis of coherent and noncoherent space time receivers," *IEEE Trans. Inform. Theory*, vol. 47, pp. 2383–2399, September 2001.
- [99] I. Kammoun and J.-C. Belfiore, "A new family of Grassmann Space-Time codes for non-coherent MIMO systems," *IEEE Commun. Lett.*, vol. 7, pp. 528–530, November 2003.
- [100] E. Viterbo, "Table of full diversity algebraic rotations," Online, <http://www.tlc.polito.it/~viterbo/rotations/rotations.html>.

- [101] M. Daberkow, C. Fieker, J. Klner, M. Pohst, K. Roegner, and K. Wildanger, "Kant v4," *J. Symbolic Comp.*, vol. 24, 1997.
- [102] E. Viterbo and J. Boutros, "A universal lattice code decoder for fading channels," *IEEE Trans. Inform. Theory*, vol. 45, pp. 1639–1642, July 1999.
- [103] Z. Guo and P. Nilsson, "Reduced complexity Schnorr-Euchner decoding algorithms for MIMO systems," *IEEE Commun. Lett.*, vol. 8, pp. 286–288, May 2004.
- [104] A. D. Murugan, H. El Gamal, M. O. Damen, and G. Caire, "A unified framework for tree search decoding: rediscovering the sequential decoder," *IEEE Trans. Inform. Theory*, vol. 52, no. 3, pp. 933 – 953, March 2006.
- [105] J. Luo, R. S. Blum, L. Greenstein, L. Cimini, and A. M. Haimovich, "New approaches for cooperative use of multiple antennas in ad hoc wireless networks," in *IEEE Conference on Vehicular Technology*, September 2004, pp. 2769 – 2773.
- [106] P. Tarasak, M. Hlaing, and V. K. Bhargava, "Differential modulation for two-user cooperative diversity systems," *IEEE J. Select. Areas Commun.*, vol. 32, pp. 1891–1900, September 2005.
- [107] Z. Yimin, "Differential modulation schemes for decode-and-forward cooperative diversity," in *IEEE International Conference on Acoustics Speech and Signal Processing*, vol. 4, March 2005, pp. 917 – 920.
- [108] Y. Chao and R. Scholtz, "Optimal and suboptimal receivers for ultra-wideband transmitted reference systems," in *Proceedings IEEE Conference on Global Telecommunications*, vol. 2, March 2004, pp. 759–763.
- [109] G. Durisi and S. Benedetto, "Performance of coherent and non-coherent receivers for uwb communications," in *Proceedings IEEE International Conference on Communications*, vol. 6, June 2004, pp. 3429–3433.
- [110] Y. Souilmi and R. Knopp, "On the achievable rates of ultra-wideband ppm with non-coherent detection in multipath environments," in *Proceedings IEEE International Conference on Communications*, vol. 5, 2003, pp. 3530–3534.
- [111] F. Adachi and M. Sawahashi, "Decision feedback differential phase detection of m-ary dpsk signal," in *IEEE Trans. Vehicular Technology*, vol. 44, May 1995, pp. 203–210.
- [112] M. O. Damen, H. El-Gamal, and G. Caire, "On maximum-likelihood detection and the search for the closest lattice point," *IEEE Trans. Inform. Theory*, vol. 49, pp. 2389–2402, October 2003.
- [113] E. Agrell, T. Eriksson, A. Vardy, and K. Zeger, "Closest point search in lattices," *IEEE Trans. Inform. Theory*, vol. 48, pp. 2201–2214, August 2002.
- [114] N. A. Kumar and R. M. Buehrer, "Application of layered space-time processing to ultra-wideband communications," in *IEEE Midwest Symp. on Circuits and Systems*, vol. 3, August 2002, pp. 597–600.

- [115] F. Q. Gouvêa, *P-Adic Numbers: An introduction*, 2nd ed. Berlin, Germany: Springer-Verlag, 1997.
- [116] T. De-Mazancourt and D. Gerlic, “The inverse of a block-circulant matrix,” *IEEE Trans. Antennas Propagat.*, vol. 31, no. 5, pp. 808–810, September 1983.